UNIVERSITY OF ALBERTA

Acid Mine Drainage at Sub-Zero Temperatures

by

Roderick Cameron Godwaldt

A thesis submitted to the Faculty of Graduate Studies and Research in partial fulfillment of the requirements for the degree of Master of Science.

in

Geoenvironmental Engineering

Department of Civil and Environmental Engineering

EDMONTON, ALBERTA

Spring 2001

National Library of Canada
Acquisitions and Bibliographic Services
395 Wellington Street
Ottawa ON K1A 0N4
Canada

Bibliothèque nationale du Canada
Acquisitions et services bibliographiques
395, rue Wellington
Ottawa ON K1A 0N4
Canada

Your file Votre référence

Our file Notre référence

The author has granted a non-exclusive licence allowing the National Library of Canada to reproduce, loan, distribute or sell copies of this thesis in microform, paper or electronic formats.

The author retains ownership of the copyright in this thesis. Neither the thesis nor substantial extracts from it may be printed or otherwise reproduced without the author's permission.

L'auteur a accordé une licence non exclusive permettant à la Bibliothèque nationale du Canada de reproduire, prêter, distribuer ou vendre des copies de cette thèse sous la forme de microfiche/film, de reproduction sur papier ou sur format électronique.

L'auteur conserve la propriété du droit d'auteur qui protège cette thèse. Ni la thèse ni des extraits substantiels de celle-ci ne doivent être imprimés ou autrement reproduits sans son autorisation.

0-612-60432-2

Canada

University of Alberta

Library Release Form

Name of Author: Roderick Cameron Godwaldt

Title of Thesis: Acid Mine Drainage at Sub-Zero Temperatures

Degree: Master of Science

Year this Degree Granted: 2001

Permission is hereby granted to the University of Alberta Library to reproduce single copies of this thesis and to lend or sell such copies for private, scholarly, or scientific purposes only.

The author reserves all other publication and other rights in association with the copyright in the thesis, and except as hereinbefore provided, neither the thesis nor and substantial portion thereof may be printed or otherwise reproduced in any material form whatever without the author's prior written permission.

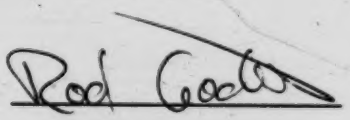

Roderick Cameron Godwaldt
2 Village Road
Sherwood Park, Alberta
T8A 0Z4

January 6, 2001

UNIVERSITY OF ALBERTA

FACULTY OF GRADUATE STUDIES AND RESEARCH

The undersigned certify that they have read, and recommend to the Faculty of Graduate Studies and Research for acceptance, a thesis entitled **Acid Mine Drainage at Sub-Zero Temperatures** submitted by **Roderick Cameron Godwaldt** in partial fulfillment of the requirements for the degree of **Master of Science** in **Geoenvironmental Engineering.**

Dr. K.W. Biggar (Supervisor)

Dr. D.C. Sego (Co-Supervisor)

Dr. S. Guigard (Internal Examiner)

Dr. R. Brachman (Internal Examiner)

Dr. M. Dudas (External Examiner)

14 July 2000

Date thesis approved by committee.

ABSTRACT

Acid mine drainage is the oxidation of sulfide minerals in the presence of water resulting in the generation of acidity and increased metal solubility. Elevated heavy metal concentrations in mine runoff makes acid mine drainage a serious environmental concern for many hard rock and coal mines.

The main objective of this research was to determine the effects of sub-zero temperatures on the generation of acid mine drainage from mine tailings. Site visits were made to conduct field tests and collect samples for physical, thermal, microbial and weathering characterization. As the temperature decreases near 0°C, there is a decrease in the production of sulfate and an increase in the lag time to the onset of acid generation.

In combination with previous research and field investigations, the results of testing suggest that the acid generation mechanisms will continue at sub-zero temperatures in the presence of unfrozen water and oxygen.

ACKNOWLEDGEMENTS

I would like to express my thanks firstly to my supervisor, Dr. Kevin Biggar, and co-supervisors Dr. David Sego and Dr. Julia Foght for their patience, direction and support. during the course of these three years. Thanks also to the many other advisors around the University of Alberta, in various faculties, including Dr. Selma Guigard and Dr. Marvin Dudas for their patience under a continual barrage of questions. Thanks also to the many people at various mine sites, government organizations and private consultants for their advice and willingness to participate.

This project was made possible by Public Works and Government Services Canada. Environmental Services, and Indian and Northern Affairs Canada. Thanks to Mike Nahir for taking the risk of sponsoring the thesis, and to Giselle Cotta, who managed to be both a classmate during the first year of courses and then a boss during the final months of the project.

To Christine Hereygers, a very special thank-you. You deserve to be a co-author for the countless hours of help, for going out of your way so many times, for covering for me so I could actually take time off and for your cheerful spirit. To Steve Gamble, Gerry Cyre and Sally Petaske, thanks for your help in many different ways.

To the many international students and friends in the faculty, thank you for opening my eyes to the many wonderful cultures around the world.

Finally, to my family for always being there - knowing you were there allowed me to venture out a little further - and to the many roommates for making this such a good time.

TABLE OF CONTENTS

1 INTRODUCTION 1

1.1 STATEMENT OF PROBLEM 1

1.2 THESIS OBJECTIVE 2

2 BACKGROUND INFORMATION 4

2.1 FUNDAMENTALS OF ACID MINE DRAINAGE 4

2.1.1 Chemical Oxidation Processes 4

2.1.2 Biochemical Oxidation 6

2.1.2.1 Bacteria Physiology and Mechanisms 6

2.1.3.2 Factors Affecting Biochemical Activity 8

2.1.5 Acid Neutralizing Mechanisms 11

2.1.5.1 Carbonate Dissolution 12

2.1.5.2 Hydroxide Dissolution 12

2.1.5.3 Aluminosilicate Dissolution 13

2.1.5.4 Reaction Kinetics 13

2.1.6 Conclusions 14

2.2 ACID MINE DRAINAGE AT LOW TEMPERATURES 14

2.2.1 Unfrozen Water Content 15

2.2.1.1 Effect of Solutes 15

2.2.1.2 Mineral Grain Effects 18

2.2.1.3 Charged Surfaces 19

2.2.1.4 Bacteria Effects 21

2.2.2 Biochemical Activity 21

2.2.2.1 Effects of Cold Temperatures on Microorganisms 23

2.2.2.2 Microbial Adaptation to Cold Temperatures 25

2.2.3 Oxygen / Water Availability 25

2.2.4 Consequences 26

2.3 ACID BASE ACCOUNTING 28

2.3.1 Static Geochemical Tests 29

2.3.1.1 Sobek Test 29

2.3.1.2 Other Static Tests 31

2.3.1.3 Comparison of static test techniques 32
2.3.2 Kinetic Geochemical Tests 33
2.3.2.1 Humidity Cells 34
2.3.2.2 Batch Cells 37

3 SITE VISITS AND PREVIOUS STUDIES 59

3.1 DISCOVERY SITE 59
3.2 PREVIOUS STUDIES FROM DISCOVERY MINE 62
3.2.1 Acid Generating Studies 62
3.2.2 Summaries of Cold Temperature Considerations 63
3.3 PREVIOUS STUDIES FROM FARO MINE 64
3.4 FARO MINE VISIT 65

4 EXPERIMENTAL PROGRAM AND RESULTS 84

4.1 PHYSICAL CHARACTERIZATION 84
4.1.1 Grain Size Distribution 85
4.1.2 Atterberg Limits 85
4.1.3 Mineralogical Speciation 86
4.1.4 Metals analysis 87
4.1.5 Acid Base Accounting 89
4.1.6 Soil-Moisture Characteristic Curves 90
4.2 THERMAL CHARACTERIZATION 90
4.2.1 Unfrozen Water Content / Freezing Point Depression 91
4.2.2 Thermal Conductivity 93
4.3 MICROBIAL CHARACTERIZATION 93
4.3.1 Agar Plate Counts 94
4.3.2 Enrichment Cells 97
4.3.3 Transmitting Electron Microscope 98
4.3.4 Batch Cell Inoculations 98
4.4 ACID GENERATING CHARACTERIZATION 98
4.4.1 Humidity Cells 99
4.4.1.1 Apparatus 100
4.4.1.2 Sample Preparation 102
4.4.1.3 Humidity Cell Operation 102
4.4.1.4 Humidity Cell Results 104

4.4.2 Batch Cell Test *106*
4.4.2.1 Sample Preparation 107
4.4.2.2 Experimental Constraints 108
4.4.2.3 Batch Test Results 108

5 DISCUSSION AND ANALYSIS 142

5.1 PHYSICAL PROPERTIES ANALYSIS 142
5.1.1 Grain Size Distribution *142*
5.1.2 Mineralogy *143*
5.2 THERMAL PROPERTIES ANALYSIS 144
5.2.1 Discovery Mine – Unfrozen Water *144*
5.2.2 Faro Mine – Unfrozen Water *146*
5.2.3 Thermal Conductivity *146*
5.3 BIOTIC EFFECTS ON ACID GENERATION 148
5.4 EFECTS OF TEMPERATURE ON HUMIDITY CELLS 150
5.4.1 Effects of Temperature on pH for Faro Tailings *150*
5.4.2 Effects of Temperature on Sulfate Leaching *151*
5.4.3 Effect of Redox Potential *153*
5.4.4 Humidity Cell Operation *153*
5.4.5 Humidity Cells – Comparison to Other Studies *154*
5.5 EFFECTS OF TEMPERATURE ON BATCH TESTS 156
5.5.1 Predicted Batch Test Results *156*
5.5.2 Sources of Error *157*
5.5.3 Consequences of Membrane Failure *159*
5.6 CORRELATION BETWEEN HUMIDITY CELLS AND BATCH CELLS 160
5.7 RECOMMENDED CHANGES TO TESTING PROGRAM 160

6 CONCLUSIONS AND RECOMMENDATIONS 170

REFERENCES 173

LIST OF FIGURES

Chapter 2

2-1 Intermediate Reactions in Acid Mine Drainage Reaction 39

2-2 Progression of Stages in Acid Generation with Time as a Function of pH 40

2-3 Changes in Relative Biological and Chemical Oxidation Rates of Pyrite as a Function of pH 41

2-4 Bacterial Physiology 42

2-5 Solubility of Oxygen and Nitrogen in Water vs. Temperatures with Critical Oxygen Concentration 43

2-6 Progressive pH Levels of Dissolution of Acid Buffering Minerals 44

2-7 Phase Diagram for Sodium Chloride 45

2-8 Increasing Unfrozen Water Content as a Function of Various NaCl Solution Concentrations at Temperatures Below 0°C 46

2-9 Unfrozen Water Content for Antarctic Moraine and Alluvial Soils vs. Temperature 47

2-10 Increasing Confining Pressure Resulting in Finer Pore Radii Resulting in Increased Unfrozen Water Content 48

2-11 Increase in Unfrozen Water Content with Increase in Confining Pressure and Void Ratio for Devon Clayey Silt 49

2-12 Increase in Unfrozen Water Content with Increases in Material Surface Charge for Five Soils 50

2-13 Sudden Change in Biological Oxidation Rate Curve as Modeled by RATAP Software Unsupported by Experimental Data 51

2-14 Sudden Changes in Biological Oxidation Rates Due to Assumed 0°C Intercept 52

2-15 Biological Oxygen Demand Curve Suggesting Biological Activity at Temperatures Below 0°C 53

2-16 Growth Rate for Thiobacillus Ferrooxidans at Near 0°C 54

2-17a Arrhenius Plot of Growth Rate Constant for Thermophilic Bacteria 55

2-17b Square Root Model Plot for Reaction Rates for Thermophilic Bacteria – Alternative to Arrhenius Curve for Biological Activity 55
2-18 Minimum Temperature – Water Activity Limits for Two Psychrophiles 56

Chapter 3

3-1 Discovery Mine Base Camp 67
3-2 Discovery Site Characterization Team 67
3-3 Collection Site of Discovery Tailings for Bulk Test Sample 68
3-4 Exposure of GCL During Sample Collection on Tailings Delta at Discovery Mine 68
3-5 Standard X-cut in GCL Revealing Organic Matter During Sample Collection on Tailings Delta 69
3-6 Tailings Extracted Using Hand Auger on Tailings Delta 69
3-7 Sample Collection and Labeling of Bulk Samples from Tailings Delta 70
3-8 Sealing Hole in GCL from Sample Extraction Site Using Bentonite Chips 70
3-9 Bentonite Chips with Geotextile in Final Step of GCL Repair 71
3-10 Thermistor String 'A' Identification on Tailings Delta 71
3-11 Completed Site of Thermistor 'A' on Tailings Delta 72
3-12 Initial Site Location for Collection of Weathering Profile of Tailings at Discovery Site 72
3-13 Air Strip Sampling and Thermistor String 'B' Location Approximately 200m from Town Site 73
3-14 Weathering Zones in Air Strip Tailings Revealing Significant Zones of Iron Enrichment and Sulfide Oxidation 73
3-15 Core Extracted Using Shelby Tubes at Air Strip Thermistor String 'B' Location 74
3-16 Tube Labeling and Site Repair at Discovery Airstrip Sampling Location 74
3-17 Ground Temperatures at Discovery Mine, NWT with 0°C Line 75
3-18 Sample Collection Sites for Soil Analysis at Discovery Mine 76
3-19 Faro, Yukon Territory 77
3-20 Selected Sites for Faro Mine Samples on Tailings Impoundment 78

3-21 Depth to Frozen Material at Initial Mine Sampling Location on Tailings Impoundment 79
3-22 Final Depth for Bulk Sampling at Faro Mine 79

Chapter 4

4-1 Grain Size Distribution Curves for Discovery and Faro Mine Tailings 111
4-2 XRD Patterns for Unoxidized Discovery Tailings 112
4-3 XRD Patterns for Oxidized Discovery Tailings 112
4-4 Increasing Batch pH with Depth in Profile of Discovery Core Sample 113
4-5 Pressure Plate Apparatus for Determining Soil Moisture Characteristic Curve 114
4-6 Ceramic Plates for Pressure Plate Apparatus for Soil Moisture Characteristic Curve 114
4-7 Soil-Moisture Characteristic Curves for Discovery Tailings 115
4-8 TDR Cell for Measuring Unfrozen Water Content 116
4-9 Example of TDR Pulse 116
4-10 Unfrozen Water Content for Discovery and Faro Mine Tailings 117
4-11 Thermal Conductivity Probe 118
4-12 Thermal Conductivity of Discovery and Faro Mine Tailings 119
4-13 Enrichment Cell pH vs Time for Different Test Conditions 120
4-14 Transmitting Electron Microscopy – Sulfur Oxidizing Bacteria from Discovery Tailings 121
4-15 Transmitting Electron Microscopy – Iron Oxidizing Bacteria from Discovery Tailings 121
4-16 Humidity Cell Schematic 122
4-17a 20°C Humidity Cell Setup Using Discovery Mine Tailings 123
4-17b Humidity Cell Manifold in 20°C Humidity Cell Setup 123
4-18 Air Temperature Regulating Coil for 3°C Humidity Cell 124
4-19 Discovery Tailings – Humidity Cell pH and Sulfate vs Time at 20°. 3° and 1°C 125
4-20 Faro Tailings - Humidity Cell Average pH vs Time 128

4-21 Faro Tailings Humidity Cell pH vs Time at 20°, 3° and 1°C 129
4-22 Humidity Cell Sulfate Concentration vs Time at 20°, 3° and 1°C 130
4-23 Humidity Cell Sulfate Mass vs Time at 20°, 3° and 1°C 131
4-24 Cumulative Sulfate from Faro Humidity Cell Tests 132
4-25 Eh-pH Diagram for Iron Sulfide Species 133
4-26 Batch Cell Schematic and Apparatus 134
4-27 0.45 Micron Vacuum Filtration Unit 134
4-28 Faro Tailings – Batch Cell Sulfate vs Time 135
4-29 Inoculated Batch Cell Sulfate Concentration vs Time 136
4-30 Batch Cell Total Dissolved Sulfur vs Time 137
4-31 Batch Cell pH vs Time 138

Chapter 5

5-1 Comparison of Volumetric Water Content for 5 Soils with Faro and Discovery Tailings 162
5-2 Effects of Grain Size and Solute Strength on Volumetric Unfrozen Water Content 163
5-3 Cullaton Lake Humidity Cells – pH vs Time 164
5-4 Cullaton Lake Humidity Cells - Sulfate vs Time 164
5-5 Windy Craggy Humidity Cells - pH vs Time 165
5-6 Windy Craggy Humidity Cells - Sulfate vs Time 165
5-7 pH vs Time for Enrichment Cultures Using Elemental Sulfur at Temperatures Approaching 0°C 166
5-8 Oxidation Reaction Rates with Elemental Sulfur, Pyrite and Pyrrhotite at Temperatures Approaching 0°C 167
5-9 Measured and Predicted Behavior of Batch Sulfur Concentration vs Time 168

LIST OF TABLES

Chapter 2

2-1 Growth Conditions for Acidophilic Bacteria 57

2-2 Principle Acid Neutralizing Minerals 57

2-3 Mineral Equilibrium pH for Acid Buffering 58

2-4 Vapor Pressures for Water and Ice 58

Chapter 3

3-1 Thermistor Strings at Discovery Mine 80

3-2 Comparison of Oxidized and Unoxidized Zones in Discovery Core 81

3-3 pH of Tailings. Leachate and Lake Water 82

3-4 Concentration of Elements in Water Samples from Discovery Tailings 83

Chapter 4

4-1 Discovery Tailings Soil Analysis of Unoxidized Tailings 139

4-2 Composition of Discovery Tailings by Neutron Activation Analysis 140

4-3 Bacteria Plate Counts 141

Chapter 5

5-1 Thermal Conductivities for Various Minerals 169

APPENDICES

Appendix A X-ray Diffraction Patterns.....186
Appendix B Klohn Leonoff Total Metals Analysis 192
Appendix C Modified Sobek Test.....195
Appendix D Thermal Conductivity Tests.....198
Appendix E Bacteria Culture Recipes.....227
Appendix F pH and Sulfate Tracking for Humidity Cells and Batch Cells 231

LIST OF SYMBOLS

β - characteristic soil parameter

α - characteristic soil parameter

θ - constant

θ - temperature below 0°C

ΔH - molar heat of fusion

σ_{iw} - ice water interfacial tension

ΔT - freezing point depression

A - constant

A - peak area counts

a_w - water activity

B - background counts

b - slope of regression curve

C - concentration

E - error

E - ratio of molecular weight of water to molecular weight of solutes

E_a - activation energy

EC - electrical conductuvity

I - ionic strength

K - oxygen adsorption constant

K - rate constant

k - specific growth rate

K_a - apparent dielectric constant

L_f - latent heat of fusion

LL - liquid limit

m_B - molality

N - pyrite concentration

R - universal gas constant

r_{iw} - radius of interface

T - absolute temperature

t - time

T_0 - freezing point of pure solvent

T_{min} - temperature where regression line cuts temperature axis

V_w - specific volume of water

w_u - unfrozen water content

x - cycle number

X_s - solute concentration

1 INTRODUCTION

1.1 STATEMENT OF PROBLEM

With exploration and mining activity recovering in the Arctic, and due to intense environmental scrutiny, attention is again being focussed on waste treatment issues in the North. Decades of careless resource management have left a legacy of abandoned mine sites, waste dumps, and ongoing cleanup requirements. Over 75 sites in the Canadian territories have been identified by Indian and Northern Affairs Canada as requiring investigation into their potential for acid mine drainage (AMD) (Klohn Leonoff, 1994), a condition in which sulfide minerals reacts with oxygen and water to generate acid through a combination of chemical and biological activities. These sulfides may be present in a mineral or material of economic interest, waste generated from mining operations, or from disturbed material on a construction site. The resulting acidic conditions are responsible for increased heavy metal concentrations in the water, which are toxic to plant and animal life.

One of the recommended strategies for control of acid mine drainage in northern regions is the use of permafrost to permanently encapsulate the reactive material. Preliminary results indicate that this method has been successful in continuous permafrost regions, although no long-term data or performance monitoring have been published. While permanent storage may be achievable in extreme cold regions for some material, it is necessary to examine the factors that determine whether a specific material remains inert in a given environment.

Due to the extreme temperatures experienced in the North, a fundamental shift occurs with respect to the prediction, prevention and containment of acid rock drainage compared to generally accepted methods in more temperate climates. Some of the constraints include:

- Extremely low temperatures (averaging less than –30°C at times);
- Relatively short frost free period;
- Long duration of ice and snow cover (7 to 10 months);
- The presence of permafrost (ground temperature less than 0°C for more than 12 continuous months);
- Annual precipitation varying from high to very low (less than 300mm);
- Extreme seasonal variation in runoff volumes due to melting snow;
- Lack of reliable data to characterize climate; and
- Remoteness of most regions.

Combined, these factors complicate prediction of acid mine drainage (AMD) potential, including depths of active zones due to permafrost, the activity of microbes at sub-zero temperatures, the presence of unfrozen water at temperatures less than 0°C, the mobility of moisture during freezing, and the availability of oxygen.

According to classical thermodynamics, as the temperature of a system decreases, the chemical, and in most cases biological, activity also decreases. Though the principle of reduced activity with decreasing temperature is valid, the interactions between microbial and geochemical systems make simplified models inadequate for complex modeling. It is important to realize that subzero temperatures do not predicate the absence of biological activity, water flow, or chemical reactivity. It is also important to identify that the oxidation of pyrite is an exothermic reaction which may affect local temperature regimes.

The kinetics of these reactions are therefore much more complicated, with rate of oxygen availability, contact surface area, bacterial presence and acitivity, and temperature acting as variables.

1.2 THESIS OBJECTIVE

The primary objective of this research project is to evaluate the effects of sub-zero temperatures on acid mine drainage. This objective is resolved into three components:

- To examine the physical, chemical and microbial roles in the acid generating process, as described in published literature, and to determine the theoretical effects of low and sub-zero temperatures on the mechanisms involved (Chapter 2);
- To investigate the effects of the thermal regime in the field on acid generation at Discovery Mine, NWT, and Faro Mine, YT (Chapter 3); and
- To design and implement a physical, chemical, microbial and thermal testing program that determines the effect of near and sub-zero temperatures on the generation of acid mine drainage (Chapter 4).

Chapter 5 analyses the data from the testing program and evaluates the consequences for mine sites experiencing similar environmental conditions to Faro and Discovery mines. Chapter 6 summarizes the main conclusions and suggests further areas of research.

2 BACKGROUND INFORMATION

2.1 FUNDAMENTALS OF ACID MINE DRAINAGE

The classic understanding of acid mine drainage is the generation of acidity and the release of metals into solution through the direct oxidation of sulfide minerals with oxygen, or indirectly with ferric iron (Hutchison and Ellison, 1992). In its simplest form, oxidation of pyrite by oxygen is described stoichiometrically as:

$$FeS_2 + \frac{7}{2}O_2 + H_2O \longrightarrow Fe^{2+} + 2SO_4^{2-} + 2H^+ \qquad \text{Eq. 2-1}$$

In reality, the acid generation process is a combination of intermediate reactions, which vary with pH, time, bacterial activity, temperature and other variables (Figure 2-1).

This section reviews the factors contributing to the generation of acid mine drainage and describes the mechanisms that control the kinetic response.

2.1.1 Chemical Oxidation Processes

The chemical oxidation processes involved in acid mine generation are very well understood and are described at length in the literature (Otwinowski, 1994; Nicholson, 1994). As noted above, the oxidation reactions vary with a number of factors and can be divided into a three-stage process corresponding to the pH of the environment. Though other pathways do exist, Figure 2-2 shows the main reaction sequence.

Stage 1

The initial stage of acid generation is characterized by a pH above 4.5 with high sulfate and low iron concentrations. The environment is characterized by the direct oxidation of pyrite by elemental oxygen, generating 2 moles of H^+, 2 moles of sulfate ion and 1 moles

of iron (II). In this early stage, at elevated pH, the process is predominantly abiotic (involves no microbes) (Eq. 2-2).

If the environment is oxygen rich, iron (II) will also be oxidized to iron (III) (Eq. 2-2).

$$4Fe^{2+} + O_2 + 4H^+ \longrightarrow 4Fe^{3+} + 2H_2O \qquad \text{Eq. 2-2}$$

In these elevated pH (>4.5) environments though, the iron (III) will be precipitated (Eq. 2-3).

$$Fe^{3+} + 3H_20 \longrightarrow Fe(OH)_3 + 3H^+ \qquad \text{Eq. 2-3}$$

Stage 2

The second stage is transitional, and is characterized by a higher biochemical activity. Oxidation of pyrite continues to occur (Eq. 2-2), but is now catalyzed greatly by direct bacterial oxidation. In this stage, the calcium-based carbonate is consumed or becomes unavailable alleviating any buffering and the pH decreases to between approximately 4.5 and 2.5.

At this point, the water has high sulfate levels, acidity, total dissolved iron, and a low soluble Fe^{3+}/Fe^{2+} ratio. This ratio is a key indicator, for as the acid generation process passes to the third stage, the ratio increases.

Stage 3

$$FeS_2 + 14Fe^{3+} + 8H_2O \longrightarrow 15Fe^{2+} + 2SO_4^{2-} + 16H^+ \qquad \text{Eq. 2-4}$$

Once the pH decreases below 2.5, the iron (III) no longer precipitates, and it oxidizes the pyrite directly, without the need for oxygen. This direct oxidation accelerates the process

dramatically. It is important to note the significance of the stoichiometric value of the protons in these reactions. In Equation 2-1, oxidation of one mole of pyrite generates two moles of acidity, and the reaction rate is low. However, once the iron (III) is present to oxidize the pyrite directly, *sixteen* moles of acidity per mole of pyrite are produced (Eq. 2-4).

This stage is characterized by a pH below 2.5, with high sulfate levels, acidity, total dissolved iron content and a higher Fe^{3+}/Fe^{2+} ratio.

2.1.2 Biochemical Oxidation

In addition to the purely chemical reactions that generate acid, there is a biological component that affects the sulfide tailings environment. Given the right conditions, microorganisms have the ability to catalyze the oxidation process (Norris and Johnson, 1998; Ingledew, 1990). Figure 2-3 shows the normalized curves for the sulfide oxidation rate for the chemical and biological reaction conditions. Because the bacteria have such a catalytic effect on the rates of acid generation, it is important to recognize their mechanisms and the factors that affect them.

Despite the increasing interest into the relative contribution of microbial oxidation, the opinions of the scientific community are not unanimous. Morin and Hutt (1998) challenge the usefulness of determining the biological effects. They state that the bacterial contribution appears to be relatively constant across most natural conditions and can therefore be considered a constant without having to quantify these effects any further.

2.1.2.1 Bacteria Physiology and Mechanisms

Acidophiles are bacteria that thrive in acidic media, though only in sulfate based systems at extreme pHs (Ingledew, 1990). Cytoplasmic membranes (Figure 2.4) form an osmotic

barrier sustaining a neutral pH within the membranes (between 5 and 7) while being supported in an acidic environment (Norris and Johnson, 1998). A survey of the literature revealed that the lowest reported pH environment supporting bacterial life was near 0.5.

Table 2-1 (Norris and Johnson, 1998) lists several acidophilic bacteria that are capable of growing in acidic environments, with their preferred pH and temperature ranges. Several other types exist, but this discussion is limited to the bacteria capable of surviving at lower temperatures.

The bacteria that has generated the most interest is the acidophilic Thiobacillus ferrooxidan which derives its energy from the oxidation of sulfides (or any reduced sulfur) or iron (II), according to Eqs. 2-3 and 2-4. Research into the Thiobacillus genus has been extensive due to its ubiquitous nature in acid mine drainage, and for its biohydrometallurgical benefits in metal leaching. In addition to the energy source, they also require CO_2 as a carbon source.

Abiotic oxidation of pyrite by iron (III) occurs at pH less than 4, but a dependence upon abiotic generation of iron (III) would limit the rate of this reaction. It is in the generation of iron (III) that the microbial action enhances the pyrite oxidation. Reports differ as to the extent of this catalyzing effect, from 10^6 (Singer and Stumm, 1968; Otwinowski, 1994) to a more modest 10 or 100 times more rapid, though other reports cast doubt upon even these figures (Morin et al., 1991). In addition to its role as a catalyst, reports also suggest that Thiobacillus is capable of oxidizing sulfide minerals upon contact with the mineral surface without requiring ferric iron as an oxidant (Morin et al., 1991).

For a complete discussion of the bacterial mechanisms involved, the reader is directed to Nordstrom and Southam (1997).

2.1.3.2 Factors Affecting Biochemical Activity

There are numerous environmental factors that affect the bioactivity within the tailings environment. These include, but are not limited to:

- pH
- Temperature
- Oxygen and nutrient availability
- Presence of carbon source
- Presence of moisture

As shown in Table 2-1, each strain of bacteria has an optimum and range of pH levels for growth. The bacteria may not die outside of these ranges, but are severely limited in their activity. Their re-emergence upon amelioration of environmental conditions suggests that they are still present, but may have been dormant.

Table 2-1 also shows the preferred temperature ranges for each strain. It is important to note the uncertainty in the lower end of the growth range. This factor will be discused further.

Morin et al. (1991) report that ammonium-nitrogen, phosphorous, sulfate and magnesium are essential for cellular processes of Thiobacillus ferrooxidans. The nitrogen and phosphorous requirements are typically not limiting, as only very small concentrations are necessary. The magnesium is used in carbon dioxide fixation and the phosphorous in energy metabolism.

Carbon dioxide is necessary for cell biosynthesis. In the early stages of acid generation, the dissolution of the carbonate minerals present provides an abundant source, but as the carbonates are depleted, the CO_2 supply can be limited. This depletion is augmented by its low solubility in acid waters, as carbonic acid dominates the carbonate continuum at low pH.

Though water is required for survival, too much water in the tailings system can be inhibitory. As the saturation levels increase, the oxygen transport decreases, reducing oxygen levels to diffusion controlled concentrations. At moderate temperatures in the tailings environment, lack of water is rarely a concern; however, at sub-zero temperatures when unfrozen water content decreases, the issue becomes important. Brock (1976) determined that a suction of less than -15 bars (indicative of unsaturated conditions) was required to sustain biological activity. This suction relates to a different moisture content for each tailings mass, as the grain size distribution varies.

Acid Generating Capacity

The presence of potential acid forming minerals does not predicate the production of acid runoff; rather, there exists a dependence on several key factors, including sulfide abundance and type, acid-neutralizing processes, and availability of moisture and oxygen. Additionally, carbon dioxide transport and nutrient levels present in the soil are significant as they contribute to the biochemical activity; however, these have been described above and will not be discussed further. The purpose of this section is not to provide quantitative calculations for predicting acid generation, but to demonstrate the diversity of factors and how they may inhibit or contribute to acid mine drainage generation.

Sulfide abundance, morphology and surface area

Hutchison et al. (1992) suggests two mechanisms affecting acid generation:

- Disseminated sulfides (i.e. finer grained materials) will generally be stronger acid generators than massive sulfides, as the extent of sulfide encapsulation by other minerals limits the physical accessibility to the oxidation reactants.

- The morphology of the sulfide also has an effect. Yanful et al. (1990) report that framboidal pyrite is more reactive than the euhedral form. No definitive relationship between surface area and oxidation rate has been accepted. Early papers report linear relationships (Cornelius and Woodcock, 1958), while others include exponential roughness factors (Lowson, 1982).

Oxygen transport

It is well understood that oxygen is a key component of the acid generating process, whether it is atmospheric or dissolved. As seen in Equations 2-1 and 2-2, oxygen acts as the primary oxidizer. Myerson (1981) introduced the concept of a critical oxidation concentration, defined as 5% of the oxygen saturation concentration (Figure 2-5), at which oxidation of sulfides occurs unimpeded.

It remains uncertain if the principle of critical oxidation concentrations can be extrapolated to include psychrotrophic (cold tolerant) bacteria living at near and sub-zero temperatures, as the relationship is empirical, and was modeled at temperatures greater than 25°C. At oxygen concentrations lower than the critical concentration, the rate of oxidization may be described as (Stumm and Lee, 1961):

$$-\frac{dN}{dt} = \theta \cdot K \cdot C \cdot \exp\left(\frac{-E_a/RT}{1+KC}\right) \qquad \text{Eq 2-5}$$

where $-dN/dt$ is the change in pyrite concentration with time; C is the oxygen concentration; K, the oxygen adsorption constant for pyrite; T, the absolute temperature; E_a, the activation energy; R, the universal gas constant; and θ, a constant.

The presence of elemental oxygen beneath the surface of the tailings remains essential to the ongoing oxidation of the sulfides. For sulfide oxidation to continue, the oxygen must either diffuse through the tailings or come out of solution in the gas-filled pore space available. Both of these processes are limited by low porosity and high saturation levels. The partitioning of oxygen from the water in the pore spaces is controlled by Henry's Law, which defines the equilibrium between dissolved oxygen and the water. These oxygen concentrations will also vary with temperature and presence of other gases.

2.1.5 Acid Neutralizing Mechanisms

Even if all the factors described above are present and active, acidic drainage may still not be generated from sulfide tailings. This section describes the mechanisms that can occur within the sulfide tailings that are capable of neutralizing the acid.

When acidity that has been released into solution reacts with carbonate, hydroxide or aluminosilicate minerals, the solution is buffered, reducing the acidity and maintaining the pH. This buffering results in the re-precipitation of secondary or tertiary minerals, such as marcasite and jarosite. The presence of these minerals can indicate an active, or previously active, acid-neutralizing regime. This mineralization is capable of retarding the acid generation by coating the reactive sulfide minerals, and by limiting the oxygen transport down-gradient. These phenomena will not be discussed here, but are described at length in Jambor (1994) and Cravotta III (1994).

As mentioned above, the neutralizing of the acidic drainage is controlled by the dissolution of carbonates, hydroxides and aluminosilicates (Table 2.2). As the pH of the pore-water drops, the primary buffering material changes accordingly. Table 2-3 shows the approximate ranges for the mineral suites (Morin et al., 1991).

The first stage in this sequence is the dissolution of carbonates.

2.1.5.1 Carbonate Dissolution

Carbonate dissolution is the most significant buffering mechanism, as it alone may completely neutralize all of the acid generated. The dissolution (of the more active carbonates) and buffering reactions are capable of maintaining equilibrium conditions during sulfide oxidation, and are dependant only on the volume and availability of the carbonates. Equation 2-6 shows the neutralizing reaction for carbonate dissolution in the form of calcite.

$$CaCO_3 + H^+ \Leftrightarrow Ca^{2+} + HCO_3^- \qquad \text{Eq. 2-6}$$

As shown, this reaction consumes both the carbonate and the hydronium ion and releases the calcium cation, maintaining the pH at 6.5-7.5. Evidence of carbonate dissolution is an increase in the discharge alkalinity. Combining Equation 2-1 with 2-6 for pyrite oxidation, it can be shown that 200g of calcite can neutralize 120g of pyrite.

The order of carbonate buffering is shown in Table 2-3 with calcite being the most favorable and siderite the least. Dissolution of the lesser reactive carbonates (i.e. dolomite and siderite) is slower, and equilibrium conditions are less common. As each decreasingly reactive carbonate is depleted, the pH is buffered to that of the newly preferred dissolving mineral. Figure 2-6 shows the sequence of the buffering reactions. By the time siderite is the most favorable buffer, the pH is between 4.8 and 6.3.

2.1.5.2 Hydroxide Dissolution

As the carbonates become depleted and the pH of the solution decreases below 4.5, dissolution of the hydroxide minerals, such as gibbsite and ferrihydrite, becomes favorable. Dissolution of $Al(OH)_3$ buffers the solution to between 4.0 and 4.3. These reactions have been shown to be capable of maintaining equilibrium buffering conditions (Blowes and Ptacek, 1994). With the depletion of $Fe(OH)_3$, the pH drops below 3.5.

2.1.5.3 Aluminosilicate Dissolution

The final stage in the buffering process involves the dissolution of the aluminosilicate minerals. Evidence for this includes an increase in Al and Si concentrations in the leachate. Unlike the carbonates and hydroxides, the dissolution of the different aluminosilicates can occur simultaneously.

Buffering with aluminosilicates is more complex, as their acid-consuming mechanisms include (Hutchison and Ellison, 1992):

- In contact with water, they tend to produce an alkaline pH.
- In contact with acid, they tend to degrade, consume hydrogen ions and produce clay minerals.
- Some silicates are capable of removing hydronium ions by ion exchange.

Though relatively slow, the buffering with aluminosilicates has been shown to consume the acid generated by sulfide oxidation where the initial sulfide content is less than 0.8% (Lapakko, 1987).

2.1.5.4 Reaction Kinetics

In addition to balancing the acid generating and consuming processes stoichiometrically, predicting the acid generating potential of a material requires an understanding of the rates of the reactions. As mentioned above, equilibrium, which is not always instantaneous, must be established. Additionally, in stratified deposits the leachate may be acidic and passing over neutralizing material; however, the reverse may also occur. Depending on the order of contact, the resulting leachate may vary.

Data in the published literature on reaction kinetics for the acid consuming processes are limited. The rate of reaction between acids and carbonates is described as rapid, such as

with fresh calcite and sulfuric acid. Limestone has a much slower reaction rate and may require days to reach equilibrium (Hutchison and Ellison, 1992). As with the kinetics of acid generation, any coating that forms around the buffering mineral grains is capable of further impeding the reaction. Unlike the acid generation reactions though, the reactions are abiotic and anaerobic, so the problems associated with oxygen diffusion or bacterial activity are not present.

Tuszynski et al. (1993) attempted to model numerically the principal acid neutralizing reactions, namely $CaCO_3$ and $Al(OH)_3$. They concluded that process is dominated by the concentrations of $CaCO_3$ and H^+. When buffering with aluminosilicates, the ion exchange mechanism is rapid but the rate of dissolution of the silicate is described as slow (Hutchison and Ellison, 1992).

2.1.6 Conclusions

Due to the significant number of variables in the acid generation process quantitative rate predicting analysis is extremely difficult, making numerical modeling questionable. This thesis does not attempt to predict or model the acid generating capacity for potentially acid generating tailings; however, an understanding of the principles governing and / or preventing sulfide oxidation is essential for understanding the *relative* effects of sub-zero temperatures on the generation of acid mine drainage. The best method of predicting the acid drainage potential is by conducting laboratory kinetic testing to determine actual reaction characteristics, though even these tend to vary with laboratory conditions.

2.2 ACID MINE DRAINAGE AT LOW TEMPERATURES

Although the chemistry and kinetics of AMD generation have been examined at length at moderate temperatures, few investigations have explored the process at near and sub-zero temperatures. This section re-examines several fundamental acid-generating principles including microbial activity and water and oxygen availability, taking into account frozen state soil behavior. Before any investigation into acid generation can occur though, the

presence of unfrozen water must be established. Until recently, assumptions that acid generation ceased at 0°C preempted any further investigation into the potential of biotic catalysis of the acid generating reactions. Though no definitive evidence is provided for biochemical oxidation of sulfide minerals at sub-zero temperatures, this section does provide significant grounds for prospective biochemical interactions. This establishes the foundation for the experimental program aimed at investigating the effects of sub-zero temperatures on acid generation.

2.2.1 Unfrozen Water Content

Another issue associated with the determination of the minimum temperature of acid generation relates to the presence of unfrozen water. This section discusses the factors that could enhance the acid generating environment, but does not propose new models for predicting unfrozen water content with temperature or freezing point depression. For the purposes of this thesis, the hysteretic effects of temperature on unfrozen water content are ignored and the temperatures are assumed to be reached by cooling. This section will review the significant factors including temperature, soil suction and the presence of solutes and charged surfaces. Research into predicting unfrozen water content is extensive, with many models employed for the various factors involved; however, a review of the literature did not reveal any all-encompassing relationships. Additional factors affecting unfrozen water content such as rate of freezing (Xiaozu et al., 1997) will not be examined due to their minor effects.

2.2.1.1 Effect of Solutes

The factor that has received the most attention is the effect of solutes on the unfrozen water content. The freezing point depression, or increases in the solubility of ice, is related to water activity. By definition, water activity is the availability of water in a solution. According to solvate theory, as described by Chen and Nagy (1986), part of the water can combine with the dissolved substances (non-electrolytes) or ions (electrolytes) to form hydrates. This water no longer acts as a solvent. Calculations of

freezing point depression due to solutes are still very approximate as little is known about the thermodynamic properties of electrolytes in solution below 0°C, with the exception of sodium chloride. Recent software packages like FREEZCHEM have added a number of additional electrolytes, but are restricted to solutions with low concentrations. It is known though, that at high concentrations of calcium chloride, brines can remain entirely unfrozen at -50°C (Thurmond and Brass, 1987). When solutions reach their eutectic point, or coldest temperature at which unfrozen water is present, the solute precipitates and ice is formed (Fig 2-7).

The equations for predicting the freezing point depression vary significantly in complexity, the simplest considering only the effects of dilute solutes. In dilute solutions the freezing point depression can be calculated using the molality of the solutes, derived from the Van't Hoff equation (Eq. 2-9):

$$\frac{dT}{dm_B} \approx \frac{-RT^2}{55.5 \cdot \Delta H} \qquad \text{Eq. 2-9}$$

where m_B is the molality of the solute (mol kg^{-1}), T is temperature (Kelvin), R is the universal gas constant (J K^{-1} mol^{-1}), and ΔH is enthalpy of fusion of ice (J mol^{-1}) (Marion, 1995). This model is limited to single solute, and is insufficient for complex systems compounded by the effects of solute redistribution, or solute exclusion. The redistribution of solutes during freezing can concentrate the solution at the freezing front by up to 80 times the original concentration, provided that there is no solute inclusion or salt precipitation (Marion, 1995). Figure 2-8 shows the effect of temperature on ice content for various initial NaCl concentrations. As the ice crystals form from pure water, the solute is excluded into the remaining unfrozen water, increasing the concentration in the remaining unfrozen water, further decreasing the freezing point. Given the high concentrations of metals at low pH in solution associated with acid mine drainage, one can anticipate the potential for significant freezing point depression. Due to the limited applicability, freezing point depression in these environments has not been well addressed and reported data has been restricted predominantly to saline waters.

The effect of solutes on unfrozen water was demonstrated by Anderson and Tice (1989). Figure 2-9 shows the unfrozen water for two Antarctic soils, and the considerable change when the natural solutes had been rinsed. Soil A was described as having angular grains indicative of a low degree of weathering, containing magnetite, silicate, iron, $CaCl_2$ and KCl. Soil B was an evaporitic soil, containing weathered quartz, potassium, calcium and iron.

Another relationship often used to determine the freezing point depression of a solution is derived from the Clausius-Clapeyron equation (Eq. 2-10):

$$\Delta T = \frac{-R \cdot T \cdot T_0}{\Delta H} \ln a_w \qquad \text{Eq. 2-10}$$

where ΔT is the freezing point depression, T_0 is the freezing point of pure solvent. T is the freezing point of the solution, R is the universal gas constant, ΔH is the molar heat of fusion and a_w is the water activity. The inclusion of the water activity is useful for this discussion as it is also employed in biological systems. For an ideal system, Raoult's law of water activity is:

$$a_w = \frac{1 - X_S}{1 - X_S + E \cdot X_S} \qquad \text{Eq. 2-11}$$

where X_S is the solute concentration in weight fraction, and E is the ratio of the molecular weight of water to the molecular weight of solutes (Chen and Nagy, 1986).

At higher solute concentrations, additional parameters are necessary (except for simple solutions, ie. NaCl). The complex systems, as modeled by the Pitzer equations, relate ion activity coefficients and osmotic coefficients to enthalpies, entropies, Gibb's energies, heat capacities and molal volumes of highly concentrated aqueous electrolyte solutions, for temperatures to below -50°C (Marion and Grant, 1997). The Pitzer equations are

algebraically extremely complex and have been simulated by computer (Mironenko et al., 1997), but are limited with respect to chemical interactions. According to Marion and Grant (1997), this theory cannot be applied to frozen ground until:

- Sufficient heat capacity and density data are collected for supercooled electrolyte solutions at sub-zero temperature; and
- The interaction of ionic solutes with layered silicates can be incorporated.

The relationship between unfrozen water content and solute content is further complicated due to electrolyte effects on capillary pressures of frozen soils. Additional capillary pressure is generated as the solute distorts the ice-liquid interface (Marion and Grant, 1997). The consequence of all the above is that the ability to predict the temperature at which sulfide-oxidizing solutions will completely freeze is indeterminate.

Several software packages are available that model electrolytic interactions, such as PHREEQC, WATEQ or MINTEQ, though these are only for solutions having ionic strengths of less that 0.1 (Marion, 2000).

2.2.1.2 Mineral Grain Effects

Despite the influence of solutes on freezing point depression, Williams (1991) suggests that it is not the presence of dissolved material that is responsible for the unfrozen water. Williams suggests that suction has a far greater effect, and that freezing point depression is a modeled by the Clausius-Clapeyron equation (Eq 2-12):

$$T - T_0 = \frac{V_w \cdot 2\sigma_{iw} \cdot T_0}{r_{iw} L_f} \qquad \text{Eq. 2-12}$$

where T_0 is the 'normal' freezing point, V_w is the specific volume of water (m^3/kg), σ_{iw} is the ice-water interfacial tension, r_{iw} is the radius of interface between ice and water, and L_f is the latent heat of fusion (Williams and Smith, 1989).

Williams (1991), though not well supported in the literature, points to the 'properties of the mineral particle surface' as being the most significant. It is uncertain if this refers to the presence of charged surfaces, or is based entirely on pore space capillary pressure.

It is necessary here to clarify the difference between capillary space and adsorption space. Capillary space, as used in this thesis, is the zone in which soil water is only affected by the laws of surface tension, as in the case of granular soils. Adsorption space is the zone in which soil water is strongly affected by the charged surfaces of the colloidal material (Black, 1990), whether mineral or bacterial, typical of highly colloidal soils.

The effects of external pressure on freezing point depression are described by Williams (1964), but are limited to a 1°C difference. Though the pressure itself has little effect. Konrad (1989) has proposed that the unfrozen water content is affected by soil structure (ie. void ratio), which does change with applied pressure. As the confining pressure increases, the angle between clay particles sharpens, the void ratio decreases and the capillary pressure increases (Fig. 2-10). No model has been proposed for this mechanism, but Figure 2-11 demonstrates the effects on the unfrozen water content. This concept has also been verified in similar work by Ruijie et al. (1993) and may become an issue for larger tailings deposit structures.

2.2.1.3 Charged Surfaces

The final factor affecting the presence of unfrozen water is the presence of charged surfaces in the form of clay minerals (Marion, 1995) or bacteria (Cullimore, 1998). The charged surfaces contain a region known as the diffuse double-layer, in which water, a dipole molecule, is sorbed to the surface in proportion to the strength of the surface charge (Marion, 1995). It is known that with the addition of solutes, the volume of water influenced by the mineral surface is reduced due to positive charged ions balancing the negative surface charge (Yong et al., 1978). As stated previously, the addition of a solute

to a pure solution will increase the unfrozen water content. Clearly then, a model is required which is capable of determining the relative effect of these factors. Simple models have been created which expand this relationship to include effects of salts on the diffuse double-layer, but are limited to two test soils and NaCl solutions (Yong et al., 1978).

Due to this limited understanding, the relationship between unfrozen water content and surface charges is restricted to empirical equations based on specific soils. They show that the relationship can be represented by a simple power curve (Eq. 2-13),

$$w_u = \alpha \cdot \theta^{\beta} \qquad \text{Eq. 2-13}$$

where w_u is unfrozen water, α and β are characteristic soil parameters and θ is the temperature (°C below zero). Figure 2-12 shows the power law curve for a series of soils; however, while these curves are effective for material that has been previously tested, no direct relationship has been established between the strength of the charged surface and the unfrozen water content with temperature. Over 30 sets of values have been compiled by Andersland and Ladanyi (1994); for the soils not listed, the liquid-limits (Eq. 2-14) have been used as an indirect method for determining unfrozen water content (Tice et al., 1976).

$$w_{u,\theta=-1} = 0.346 \cdot LL - 3.01 \qquad \text{Eq. 2-14}$$

where LL liquid limit at the test temperature and $w_{u,\theta=-1}$ is the unfrozen water content at -1°C. These equations are based on tests only to -4°C and are recommended only for liquid limits above 0°C of less than 100.

2.2.1.4 Bacteria Effects

This section briefly describes how the presence of bacteria also accounts for the presence of some unfrozen water. This is expanded upon further below. Taylor (1987) describes three types of water found in proximity to the bacteria:

- Internal water within the protein as part of the structure which is irrotationally bound. and is intimately involved in the function of proteins. This may be as a co-enzyme and it cannot be resolved by methods other than diffraction as its motions are determined by the protein itself.
- Water molecules bound at various peripheral sites on the surface of the protein which can be distinguished by diffraction but may be quite mobile.
- There exists an undefined region where the influence of the protein competes with the normal tetrahedral-like order in the water. The hydration helps to maintain the structural stability of the protein and influences both the mechanical and hydrodynamic properties of the protein as well as the transport of the protein and of substrates or ions.

It is uncertain what volume of water this comprises, though if a large biomass accumulates, this may assist in the sustenance of an unfrozen region.

2.2.2 Biochemical Activity

As described above, even at moderate temperatures, the biological oxidation processes are relatively poorly understood. A key assumption in reviewing the effects of cold temperature on microbial sulfide oxidation catalysis is that microbial growth depends on the presence of liquid water. It is likely incorrect, however, to assume that all microbial activity ceases at 0°C, although two models described in the literature make this assumption (GEOCON, 1993; Davé et al., 1996). This is reflected by the sudden change in the reaction rate gradient as shown in Figures 2-13 and 2-14. In Figure 2-13, the data do not actually extend below 6°C, yet the curvature changes sharply at 4°C to pass

through the origin. Figure 2-14 smoothes the curve, but retains this assumption. Figure 2-15, however, shows data for biological oxygen demand tests in which the intercept of the growth rate at 0°C is greater than zero (Heroux and Rowney, 1987). If this curve is valid for the oxidation of sulfides, the previous models would be in error.

The presence of psychrophiles (cold loving bacteria) and psychrotrophs, (cold tolerant bacteria) is well documented (Vincent, 1988; Russell and Hamamoto, 1998) and demonstrates that bacteria are capable of existing in cold environments. It is thus important to determine to what degree the sulfide oxidation reaction is catalyzed at sub-zero temperatures. It is possible that at lower temperatures, the catalyzing effect is still present, though reduced. Given that early studies in food science have demonstrated bacteria are capable of germinating at -6°C (Halvorson et al., 1961), an examination into microbial activity at sub-zero temperatures within sulfide rich materials is in order.

A review of the literature revealed several studies examining the effects of temperature on *Thiobacillus ferrooxidans*. Leduc et al. (1993) reported isolating 4 strains of psychrotophic T. ferrooxidans, capable of growth at temperatures of 2° and 5°C. These isolates were capable of iron oxidation and growth to various degrees from 2° to 35°C. Figure 2-16 shows the change in growth rate, as defined by the mean generation time, over these temperatures. This report was the first to positively identify psychrotrophic strains of sulfide oxidizers.

More recently, Dawson and Morin (1996) suggested that by extrapolating activation energies according to the Arrhenius equation, bacteria growth may occur at -2°C to -5°C; however, they are unsure as to the method of extrapolation. They also report an unpublished research proposal by Mehling (1993) suggesting that T. ferrooxidans may be active to -6°C. More promising work by Meldrum (1998) has indicated oxygen may have been consumed in a sulfidic environment at -2°C, that the author attributes to bacterial activity. To date, this report is the most indicative of the existence of acidophilic sulfide oxidizers below 0°C, but is yet unconfirmed.

Despite all hypotheses to date, there have been no reports of naturally occurring psychrophilic sulfide oxidizing bacteria. Psychrophiles require very constant temperatures and would therefore only occur in places like the sea bottom in the arctic. As such, any bacteria of interest for acid generation in cold climates would likely be psychrotrophs. The reports do all concur on one principle though: bacteria demonstrate an ability to adapt to changing environmental conditions (Morin and Hutt, 1998) and that strains of T. ferrooxidans have been isolated that reproduce at significantly colder temperatures than previously believed possible.

Additionally, though no reference has been found listing specific sulfide oxidizing bacteria that grow in the sub-zero temperature ranges, it is recognized that there are many species of bacteria that have not been identified. Each species of bacteria has different optimum, preferred and growth limiting temperature ranges, and the well-known sulfide oxidizing species may not be able to survive at sub-zero temperatures. As such, research into isolating these bacteria and characterizing their growth temperatures represents an important step in predicting acid generation at sub-zero temperatures.

Therefore, due to the absence of earlier research on psychro*philic* organisms from the soil science arena, parallel principles must be borrowed from the frozen food industry. Beard and Cleary (1932) states that certain microorganisms survived in greater numbers at -4°C than at room temperature in an acid medium. Unlike the soil science research, however, isolates have been documented that show actual bacteria surviving and growing at sub-zero temperatures. Though significant damage occurs during freezing, the microorganisms that survive are capable of living for prolonged periods (Goresline, 1961).

2.2.2.1 Effects of Cold Temperatures on Microorganisms

The slowing of the physiological processes, and therefore also the catalyzing effects in cold temperatures, is due to 'gelling' of a fluid layer of lipids within the cell membrane

(Vincent, 1988). As the temperature decreases, the membrane loses its fluidity and impairs the activity, or activation energy, of certain proteins. The rate at which the bacteria slows its physiological processes due to the cold has been described by a form of the Arrhenius equation (Eq. 2-15), where k is the rate constant, E_a is the activation energy and T is the temperature (K); A is a constant and R is the universal gas constant.

$$k = A \cdot \exp\left(\frac{-E_a}{RT}\right) \qquad \text{Eq. 2-15}$$

The Arrhenius relationship contains certain inherent weaknesses though, as it does not consider systems containing more than one enzyme, nor complex systems in which a single enzyme may have several stages (Vincent, 1988). Additionally, it fails to consider that activation energies tend to increase as temperature decreases (McMeekin et al., 1988). As such, the Arrhenius plot for one strain of bacteria is not necessarily transferable to another strain.

A second model that has been used to predict microbial activity is the square root model (Equation 2-16), proposed by Ratkowski et al. (1982), which utilizes the temperature difference between the optimum temperature for growth and the actual temperature.

$$\sqrt{k} = b \cdot (T - T_{min}) \qquad \text{Eq. 2-16}$$

This relationship applies for the temperature range between the minimum and optimum temperatures for growth, where k is the specific growth rate, b is the slope of the regression line, T is temperature of concern, and T_{min} is the temperature, in Kelvin, where the regression line cuts the temperature axis. Figure 2-17 shows plots of the Arrhenius data and the square root model. The data shown is for thermophilic bacteria. Psychrotrophic bacteria demonstrate the same curve, though shifted to colder temperatures (Russell and Hamamoto, 1998).

For some complex systems, the square root model is an improvement over the Arrhenius model as it incorporates a changing activation energy, E_a, and has met with success in the food industry at temperatures from -2°C to 15°C.

2.2.2.2 Microbial Adaptation to Cold Temperatures

Although it is assumed that complete freezing does preclude biological activity and acid generation, it must be proven that bacteria are capable of resisting the extreme temperatures and can survive in super-cooled environments (Vincent, 1988). Bacteria are equipped with cell membranes and plasma membranes surrounding the bacteria which contain very small aqueous channels. As the external environment cools, the external water begins to crystallize; however, the ice growth is restricted as it reaches the channels. According to surface tension / capillary pressure theory, the size of the ice crystal is proportional to its freezing point. Vincent (1988) reports super-cooling of bacteria to at least -10°C, which corresponds to an ice crystal radius, and therefore membrane channel, of 30nm.

As the temperature continues to decrease, ice crystals form in the water and the remaining solute concentration increases, resulting in an osmotic pressure gradient across the plasma membrane. To maintain equilibrium, the bacterium rejects water, increasing its internal solute concentration, thereby lowering the freezing point of the water within the bacterium further. As the concentration of solutes reach the solubility level, certain compounds will precipitate, and the eutectic temperature will be reached. For further detail, the reader is directed to Hayashi (1991). At this temperature, complete freezing is assumed to preclude further biological activity.

2.2.3 Oxygen / Water Availability

In addition to the presence of unfrozen water at sub-zero temperatures, the presence of *biologically active* water is also a factor. As described above, with the addition of solutes, the water is less available for ice crystal formation. However, for the purposes of

microbial survival and growth, the water available for biological activity must also be considered. In the presence of ice, this activity, or chemical potential, is described in terms of relative vapor pressures. At the freezing point, the vapor pressure is equal to the vapor pressure of the unfrozen solution. Table 2-4 shows the vapor pressures of water and ice at sub-zero temperatures.

In similar fashion with pH and temperature dependence, different bacteria also have different survival water activities. Figure 2-18 plots the water activity against temperature and shows the region of growth for two psychrophiles.

The combined effects of decreased water activity due to electrolytic interference and further impact of relative ice-water vapor pressures are unknown, yet undoubtedly significant competition for the unfrozen water exists.

The final consideration for biologically catalyzed AMD is the availability of oxygen. Water covers have been demonstrated to be effective barriers against acid generation (Davé, 1996), but the effects of dissolved oxygen in the water must be considered. A review of the literature did not locate any data for oxygen levels in sub-zero water, but it is known that the levels of dissolved oxygen increase as the temperature decreases (Otwinowski, 1995). Studies would have to be performed to determine these concentrations, in addition to an oxygen mass balance to determine if sufficient oxygen is present to prevent the environment from becoming anaerobic.

2.2.4 Consequences

The natural progression of the argument discussed above is to question the long-term behavior of sites that use freeze-back techniques for the disposal of acid generating mine tailings. For these facilities, it must also be determined if the amount of unfrozen water present is sufficient to propagate further melting of the ice as described below.

As the sulfide grains oxidize, 22,500 kJ/kg of sulfur is released at a rate of 1.2×10^{-2} J/kg/s at 30°C, and 5.5×10^{-4} J/kg/s at -2°C. These reaction rates are reported for pyrrhotite (Meldrum, 1998); 334 kJ are required to melt 1 kg of ice. Given these rates, if there are high pyrite concentrations present and the super-cooled solution has elevated electrolyte concentrations in addition to oxygen availability, a zone may develop in which the rate of heat loss to the surroundings is low enough to maintain elevated temperatures and propagate further melting and oxidation. Once these warmer microclimates are established, the integrity of the structure may be at risk due to water lenses that decrease the strength of the material.

The following iterative steps describe a self-propagated oxidation environment (adapted from GEOCON, 1993):

Step 1. A grain of sulfide mineral is oxidized by elemental oxygen or another oxidizing agent, such as Fe^{3+}, generating heat. The rate and amount of heat generated depends on the sulfide type.

Step 2. The heat is either absorbed by the proximate pyrite grains or is conducted away by non-reactive grains and/or porewater. The amount of heat that is conducted away from the grain is dependent on the thermal conductivity and temperature gradient of the surrounding mass. The conductivity varies with moisture content, material type, and temperature.

Step 3. The heat that is not conducted away from the area either increases the temperature locally or is used in other energy consuming processes, such as melting ice. The melting of ice may result in the release of available dissolved oxygen.

Step 4. If the temperature of the local area increases, the rate of further oxidation is increased (as the rate of oxidation is a function of the temperature). If additional oxidizing agents and sulfide minerals remain, the process repeats Step 1 at a higher rate of oxidation.

Step 5. If the thermal gradient surrounding the oxidizing zone is sufficiently great, the heat will dissipate into the surrounding mass and no change in the oxidation reactions will occur. If the heat lost to the mass is greater than the heat generated in the zone at any time, the local temperature will decrease, thereby decreasing the oxidation rate.

Facilities constructed for permanent disposal in permafrost regions should consider ongoing observations of the site to ensure that the bacterial growth rate remains very low. It is also recognized that the bacterial component of the oxidation process is significantly greater at low pH (Davé et al., 1996). It is conceivable that over long periods, if the unfrozen water develops a low pH, the increase in bacterial activity due to the preferred acidic environment could offset the decrease in activity due to cold temperatures. This could lead to an eventual failure of the containment system.

Several factors must be better understood for accurate prediction of acid generation from mine tailings at sub-zero temperatures:

- The behavior of supercooled electrolyte solutions
- The relationship between charges surfaces and unfrozen water content
- The solubility of oxygen at sub-zero temperatures
- The coupled reaction and thermal kinetics.

2.3 ACID BASE ACCOUNTING

There are two main stages to predictive testing for a material's long term acid mine drainage behavior, material characterization (which identifies the acid generating potential of a sample), and the drainage prediction (SRK, 1992). Material characterization is the simpler task, as it requires only static accounting of the mineralogy of the sample, a summation of the reactive components. Drainage prediction requires a kinetic approach, considering factors such as the leachate flow rates, relative solubility, partial reactions due to particle coating, secondary mineral precipitation, or preferential

flow, as well as bacterial and temperature effects. To some degree, modeling of the flow regime is also necessary.

Due to the complexity of the problem of leachate quantity and quality, many different predictive tests have been proposed and utilized. This is partially due to the fact that several of the tests were originally designed for testing coal, and later adapted for hard rock uses. Additionally, the test selected will vary with its purpose, whether for predicting, confirming or quantifying the production of acidic leachate. For the purpose of this investigation, the tests intended as field tools, such as the hydrogen peroxide oxidation procedure (Finkelman and Giffin, 1986) will not be analyzed. The remainder of the tests can be divided into two groups, static tests and kinetic tests.

2.3.1 Static Geochemical Tests

The traditional acid-base accounting techniques provide a measurement of the likelihood to produce acid drainage, literally accounting for the different total contents of acids and bases within the mineral geochemistry (Morin, 1990).

2.3.1.1 Sobek Test

The first widely used acid base accounting system was introduced by Sobek et al. (1978), in which the variables include maximum potential acidity (MPA), or acid potential (AP), neutralizing potential (NP), and net neutralizing potential (NNP).

The acid potential (AP) was originally obtained using a LECO furnace to determine the sulfur content of a coal sample. This % total sulfur content is multiplied by 31.25, derived from the stoichiometric relationship for the complete oxidation of pyrite and hydrolysis of Fe^{3+}. This converts the sulfur to tonnes $CaCO_3$ equivalent per 1000 tonnes. The neutralizing potential (NP) is calculated by adding excess hydrochloric acid to the raw tailings, heating them to ensure complete reaction, then titrating the mixture with standard sodium hydroxide to a pH of 7. This is then converted to tonnes $CaCO_3$

equivalent per 1000 tonnes. The difference between these values is the net neutralization potential (NNP), expressed in tonnes $CaCO_3$ equivalent per 1000 tonnes.

A net neutralization potential of -20 tonnes $CaCO_3$ per 1000 tonnes or greater indicates that the sample is potentially acid generating. If the NNP is between 20 and -20, it is considered potentially acid generating, and non-acid generating if greater than 20 (Hutchison and Ellison, 1992). The ratio of NP/AP is also considered, where a sample having an NP/AP ratio of 1.2:1 is generally considered non-acid rock generating, yet ratios in the range of 1:1 to 3:1 may be inconclusive for reasons described below.

Several assumptions are made in this process that make the Sobek method of acid base accounting imprecise. The 31.25 conversion factor assumes (Morin, 1990) that:

- the sulfur occurs only as S_2^{2-};
- the sulfur oxidizes completely to sulfate;
- pyrite is the only sulfide mineral;
- molecular oxygen and water are the only oxidants;
- all iron oxidizes to the ferric state; and
- all iron precipitates from solution in the form of $Fe(OH)_3$.

In fact, the sulfur may exist in several forms, as sulfide, elemental sulfur, polythionates, thiosulfate, sulfite, sulfate, or organically bound sulfur (Morin, 1990). It has also been shown that the pyrite can be replaced by pyrrhotite, or that ferric ion can replace oxygen as the oxidant (Morin, 1990). Morin describes in detail many other deviations from the initial assumptions that are made in the standard acid base accounting. For example, with no precipitation of ferric iron, the conversion factor is reduced to 7.81. The factor may also be increased, as when ferric iron replaces oxygen as the oxidizer, and the conversion factor increases to 125.0.

Uncertainty is also generated from the determination of the neutralization potential. Unlike the acid potential which is calculated directly, the neutralizing potential is subject

to uncertainties which are derived from the variation in time between the acid soak and the base titration, and the impact of the length of time during which the sample soaked in excess acid (Morin, 1990).

Both carbonate and hydroxide minerals are commonly found as neutralizing minerals. During the acid bath, these minerals are dissolved, and some of the dissolved carbonate will be lost as carbon dioxide gas, as described by open-system carbonate equilibrium levels. During the titration with base, some of these minerals may re-precipitate due to decreased solubility at higher pH values. It is possible that the loss of carbonate from the solution will result in a precipitation of more hydroxide minerals than previously present. This precipitation of hydroxide minerals consumes the additional base, giving the impression that less acid had actually been neutralized by the original minerals. This inaccuracy is dependent on the time for base titration, as this governs the metal precipitation.

Another difficulty in the sample preparation for neutralization potential is the possibility for incomplete dissolution of the neutralizing constituents of the sample, and the resultant measurement of the neutralizing potential of only the rapidly dissolving minerals. Examples of these minerals include aged oxides and feldspars (Morin, 1990).

2.3.1.2 Other Static Tests

A more recent improvement upon the Sobek method proposed by Konsten et al. (1988) involves the determination of total sulfide acidity (TSA), total potential acidity (TPA), and total actual acidity (TAA). This method eliminates some of the problems using sulfur speciation, which considers the oxidizing potential of the sulfur, but still retains difficulties with organic matter interference. According to Clark et al. (1996), the oxidation of the organic matter can result in overestimating the acid potential, as substantial amounts of organic acids are generated. Ideally, the static test must be able to isolate and distinguish between the oxidizable sulfur species and calculate the net difference between the acid neutralizing potential.

For these reasons, unless a complete delineation of the oxidation processes is performed, which requires significantly more time and effort, static tests performed alone will present an unclear picture of the acid potential. Therefore, static tests should be used only as an indicator of acid drainage, and a guide for future testing.

2.3.1.3 Comparison of static test techniques

As part of the Mine Environmental Neutral Drainage Program, a study was conducted, in 1989, directly comparing five static tests, the BC Research Initial Test, the Sobek and Modified Sobek test, the Alkaline Production test and the Net Acid Production test, with field observations. The conclusions of the study are (Hutchison and Ellison, 1992):

- With the exception of the Net Acid Production Test, all the tests provide NNP values that are of similar magnitude. The Net Acid Production Test results predicted higher NNP for the samples that were acid producing.
- The tests on tailings were conservative, as they predicted acid generation when the field observations showed none.
- The tests on waste rock were variable, as the Modified Sobek Test indicated a positive NNP, where the others and field observations showed acid production.
- Using sulfide sulfur analysis to calculate AP is preferable to total sulfur as sulfide sulfur does not consider the presence of other sulfates (ie. gypsum).

Steffen, Robertson and Kirsten Inc. (SRK, 1992), obtained similar results. No direct field correlation was mentioned in the report.

- The Modified and Standard Sobek procedures may overestimate the neutralizing potential under field conditions if siderite is present, as it is capable of neutralizing hydrochloric acid, but not sulfuric acid.

- The BC Research Initial method may provide a more realistic estimate of the readily available neutralizing potential of the sample. It may also overestimate the NP for samples having a low NP value.
- The Net Acid Production test predicts lower net acid generating potential than the acid base accounting.
- The Net Acid Production test requires an acid-base calibration curve for the specific waste rock type to determine the acid generation potential.

Despite the fact that the Sobek test is not the most accurate, it is however, the most widely used. Due to the extensive database of Sobek results, the test continues to be used as it is an established baseline for comparison against other material (Morin, 1998).

2.3.2 Kinetic Geochemical Tests

Whereas static tests are useful for predicting the potential of a sample to generate net acidity, kinetic tests are used for (Hutchison and Ellison, 1992):

- confirming the potential acidity,
- determining the rates of sulfide oxidation and neutralization,
- determining the typical concentrations that occur in the acid drainage, and for
- evaluating the effectiveness of proposed control and treatment methods.

Where a static test uses the soil mineralogy as its sole source of data, kinetic tests add the dimension of time, introducing reaction rates to the equation. In these tests, factors such as particle size, temperature, relative solubility, hydraulic conductivity, and bacterial activity may extend the testing period over several weeks, months, or years. Another advantage to kinetic testing is the added control over environmental factors, including atmospheric gases, humidity, microbial catalysts and water leachate rates.

Depending on the purpose of the investigation, many different kinetic tests are available. Of these, the most commonly used are the Humidity Cell Test and the Column Test.

Specialized tests, such as the Shake Flask Test, are also used in select cases. Column tests are typically used for determining the kinetics of weathering, oxidation and metal leaching for waste rock in large-scale laboratory tests (SRK, 1992). They feature a column of material, with height and diameter greater than 8 times the particle size. At field representative intervals, water is added in the top. The volumes added should match the conditions at the material's site of origin. Additionally, air is passed through the system to increase the rate of drying between leaches. The benefits of the column test include:

- capacity for retaining size distribution and representative surface exposure of material found in rock piles
- selected control options can be examined (i.e. seasonal precipitation variances)
- capacity for modeling site specific seepage quality
- capacity for including potential control options

Though the column tests are effective at predicting drainage quality and acid generation rates, the humidity cell remains the test of choice for finer grained material, as the test has been standardized which facilitates comparisons. In effect, the humidity cell is a specific case of the more general column test. Like the humidity cell though, the column test is unable to test for reactions at sub-zero temperatures, due to the necessity for water drainage.

2.3.2.1 Humidity Cells

The humidity cell is an accelerated weathering test designed to increase the geochemical weathering rate for selected 1000-g solid material samples and produce a weekly effluent that can be characterized for solubilized weathering products. The test apparatus employed is similar to the method described in ASTM Standard D 5744 – 96, Standard Test Method for Accelerated Weathering of Solid Materials Using a Modified Humidity Cell, and is used widely for predicting potential acid drainage from reactive material which is exposed to weathering. The cells simulate the processes of geochemical

weathering by providing control over air, temperature and moisture, while allowing for the removal of oxidation products which can be analyzed to determine the onset of AMD. to calculate mass loads, and to determine the concentration of metals and other species as a function of time (Lawrence, 1990).

The ASTM procedure calls for weekly cycles comprised of three days of dry air (less than 10% relative humidity) and three days of water-saturated air (approximately 95% relative humidity) pumped through the sample, followed by a leach with distilled water. A duration of at least 20 weeks (ie. 20 cycles) is recommended, though at colder temperature, it may last significantly longer.

Chapter 4 provides a detailed description of the assembly and operation of the humidity cells. This section provides theoretical support for the geochemical principles employed in the test. The alterations made to the standard apparatus and operation are noted and explained in the experimental procedure, as the recommended apparatus description contains significant allowances for modification to be made to accommodate different testing material. For the testing performed, these modifications were significant as the ASTM standard test appears to have been designed for material larger than 150 microns.

The humidity cell operates based on the principles of mineral solubilities, in which during the leaching phases, the water will react with the tailings, dissolving the most soluble components. These are dependent on temperature and pH.

Tracking Acid Generation

As described above, there are three stages to the acid generation process. In each of these stages, there are different indicators. Because of the sample disturbance, and the dissimilarities from the field, similar leachate quality at separate intervals may not represent the same geochemical regime. For instance, during the initial flushing cycles, if the sample contains stored oxidation products or a readily soluble load in the form of easily transportable salts, these will have a significant impact on the early test results.

This is also true if there has been sample pretreatment, or if control measures are being studied (SRK, 1992). The basic indicators of acid generation are pH, specific conductivity, redox potential, acidity, sulfate and metal concentrations (Coastech Research Inc., 1991).

The most obvious indicator is the *pH*, or hydrogen ion concentration. In general, any decrease in pH is associated with increasingly acidic conditions. If the pH is greater than 5, the sample is not actively generating acid and/or the geochemical regime is dominated by alkalinity. As the pH decreases to between approximately 3 and 5, the biological contribution is stronger and the leachate is considered acid generating. pH is different than *acidity* in that acidity is the measure of the combined concentrations of Fe^{2+}, Fe^{3+}, Al^{3+}, H^{+} and HSO_4^{-}.

The *specific conductivity* is a measure of the strength of the leachate and reflects the reactivity of the sample. An increase in conductivity is a potential indicator of AMD generation as it reveals a greater presence of ions in solution, which in turn is indicative of higher solubilities as a result of increased acidity . The *redox potential* is a measure of the electrochemical regime. A potential of greater than 450 mV can indicate an oxidizing environment. Unfortunately, the redox potential readings are extremely time dependant as the iron species are quickly oxidized in an aerobic environment. Due to the nature of the humidity cell tests, it is not possible to maintain this.

The presence of *sulfate* is significant in that the sulfate ion originates primarily from the oxidation of sulfides, such as pyrite. SRK (1992) reports that the sulfate production is indicative of acid generation where:

- all of the oxidized sulfur is flushed from the system,
- sulfur is fully oxidized to sulfate, and
- solubility constraints do not result in precipitation of gypsum or other sulfate salts.

Ferguson and Morin (1991) also report that the shape of the cumulative sulfate production curve is important. When conditions are neutral, a linear curve may indicate reaction controlled kinetics, such that the leachate is saturated with sulfate or that the concentration is controlled by the rate of oxidation. A concave down curve typically demonstrates the effects of initial flushing; however, it can also represent a reduction of the oxidation due to mineral coating. Finally, a concave curve up can be the result of increased surface area contact.

The last indicator of acid generation is an increase in the *metal* load. The solubility of metals increases with decreased pH, so with increased metal load, one would expect increased acid.

2.3.2.2 Batch Cells

The batch tests utilized in this investigation are similar in principle to a static shake flask test (ASTM D 3987 – 85), in that no cyclic leaching is employed, as a sample is removed at each interval for total analysis and tested for indications of acid generation. In the batch test, environmental oxygen and the moisture contained within the pore water oxidize the sulfide tailings with the assistance of catalyzing bacteria.

The static batch test has several significant modifications from the shake flask test:

- The sample is not continuously agitated.
- The sample is open to the environment to ensure oxygen supply.
- The sample has a much lower water content (15% vs up to 900%) and a greater mass of solid.

These modifications are necessary due to the effects of sub-zero temperatures. Because some samples will contain small amounts of unfrozen water, the agitation, which is useful for effective mixing, is severely hampered. Furthermore, a low moisture content environment enables the oxygen to reach the oxidizing zones, and, because of the

increased solids mass, the amount of oxygen necessary to oxidize the reaction is greater than the volume of the closed flask. The increased solids mass is necessary to provide sufficient water for analysis upon completion.

The interpretation of the leachate is similar to the humidity cells. The notable exceptions include in increased reliance upon the sulfate and metals in solution. This is due to the rapid pH flux once the water has been extracted. The fines contained in the extract have a high reactivity and result in considerable uncertainty in pH readings. Additionally, if the electrochemical conditions within the batch cell were reduced, they would quickly oxidize upon exposure to the atmosphere. The dissolved metals and sulfate concentrations are better indicators in this case, as the concentration of sulfate and especially metals are dependent upon the pH within the cell and provide a 'signature' of the insitu conditions.

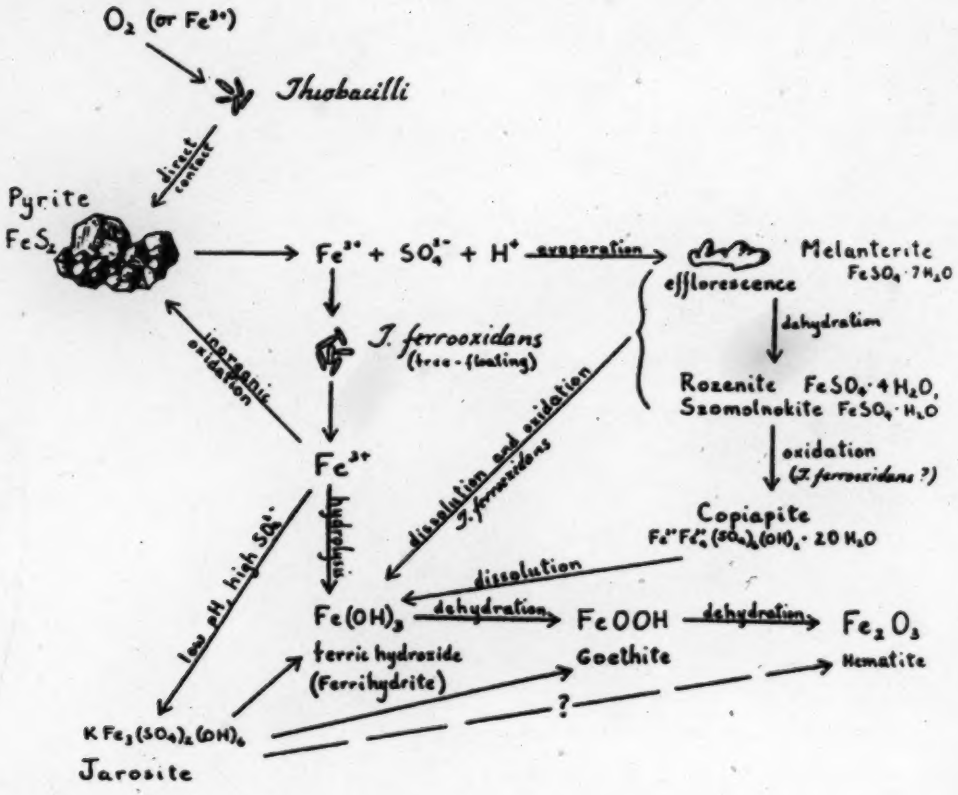

Figure 2-1. Intermediate Reactions in Acid Mine Generation
(Dudas, 1998)

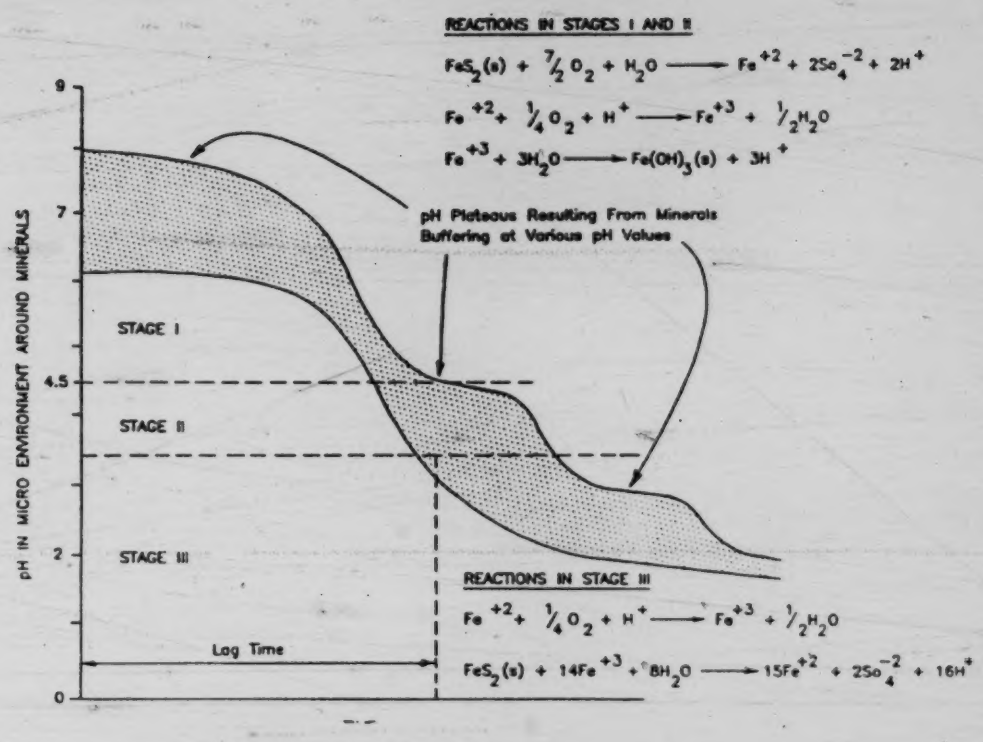
REACTIONS IN STAGES I AND II
$FeS_2(s) + \frac{7}{2}O_2 + H_2O \longrightarrow Fe^{+2} + 2So_4^{-2} + 2H^+$
$Fe^{+2} + \frac{1}{4}O_2 + H^+ \longrightarrow Fe^{+3} + \frac{1}{2}H_2O$
$Fe^{+3} + 3H_2O \longrightarrow Fe(OH)_3(s) + 3H^+$
pH Plateaus Resulting From Minerals Buffering at Various pH Values
pH IN MICRO ENVIRONMENT AROUND MINERALS
9
7
4.5
2
0
STAGE I
STAGE II
STAGE III
Lag Time
REACTIONS IN STAGE III
$Fe^{+2} + \frac{1}{4}O_2 + H^+ \longrightarrow Fe^{+3} + \frac{1}{2}H_2O$
$FeS_2(s) + 14Fe^{+3} + 8H_2O \longrightarrow 15Fe^{+2} + 2So_4^{-2} + 16H^+$

Figure 2-2. Progression of Stages in Acid Generation with Time as a Function of pH (Adapted from SRK, 1992)

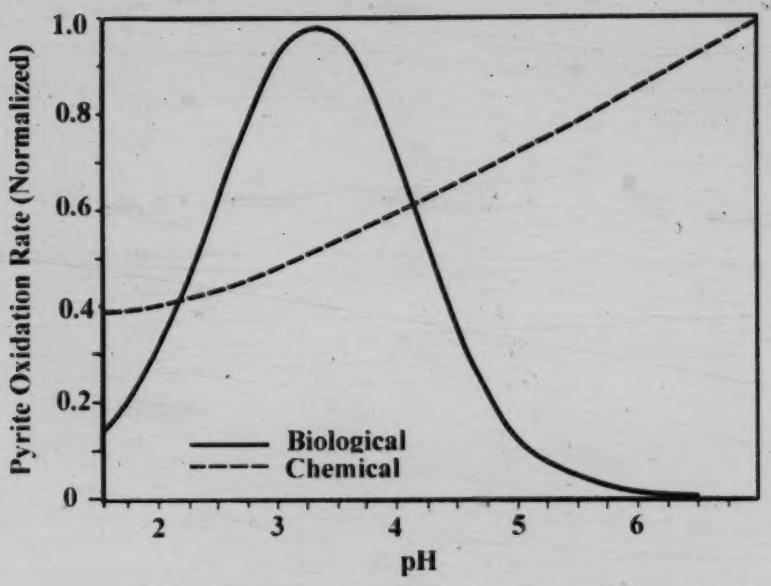

Figure 2-3. Changes in Relative Biological and Chemical Oxidation Rates of Pyrite as a Function of pH (Modified from Knapp, 1987)

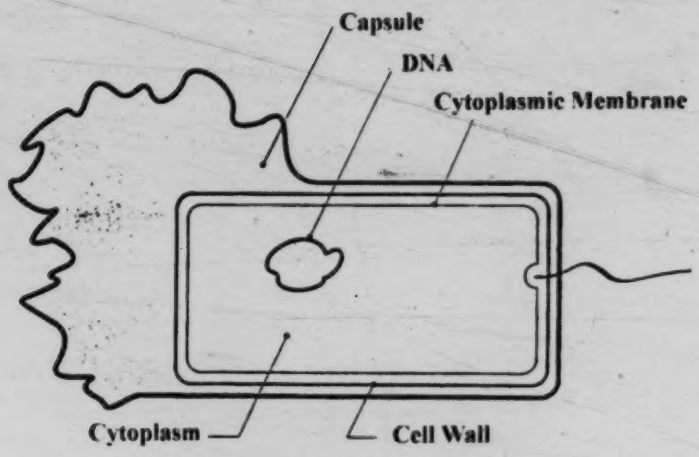

Figure 2-4. Bacterial Physiology
(Modified from Gould et al., 1994)

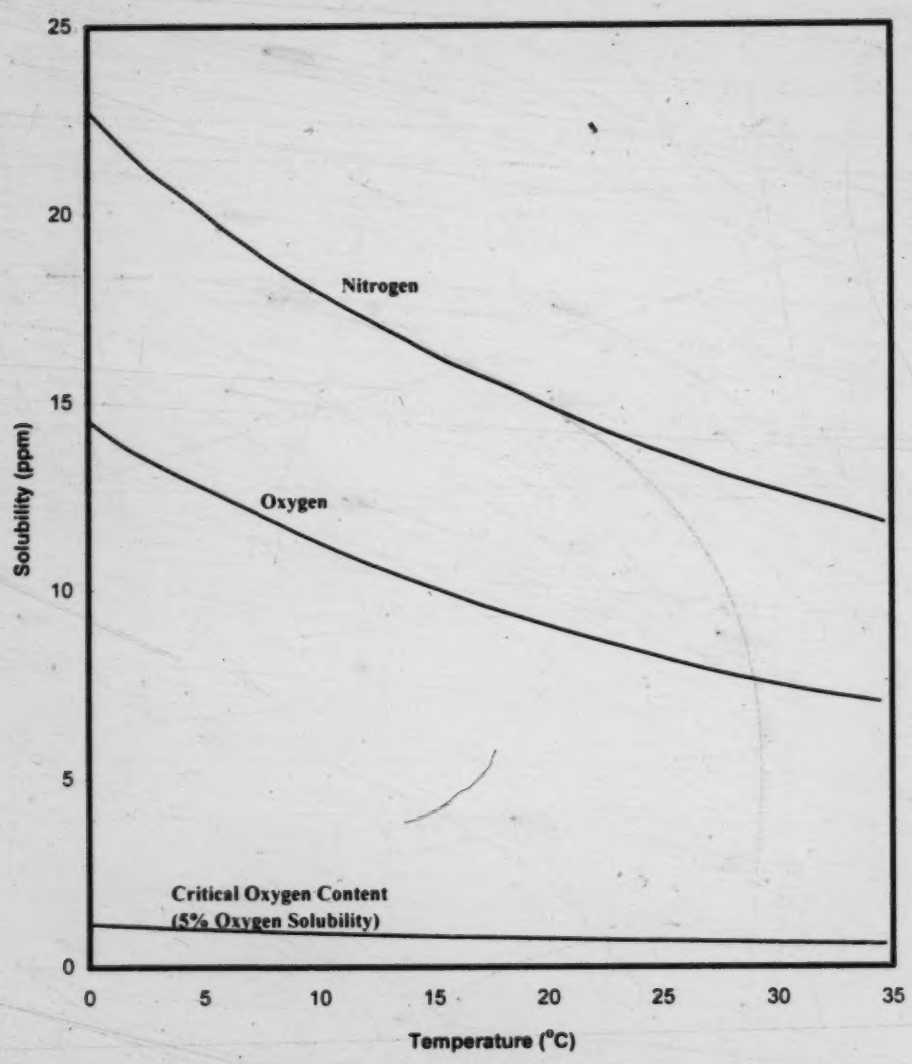

Figure 2-5. Solubility of Oxygen and Nitrogen in Water vs. Temperature with Critical Oxygen Concentration (Modified from Sawyer et al., 1994)

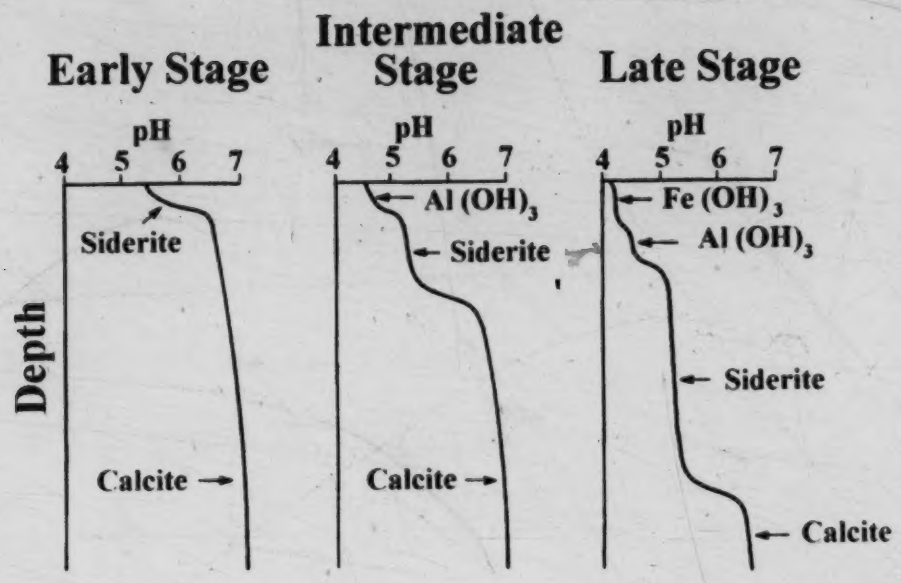

Figure 2-6. Progressive pH Levels of Dissolution of Acid Buffering Minerals (Modified From Blowes and Ptacek, 1994)

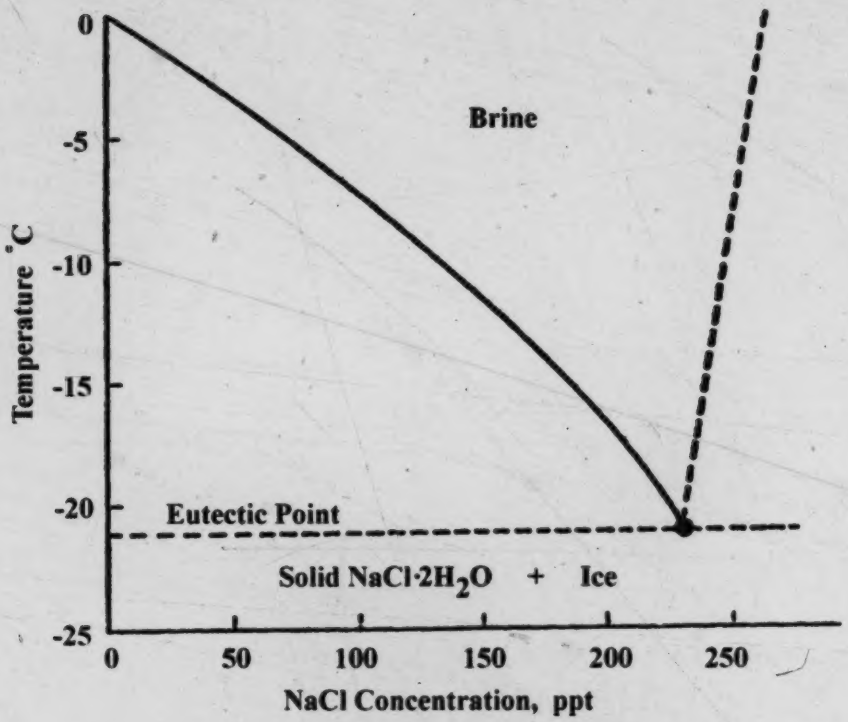

Figure 2-7. Phase Diagram for Sodium Chloride Solution
(Modified from Sheeran and Yong, 1975)

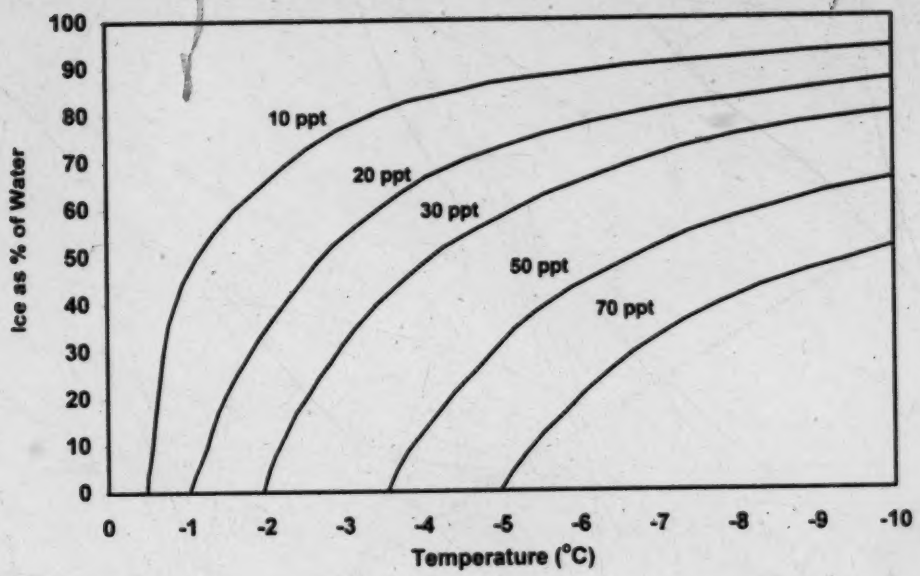

Figure 2-8. Increasing Unfrozen Water Content as a Function of Various NaCl Solution Concentrations at Temperatures below 0∘C (ppt – parts per thousand)

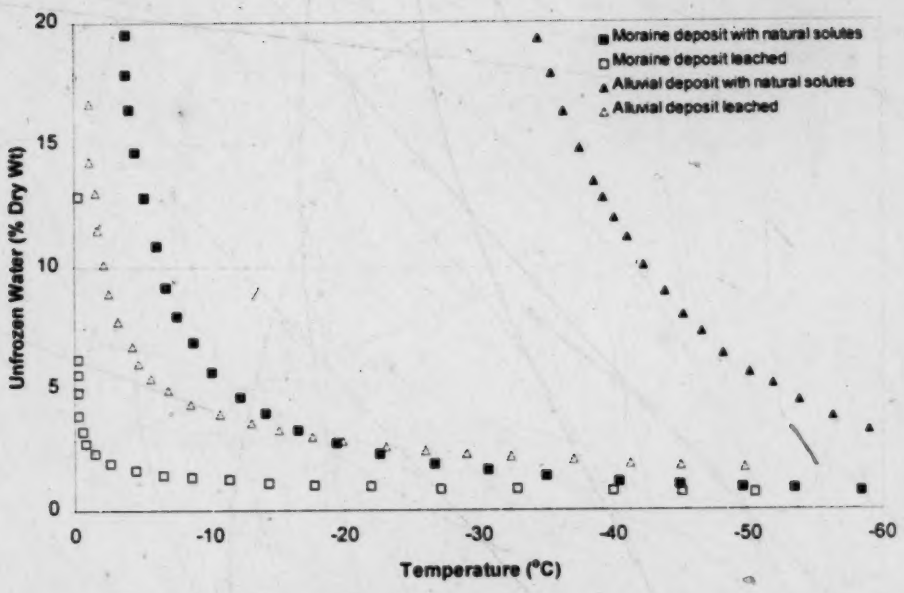

Figure 2-9. Unfrozen Water Content for Antarctic Moraine and Alluvial Soils vs Temperature (after Anderson and Tice, 1989)

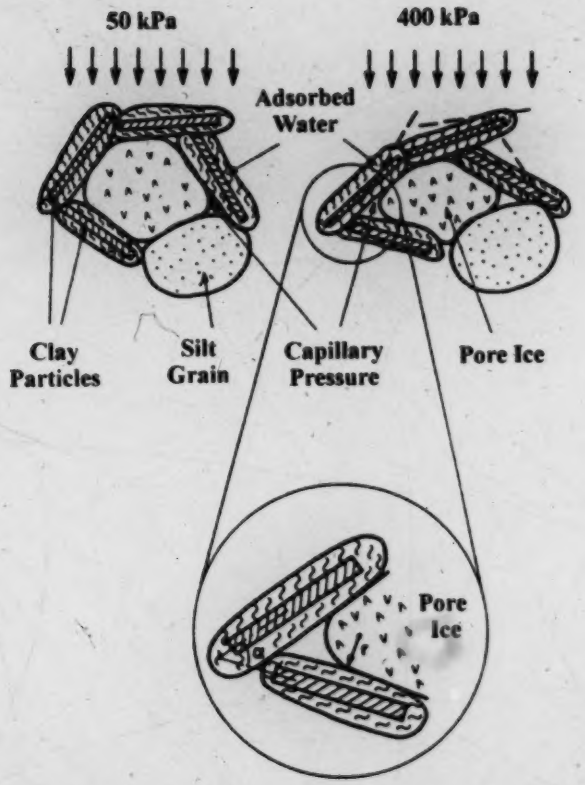

Figure 2-10. Increasing Confining Pressure Resulting in Finer Pore Radii Resulting in Increased Unfrozen Water Content (Modified from Konrad, 1989)

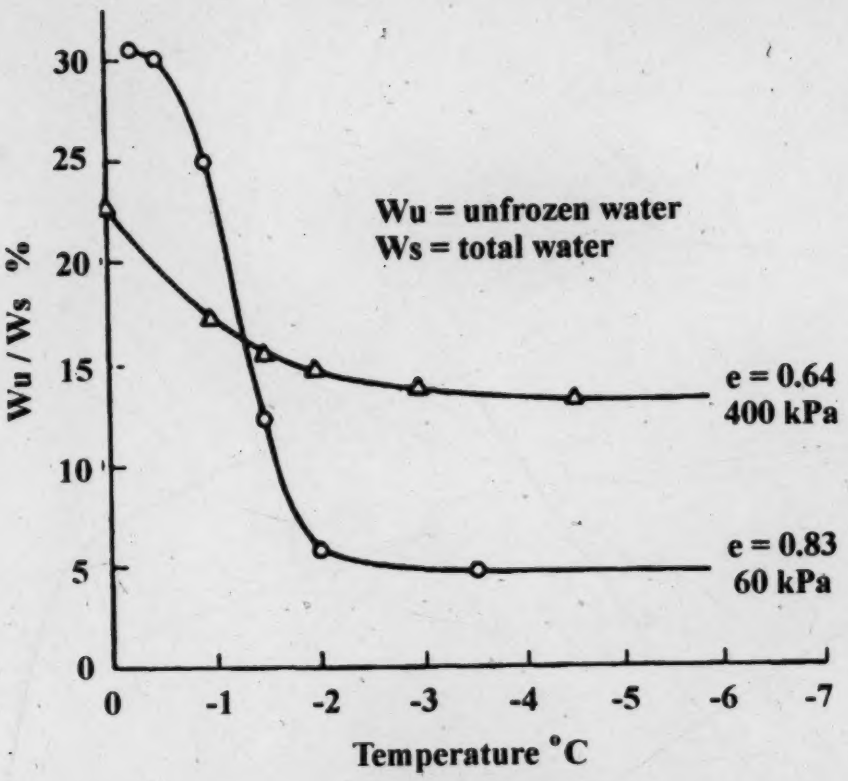

Figure 2-11. Increase of Unfrozen Water Content with Increase in Confining Pressure and Void Ratio for Devon Clayey Silt (Modified from Konrad, 1989)

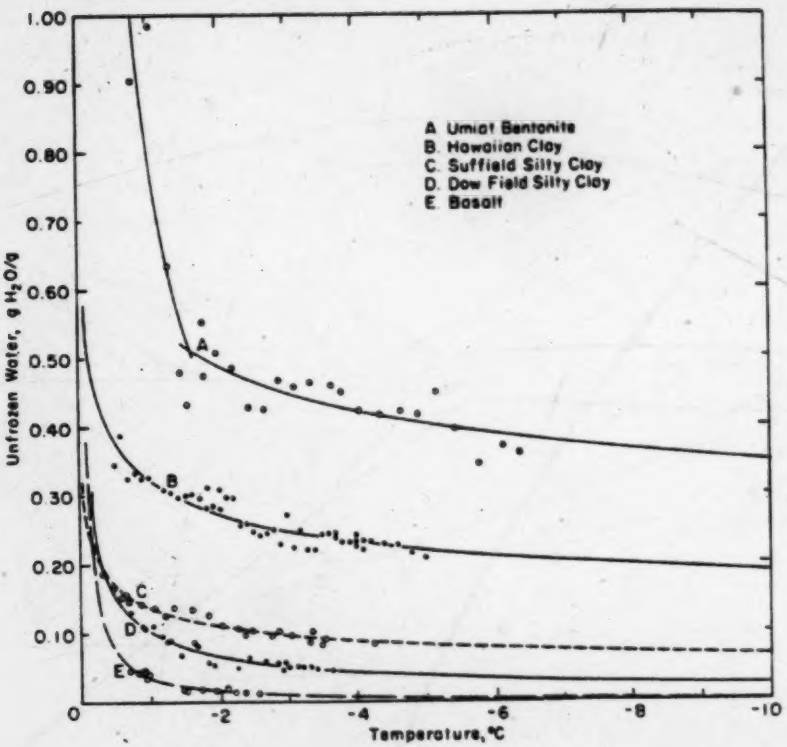

Figure 2-12. Increase in Unfrozen Water Content with Increases in Material Surface Charge for Five Soils (Modified from Anderson and Morgenstern, 1973)

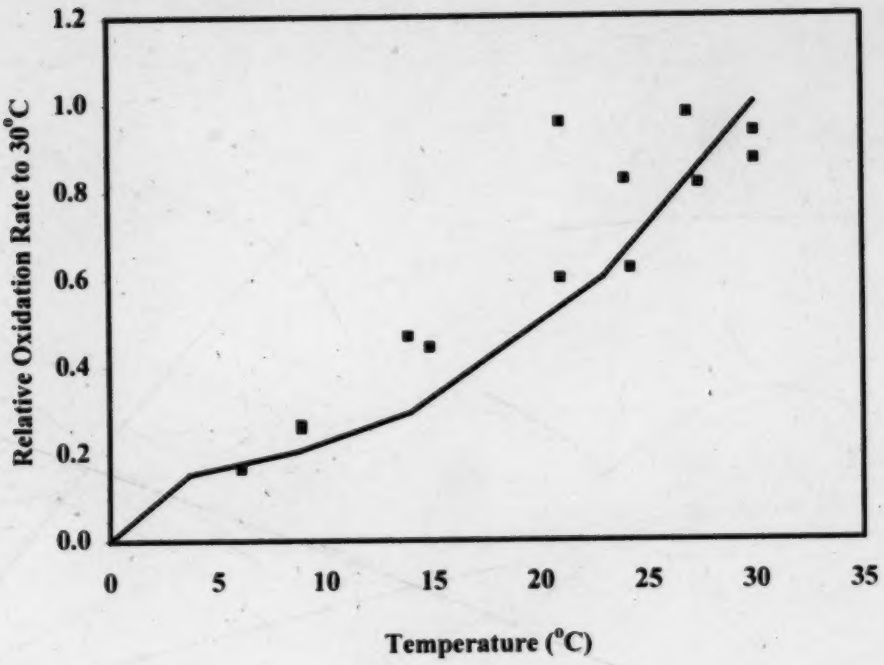

Figure 2-13. Sudden Change in Biological Oxidation Rate Curve as Modeled by RATAP Software Unsupported by Experimental Data (Modified from GEOCON, 1993)

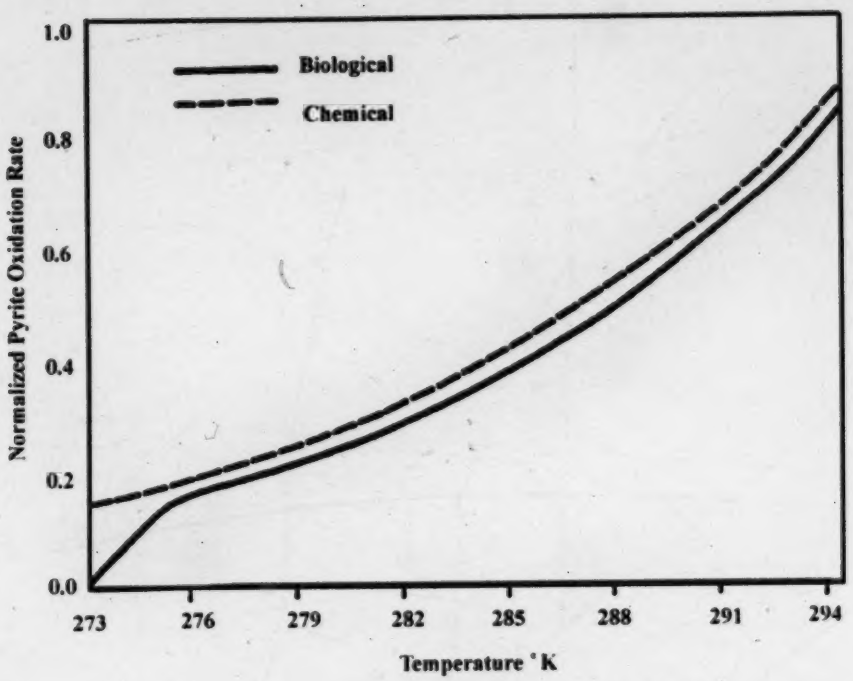

Figure 2-14. Sudden Changes in Biological Oxidation Rates Due to Assumed Zero Degree Celsius Intercept (Modified from Dave et al., 1996)

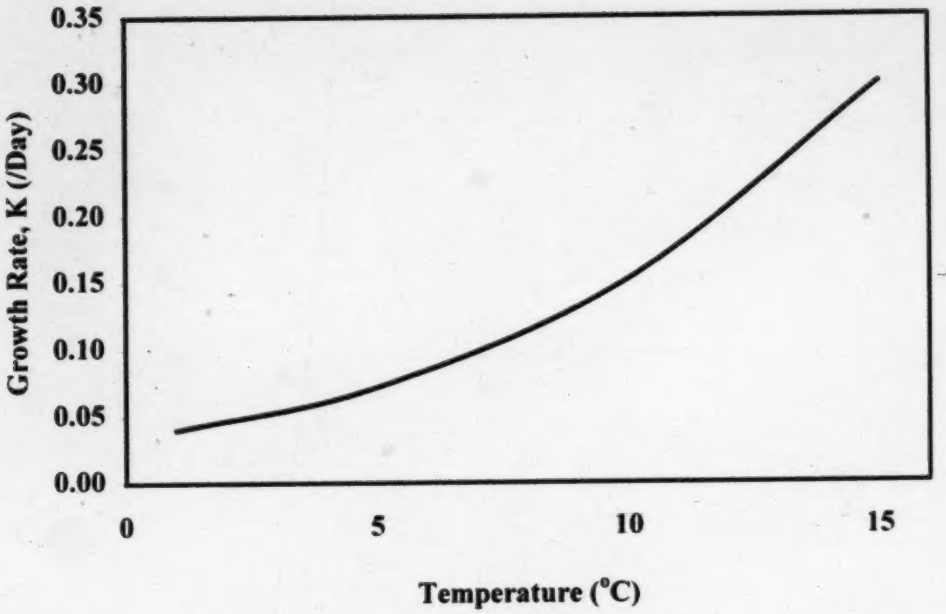

Figure 2-15. Biological Oxidation Demand Curve Suggesting Biological Activity at Temperatures Below Zero Degrees Celsius
(Modified from Heroux and Rowney, 1987)

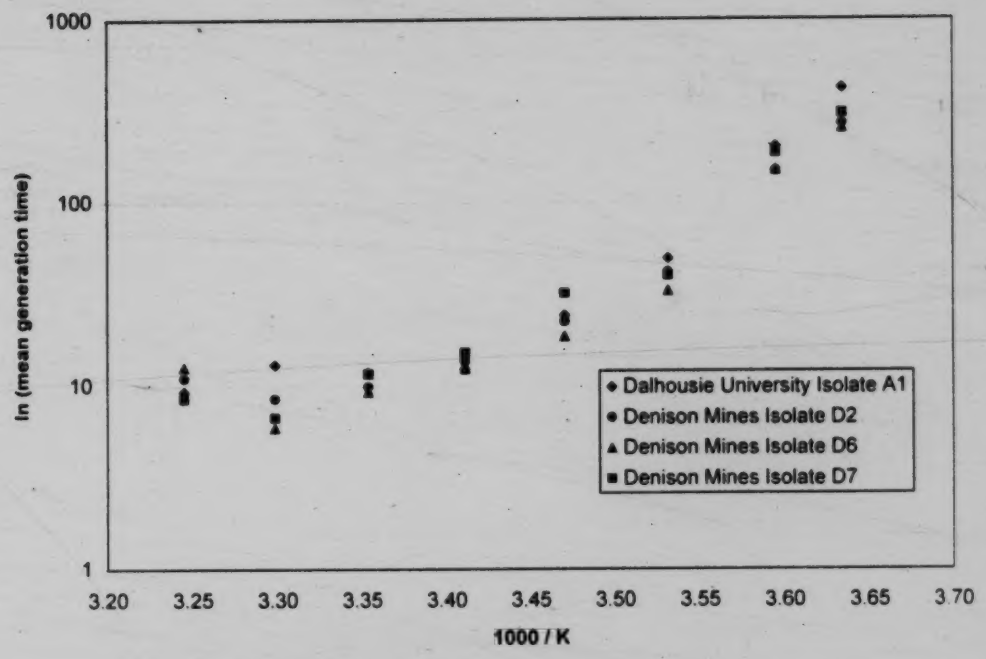

Figure 2-16. Growth Rate for Thiobacillus Ferrooxidans at Near 0°C
(modified from Leduc et al., 1993)

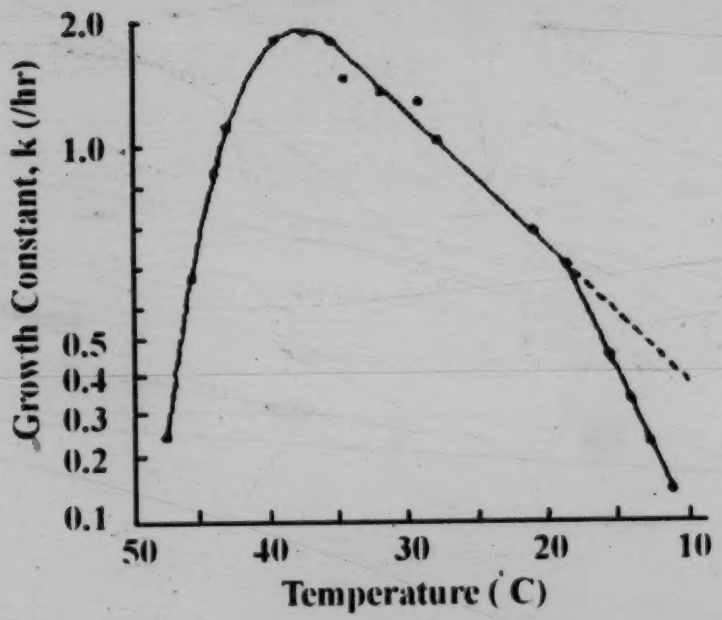

Figure 2-17a. Arrhenius Plot of Growth Rate Constant for Thermophilic Bacteria

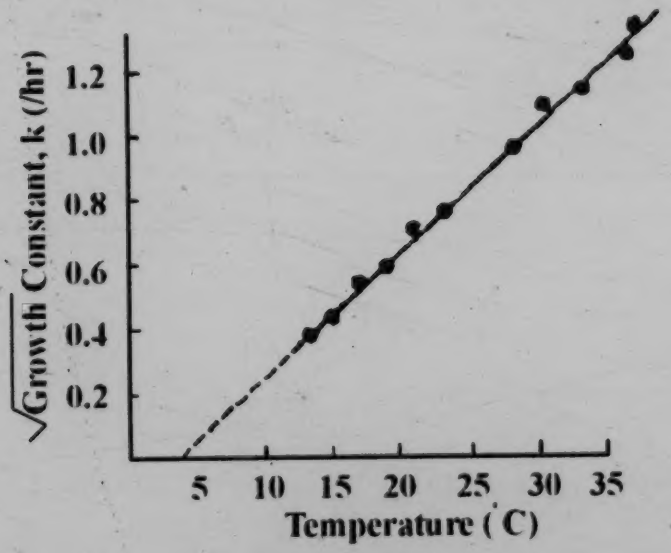

Figure 2-17b. Square Root Model Plot for Reaction Rates for Thermophilic Bacteria – Alternative to Arrhenius Curve for Biological Activity

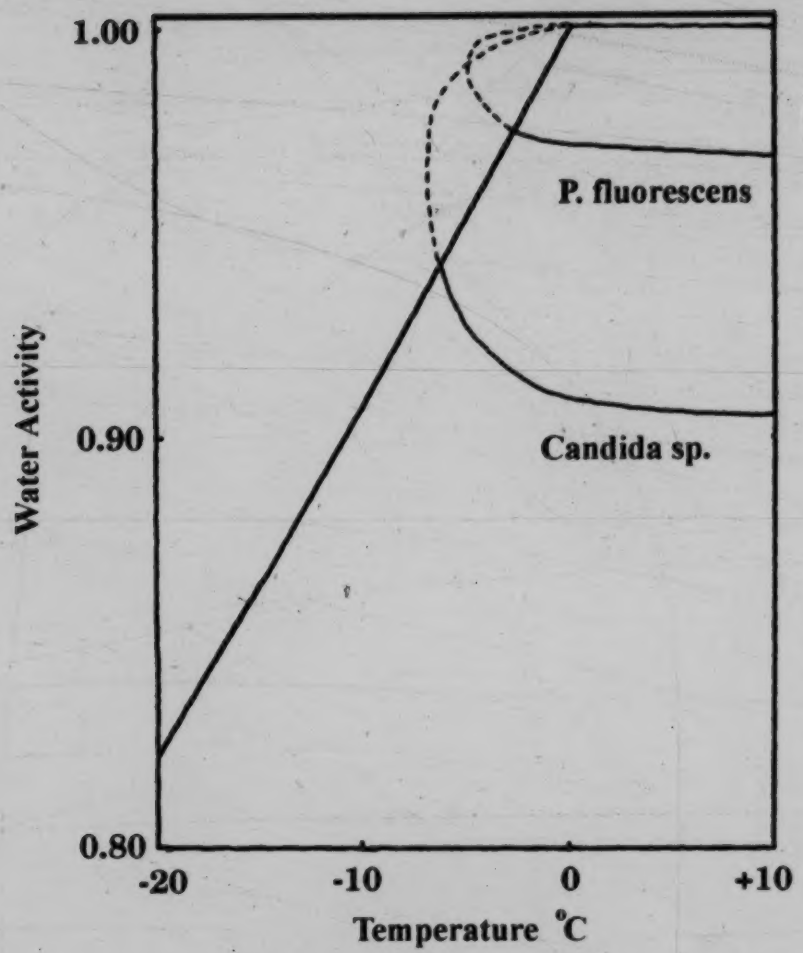

Figure 2-18. Minimum Temperature - Water Activity Limits for Two Psychrophiles (Modified from Scott, 1961)

Table 2-1. Growth Conditions for Acidophilic Bacteria

	pH		Temperature °C	
Organism	**Optimum**	**Range**	**Optimum**	**Range**
Leptospirillum ferrooxidans	1.5 - 2.0	---	30 - 37	< 10 - 45
Thiobacillus thiooxidans	2.0 - 3.0	0.5 - 5.5	28 - 30	< 10 - 37
Thiobacillus albertis	3.5 - 4.0	2.0 - 4.5	28 - 30	---
Thiobacillus ferrooxidans	2.5	1.3 – 4.5	30 - 35	< 10 - 37

Table 2-2. Principle Acid Neutralizing Minerals (Blowes and Ptacek, 1994)

MINERAL	FORMULA
CARBONATES	
Calcite	$CaCO_3$
Dolomite	$CaMg(CO_3)_2$
Ankerite	$Ca(Fe.Mg)(CO_3)_2$
Siderite	$FeCO_3$
HYDROXIDES	
Gibbsite	$Al(OH)_3$
Ferrihydrite	$Fe(OH)_3$
Goethite	α-FeOOH
K-Jarosite	$KFe_3(SO_4)_2(OH)_6$
ALUMINOSILICATES	
Chlorite	$(Mg,Al,Fe)_6(Si,Al)_4O_{10}(OH)_8$
Muscovite	$KAl_2(Si_3Al)O_{10}(OH,F)_2$
Alkali Feldspars	$(K,Na)AlSi_3O_8$
Plagioclase Feldspars	$NaAlSi_3O_8$-$CaAl_2Si_2O_8$
Pyroxene Group	-
Amphibole Group	-

Table 2-3. Mineral Equilibrium pH for Acid Buffering

Mineral Type	Equilibrium pH
Calcium-based carbonates (i.e. calcite)	5.5 – 6.9
Iron-based carbonate (i.e. siderite)	5.1 – 6.0
Aluminun-hydroxide-bearing minerals (i.e. muscovite)	4.3 – 5.0
Iron-hydroxide-bearing minerals (i.e. chlorite)	3.0 – 3.7

Table 2-4. Vapor Pressures for Water and Ice

Temp	Liquid water (mm Hg)	Ice (mm Hg)	Activity
0	4.579	4.579	1.00
-5	3.163	3.013	0.95
-10	2.149	1.95	0.91
-15	1.436	1.241	0.86
-20	0.943	0.776	0.82
-25	0.607	0.476	0.78
-30	0.383	0.286	0.75
-40	0.142	0.097	0.68
-50	0.048	0.03	0.63

3 SITE VISITS AND PREVIOUS STUDIES

3.1 DISCOVERY SITE

The Discovery Mine and townsite are located approximately 100km from Yellowknife. NWT, and cover approximately 1.5 km^2. The areas of interest for this thesis include an airstrip south of the Discovery Town site and a tailings delta in the adjacent Giauque Lake. From 1949 to 1969, the mine generated approximately 1,100,000 tonnes of tailings, that for the first 25 years were deposited at the location of the present day airstrip. From 1965 to 1969, these tailings were allowed to flow into Giauque Lake. eventually forming a land bridge across to an island. The delta covers approximately 25,000 m^2, and is scheduled for encapsulation. The depth of tailings varies significantly over the site, as little effort was made to contain them.

The Discovery site is situated at the top of the hill overlooking Giauque Lake. approximately 40m below. The topography of the area surrounding the airstrip is rolling. with relief in the order of 5-10 m over half a kilometer. Where the tailings are deposited. the ground is relatively bare of vegetation. The surficial tailings are unsaturated and significantly oxidized to a depth of approximately 1m, as indicated by a yellow-brown color. Where the tailings are thicker than 1m, they become more saturated and are dull grey in color, remaining unoxidized since deposition. The average depth to original ground is not known.

Travel to the Discovery Site occurred on 14 September, 1998, by single Otter. Weather conditions were rainy and cold. After setting up the base camp (Fig. 3-1), travel to the study site was organized by North Slave Metis Alliance project manager. At this time. the team expanded to include scientists and engineers involved with the fisheries. physical, terrestrial, tailings and sediment monitoring program (Fig. 3-2). The U of A team was a late addition to the team, but no significant changes had to be made.

Since the tailings delta on Giauque Lake was 300m from the townsite and base camp and over rugged terrain, it was decided to transport the equipment by water. The sampling buckets and digging equipment were loaded into the dinghy supplied by the biological team. Preparation of the site on the tailings delta from where the samples would be collected is shown in Figure 3-3.

The cover material was removed using shovels, until the geosynthetic clay liner (GCL) was reached (Fig. 3-4). According to SRK guidelines, an X-cut was made in the GCL (Fig. 3-5), exposing the tailings. The first hole dug showed significant organic matter at the surface of the hole. Because of the uncertainty of the amount of oxidation/reactions that had occurred due to the organics, a second hole was dug in what would be the final location (Fig. 3-6). As in the first hole, the GCL was cut and pulled back according to SRK guidelines.

Samples were obtained using a hand auger. The upper ~30cm saturated. Samples were placed in 6 - 20L buckets, at which time, the sides of the auger hole began to collapse, forming a slurry. Due to the difficulty in obtaining samples, the remainder of the final two buckets were collected from the first hole. The buckets were labeled upon filling (Fig. 3-7). Additional samples of cover material and lake water were placed in 20L buckets.

The void created from the removed tailings was self-filling as the surrounding tailings collapsed inward. The flaps from the cut GCL were replaced and covered with a layer of bentonite powder and chips (Fig. 3-8). A layer of geotextile was placed over the bentonite layer and covered with original cover material (Fig 3-9).

After supper, the first thermistor string (String A) was installed, composed of 8 resistance temperature detectors (RTDs), labeled and spaced at 25cm intervals as shown in Table 3-1. The string was pushed down into the tailings and covered on the surface with a plastic piping (Fig. 3-10). Figure 3-11 shows the location and condition of the site upon completion.

A search was conducted for a location that would provide a weathering profile, a column less than 2m in depth that showed the transition from weathered to non-weathered tailings material. The second thermistor string was to be placed nearby.

The first location selected was near the road leading west running parallel to the airstrip. 150m south of the strip and approximately 200m from the town site (Fig. 3-12) near the tailings line. The sand was augered to a depth of approximately 90 cm, where contact was made with a layer of organics. The entire length of tailings was weathered. It was interpreted that original ground surface had been reached, so the site was abandoned.

The second location was 20m north from the center of the airstrip, approximately 250m west of the powerhouse (Fig. 3-13). A hole was augered revealing the profile that was required. A closer view revealed the visible weathering that had occurred in the surficial tailings (Fig. 3-14). No organics were encountered and the hole was stable along its entire length.

A core sample was obtained using Shelby tubes, driven by a sledge hammer (Fig. 3-15). The upper meter was sampled without difficulty, using the Shelby tube extension. To proceed deeper required widening the hole made by the tube, using the auger and shovels. The expanded hole permitted lowering tubes beyond surface level. Each successive tube was labeled indicating the depth and the sample recovery (Fig. 3-16).

As the depth increased, it became more difficult to recover significant lengths of sample, as the tailings were increasingly saturated, making them more difficult to extract as they slipped from the tube upon lifting. This problem was solved by denting the base of the tubes which provided additional support for the tailings, and by sampling smaller lengths.

When the tube had been lifted from the hole, the looser material was removed, assuming that this material was merely slough from the sides of the hole. The ends were then capped with fitted ends. The total depth of the core was 200cm, with 185cm of sample

recovered. This loss of sample was attributed primarily to compression, but some loss of sample is also possible. The bottom 15-20 cm of the last core sample were completely saturated and required several attempts to extract them.

The second thermistor string (String B) was installed near the sample collection site. The two thermistor strings were identical, again having RTDs at 25cm intervals. The first readings from the strings were made later that afternoon, before leaving the mine site for Yellowknife. A second reading was made the following spring. These results are shown in Figure 3-17.

3.2 PREVIOUS STUDIES FROM DISCOVERY MINE

Due to the extensive contamination by mine tailings at the Discovery Mine, there have been several investigations since its closure. In reports compiled and summarized by SRK (1998), it was concluded that the Discovery site has developed an acid generating environment conducive to metal leaching and that there remains significant potential for further acid production. Though not extensive, this section includes the summaries with respect to acid generating behavior recorded, as well as any references to temperature data or thermal regimes.

3.2.1 Acid Generating Studies

Tests indicating the presence of an acidic environment are reported here. Elevated metal levels *not* associated with low pH are not included.

Klohn Leonoff (1992) Discovery Mine – Options for Tailings Reclamation

The Klohn Leonoff study sampled two sites, and blended the oxidized surface material and unoxidized subsurface material from each. Table 3-2 shows the comparison. The significant difference between the two samples is primarily the change in pH, from 7.36 in the unoxidized material, to 3.80 in the surface oxidized material. Also of significance

in this data is the remaining total sulfur in the oxidized material. The report suggests that there is potential for the tailings to become even more acidic.

Samples of water, tailings and sediments were collected at sites shown in Figure 3-18. and tested for pH and mineral content. These tests show that the pH ranged from 3.8 to 6.2 for the tailings, concluding that the surface tailings were producing acid. Table 3-3 shows the results. Typically, the pH increased with depth. In Table 3-4, higher metal levels in Pit 9, which had the lower pH, suggests a relationship between increased acidity and increased levels of copper, lead and zinc.

3.2.2 Summaries of Cold Temperature Considerations

The acid generating and metal leaching potential of the tailings on site has been partially examined (Klohn Leonoff, 1992), but no previous effort has been taken to determine the effects of the thermal regime.

An investigation of the effects of the thermal regime was originally included in the program proposed by SRK Inc., but was later removed. As such, the thermal monitoring program is limited to the work summarized in this report.

Considering the potential role that the arctic temperatures could play in the reclamation of the Discovery site, relatively few studies have been performed predicting these effects. though several reports do consider using freezing as a reclamation technique. This application has not experienced wide use however, which may be due in part to its uncertainty for long term durability. The following sections summarize previous Discovery Mine reports with respect to acid mine drainage and temperature considerations.

Klohn Leonoff (1992) Discovery Mine – Options for Tailings Reclamation

The report by Klohn Leonoff reported more qualitative characterization, describing the site as being within the zone of discontinuous permafrost, as evidenced by the presence

of heaved ice blocks and ice lenses. During the mining activities, permafrost was reported as deep as 38m.

Proposals to freeze the tailings to contain them were discounted because Giaugue Lake acts as a heat source. It was also recognized that the oxidation of the tailings is an exothermic reaction, which further complicated the conditions. As part of the evaluation, the report recommended that studies would have to be performed capable of defining the required thickness and type of cover material to keep the underlying tailings frozen year round. This study would require thermistor installation and temperature monitoring within the tailings.

3.3 PREVIOUS STUDIES FROM FARO MINE

Due to the lack of success with the laboratory testing of the Discovery Mine material due to its low sulfur concentration, further investigations were made to find a different site with material having higher sulfur content, more likely to generate acid drainage in a laboratory setting. Ongoing communication with Mr. Benoit Godin at Environment Canada led to contacting Eric Denholm, the environmental specialist at the Faro Mine, located near Faro, Yukon (Figure 3-19).

Portions of the Down Valley Tailings Impoundment Decommissioning Plan (Curragh Resources Inc. and SRK, 1991) were obtained, which described zones of the tailings facility that had been tested previously. This report showed regions that had undergone significant testing, including acid generating characterization. One drill site listed the results from previous humidity cell testing when the leachate with an initial pH ranging from 6.0 to 6.6 dropped to between 4.1 and 4.2 after 42 days of testing. This material was from a depth of 2 m. The report described this target as having "a high sulphide content and negative net neutralization potential (NNP) indicating potentially acid generating material". Sulfur content averaged 31.2 percent total sulfur with 1.2 percent sulfate sulfur, and NNP of –917 kg $CaCO_3$ equivalent/tonne. The sulfide content was variable, ranging from less than 0.1 to 49.9 percent total sulfur. The goal of the investigation was to obtain samples of these tailings.

Portions of a second report was provided by the Anvil Range Mining Corporation, a previous operator of the Faro Mine (Cron, 1996). This report describes a sampling program, aimed at providing data for feasibility of reprocessing the original mill tailings pond. The work performed under this program described in the section of the report consisted of 10 test pits, from which 10 – 200L drums of tailings were collected. A description of the material in each drum was listed in addition to the paste pH. Test pit D1 showed paste pHs increasing from 2.79 in drum 5 (depth of 2 – 2.5m) to 4.88 in drum 6 (2.5 – 3m) and 5.2 in drum 7 (3 – 4m). The report noted that "although wet paste appears to increase in moisture with depth, no free water was observed."

The results from these reports did not present completely corroborating analyses, though it appeared that the material listed in the Curragh Resources and SRK report was similar in description and location to the material reported in the Cron report. Due to the simplicity of performing paste pH tests on site, it was decided to use this form of testing to confirm that the appropriate material was being collected.

3.4 FARO MINE VISIT

A visit was made in October, 1999, to collect additional tailings samples with a higher sulfur content from Faro Mine, near the townsite of Faro, Yukon Territory. The tools necessary for the sample collection and the insulated crate for returning the samples were sent in advance through Canadian Air Cargo. Upon arrival in Whitehorse, YT, on October 14, 1999, a truck was rented, and the team drove to Faro townsite, meeting the site environmental specialist for an introductory overview of the planned project.

The following morning, he provided a site visit and indicated the location of the target material, as described by the Cron report (Figure 3-20). After approximately 3 hours of digging by spade, a depth of approximately 5 feet was reached (Figure 3-21), where a layer of frozen material was reached. Digging became slower until a layer of dry and cracked hardpan was reached. This material did not match the description of any material in the Cron report (1996), so the digging site was relocated.

A second hole was begun late in the afternoon, and a depth of approximately 1 meter was reached before the work ended for the day. The following morning, digging resumed, with paste pHs being obtained every 0.5m. A portable pH probe was used, though as the testing proceeded, confidence in the readings became increasing poor, due to apparent disparity between successive tests. The surface material had a paste pH of approximately 1.5, and was increasing slightly with depth. At a depth of approximately 2m, the paste pH was 4, and had not changed for over half a meter. Finally, at a depth of 2.5m (Figure 3-22), a paste pH of 5 was recorded. Due to the increasingly difficult excavating conditions using spade and 20L buckets, and the time of day, it was decided to collect the samples from this depth. Six – 20L buckets were collected, in addition to smaller samples of material from the hole walls at 10 cm intervals for the upper meter, and 50 cm intervals to a depth of 2.5 m.

Upon returning to the University of Alberta, testing of the material paste pH revealed that the pH probe used in the field was inaccurate. The material obtained had a paste pH of 6.0, indicating that the collection site was selected appropriately.

Figure 3-1. Discovery Mine Base Camp

Figure 3-2. Discovery Site Characterization Team

Figure 3-3. Collection Site of Discovery Tailings for Bulk Test Sample

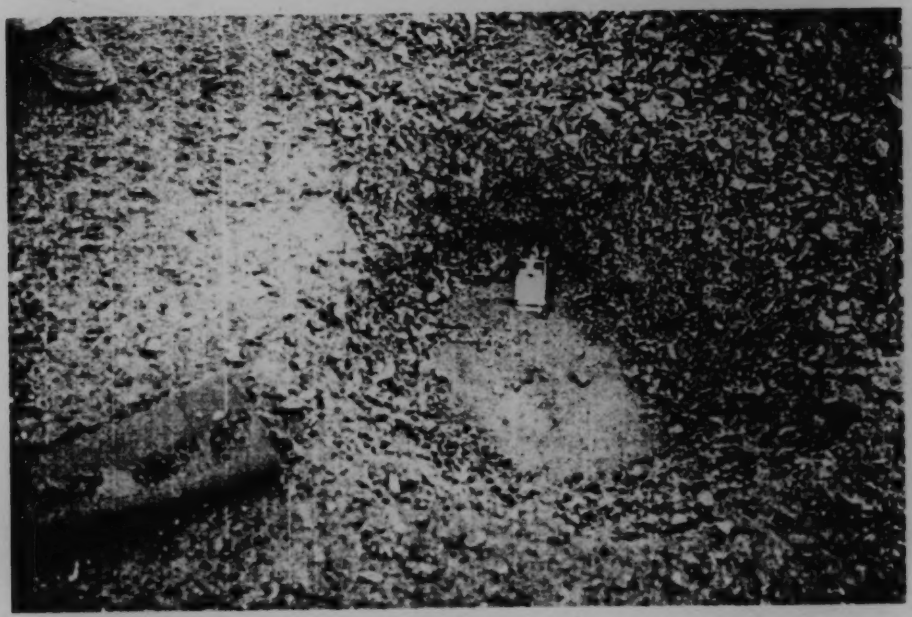

Figure 3-4. Exposure of GCL During Sample Collection on Tailings Delta at Discovery Mine

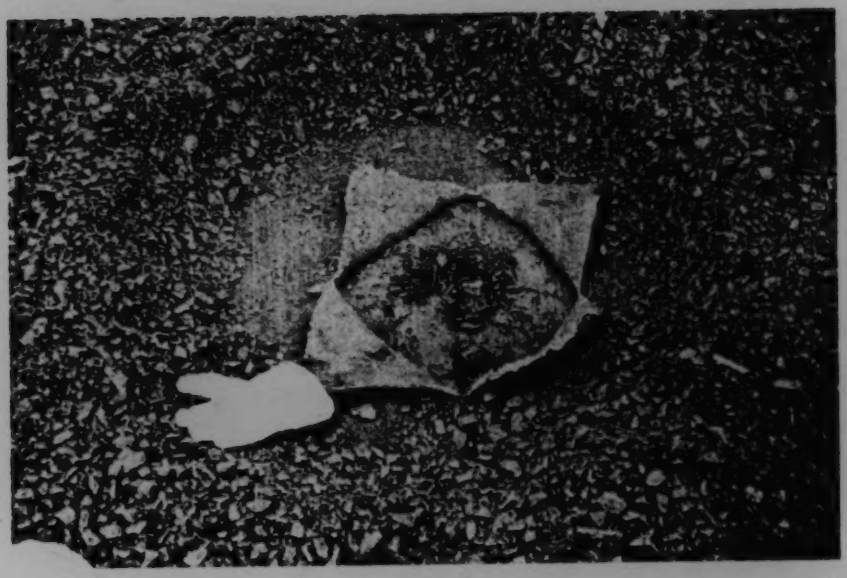

Figure 3-5. Standard X-cut in GCL Revealing Organic Matter During Sample Collection on Tailings Delta

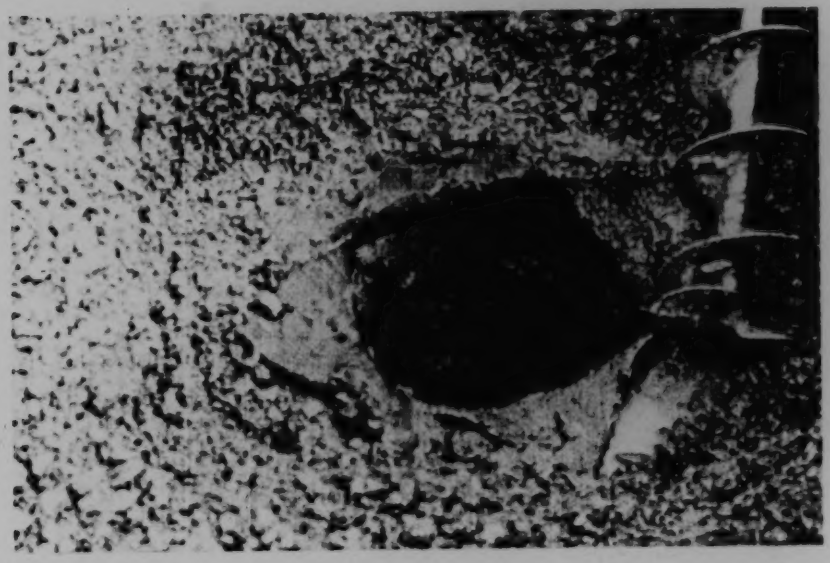

Figure 3-6. Tailings Extracted Using Hand Auger on Tailings Delta

Figure 3-7. Sample Collection and Labeling of Bulk Samples from Tailings Delta

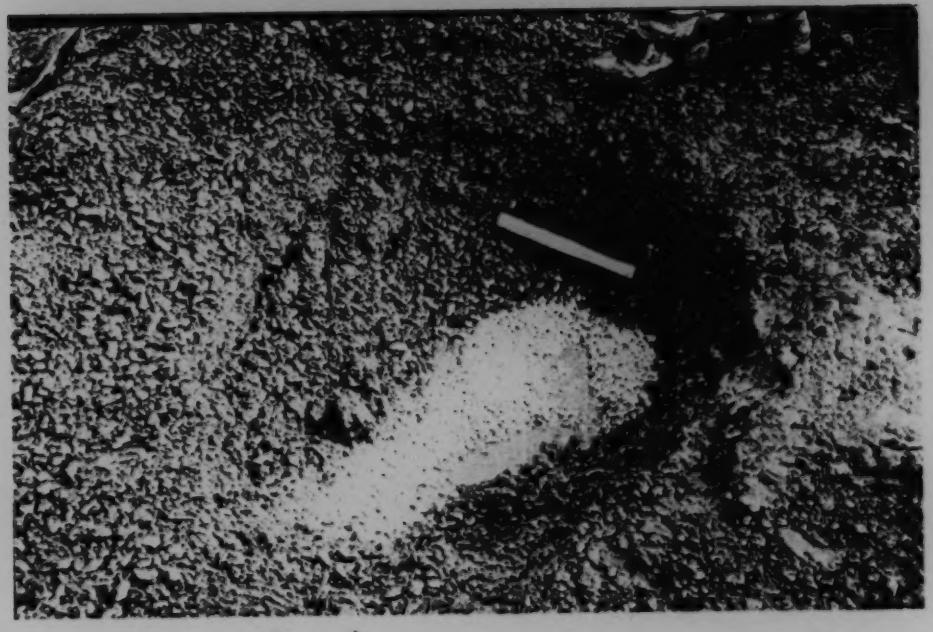

Figure 3-8. Sealing Hole in GCL from Sample Extraction Using Bentonite Chips

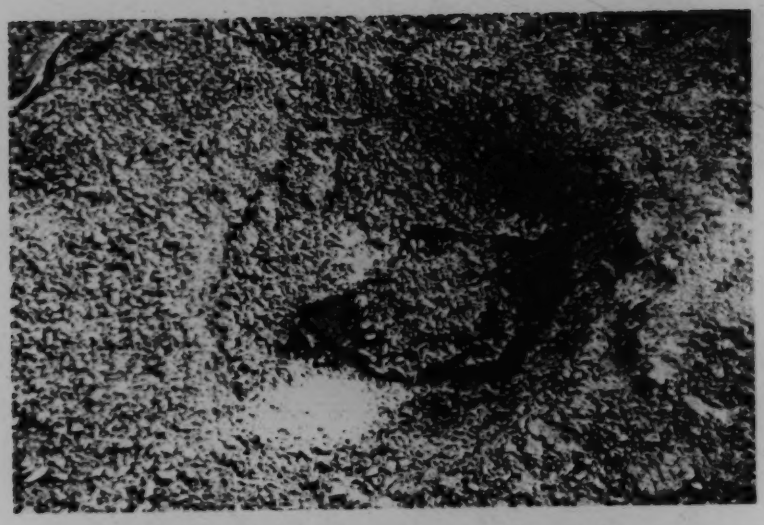

Figure 3-9. Bentonite Chips Covered with Geotextile in Final Step of GCL Repair

Figure 3-10. Thermistor String 'A' Identification on Tailings Delta

Figure 3-11. Completed Site of Thermistor String 'A' on Tailings Delta

Figure 3-12. Initial Site Location for Collection of Weathering Profile of Tailings at Discovery Site

Figure 3-13. Air Strip Sampling and Thermistor String 'B' Location Approximately 200m from Town Site

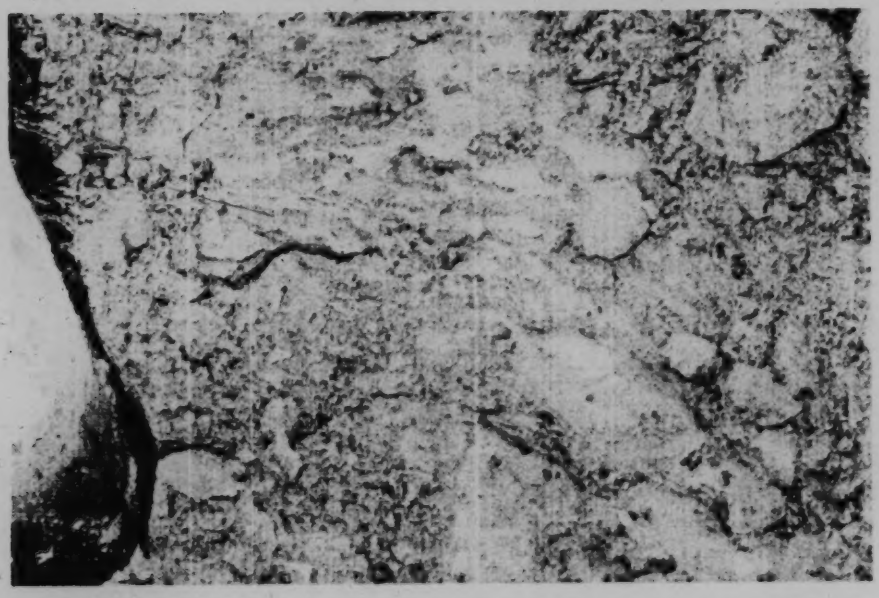

Figure 3-14. Weathering Zones in Air Strip Tailings Revealing Significant Zones of Iron Enrichment and Sulfide Oxidation

Figure 3-15. Core Extracted Using Shelby Tubes at Air Strip Thermistor String 'B' Location

Figure 3-16. Tube Labeling and Site Repair at Discovery Airstrip Sampling Location

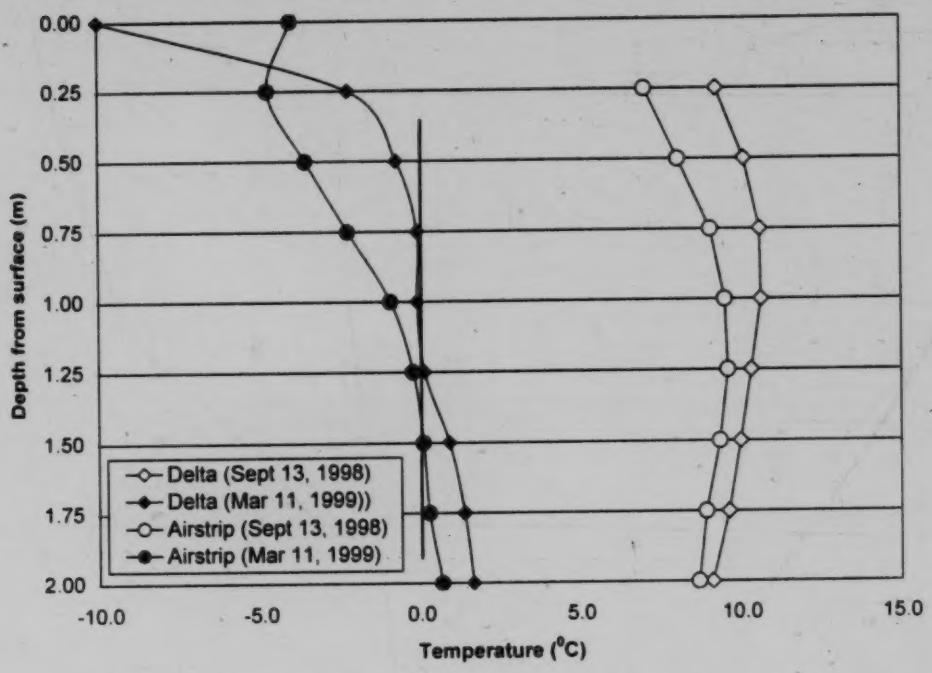

Figure 3-17. Ground Temperatures at Discovery Mine, NWT with 0∘C Line

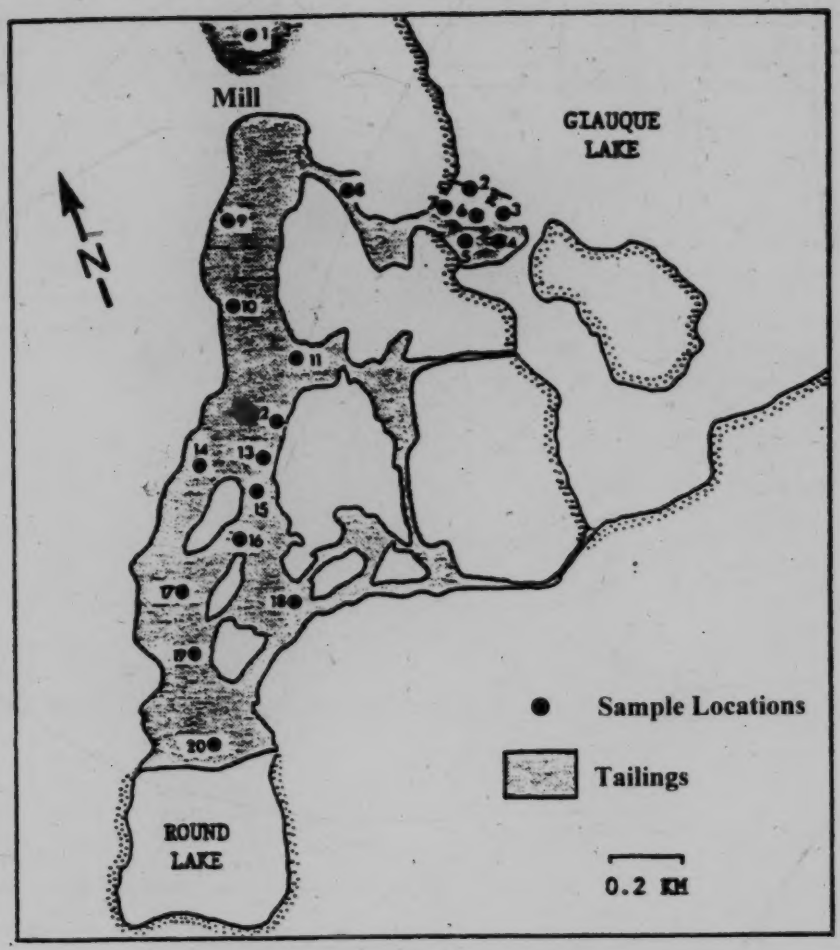

Figure 3-18. Sample Collection Sites for Soil Analyses at Discovery Mine
(Modified from Klohn Leonoff, 1992)

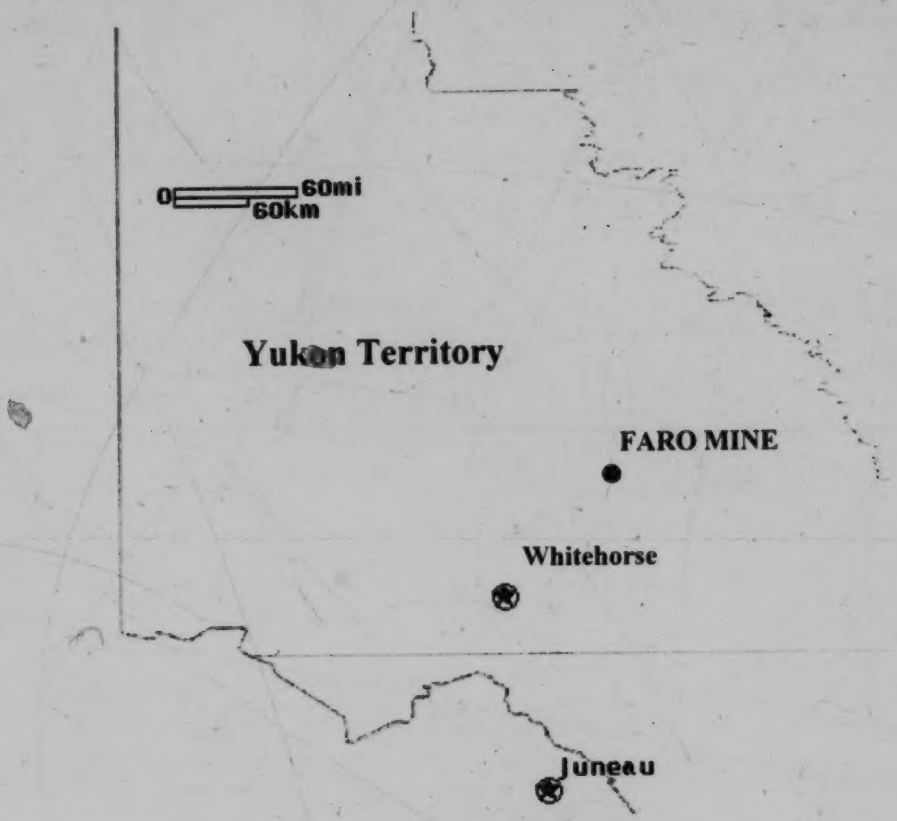

Figure 3-19. Faro, Yukon Territory
(modified from MapQuest.com, Inc.)

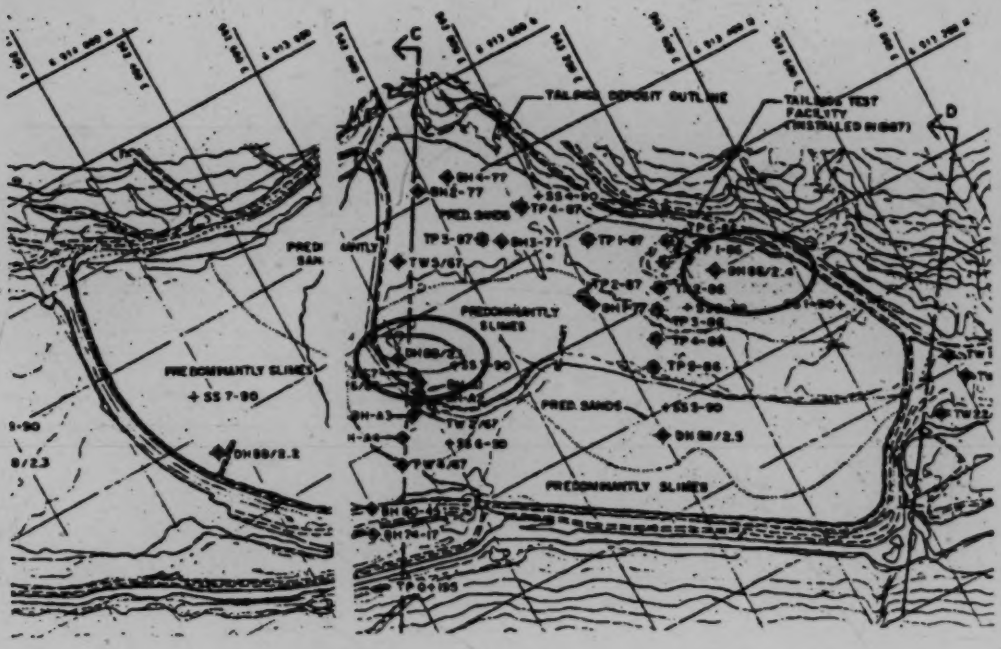

Figure 3-20. Selected Sites for Faro Mine Samples on Tailings Impoundment (Curragh Resources Inc. and SRK, 1991)

Figure 3-21. Depth to Frozen Material at Initial Faro Mine Sampling Location on Tailings Impoundment

Figure 3-22. Final Depth for Bulk Sampling at Faro Mine

Table 3-1. Thermistor Strings at Discovery Mine

String A - on tailings delta

	String	Color	Depth	Date	Ohm	Temp
A1	1	green	2.00m	13-Sep-98	10.3	9.1
				11-Mar-99	14.9	1.6
A1	2	black	1.75m	13-Sep-98	10.0	9.6
				11-Mar-99	15.1	1.4
A1	3	red	1.50m	13-Sep-98	9.8	10.0
				11-Mar-99	15.4	0.9
A1	4	blue	1.25m	13-Sep-98	9.6	10.3
				11-Mar-99	16.0	0.1
A2	5	green	1.00m	13-Sep-98	9.5	10.6
				11-Mar-99	16.1	-0.1
A2	6	blue	0.75m	13-Sep-98	9.5	10.6
				11-Mar-99	16.1	-0.1
A2	7	black	0.50m	13-Sep-98	9.7	10.1
				11-Mar-99	16.6	-0.7
A2	8	red	0.25m	13-Sep-98	10.2	9.3
				11-Mar-99	17.9	-2.2
					5.1	25.0

String B - on airstrip

	String	Color	Depth	Date	Ohm	Temp
B2	1	green	2.00m	13-Sep-98	10.5	8.7
				11-Mar-99	15.6	0.7
B2	2	red	1.75m	13-Sep-98	10.4	8.9
				11-Mar-99	15.9	0.3
B2	3	blue	1.50m	13-Sep-98	10.1	9.3
				11-Mar-99	16.0	0.1
B2	4	black	1.25m	13-Sep-98	10.0	9.6
				11-Mar-99	16.2	-0.2
B1	5	green	1.00m	13-Sep-98	10.1	9.5
				11-Mar-99	16.8	-0.9
B1	6	blue	0.75m	13-Sep-98	10.3	9.1
				11-Mar-99	17.9	-2.2
B1	7	black	0.50m	13-Sep-98	10.8	8.1
				11-Mar-99	19.0	-3.6
B1	8	red	0.25m	13-Sep-98	11.4	7.0
				11-Mar-99	20.1	-4.7

Table 3-2. Comparison of Oxidized and Unoxidized Zones
Discovery Mine Tailings

Parameter	Oxidized Zone	Unoxidized Zone
EC (ms/cm)	3.65	1.4
pH	**3.8**	**7.36**
Total carbon (%)	0.016	0.029
Total nitrogen (%)	0.015	0.007
Phosphorous (ppm)	2.25	1.5
Sulfur (ppm)	**2,736**	**398**
Total sulfur (ppm)	**12,302**	**16,465**
Chloride (ppm)	106	104
Potassium (ppm)	4.1	2.85
Calcium (ppm)	163	69.5
Magnesium (ppm)	36.5	14.5
Sodium (ppm)	14.9	3.25
Cation exchange capacity	2.9	1.25

(Klohn Leonoff, 1992)

Table 3-3. pH of Tailings, Tailings Leachate and Lake Water

Station	Tailings Depth	pH
1	surface	6.2
2	surface	4.7
	26 cm	4
	40 cm	4.3
	53 cm	5.7
3	surface	5.9
5	surface	4.7
8	surface	5.7
9	surface	5.3
10	surface	5
	26 cm	5.7
	40 cm	5.3
11	13 cm	4.4
	40 cm	5.7
	53 cm	6.2
13	13 cm	3.8
	40 cm	4
	53 cm	4.3
	79 cm	6.2
	106 cm	4.7

Tailings Leachate Station	pH
3	7.6
5	4.1
6	4
7	3.9
8	5.1
9	2.9
12	6.4

(from Klohn Leonoff, 1992)

Table 3-4. Concentration of Elements in Water Sample From Discovery Tailings

Station	As	Pb	Cu	Ni	Zn	Na	K	Ca	Mg	Fe	Hg
1 lake	0.003	0.001	0.02	0.2	0.2	21	11	122	27	0.3	<.2
3 pit	0.003	0.001	0.02	0.7	1	18	14	130	26	7	<.2
5 pit	0.1	0.13	0.2	2.6	7	60	37	306	148	70	3
6 pit	0.003	0.01	0.1	4.7	7	64	37	262	162	8	<.2
7 pit	0.001	0.01	0.3	11	29	199	42	409	615	15	<.2
8 pit	0.011	0.4	0.3	9	26	132	31	462	462	33	<.2
9 pit	**0.001**	**0.101**	**0.6**	**54**	**96**	**171**	**214**	**440**	**759**	**78**	**0.4**
12 pit	0.001	<.001	0.004	0.1	0.1	2	2	5.8	3	0.7	<.2
Avg	0.02	0.08	0.2	10	21	83	49	267	275	27	0.425
Min	0.001	<.001	0.004	0.06	0.1	2	2	5.8	3	0.3	<.2
Max	0.1	0.4	0.6	54	96	199	214	462	759	78	3

(Klohn, 1992)
All units in ppm

4 EXPERIMENTAL PROGRAM and RESULTS

The purpose of the testing program was to determine the effects of sub-zero temperatures on the generation of acid mine drainage. To do this, an initial characterization of the material was performed with respect to its physical, thermal and microbial behavior. These parameters were necessary to interpret the results from the acid producing leach tests. As described in Chapter 2, humidity cells are the standard leach test for predicting long term drainage quality from mine tailings. In this testing program, humidity cells were operated at 20°, 3° and 1°C.

The nature of the humidity cell test, however, does not permit testing at sub-zero temperatures, as the cells would dramatically reducing the permeability thus hindering the ability to leach fluid through the oxidizing solids. Therefore, in order to track the oxidation of sulfides below 0°C, the static batch test was developed to simulate insitu weathering of mine tailings at temperatures above and below 0°C. The objective of the testing program was to develop a correlation between the humidity cell tests (the standard weathering test) and the batch tests at 20°, 3° and 1.5°. Using this relationship between the humidity and batch cells, results of the batch tests conducted at 0°, -1.5°, -3° and -20°C could be extrapolated to obtain equivalent humidity cell weathering rates at sub-zero temperatures.

4.1 PHYSICAL CHARACTERIZATION

This section describes the baseline characterization testing that was performed on the non-weathered tailings excavated from below the cop in the delta as well as the core sample of weathered tailings from Discovery Mine, including physical, geochemical and microbial tests. Previous material characterization programs are included where applicable. The grain size distribution, metals content and some geochemical data were determined for the bulk Faro material. The characterization of this material is limited to the data relevant for the geochemical analyses and comparison with the tests from Discovery.

4.1.1 Grain Size Distribution

Grain size distribution curves (Fig. 4-1) were obtained for the bulk Discovery tailings sample using standard sieve and hydrometer tests, showing approximately 35% fine sand, 60% silt, and less than 5% clay sized particles. The grain size distribution assists in defining the moisture retention curves, in addition to giving insight into the specific surface area of the samples.

Previous grain size distributions have been determined on the sample of sands and gravels from the esker, the lacustrine deposit southest of the mine, the underwater tailings, and from test pits located on the 'delta' and at the north end of the airstrip. Klohn Leonoff (1992) estimated that the tailings grain sizes are approximately 75% passing the 200 mesh (i.e. less than 75 micron, or silt size or smaller).

Figure 4-1 also shows the grain size distribution for the Faro material. The bulk tailings used for the humidity and batch cells contain approximately 65% fine sand, 34% silt and less than 1% clay size particles.

4.1.2 Atterberg Limits

Atterberg limits are indicators of clay content, which is an indicator of the clay size fraction activity. The activity is useful in predicting the unfrozen water content, as well as determining soil metal sorption during leaching.

Previous Atterberg Limits have been performed on the Discovery Tailings (Klohn Leonoff, 1992). The liquid limit, plastic limit and plasticity index were 40, 28 and 12%, respectively. The tailings collected from Discovery Mine for this study exhibited no plasticity. It is uncertain, then, what material the previous study (Klohn Leonoff, 1992) had analyzed.

4.1.3 Mineralogical Speciation

Mineralogical speciation provides baseline information of the mineral composition of the material, indicating the types of minerals present. When combined with leachate data, the presence of various minerals provides insight into the insitu electrochemical and geochemical regime, not obtainable with leachate alone. By testing the core of soil that spanned weathered and non-weathered zones, an absolute scale could be made of the long-term metal migration behavior of the deposit.

It was planned to record the degree of weathering from weathered at the surface, to non-weathered and potential acid generating at depth. This would have created a reference against which the leaching tests (Section 4.4) could be compared to determine the relative oxidation state and the remaining acid potential of the tested sample, whether humidity cell or batch test. Because the humidity cells from Discovery Mine failed to generate acidic conditions however, a complete mineralogical determination was never performed along the column, and was limited to the bulk unweathered sample.

Accoring to Sutherland and Hall (1989) the source sulfidic minerals include pyrite, pyrrotite, galena, arsenopyrite and chalcopyrite. Combined, these minerals compose less than 1% of the total mass. The mineral processing resulted in the addition of mercury (in mercury amalgamation), cyanide, zinc and lead (cyanidation with zinc dust and lead salt). No previous record was found identifying the non-acid forming minerals within the tailings.

Identification of all the minerals present in the weathered and unweathered Discovery tailings was attempted using x-ray diffraction; however, the interpretation was complicated, likely due to the abundance of constituents and residual processing chemicals (Figures 4-2 and 4-3). Additional factors may include the presence of

secondary and tertiary minerals as described in Chapter 2. In decreasing % fraction. the x-ray diffraction patterns suggest the presence of:

Quartz	SiO_2
Albite	$(Na,Ca)\ Al\ (Si,Al)_3O_8$
Anorthite	$CaAl_2Si_2O_8$
Muscovite	$(K,Ba,Na)_{0.75}(Al,Mg,Cr,V)_2(Si,Al,V)_4O_{10}$
Clinochlore	$(Mg,Fe,Al)_6(Si,Al)_4O_{10}(OH)_8$
Gypsum	$CaSO_4 \cdot 2H_2O$
Ferroactinolite	$(Ca,Na,K)_2Fe_5Si_8O_{22}(OH)_2$

The complete array of x-ray patterns is included in Appendix A. Due to the low iron content (see below), these minerals do not offer significant insight into the insitu electrochemical regime.

4.1.4 Metals analysis

Klohn Leonoff (1992) contains records of a total metals analysis conducted by Norwest Labs (Appendix B). A soil analysis was also performed on several samples, and includes pH, EC, TOC, total and sulfate sulfur, major cations, and Sodium Adsorption Ratio. These are shown in Table 4-1. The assay from the Faro material is included in this table for comparison purposes.

In addition to the standard Induced Coupled Plasma spectrophotometry soil scans for 26 metals on the original non-weathered tailings, a non-conventional elemental analysis was performed using Neutron Activation Analysis. This test was made available by the SLOWPOKE Reactor at the University of Alberta on a trial basis for two samples.

Neutron Activation Analysis involves the irradiation of a sample in a nuclear reactor (the source of neutrons), in which an extremely small fraction of the isotopes of the various elements absorbs or captures a neutron and becomes a new nuclide. In many instances

these new isotopes or nuclides are radioactive and decay emitting characteristic gamma-rays. Detection and counting these gamma-rays provides the means of elemental analysis: the energy of the gamma photons is used to identify the parent element and the intensity or number of gamma-rays is directly proportional to the concentration of the element. The method is multi-elemental, nondestructive, and matrix independent (Duke. 1999).

A weathered and non-weathered sample were tested, with the results recorded in Table 4-2. The error shown is % uncertainty, which is a function of the counting statistics. Counting statistics relate to the size ("area") of the photopeak of the individual 'elements' compared to the background counts (the peaks ride on a background). The statistical uncertainty (in %) is given by:

$$E = \sqrt{A + 2B} \cdot \frac{A}{100} \qquad \text{Eq. 4-1}$$

where A = peak area counts, B = background counts. Hence, the greater the area to background ratio the lower the statistical uncertainty.

The results obtained by NAA were significantly different than the results by ICP. This difference was believed to be primarily due to heterogeneity in the tailings, though some uncertainty existed in both methods of analysis. Because the NAA sampling was performed on a trial basis, care was not taken to ensure that the tailings samples were obtained from the same location. As such, the results were not compared for inaccuracies between methods, but instead as indicators of the heterogeneity within the bulk Discovery samples. The dominant error using ICP was likely due to incomplete digestion. Some of the metals may have been incompletely dissolved, indicating concentrations less than the NAA. Additionally, the error of testing non-representative sub-samples was present, due to the lack of replicates performed. The errors involved in NAA are fewer. though still subject to sampling discrepancies. NAA involves scanning a very small surface area of material, as the gamma-rays are emitted from the surface. Within a

testing area of 1cm^2, there may be several larger grains of one mineral, resulting in non-representative concentrations.

4.1.5 Acid Base Accounting

In addition to elemental and mineralogical characterization, the bulk and core samples were also tested for their acid generation potential using the Modified Sobek Test. The traditional acid-base accounting techniques provide a measurement of the likelihood to produce acid drainage, literally accounting for the different total contents of acids and bases within the mineral geochemistry (Morin, 1990). These were described in Section 2.3. A complete description of Modified Sobek test is provided in Appendix C.

This test determines the balance between acid producing and acid consuming components of the tailings, but offers no insight into the rate of dissolution of constituents. It is possible that the acid neutralizing carbonates are preferentially dissolved in the early stages of weathering, with little acidity formed. If, after a significant portion of the neutralizing potential has been removed, the acidity begins to be generated, then the leachate will become acidic despite an overall balance of acid forming and neutralizing material. Therefore, as mentioned previously, static tests should be used only as an indicator of acid drainage potential, and a guide for future kinetic testing.

The Discovery Mine tailings sulfur content is 0.544% as determined by Norwest Laboratories analysis. The Modified Sobek method, gave an acid potential (AP) of 17 kg $CaCO_3$/tonne. The neutralizing potential (NP) is 26 kg $CaCO_3$/tonne, resulting in a net neutralizing potential (NNP) of 9 kg $CaCO_3$/tonne and NP:AP of 1.5. As described in Chapter 3, a sample with an NNP between +20 and –20 kg $CaCO_3$/tonne is considered possibly acid generating, and an NP:AP ratio between 1:1 and 3:1 is considered inconclusive. The acidity measured in the field and preliminary results of pH vs depth from the recovered core (Figure 4-4) indicates that the samples would likely produce acid if field conditions could be replicated.

The Faro tailings sulfur content is 22.1% as analyzed by Norwest Laboratories, with a NNP of –690 kg $CaCO_3$/tonne. With <1% carbonate content, the tailings will certainly generate acid.

4.1.6 Soil-Moisture Characteristic Curves

The soil-moisture characteristic curves relate the matric suction to the water content in unsaturated soils, and are important in characterizing the transport of the water, especially in the field. These curves can be used to predict the moisture content of the tailings after drying. Moisture content and related degree of saturation also affect oxygen and carbon dioxide transport.

Testing to determine the soil-moisture characteristic curve was performed using a standard pressure plate extractor apparatus (ASTM D3152) (Fig 4-5). This test involved subjecting remolded saturated specimens of tailings to suctions varying from 33 to 1500 kPa.

The samples were placed on ceramic plates (Figure 4-6) that have a specific air entry pressure, and allowed to soak for 2 hours. The plates were then placed into the pressure plate extractor, and suction was applied. Over the next 48 hours, the pressure in the cell and samples was allowed to equilibrate as the water contained in the pore space, having a capillary pressure less than the suction applied, was drained. The samples were then weighed, heated for 24 hours at 105°C and re-weighed to determine the moisture content. This procedure was repeated for each desired suction, and the results were plotted to create a soil-water characteristic curve. Figure 4-7 shows the characteristic curve for the Discovery tailings determined in this study.

4.2 THERMAL CHARACTERIZATION

The second component to the testing involved subjecting the tailings to sub-zero temperatures and determining the unfrozen water content, freezing point depression and

thermal conductivity. The characterization performed included both the bulk material from Discovery and Faro mines.

4.2.1 Unfrozen Water Content / Freezing Point Depression

One of the key parameters in sub-zero thermal property testing is the determination of the unfrozen water content. Like water, ice inhibits the transport of dissolved oxygen to the reactive surfaces, thereby restricting sulfide oxidation. It also inhibits water movement and requires significant heat to generate a phase change, thereby acting as a heat sink. Additionally, as the ice content increases, the permeability of the soil decreases, limiting the amount of leachate.

There are two common methods utilized to determine the unfrozen water content of a sample, Time Domain Reflectometry (TDR) and Nuclear Magnetic Resonance (NMR). The NMR operates on the basis of energy absorption of radio frequencies by the hydrogen protons contained in the liquid water. When a soil-water mixture is placed in a pulsed NMR analyzer and a single radio frequency pulse is applied, a voltage is induced in a receiver coil that surrounds the specimen. This voltage is detected by the analyzer and compared against the background value. This difference is proportional to the amount of water in the mixture (Smith and Tice, 1988).

The unfrozen water content in the unweathered Discovery tailings was measured using TDR. These tests operate on the principle of measuring the dielectric constant of a material (K_a – no units), a measurement of the capacity to store electrical potential energy under the influence of an electric field relative to that of air, which is assigned a value of 1.0 (Grozic, 1997). The higher the value of K_a, the slower the propagation velocity of an electromagnetic wave as it passes through a material. Under an electric field, the charged molecules become polarized and aligned. K_a for water at 20°C is approximately 80; in its frozen state, the water molecules are not as readily aligned in the electromagnetic field. and have a K_a of approximately 3.2 (Lefebvre, 1997). The dielectric constant of a soil varies with water content, concentration of soluble salts, and soil density. The presence

of elevated metal concentrations in the soil has also been reported to affect results (Grozic, 1999)

The testing apparatus is a 4-wire probe, which is embedded in a saturated sample (Fig. 4-8). An RTD is used to determine the temperature. The TDR emits a small, fast rising step pulse that is reflected from the end of the waveguide (Fig. 4-9) and returns to the receiver producing a waveform. The relationship between the actual length of the probe and the calculated the wave length (from point A to B) generated by the pulse can be translated into the dielectric constant and ultimately, the unfrozen water content (Grozic, 1998).

The unfrozen volumetric water content was calculated using the polynomial proposed by Smith and Tice (1988).

$$\theta_u = -1.458 \times 10^{-1} + 3.868 \times 10^{-2} \cdot Ka - 8.502 \times 10^{-4} \cdot Ka^2 + 9.92 \times 10^{-6} \cdot Ka^3 \qquad \text{Eq. 4-2}$$

The Discovery Mine tailings were tested for unfrozen water content at temperatures from −10° to +2°C (Fig. 4-10). The figure shows a significant increase in the volumetric unfrozen water content from 1% at approximately −3°C, to 5% (or 4% as expressed as % dry wt.) at −1.5°C, then rose rapidly to 60% (43% dry wt.) at above 0°C. This test was run a second time in parallel with the Faro mine material. These results are also shown in Figure 4-10. The second run did not confirm any results colder than -1.5°C though, as the TDR did not register a valid waveform for the lower temperatures. It is unknown why this occurred.

The unfrozen water content for the Faro tailings are also shown on Figure 4-10. At the temperatures measured, down to approximately -20°C, the volumetric unfrozen water content did not drop below 28% (11% dry wt.). It increased slowly to 32% (12% dry wt.) at -5°C, 40% at -2°C and 56% (22% dry wt.) above 0°C.

4.2.2 Thermal Conductivity

Part of the thermal characterization includes determining the rate at which the heat will transfer. This parameter is necessary for calculating the rate and depth of freezing/thawing. This test was performed at temperatures varying from –10° to +20°C

There are two standard methods for determining thermal conductivity: by thermal needle probe (ASTM Standard D5334-92) and by the guarded hot plate apparatus (ASTM Standard C177-97). The thermal needle probe was used in this study (Fig. 4-11).

Figure 4-12 shows the changes in thermal conductivity, K, with temperature. For Discovery tailings, the frozen conductivity was 3.3 W/m°C; the unfrozen conductivity was 1.6 W/m°C. A complete record of the tests is included in Appendix D.

The Faro tailings had a frozen thermal conductivity of 5.1 W/m°C and an unfrozen conductivity of 3.1 W/m°C.

4.3 MICROBIAL CHARACTERIZATION

At the onset of the leaching program, microbial characterization was not considered important. It was assumed that the bacteria would be present and that their effects would be quantitatively assessed throughout the testing program; however, after the initial testing sequence was completed without achieving acidic conditions, this assumption was re-examined. It was postulated that this failure to generate acidic leachate was partially due to:

- An absence of AMD catalyzing bacteria due to their destruction during testing, or
- A natural absence of AMD catalyzing bacteria in the tailings

To determine if either of these reasons was accurate, a bacterial characterization of the samples was conducted. The first stage of tests included solidified media, agar plate counts.

4.3.1 Agar Plate Counts

Bacteria growth is defined in several ways (Koch, 1994):

- The ability of individual cells to multiply (i.e., to initiate and complete cell division)
- An increase in colony forming units (CFU)
- An increase in biomass
- The ability of the organisms to chemically alter their environment as a consequence of the increase in biomass

Solidified media (agar plates) are used to grow separated colonies from individual cells in a population. By adjusting the nutrients and pH of the media, and by inoculating the media with tailings, growth of certain types of bacteria can be facilitated. Due to countless number of variables though, a perfect media is not likely to be created, and the bacteria that are present and active in the field may not be the same that are grown in the laboratory. It is important to note that though the presence of a type of bacteria in the laboratory does confirm its presence in the field, the converse is not always the case, and the bacteria in the field may not grow under the controlled conditions in the laboratory. Despite this degree of uncertainty, it is possible to gain an understanding of what may be active in the field from laboratory results.

This discussion is restricted to describing the steps performed. Cultures (Appendix E) were prepared to test for the presence of sulfur oxidizing bacteria in neutral and acidic conditions, for iron oxidizing bacteria at neutral acidity and for a total count of heterotrophs.

The liquid media onto which the specimens were to be placed was mixed, adjusted for pH, then brought to a boil to completely dissolve the agar. While molten, the media was dispensed into sterile petri plates and allowed to set. Once set, the agar dishes were stored in polyethylene bags to prevent severe drying. The plates were placed in the dark, to prevent photochemical generation of hydrogen peroxide or other toxic forms of oxygen

which can render the media inhibitory for the growth of bacteria (Krieg and Gerhardt. 1994). Sterile conditions were desirable, but due to the nature of the soil inoculum. this was not deemed essential.

The plates were then inoculated with solutions of tailings using standard spread plate techniques (Koch, 1994). The inoculates included material:

- stored at 3° that had not been handled since being transported from the Discovery site.
- that had been frozen at -20° to ensure dryness,
- from a humidity cell operating at 1°,
- from a humidity cell operating at 20°, and
- from the weathered portion of the tailings core extracted from the airstrip site.

These locations were selected to determine the stage of the test, if any, at which the bacteria were dying.

Each inoculum was administered in a series of diluents, from 10^{-1} to 10^{-5}, to ensure that at least one dish contained between 30 and 300 colonies. In total, 20 sets of diluents were run. using 5 inoculum and testing for 4 types of bacteria. The colonies were counted after 2, 4 and 8 weeks. The results from these tests are shown in Table 4-3.

As seen in Table 4-3, approximately 40,000-60,000 colony-forming units (cfu) per gram of the original bulk sample grew on the PCA heterotrophic media. This represents an approximation of the total bacteria count present in the samples. On similar plates. the samples that had been frozen, dried and stored at –20°C, grew approximately 100 cfu/g. indicating that significant damage had occurred as a result of this process. In the material from both the 20°C and the 1°C humidity cells grew approximately 1,000,000 cfu/g. This demonstrates that the conditions in the different cells are similar and that no significant damage took place at the cooler temperatures. This material had also been previously dried and frozen, indicating that the bacteria was capable of recovering from

the drying/freezing process. Finally, material from the weathered portion of the tailings core grew approximately 3,500 to 7,000 cfu/g.

The second media culture was intended to grow iron oxidizers. The only samples to produce growth were the 1°C cell, at approximately 40 cfu/g and the insitu material. at roughly 1,100 to 2000 cfu/g. If the material used in the humidity and batch cells contained any iron oxidizers at all, they were very limited. That they were present in the core sample indicates that iron oxidizers are present at the site, though likely not at depth.

The third media attempted to grow acidophilic sulfide oxidizing bacteria. Between 1,300 and 3,000 cfu/g were present in the bulk media, representing approximately 10% of the bacteria present. Similar to the heterotrophs, the freezing and drying of the samples prevented the growth of bacteria, but again, these were able to recover for both humidity cells. However, in the humidity cells, the acidophilic sulfide oxidizers, at approximately 15,000 cfu/gram of soil, represent only 1% of the total heterotrophs. It is uncertain what produced this difference. Approximately 4,400 to 5,000 cfu/g grew from the weathered inoculum, indicating that they are present on the surface and at depth at the sampling site.

The final media had favorable conditions for neutrophilic sulfide oxidizers (bacteria preferring neutral pHs). The bulk sample inoculum grew between 150,000 and 200,000 cfu / gram of tailings. This is slightly more than the total heterotroph count, indicating that a large portion of the total bacteria at depth in the tailings are sulfide oxidizers. Between 160 and 200 cfu/g grew from the frozen and dried material, suggesting that these bacteria are more resilient to harsh conditions than the acidophilic bacteria. Similarly in the humidity cell samples, the number of neutrophilic sulfide oxidizers are comparable to the total number of heterotrophs present, again suggesting that a majority of the bacteria present in the samples are sulfide oxidizers. The weathered samples did not generate any bacteria growth at all. This suggests that in the lower pH zones at the site, the acidophilic bacteria are more dominant, and that even though some of the acidophilic bacteria may be able to survive in neutral conditions, the neutrophilic bacteria are incapable of surviving in an acidic environment.

4.3.2 Enrichment Cells

The second stage of microbial characterization included shake flask enrichment cells. designed to enrich / inoculate the static batch tests. The shake flask test is a standard technique used to confirm the results of static predictions in acid base accounting and is useful for determining the reactivity of material as a function of time. It is also used in the microbiological field for enriching cultures and tracking the growth of bacteria as a function of pH.

The experiment was run using 2 inoculates described below, with 3 different energy sources (elemental sulfur, pyrite and ferrous sulfate), at 3 temperatures (20°, 10° and 4°C), in acidic and neutral conditions. The inoculate came from samples of tailings from Faro Mine, Yukon, one from the surface of the tailings facility and the other from a depth of two meters in the same location. The sample from 2m depth was similar to the material used in the second round of humidity cells and static batch tests. The surface material was used for comparison purposes and as a potential source for cross-inoculation. The recipes for the liquid media are shown in Appendix E.

Each medium was prepared and 100 mL distributed into each of 14 – 250 mL flasks. Fifty grams of inoculum (bulk or surface material) was added to each and the pH adjusted to 3 or 6. The sterile samples were adjusted to the appropriate pH, but no inoculum was added. These flasks were placed on shaker tables rotating at 150 rpm in constant temperature rooms at 20°, 10° and 4°C. Including sterile controls, there were 42 shake flasks operating. These were tested for pH at regular intervals to determine the changes with time.

These results (Figure 4-13) were inconclusive in determining the presence of sulfide oxidizing microbes, due to the variation in the control sample acidity levels. While pH levels were extremely low, there was concern that this was the result of chemical activity.

4.3.3 Transmitting Electron Microscope

Based on the lack of success of the shake flask tests, attempts were made to visually confirm the presence of bacteria. At low magnification (100x), this was inconclusive, as no movement was noted; however, there were several non-mobile particles that were bacteria sized. To confirm that these were in fact bacteria, and not fine clay particles, samples of the enrichment cultures were brought to the transmitting electron microscope in the Department of Biological Sciences at the University of Alberta. Here, the particles were positively identified as bacteria. Samples are shown in Figures 4-14 and 4-15. The finer elongated bacteria are believed to be sulfide oxidizers; the more oval bacteria are believed to be iron oxidizers, based upon the media in which they grew.

4.3.4 Batch Cell Inoculations

Once it was determined that bacteria were present in the bulk tailings material from Faro, another set of 6 enrichment flasks were initiated. Each 2 L flask contained 50g tailings samples from each of Discovery Mine and Faro Mine, and either elemental sulfur (S°) or ferrous sulfate ($FeSO_4 \cdot 7H_2O$) were added (see recipes in Appendix E). Over a period of approximately 3 weeks, the pH dropped from more than 2.4 to 1.9 in the iron media, and from 3.4 to 1.9 in the sulfur media.

The flasks were then centrifuged at 8000 rpm for 20 minutes to harvest the biomass. Collected in sludge form, the biomass was then re-suspended in 50mL of water, then transferred into a 5L flask with a pH between 4 and 5. This was to prevent any undue shock to the bacteria. Once re-suspended in 5 L of water, 50mL aliquots were dispensed into selected batch cells.

4.4 ACID GENERATING CHARACTERIZATION

This section describes the tests performed to characterize the acid generating processes. The humidity cell test is a standard leaching test that has been performed on a variety of materials and provides a means for comparison with results from previous studies. This

test was run at 20°, 3° and 1°C; however, due to the nature of the test, it could not be run at sub-zero temperatures. To expand the acid generating characterization to sub-zero temperatures, the batch cell tests were developed.

4.4.1 Humidity Cells

As described in Section 2.3.2, the humidity cell (Fig. 4-16) is a weathering chamber which provides simple control over air, temperature and moisture, while allowing for the removal of weathering products in solution which can then be analyzed to 1) determine the onset of AMD, 2) calculate mass loads, 3) determine the rate of acid generation, and 4) determine the concentration of metals and other species as a function of time (Coastech Research Inc, 1990). In the current testing program, the intent was not to generate field-predictive results, but to establish a weathering pattern showing differences with temperature.

This series of tests was the central component of the testing program in this study, as it accelerated the natural weathering rate of a solid material sample so that diagnostic weathering products could be produced, collected and quantified. To simulate the effects of leaching at different temperatures, cells were operated at 20°, 3° and 1C°.

The test procedure was composed of three stages that comprise a single cycle:

Stage 1. 1000g of non-weathered tailings was placed into the cell. 500 mL of distilled water was drip-trickled into the cell, sufficient to wet all the solids. This water was allowed to soak for 1 hour, then drained through the cell base. The leachate was tested for acidity, conductivity, redox potential and sulfate, according to the testing schedule.

Stage 2. The sample was dried, using air that has passed through a dessication column (humidity < 10%), for 4-5 days, depending on the time for drying. Due to the differences in relative humidity from 20° to 1°C, the cooler samples took longer to dry.

Stage 3. Humid air (~95% RH) was then pumped through the cell for 3 days, insufficient to wet it, but enough to moisten the mineral surfaces. This completed a single cycle.

Stage 4. Steps 1-3 were repeated, using the same tailings. This cycle was repeated for 20 cycles, or until significant data was obtained to track acid production

4.4.1.1 Apparatus

The cells were 20.3 cm ID by 10.2 cm height, designed for accommodating solid material samples that pass a 150 micron sieve (Fig. 4-16). They were fabricated using cast acrylic tube and have inlet/outlet ports on the top, bottom, and side. The side port was located approximately 1 inch above the base to accommodate water collection during the leaching phase. In the second round of tests, this port was raised an inch and used for air flow instead of water.

A perforated disk, described in the ASTM standard as "comprised of materials suitable to the nature of the analysis to be performed", was suggested to support the solid material and prevent the migration of material. Due to the prohibitive cost involved, the disks were initially replaced by geo-material. Five layers of approximately ¼ inch non-reactive geonet were placed on the base of the humidity cell. These were intended to support the sample above the base of the cell and prevent the onset of a single preferential flow path through center of the sample. The upper geonet was lined with approximately 150g/m^2 nonwoven needle punched geosynthetic and was secured to the cell walls using silicon. The apparatus operated as intended, as the air flowed through several routes, and was not limited to a single area. There was some difficulty in maintaining a consistent thickness of tailings above the textile, though not unmanageable.

Later experiments showed that the geonet was not necessary, as placing the tailings directly on the base of the cell created a cell similar to a desiccation chamber (Section 4.1.6). Instead of generating a single preferred airflow path through the center of the sample, the tailings mass acted as a continuous soil-water column.

To prevent a loss of fines from the cells, two layers of glass microfibre filter (1.5 micron) were placed covering the exit port on the base of the cell. An additional layer of non-woven geotextile covered the filter as a protective shield against damage from grain penetration and/or pressure. The microfibre filter was necessary, as it is non-reactive with sulfuric acid and at the onset of the test, predictions of the final acidity of the leachate were uncertain.

The humidity cells were table-mounted at a height sufficient to accommodate the placement of both humidifier and one volumetric flask beneath the cells (Fig. 4-17). The humidifier was constructed with the suggested dimensions of 12 cm ID by 40 cm long. To operate the wetting phase of the cycle, the following equipment was required:

Aeration hose, similar to aquarium-aeration equipment, to bubble air into the humidifier water.
Copper coil, to regulate the air temperature. A length of approximately 4-5m was required for the 3° and 1° setups (Figure 4-18).

During the water-saturated and dry-air portions of each weekly cycle, feed air was metered at the bottom of each cell. The humid airflow was regulated to approximately 2 L/min/cell. Feed air for the three-day dry-air portion was routed first through the desiccant column then through the manifold to each of the cells. The dry air flow rate was varied to increase or retard the rate of drying in order to maintain similar moisture contents in each cell.

Feed air for the high humidity air portion of the cycle was routed through the water-filled humidifier and aeration hose to the humidity cells. The inlet air was routed to the top of the cell. All the air that passed through the cells was first passed through a bacteria filter which retains 99.99% of 0.1 micron particles. Each cell outlet was equipped with flexible tubing quick connect attachments and clamps to regulate flow. At the end of the

air phases, the seperatory funnels were mounted above the cells to flood leach the cells. Volumetric flasks were located beneath each cell to collect the leachate.

4.4.1.2 Sample Preparation

The tailings samples collected from the Discovery Mine were stored in a 3° cooler until the humidity cells were prepared. Due to sediment settling within the 20L buckets, a water cap was present. This ensured that the samples had little access to O_2, as only the dissolved oxygen was present with the exception of the air in the void space above the water level. The lid remained sealed until the samples were ready for testing. Prior to taking sub-samples, the bulk material was re-agitated to suspend and homogenize the solids in the water. Representative samples were collected for material characterization (sulfate, pH, Eh).

4.4.1.3 Humidity Cell Operation

Cell Loading

Each humidity cell (including lids, but not hoses) was weighed, and the tare recorded. This was important for determining the moisture content of the cells at the end of the drying stage. Approximately 1000g of tailings solids were then loaded into each cell. To minimize sample disturbance, the tailings were loaded wet, and the actual dry mass back calculated.

First Leach

The first leach designated the start of the weekly test. Half a liter of distilled water, chilled to the cell operating temperature, was measured into the separatory funnels which were drained into the cells from the inlet at the top. The cells were then flooded and allowed to sit for 1 hour. On several occasions, it became necessary to agitate the sample to ensure water and air contact with mineral grains. Depending on the volume of the non-reacting material, the sample was either rotated aggressively to cause liquefaction and induce pore fluid mixing, or the sample was physically agitated using a stir rod. This was done as quickly as possible to limit potential bacterial infiltration.

After 1 hour, the water outlet was opened and the water was drained into volumetric flasks. Due to the fine grain sizes, drainage was occasionally impeded. In these cases, to remove any pooled water on the surface, air pressure was applied to force the water through the sample.

The collected leachate was tested for pH and sulfate concentrations using ion chromatography. The pH of the samples was measured as soon as possible to prevent reaction with the atmospheric carbon dioxide. The remaining solution was stored in collection bottles at 3° that were stored for later testing.

Air Cycles

After the leachate was collected, the samples were dried to between 5 and 7% moisture content by passing dry air through the cells. The incoming air was dried using a desiccant column. The airflow rate was monitored using air-exit port bubblers to ensure even distribution. If a single cell dried earlier in the cycle, the flow to that cell was restricted by increasing the backpressure on the air exit port. This stage typically lasted 3-5 days, depending on the temperature of the cell, because at lower temperatures the relative humidity of the air is significantly greater than at higher temperatures, and the passing air is less able to draw water from the soil. To ensure that the air was cooled the correct temperature for the 3° and 1° cells, it was passed through a 4 m length of copper tubing which was at the ambient temperature of the chamber.

Once the cells were dried, the air was routed through the humidifier via an aeration tube before passing through the cells. The relative humidity of the air was known to be near 100%, as evidenced by condensation in the tubing. This stage lasted approximately 3 days.

Subsequent Cycles

Once the cells appeared moist, the cell was re-weighed and the cycle was repeated.

4.4.1.4 Humidity Cell Results

Discovery Mine

The first set of humidity cells, using material from Discovery Mine, ran from January to April, 1999. At each of the 3 temperatures, 6 individual cells were run. At the onset, 3 cells per temperature were selected for data recording. During the course of the test period, if the results from a single leach was contaminated or lost, then the data was obtained from a backup. The results for the change of pH with time are shown in Figure 4-19. Appendix F contains the data for each separate cell. For the 20°C cells, the initial pHs were 7.0 ± 0.3. Over the 12 week period, the pH in each of the monitored cells increased to between 7.5 and 8.0, with slight fluctuations of ±0.2 pH units. The 3°C cells had initial pHs of 6.5±0.3 and increased to 7.5±0.3 over the following 11 weeks. The 1°C cells had initial pHs of 7.8±0.1. Over the next 8 weeks, these did not fluctuate beyond 7.5±0.4. Early readings of the redox potential showed Eh varying from +50 to +400mV, with no differentiating between temperature or time.

Sulfate levels were also used as an indicator for acid production, however, as seen in Figure 4-19, these levels were minimal, never exceeding 300ppm.

Faro Mine

A second series of humidity cells were started in January 2000, using tailings from the Faro mine site. Each temperatures setup contained three cells.

Sulfate levels and pH were again used as indicators for acid generation. Figure 4-20 shows the average pH from the 3 readings with time for each temperature. Figures 4-21 a-c show the pH with time for each temperature. The y-axis error bars represent 1 standard deviation from the averaged values. Appendix F contains the data for each separate cell.

The 20°C cells had average initial pHs of 2.8±0.1 and increased to a maximum of 4.1±0.2. The peak for the 20°C data on Figure 4-20 occurred at approximately 6 weeks.

A 4th degree polynomial curve was fitted using MS Excel, with an coefficient of determination (R^2-value) of 0.881 (Eq. 4-1). The deviations from the curve are primarily due to the differences in the peak times between cells. After the peak at 6 weeks. the average pH drops approximately 0.05 units per cycle.

$$pH_{20°} = -0.0001x^4 + 0.0056x^3 - 0.10x^2 + 0.73x + 2.14 \quad \text{Eq. 4-1}$$

The 3°C cells had average initial pHs of 2.8±0.4 and increased to a maximum of 4.9 in two cells and 4.5 in the other. The pH peaked after 13 weeks at approximately 4.4. Similar to the 20°C cells, the data was fitted with a 4th degree polynomial curve using MS Excel, with an R^2-value of 0.902 (Eq. 4-2). After the peak, the trend line indicates a decrease in pH of approximately 0.04 units per cycle.

$$pH_{3°} = 0.00005x^4 - 0.0021x^3 + 0.21x^2 + 0.10x + 2.73 \quad \text{Eq. 4-2}$$

The 1°C cells had average initial pHs of 2.7±0.1 and increased to a maximum of 5.0 in two cells and 4.7 in the other. It remains uncertain if a peak had occurred, because the results end after 14 weeks at an average pH of 4.4. The curve was fitted using MS Excel based on subjectively selected data points (Eq. 4-3). No regression analysis was performed

$$pH_{1°} = 0.00005x^4 - 0.0015x^3 - 0.0015\,x^2 + 0.3313x + 2.3622 \quad \text{Eq. 4-3}$$

Figures 4-22 a-c show the concentrations of sulfate with time, reported in mg/L as received from the Soil Science laboratory at the University of Alberta and Norwest Laboratories. Figures 4-23 a-c show the total sulfate mass released with time, calculated by multiplying the concentration of sulfate by the volume of leachate collected. By tracking cumulative total sulfate, the effects of outlying points were limited as overall trends could be traced (Figure 4-24). Figure 4-24 does not include the sulfate from the first cycle to reduce the possible influence of rinsing soluble salts. The 20°C cells had average initial sulfate concentration of approximately 1000 mg/L, then dipped to 500 and

rose to between 1500 and 1000 mg/L for the remainder of the test. There appeared to be a peak in sulfate concentration at 7-8 cycles, with a dip at 11-12 cycles and then again rising. The 3°C cells displayed the same initial drop in sulfate levels, from 800 to 300 mg/L, which remained at approximately 300-400 mg/L for the first 12 cycles, then rose near the end of the test. The 1°C cells showed the initial drop followed by a shortened period at approximately 400 mg/L then rose near the end of the test.

The original intent was also to test for redox potential to determine the expected equilibrium constituents. Figure 4-25 shows a pH-Eh diagram for iron sulfides. By determining the redox potential and pH, it would be possible to predict the sulfur and iron species in solution after leaching, thereby assisting in the interpretation of the insitu kinetics and the intermediate reactions (Equations 2-2 to 2-5) that may or may not be occurring.

Early redox potential readings for the Faro tailings humidity cells were between +150mV and +220mV. Area A in Figure 4-25 shows the approximate operating Eh-pH state for the Faro humidity cells. As described above, the Eh readings were extremely variable. Area B shows the Eh-pH region that the Discovery humidity cells operated in for the duration of the test. Despite the fact that the Faro tailings had a lower redox potential than the Discovery material, the neutralizing potential of the Discovery material prevented the generation of acidity.

4.4.2 Batch Cell Test

Tailings were placed in 500 mL tissue culture flasks (Figure 4-26) and were subjected to a constant temperature at moisture contents slightly below field capacity for extended periods. The enclosed tailings had access to atmospheric oxygen through a tube covered with a moisture-impermeable, oxygen-permeable membrane, with the intent of maintaining aerobic conditions at original moisture contents for the duration of the test.

As described previously, the purpose of the batch cell test was to provide an index for reconciliation with the standard humidity cells. By developing a relationship between the two test methods above 0°C, the oxidation rates of the batch cells below 0°C could be converted to standardized 'equivalent humidity cell' oxidation rates.

4.4.2.1 Sample Preparation

The first round of tests on the Discovery tailings included an attempt to quantify the abiotic portion of the acid generation, using sterilized tailings samples. Initial attempts to sterilize the samples using dry heat at 170°C revealed extensive oxidation of the samples. A survey of the literature on the sterilization of soil indicated that methods included autoclaving, dry heat, gamma-radiation, microwaves, cholorform, mercuric chloride and sodium azide. Of these gamma-radiation was considered the most effective method (Trevors, 1996; Lotrario et al., 1995; McLaren,1969), but conflicting opinions were found. Several sources (Brickett et al.,1995; Tuominen et al., 1994; Wolf et al..1989) stated that irradiation has significant effects on the mineralogy of the soil, with possible results including the creation of free hydrogen and hydroxyl radicals, which may act as reducing or oxidizing agents (Tuominen, 1994), or an increase in extractable manganese (Wolf et al., 1989). McLaren (1969) also notes that increases in soluble carbohydrates and organic may occur following a dose of 3 Mrad of gamma-radiation, but he did not consider these effects significant. Trevors (1999) maintained that given the various limitations of each method, cobalt-60 radiation is the best solution.

In total, 4000 g of solid tailings were sterilized using a Gammacell 220 cobalt-60 irradiation unit. Approximately 1000 g samples could be irradiated at a time, and required 10 days of exposure at 0.21 Mrads/day for a total dose of 2 Mrads, sufficient for suppressing elemental soil sulfur oxidation (McLaren, 1969). Due to the time constraints and the extreme difficulty in maintaining a sterile environment using humidity cells, the sterile tests were limited to batch cell reaction tests at 20°, 10°, 3°, 1.5°, 0°, −1.5° and -3°C.

Until the time for sterilization, the tailings were stored in the cool room at approximately 3 °C to minimize reactions.

4.4.2.2 Experimental Constraints

Moisture Content / Oxygen Availability. Due to the high silt content (see Section 4.1.1 - Grain Size Distribution), cementing of the samples was a concern, in that oxygen flow to lower portions of the sample may have been impeded, especially in the sub-zero cells. Conversely, water had to be in sufficient supply to permit active oxidation. Thus, it was decided that the cells were to be maintained at moisture contents of approximately 15%. This corresponds to approximately 50% saturation. It was found that any increase in moisture above this led to sample liquefaction. For the first round of tests using Discovery Mine tailings, the material was dried using Buchner filtration flasks. In the second round of testing using Faro Mine tailings, 50 mL of sterile distilled water was *added* to each flask as the field moisture content was only 3%.

Oxygen Availability. Flat culture flasks were used to maximize oxygen availability to the entire sample, because when lying down, these provide increased surface area for oxygen infiltration. To maximize the air voids, the flasks were lightly agitated to place the material, enough to reduce the volume of macro-pores, but not to induce significant consolidation.

4.4.2.3 Batch Test Results

<u>Discovery Mine</u>

Because the humidity cells did not generate measurable acidity, whether in the form of pH or increased sulfate levels, the batch cells were not tested due to financial restraints and the likelihood of insignificant data.

<u>Faro Mine</u>

In the second round of tests, the Faro Mine tailings had a significantly higher sulfide content (22% sulfur vs 0.5% for the Discovery tailings). Additionally, a low (<1%)

carbonate content created a very low NP:AP ratio. This suggested a significantly increased likelihood of obtaining significant data with the Faro tailings versus the Discovery tailings.

The batch cells ran from February to May, 2000. At the end of the designated periods, the flasks were emptied into a steel cylinder and the water was extracted by applying approximately 20 MPa vertical pressure to the sample. The leachate was heavily sediment laden, so it was passed through a 0.45 micron filter to remove the fines (Figure 4-27). With 2 exceptions, the filtrate was completely clear, without any discoloration. Immediately after filtration, it was tested for pH, with readings taken instantaneously, and after 1 and 5 minutes. The filtrate was then stored at 3°C until it was tested for sulfate and total sulfur.

Figure 4-28 shows the sulfate concentrations from the batch cells. Concentrations varied from 3,000 mg/L to 19,000 mg/L with no relationships discernable with time or temperature. Figure 4-29 shows the sulfate concentrations from the inoculated batch cells. Concentrations varied from 8,000 mg/L to 23,000 mg/L. The inoculated data revealed distinct levels of sulfate, differing by a factor of approximately 2 for the samples at 20°, 1.5° and 0°C. It was believed that this division was due to contamination of some of the samples by oxygen, resulting in changes to the sulfur species in solution. Sources (Morin, 1999; Mehling, 1999) had indicated that all dissolved sulfur would be in the form of sulfide, yet this was not the case in the present results.

With the intent of utilizing total sulfur as an indicator for active oxidation, the samples from the first 6 weeks were re-tested for total dissolved sulfur (Figure 4-30). Each point represents a single batch leachate. Sulfur concentrations varied from approximately 13,000 mg/L to 25,000 mg/L. Taking the results as a whole, there did not appear to be any conclusive acid generating trends. No data set at any temperature showed a constant increase in sulfur for the period tested; however, taking the data at individual temperatures revealed trends in several figures. At 20°, 3° and 1°C, the sulfur increased for the first 3 to 4 weeks, when the curves show peaks, followed by a decrease in sulfur.

until the end of 7 weeks. This curvature was not present in the +1.5°, -1.5° or -3°C figures. In these figures, the data suggested linear relationships, with the exception of several outlying points at +1.5° and -3°C. It is uncertain if these points were significant, so these trends remained debatable.

The inoculated batch samples showed similar scatter for sulfate concentrations, so they were not tested for total dissolved sulfur. Additionally, because the Faro material was not irradiated, no conclusions could be made for abiotic vs biotic conditions.

The pH readings were typically between 4 and 6 (Figure 4-31) with no apparent relationship or trend with time or temperature. There were however, numerous outliers at pH 2 to 2.5.

At the end of the test periods, two control cells were tested for pH and Eh. One cell had been closed for the entire 4-month period, the other had an oxygen permeable membrane. The pH for the closed cell had an instantaneous pH reading of approximately 6.0, with an Eh of –69mV. The sample with the oxygen membrane had a pH of 5.3, with an Eh of +27mV.

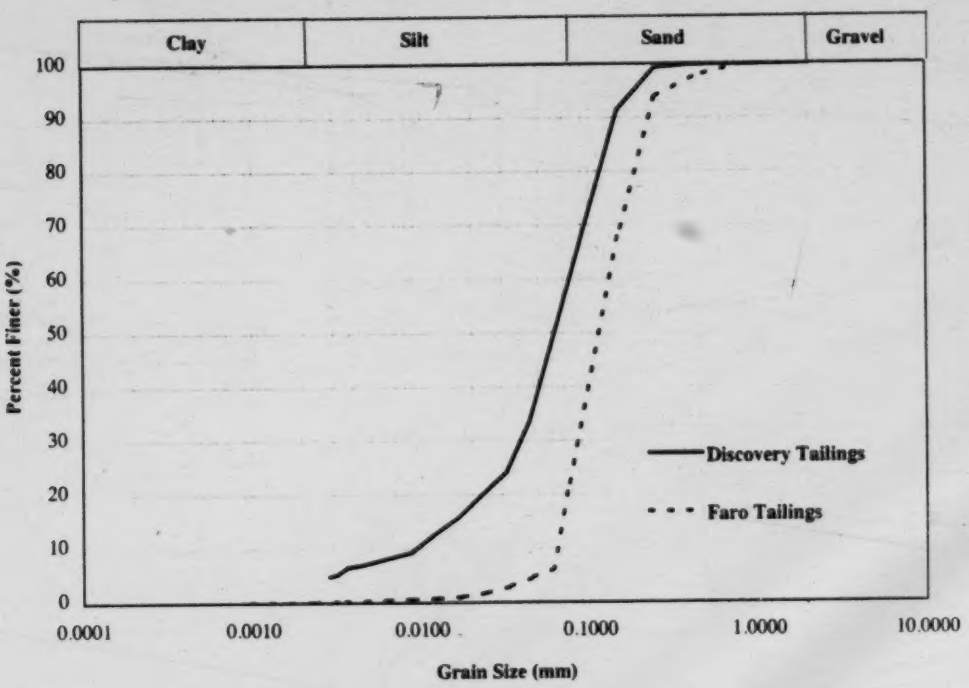

Figure 4-1. Grain Size Distribution Curves for Discovery and Faro Mine Tailings

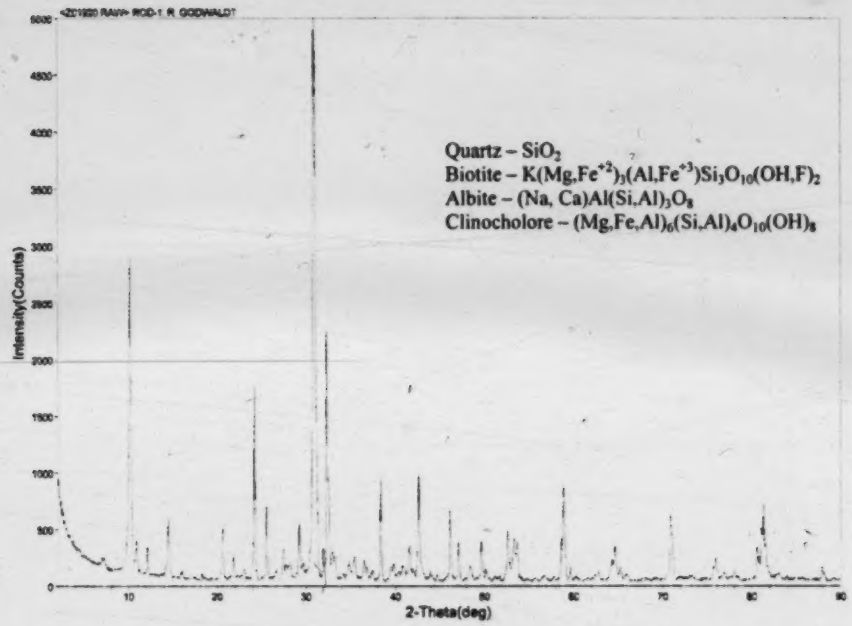

Figure 4-2. XRD Pattern for Unoxidized Discovery Tailings

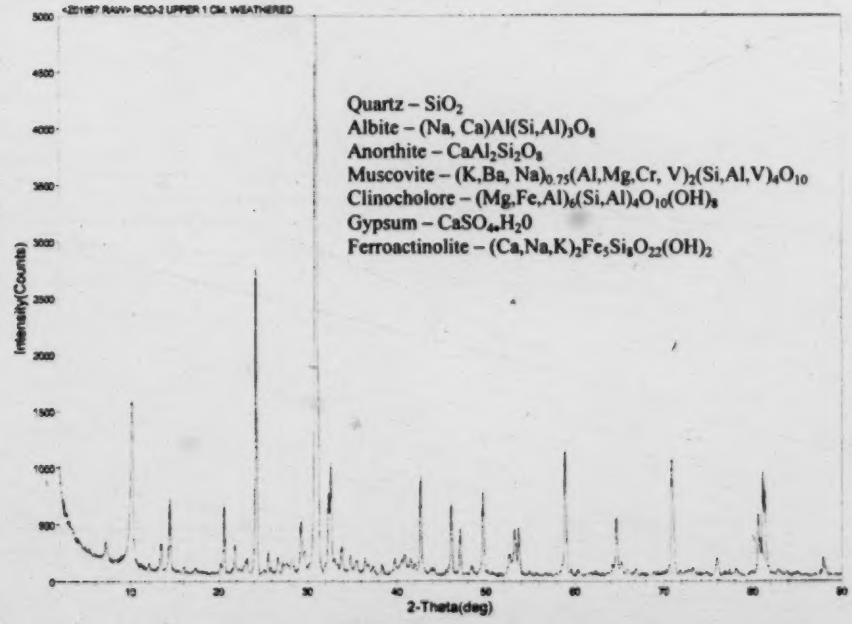

Figure 4-3. XRD Pattern for Oxidized Discovery Tailings

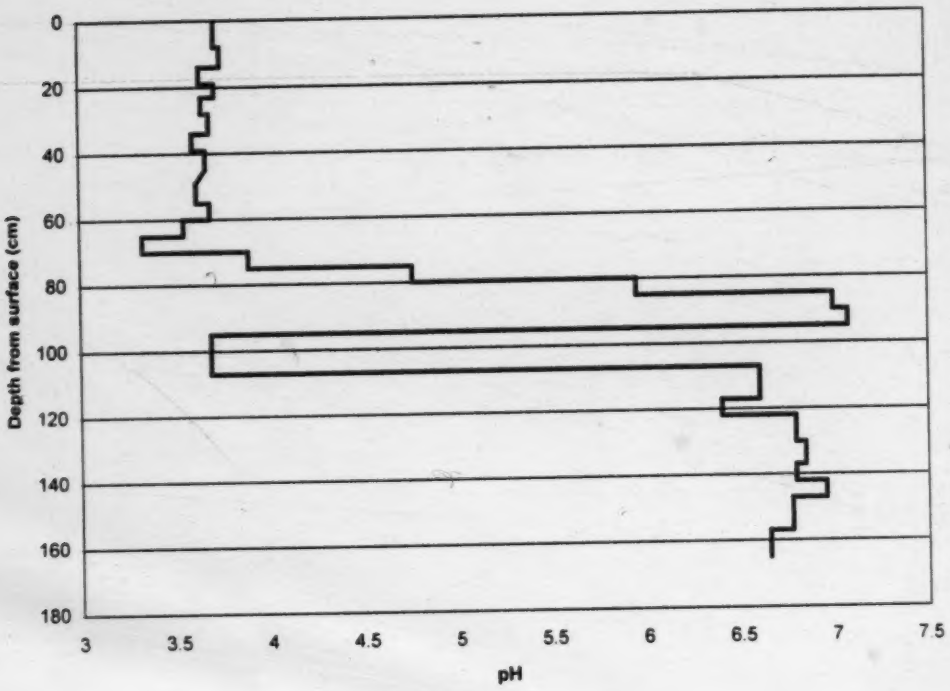

Figure 4-4. Increasing Batch pH with Depth in Profile of Discovery Core Sample

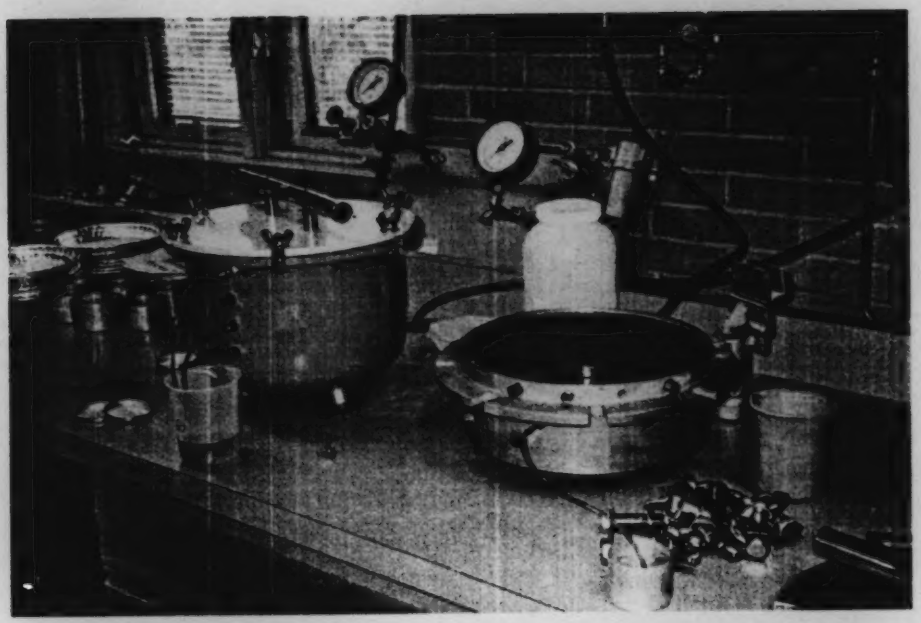

Figure 4-5. Pressure Plate Apparatus for Determining Soil Moisture Characteristic Curve

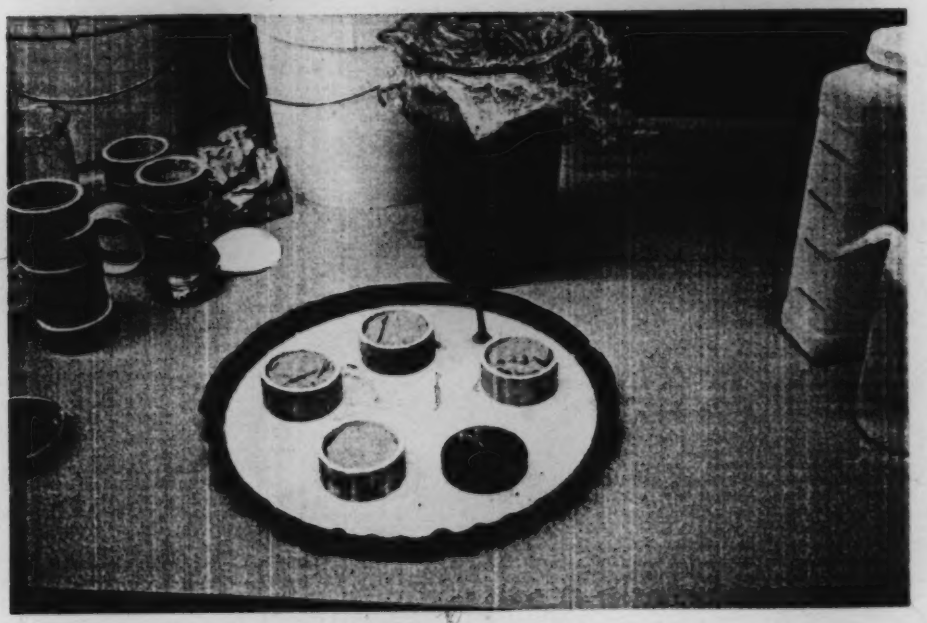

Figure 4-6. Ceramic Plates for Pressure Plate Apparatus for Soil Moisture Characteristic Curve

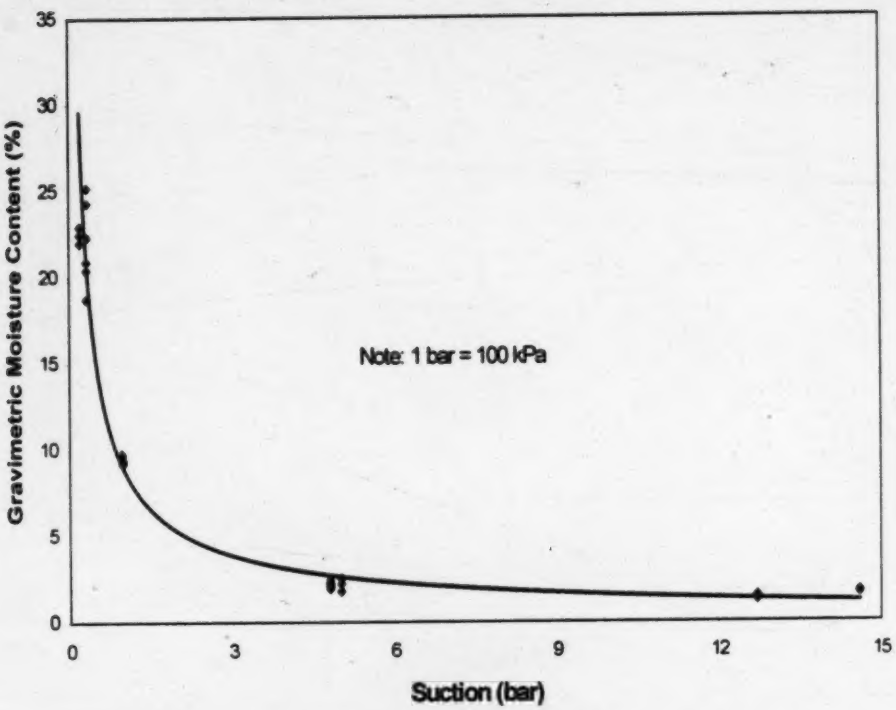

Figure 4-7. Soil-Moisture Characteristic Curve for Discovery Tailings

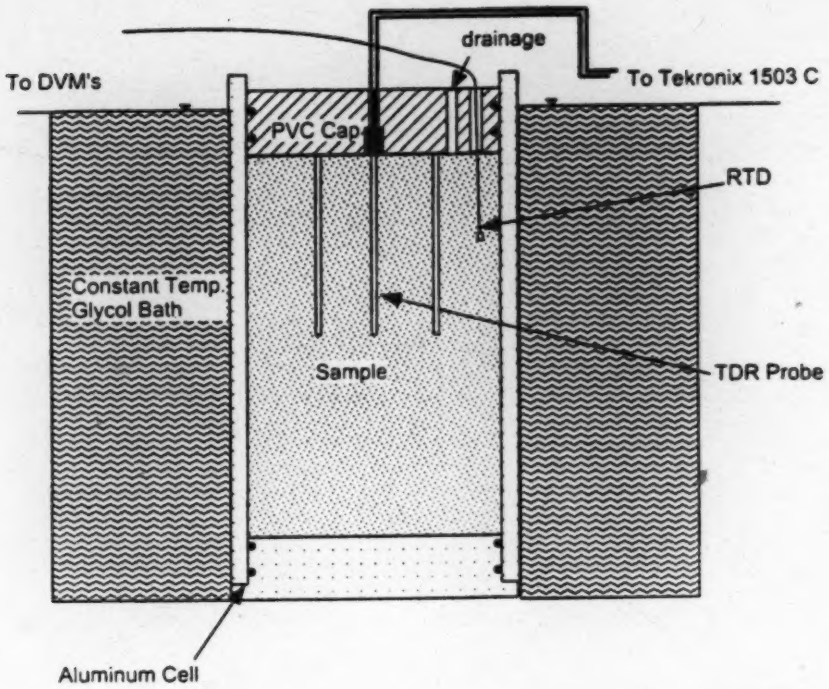

Figure 4-8. TDR Cell for Measuring Unfrozen Water Content (from Norwest, 1998)

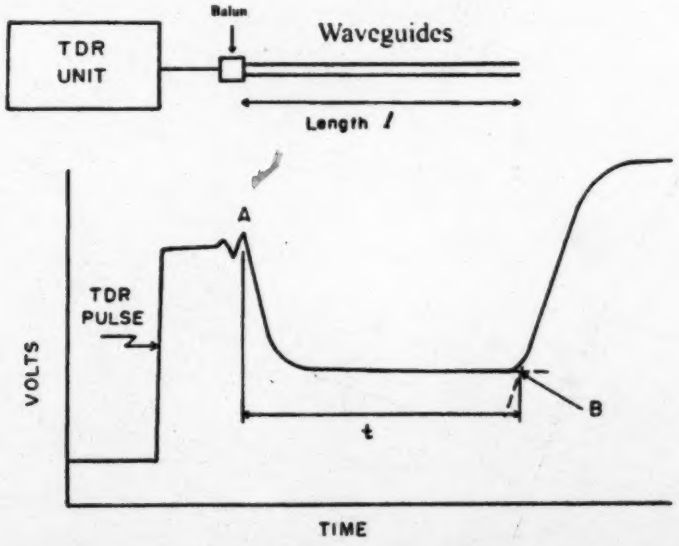

Figure 4-9. Example of TDR Pulse Reading (from Lefebvre, 1997)

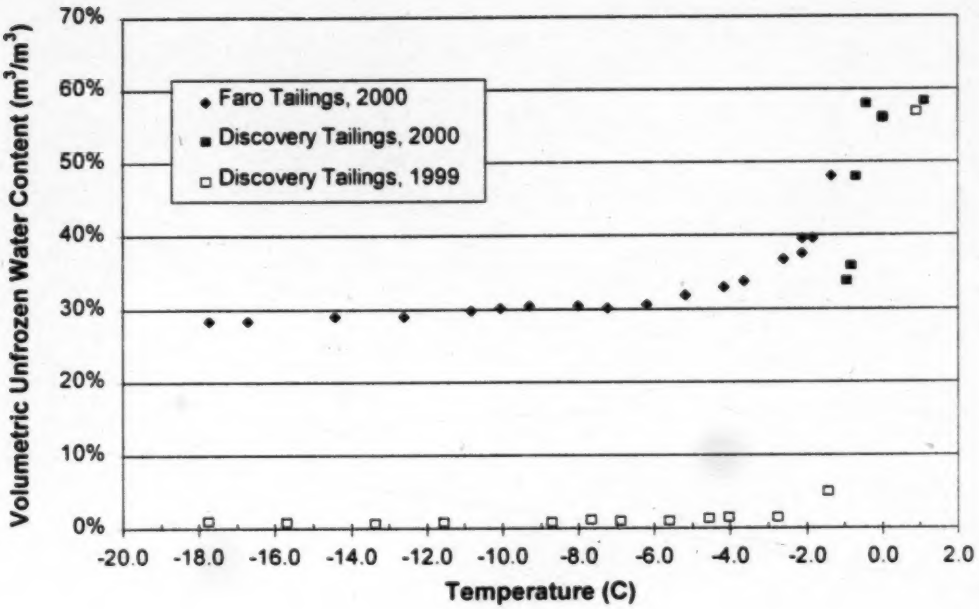

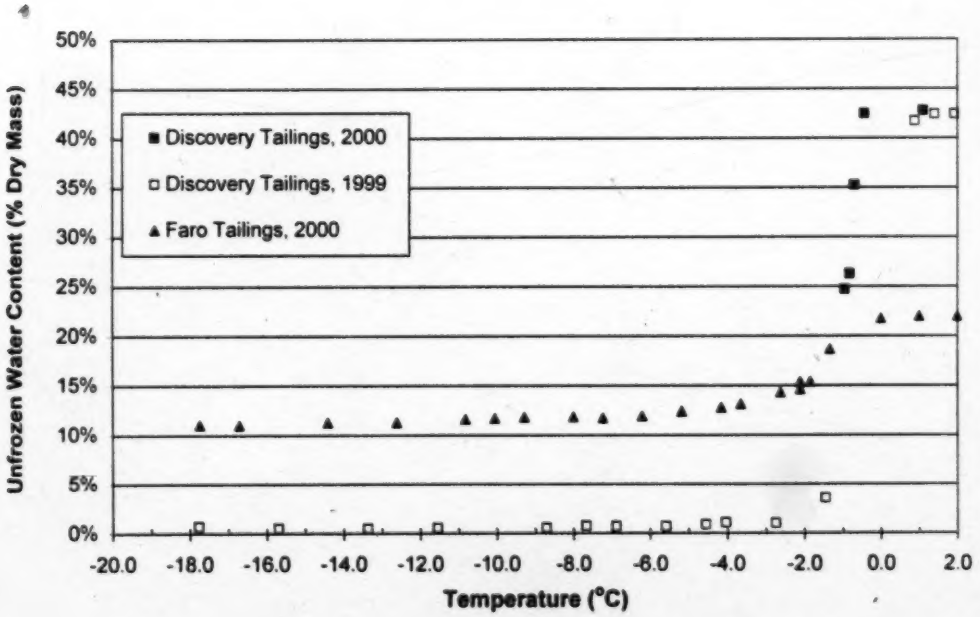

Figure 4-10. Unfrozen Water Content for Discovery and Faro Mine Tailings

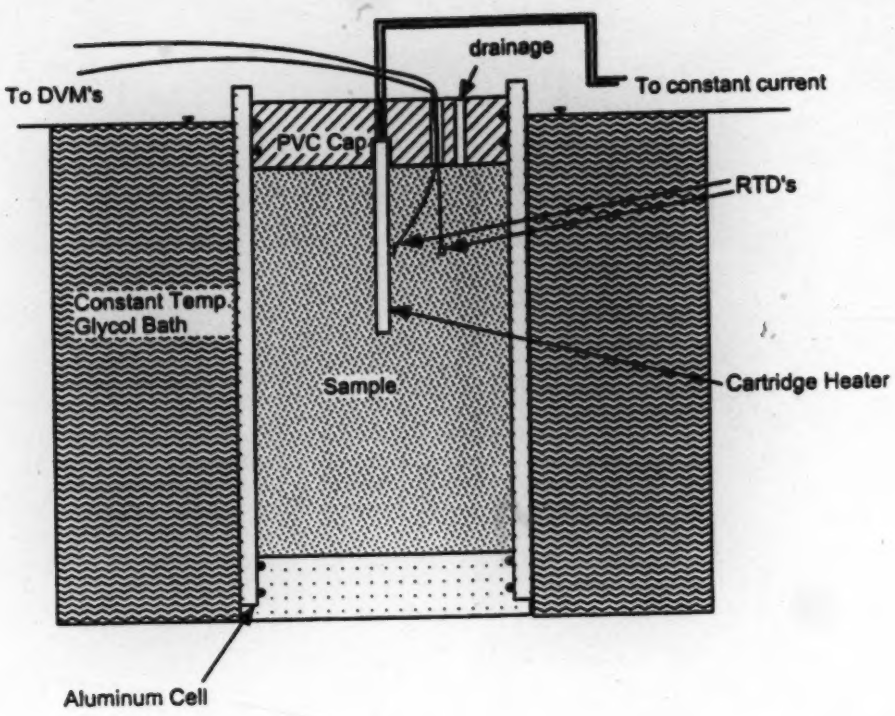

Figure 4-11. Thermal Conductivity Probe (after Norwest, 1998)

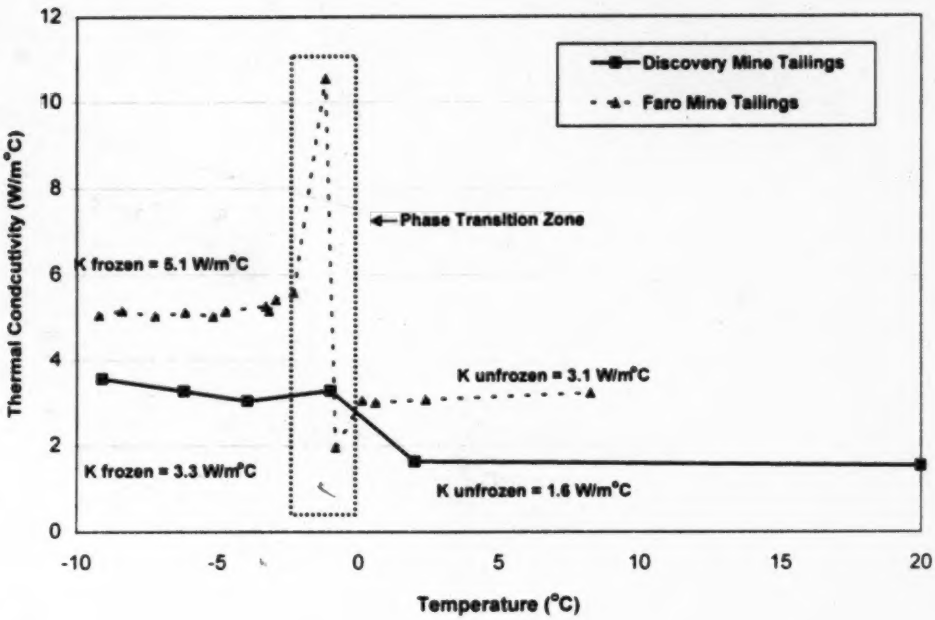

Figure 4-12. Thermal Conductivity of Discovery and Faro Mine Tailings

Figure 4-13 - Enrichment Cell pH vs Time for Different Test Conditions on Faro Tailings Temperature - Innoculum - Substrate

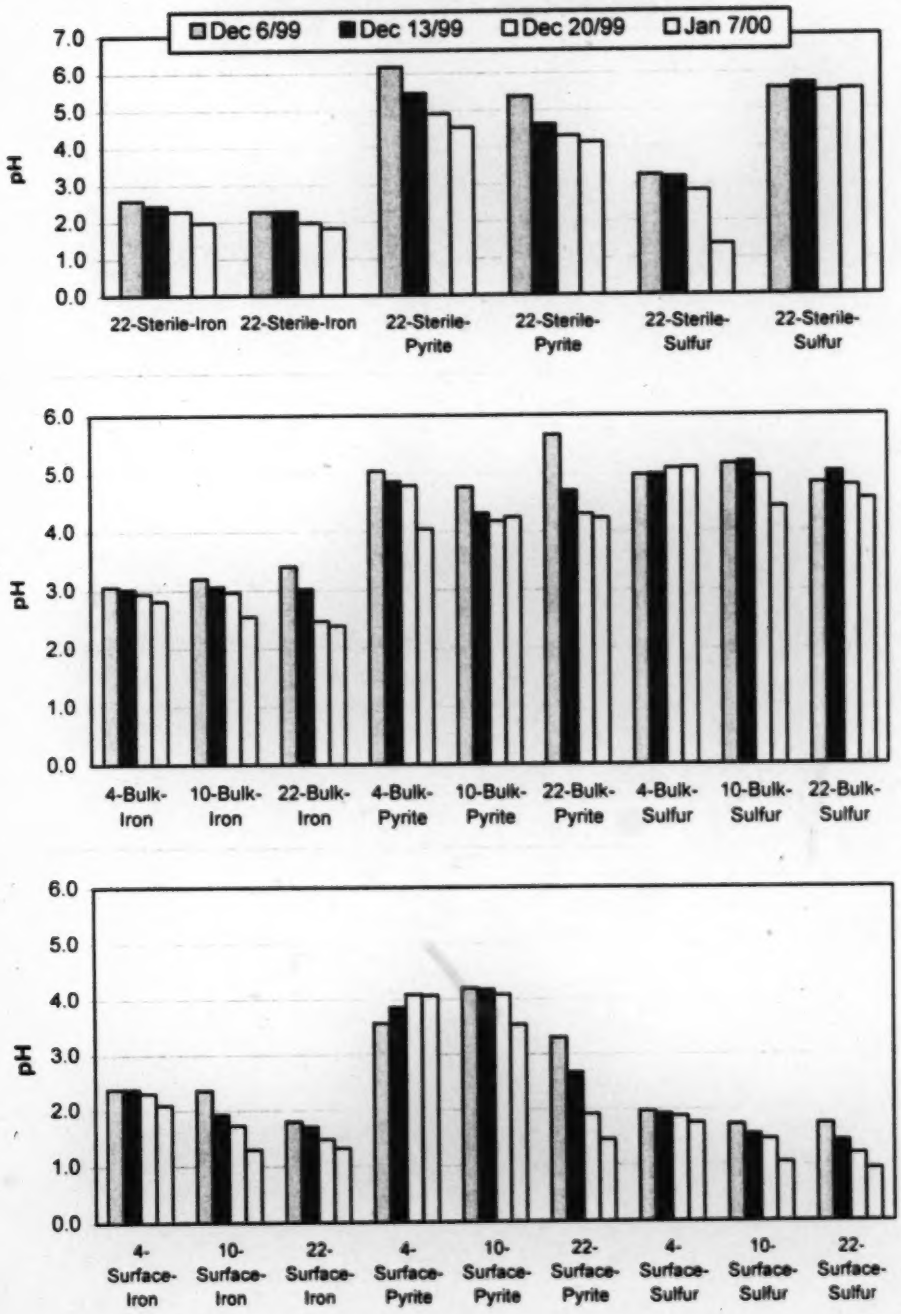

Figure 4-14. Sulfur Oxidizing Bacteria from Discovery Tailings

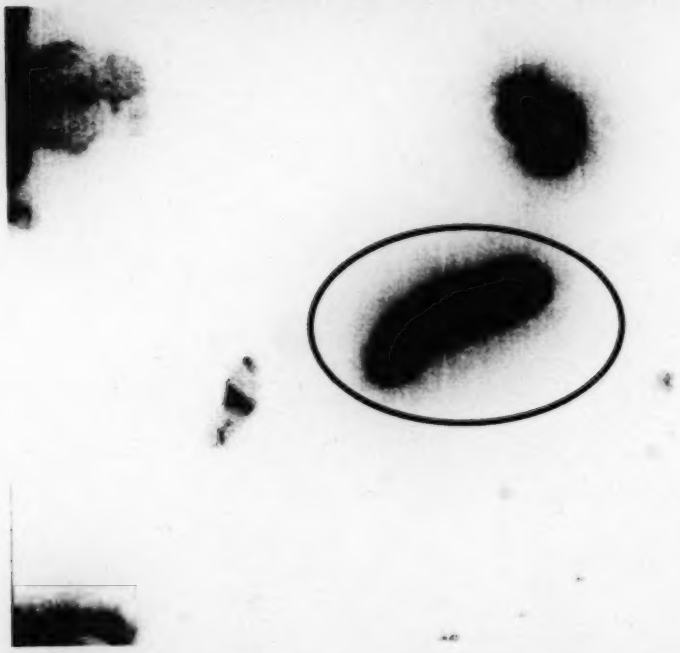

Figure 4-15. Iron Oxidizing Bacteria from Discovery Tailings

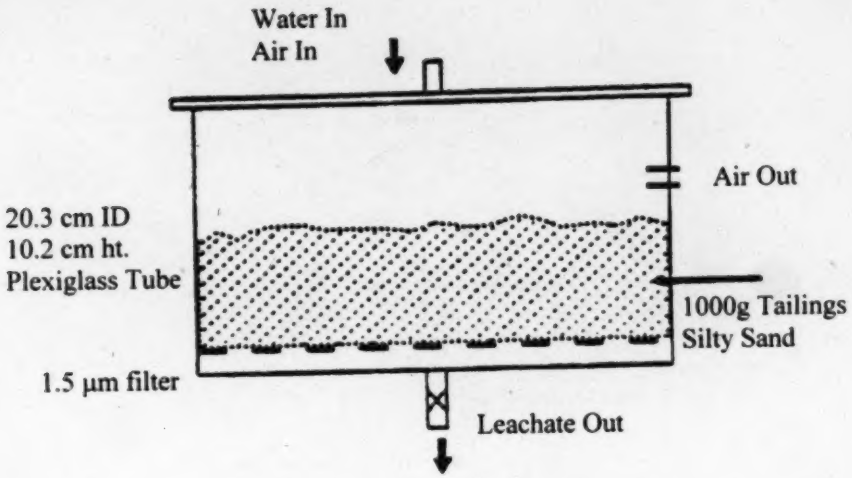

Figure 4-16. Humidity Cell Schematic

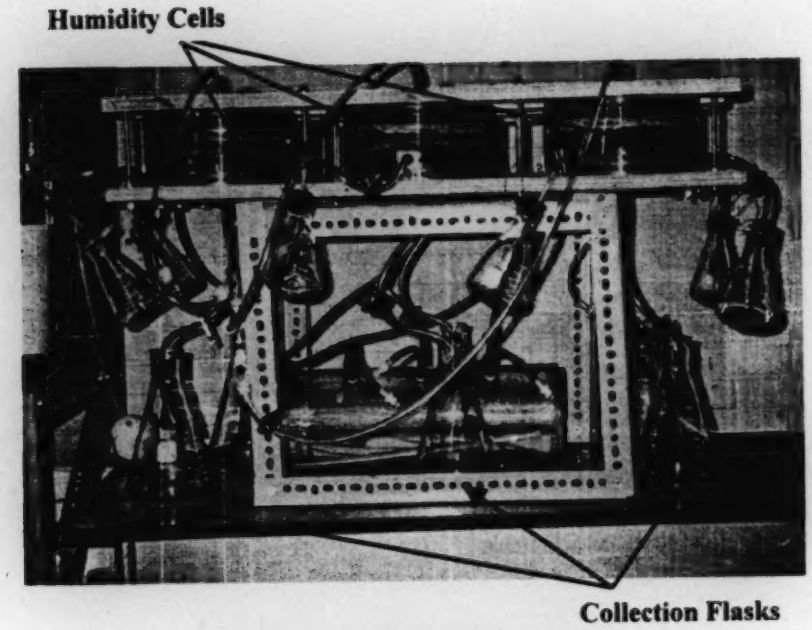

Figure 4-17a. 20°C Humidity Cell Setup Using Discovery Mine Tailings

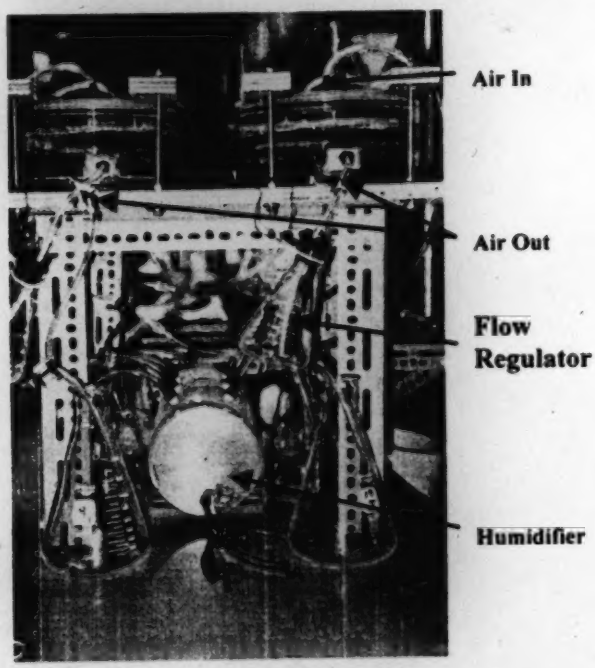

Figure 4-17b. Humidifier Manifold in 20°C Humidity Cell Setup

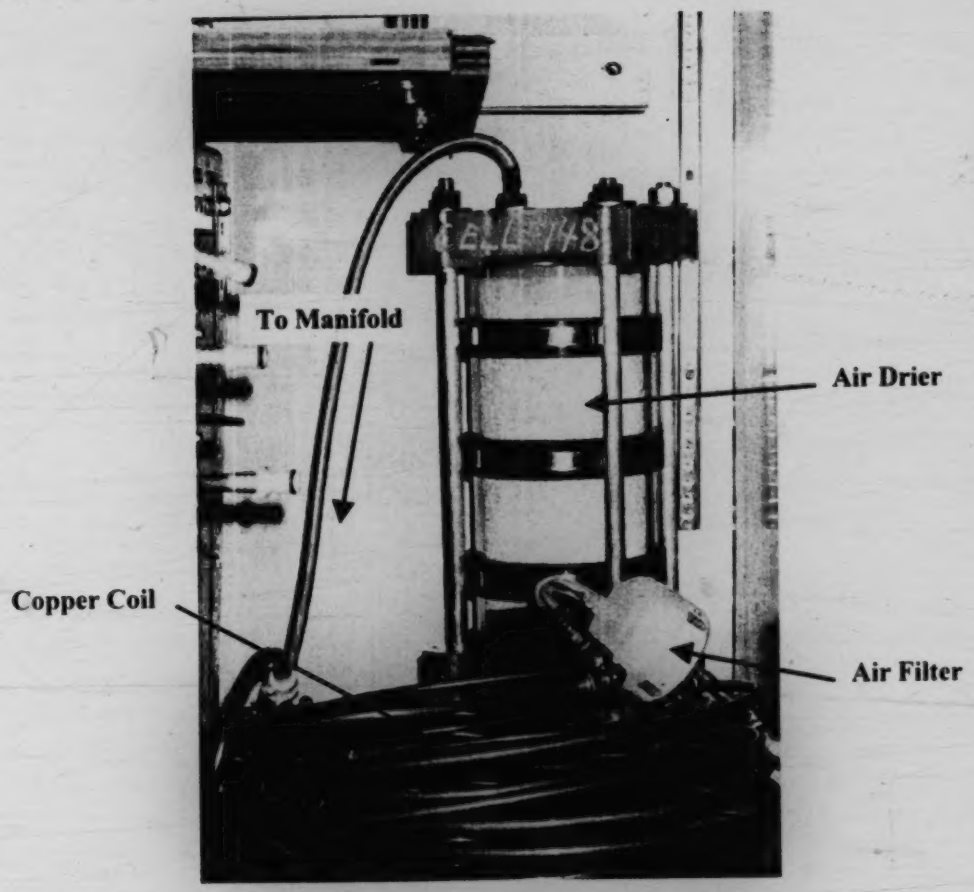

Figure 4-18. Temperature Regulating Coil for 3°C Humidity Cell

Figure 4-19a. Discovery Mine Humidity Cells
Sulfate and pH vs Time at 20°C

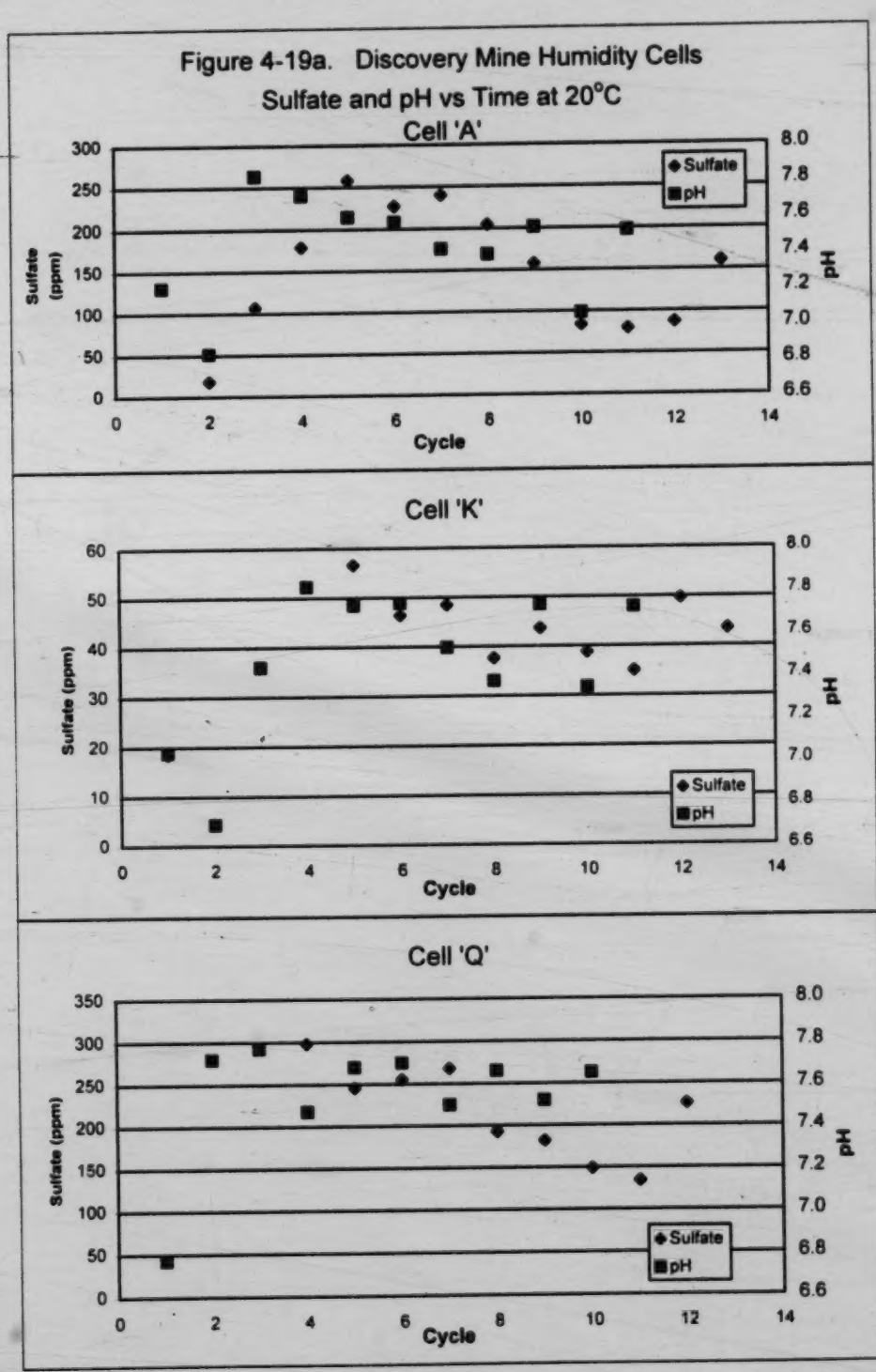

Figure 4-19b. Discovery Mine Humidity Cells Sulfate and pH vs Time at 3°C

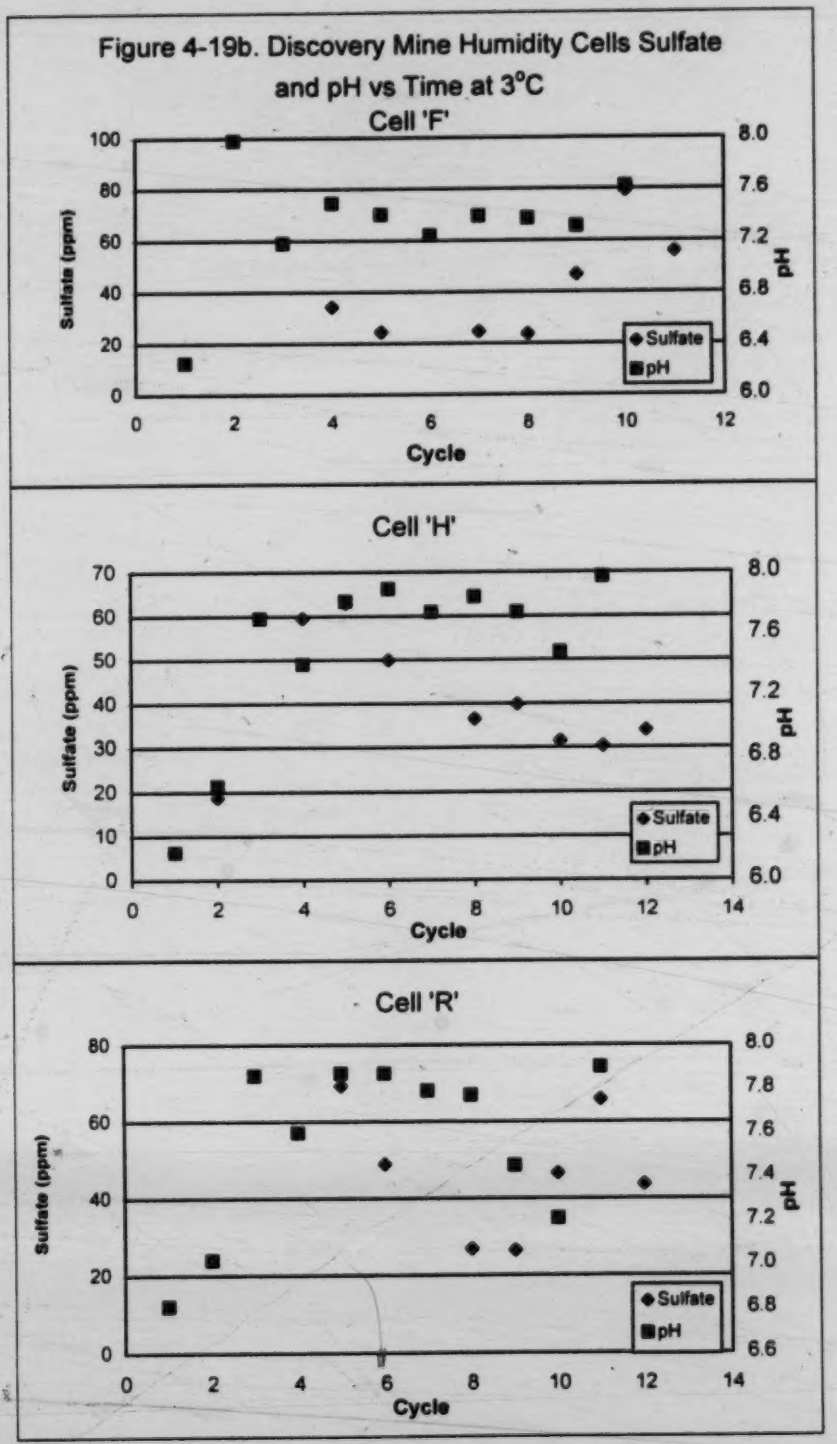

Figure 4-19c. Discovery Mine Humidity Cells Sulfate and pH vs Time at 1°C

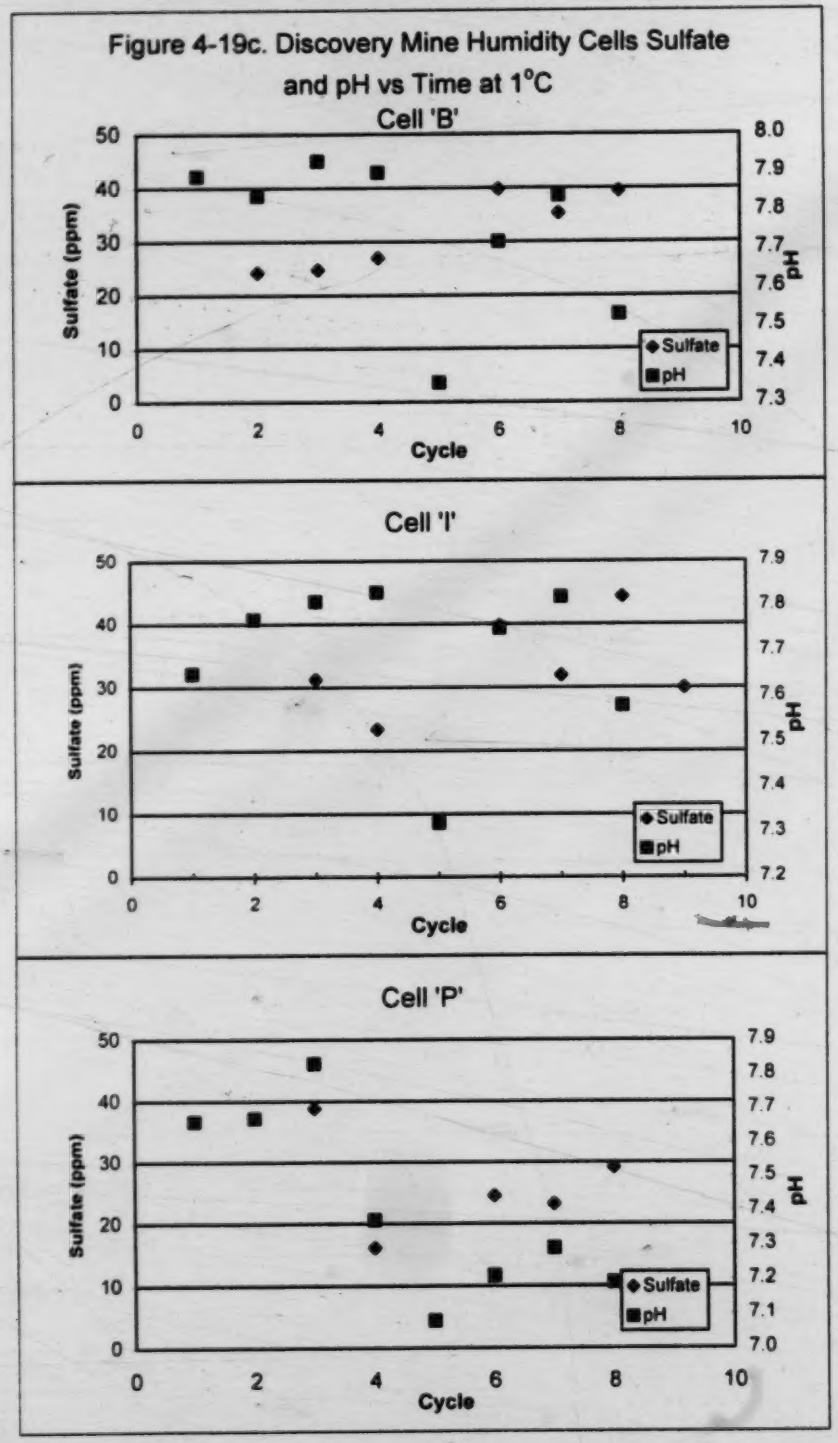

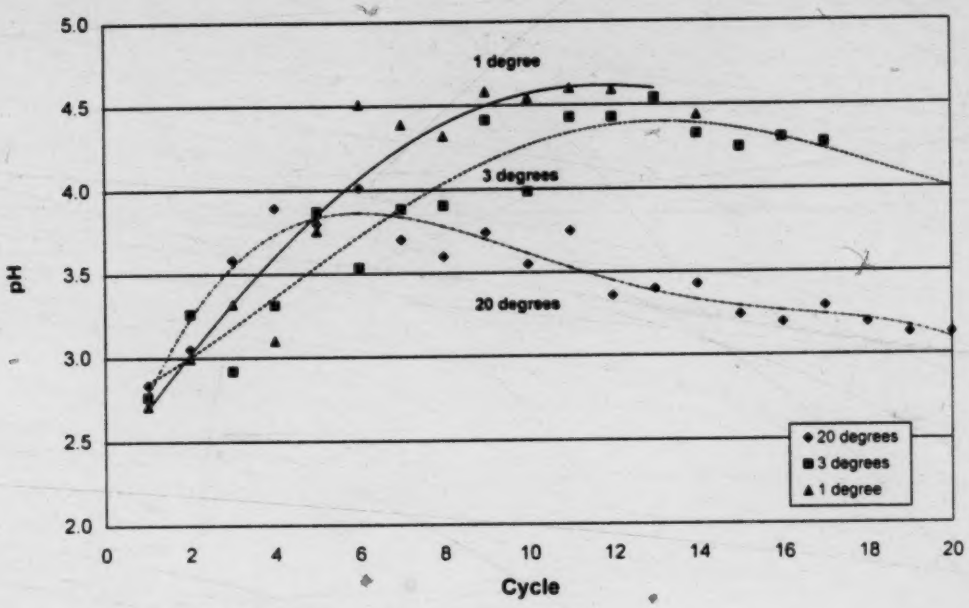

Figure 4-20. Faro Mine Humidity Cell pH vs Time

Figure 4-21a. Faro Tailings Humidity Cell pH vs Time at 20°C

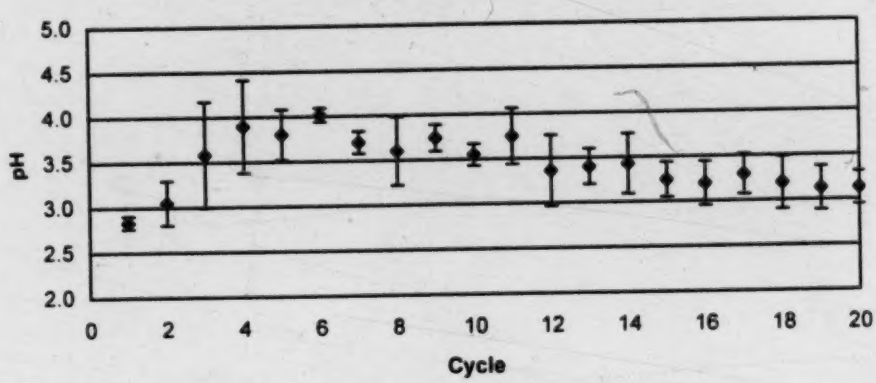

Figure 4-21b. Faro Tailings Humidity Cell pH vs Time at 3°C

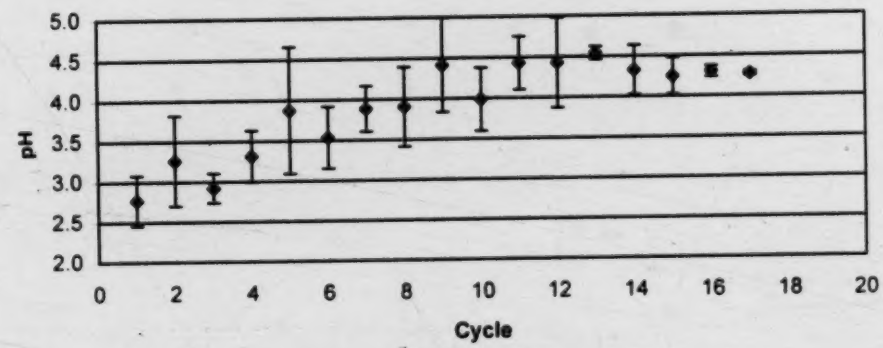

Figure 4-21c. Faro Tailings Humidity Cell pH vs Time at 1°C

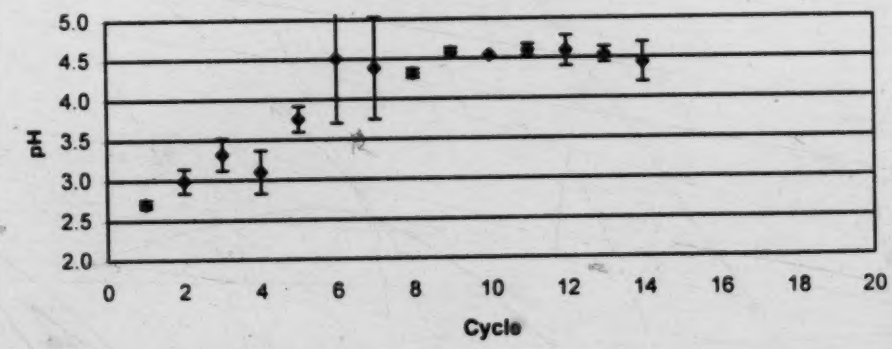

Figure 4-22a. Humidity Cell Sulfate Concentration vs Time at 20°C

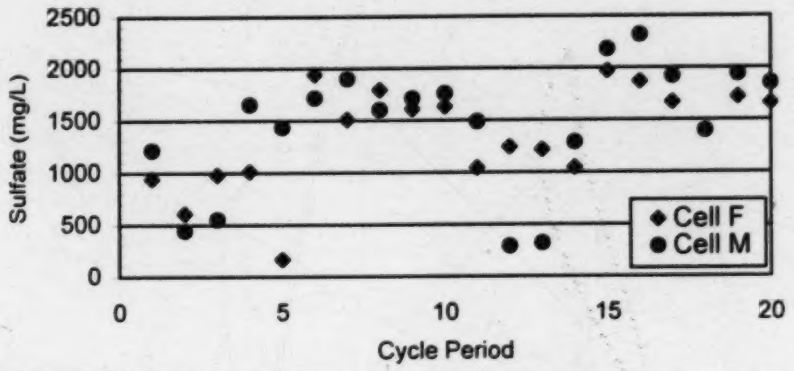

Figure 4-22b. Humidity Cell Sulfate Concentration vs Time at 3°C

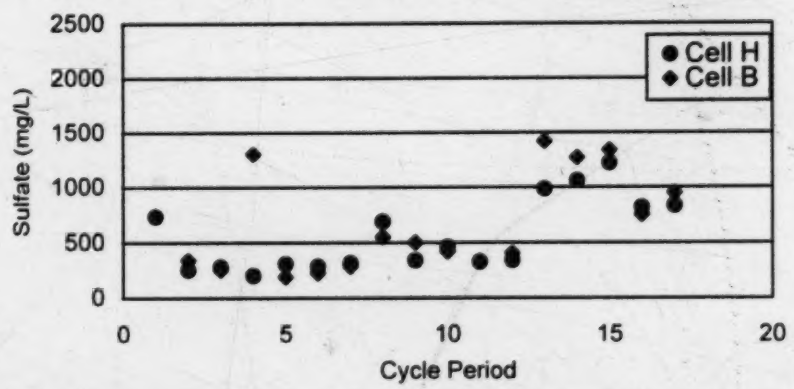

Figure 4-22c. Humidity Cell Sulfate Concentration vs Time at 1°C

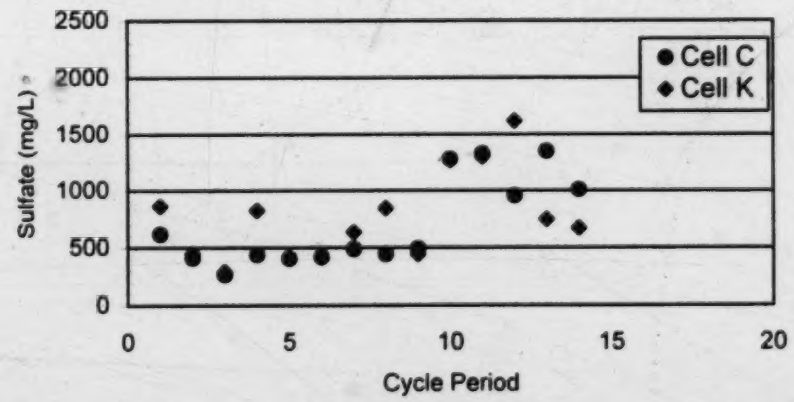

Figure 4-23a. Humidity Cell Sulfate Mass vs Time at 20°C

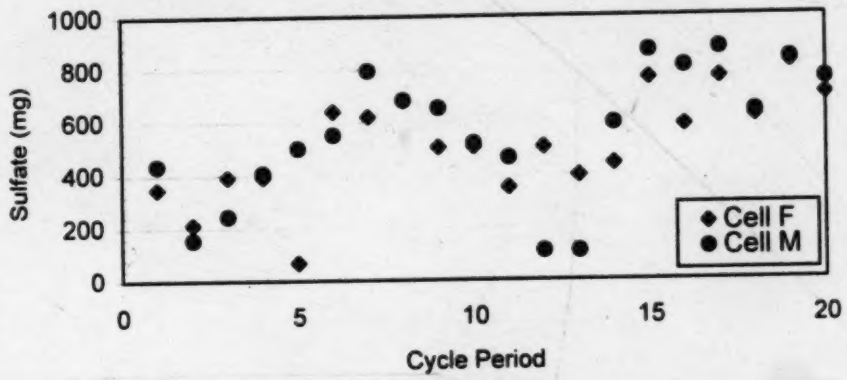

Figure 4-23b. Humidity Cell Sulfate Mass vs Time at 3°C

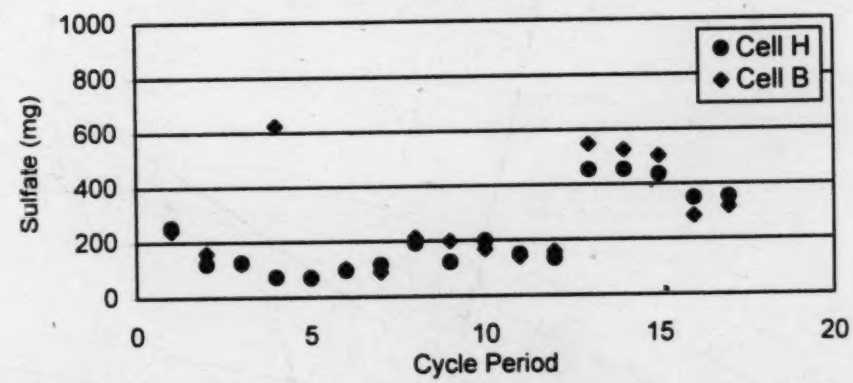

Figure 4-23c. Humidity Cell Sulfate Mass vs Time at 1°C

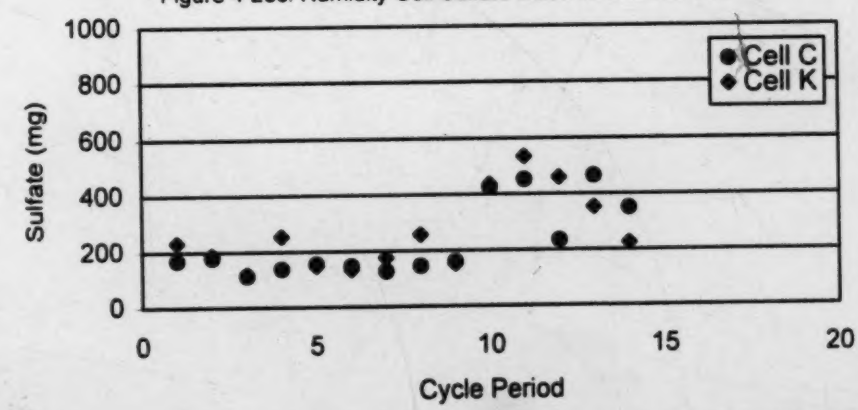

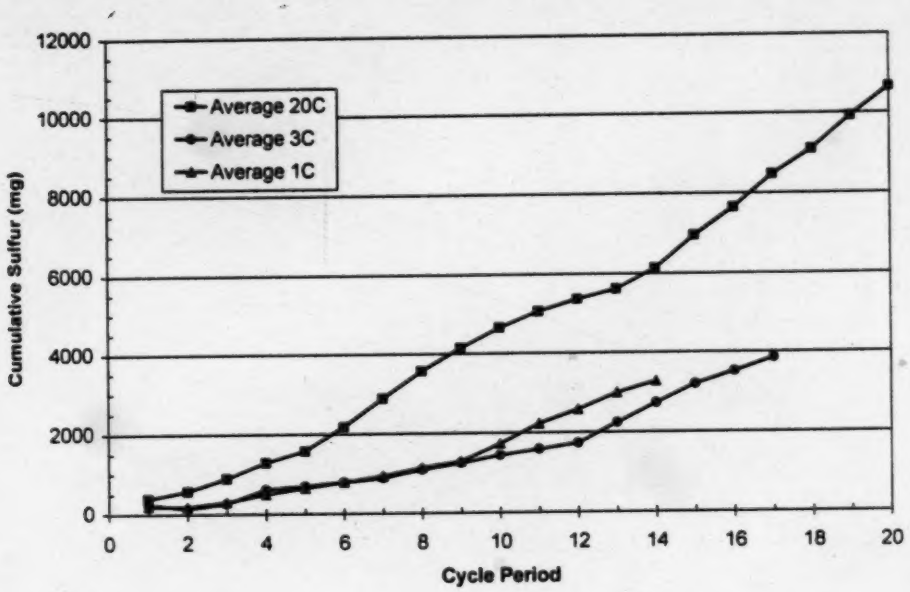

Figure 4-24. Cumulative Sulfate from Faro Humidity Cell Tests

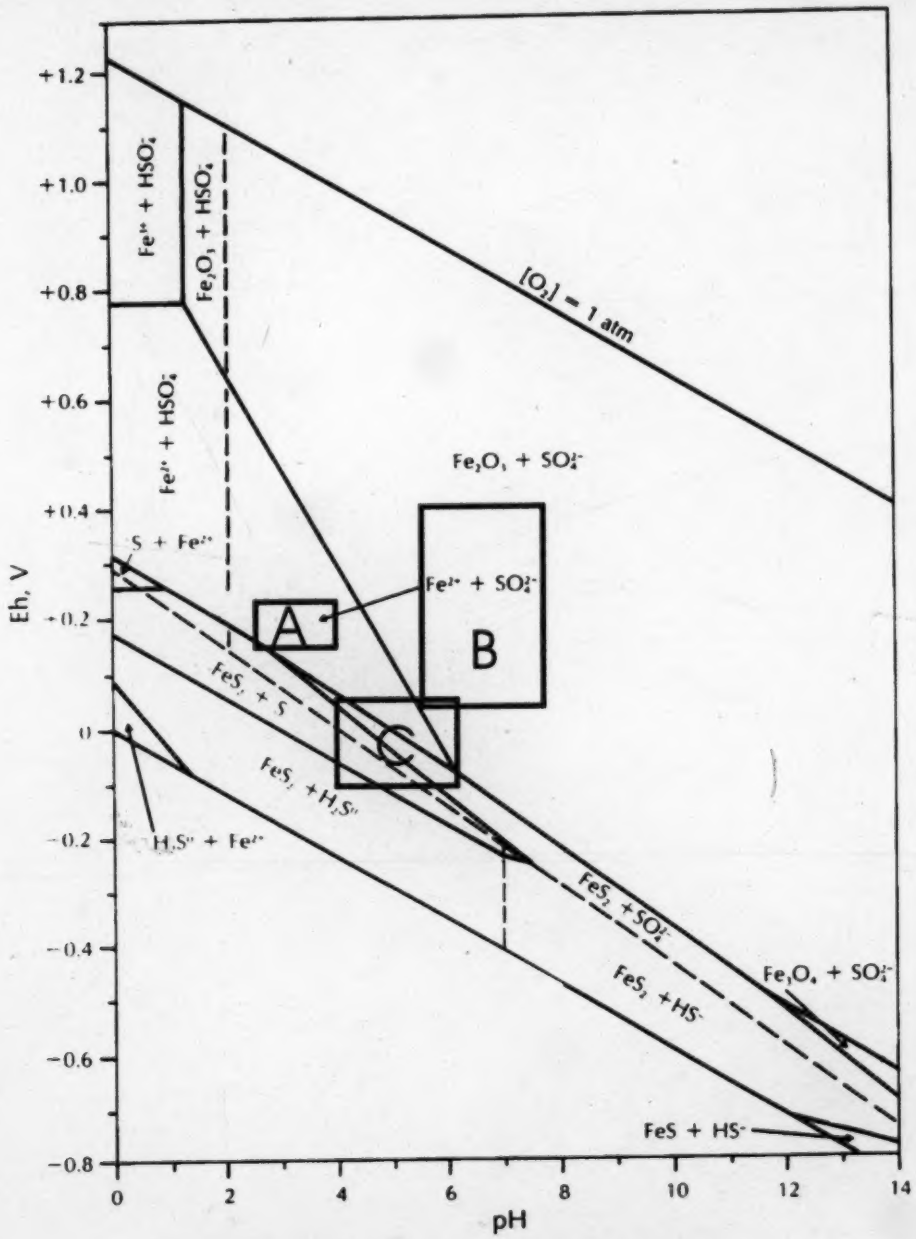

Figure 4-25. Eh-pH Diagram for Iron Sulfide Species

[S] = 0.1M at 25°C (Modified from Faure, 1991)

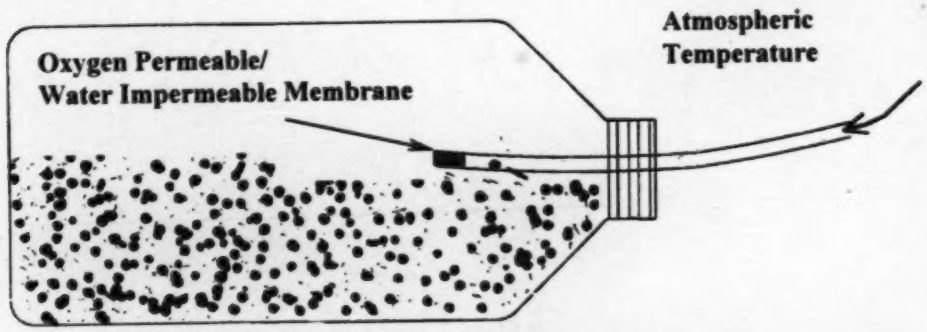

Figure 4-26. Batch Cell Schematic and Apparatus

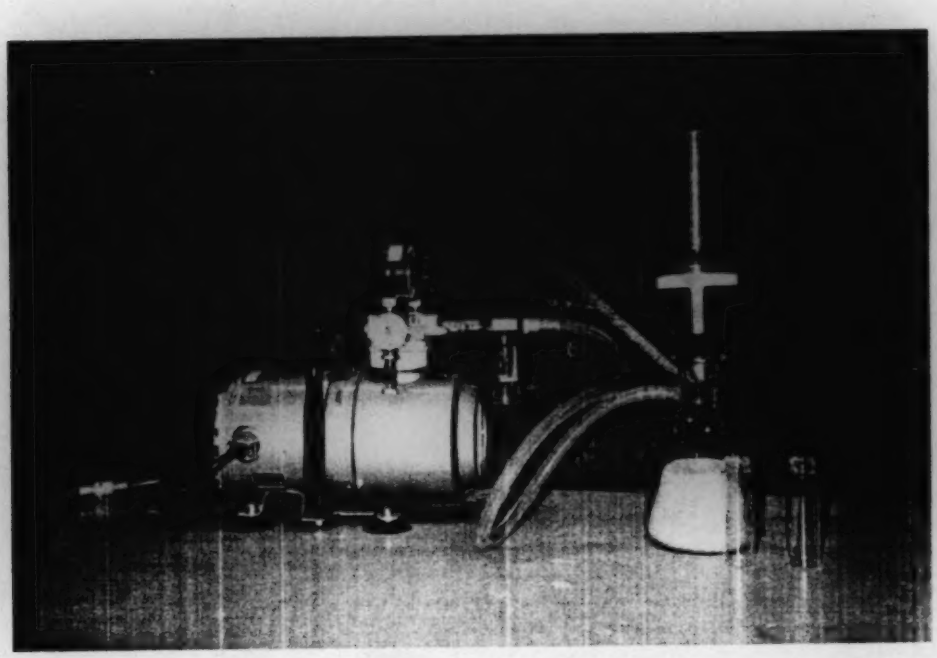

Figure 4-27. 0.45 Micron Vacuum Filtration Unit

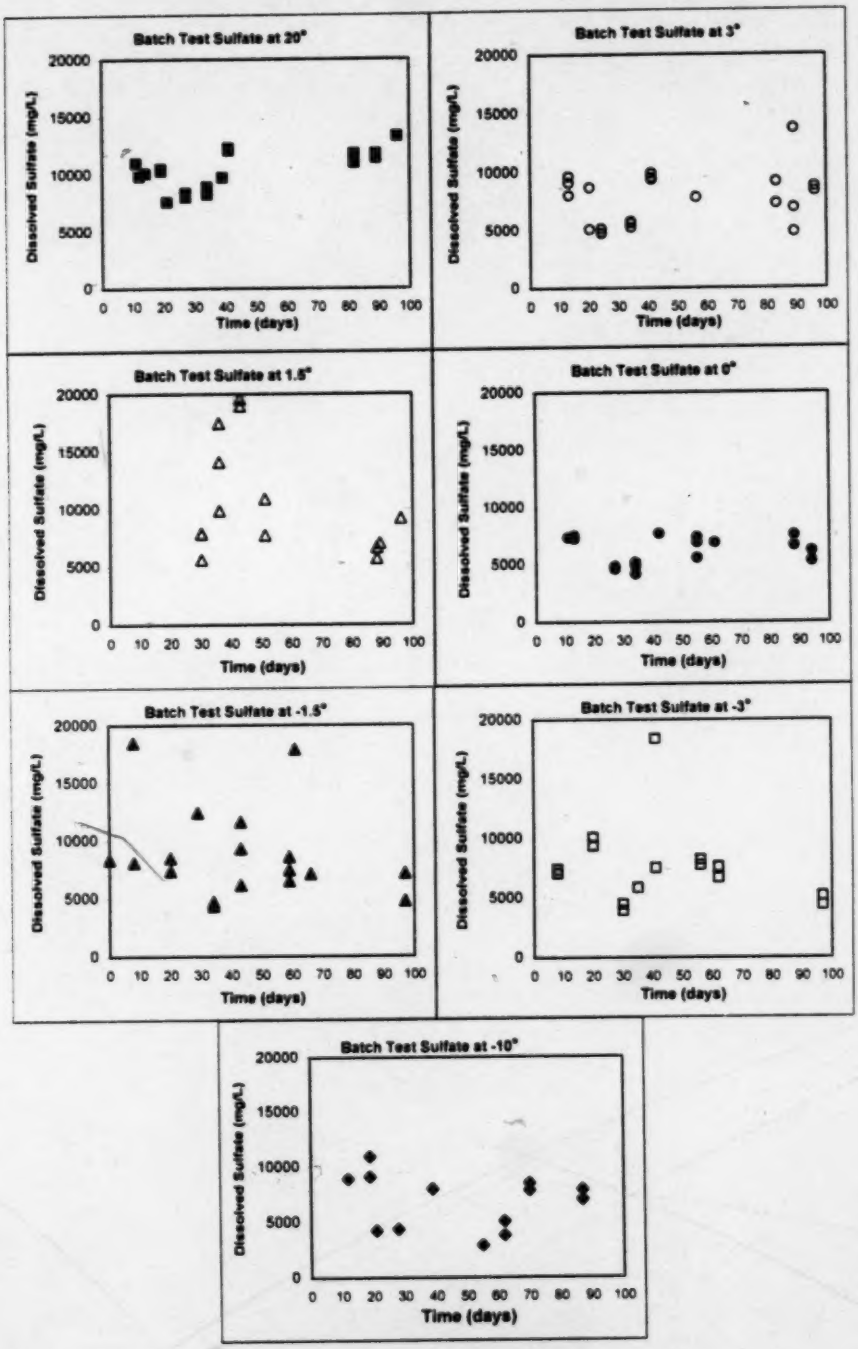

Figure 4-28. Batch Cell Sulfate vs Time

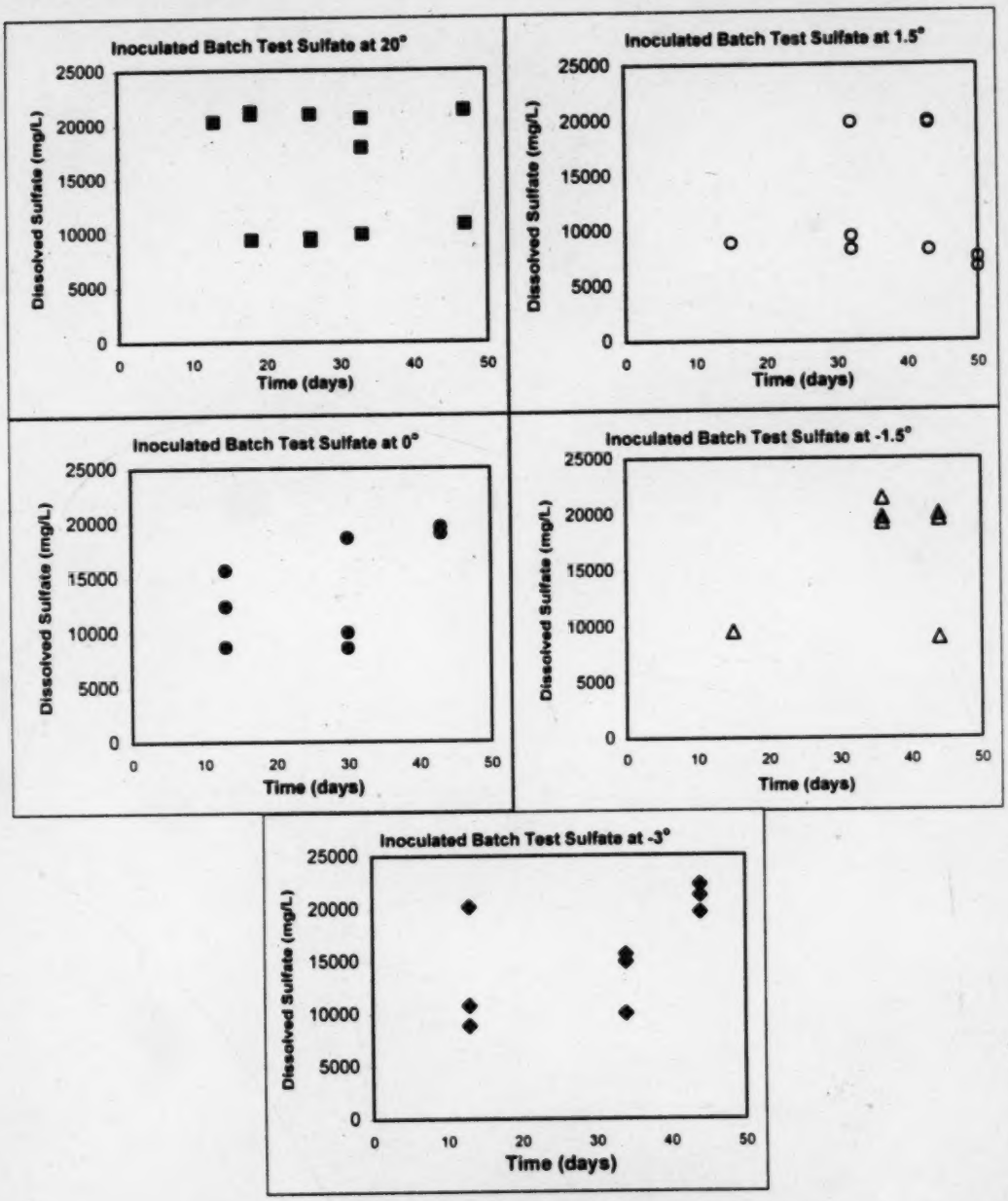

Figure 4-29. Inoculated Batch Cell Sulfate Concentration vs Time

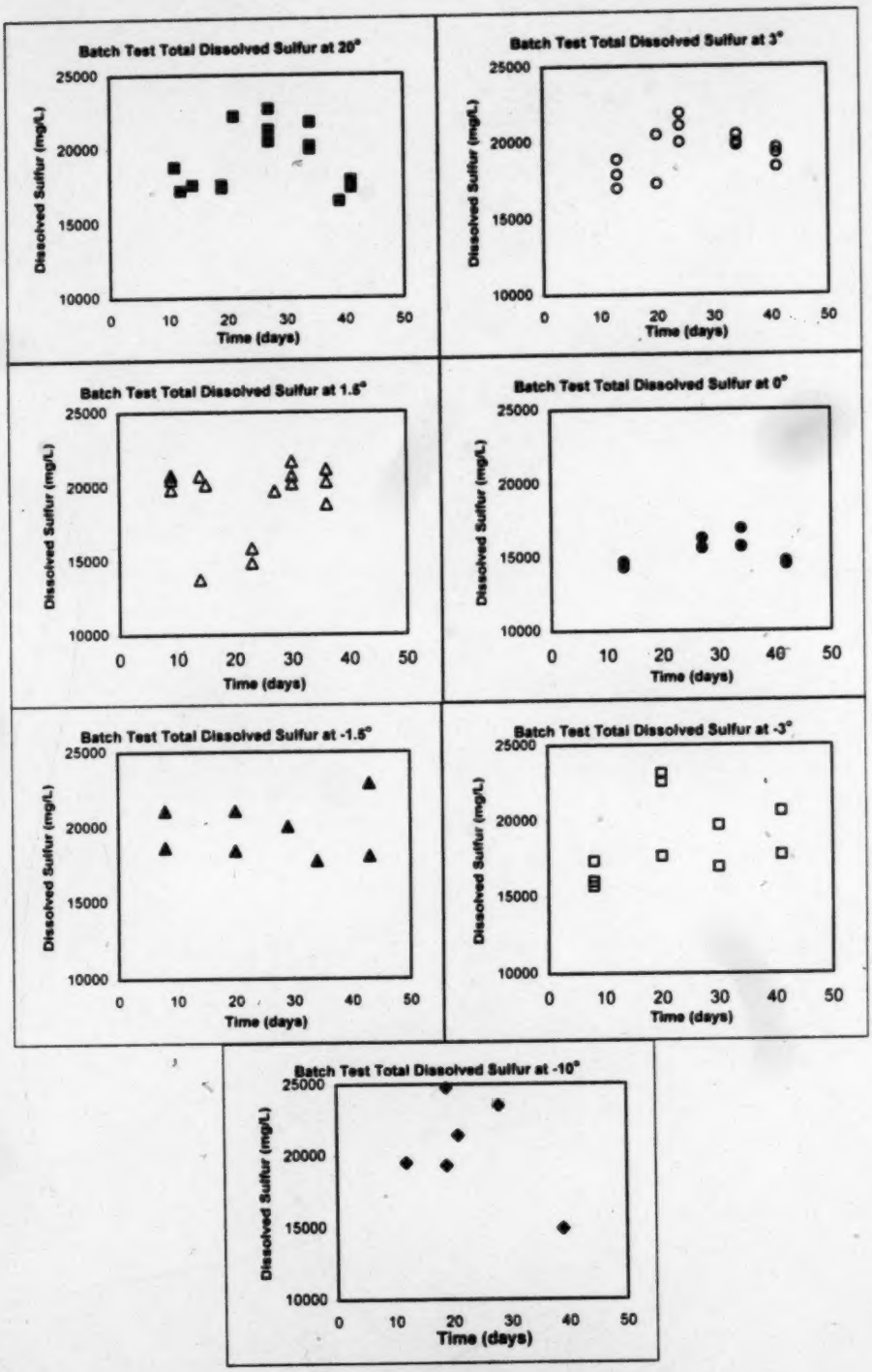

Figure 4-30. Batch Cell Total Dissolved Sulfur vs Time

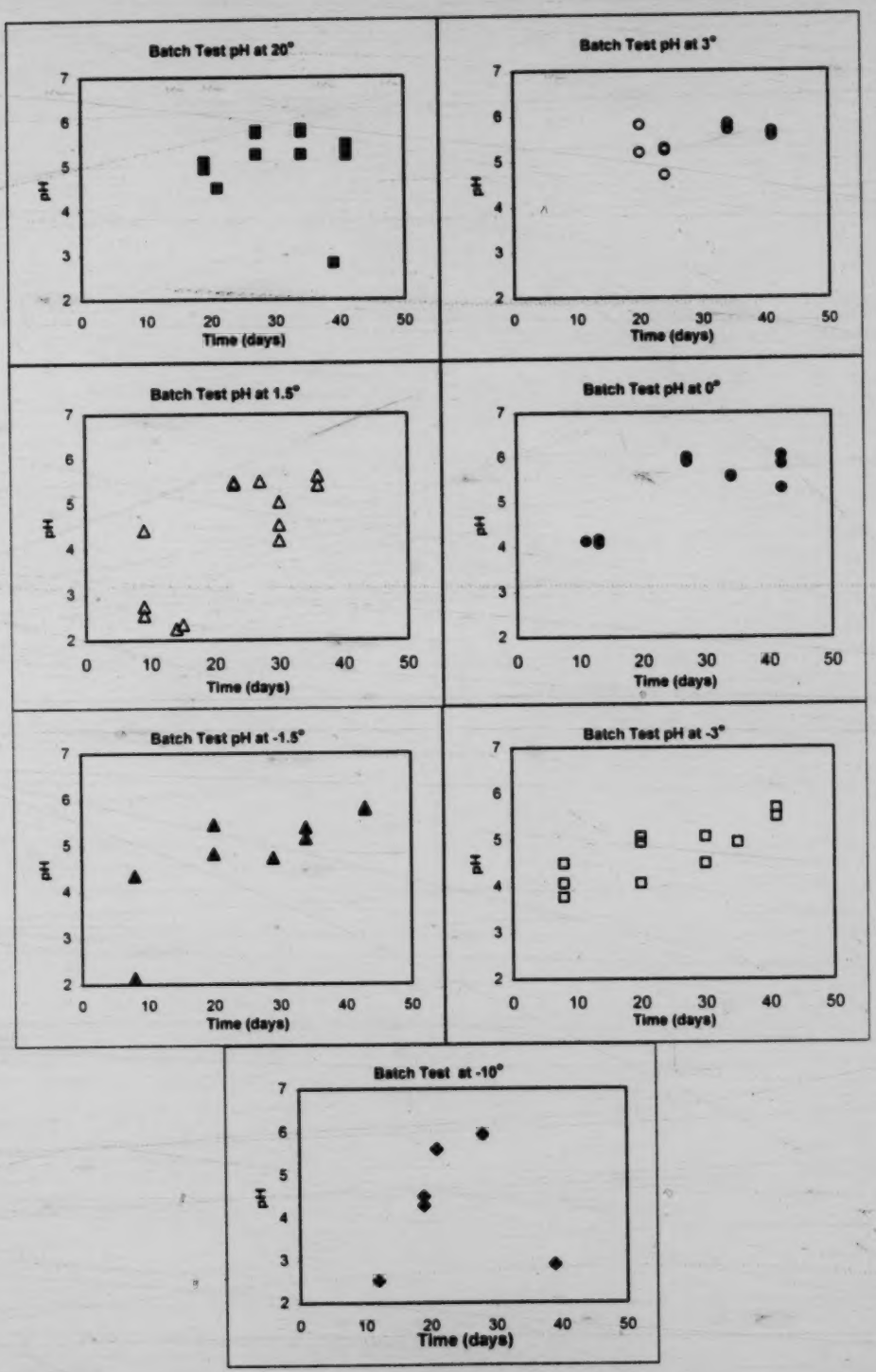
Batch Test pH at 20°
Batch Test pH at 3°
Batch Test pH at 1.5°
Batch Test pH at 0°
Batch Test pH at -1.5°
Batch Test pH at -3°
Batch Test at -10°
pH
Time (days)

Figure 4-31. Batch Cell pH vs Time

Table 4-1. Soils Analysis
Unoxidized Tailings
(Tested at Norwest Labs)

		Discovery Mine	Faro Mine
Salinity	**(units)**		
pH		7.7	6.2
Conductivity	dS/m	0.55	4.97
S.A.R.		0.8	0.1
Sulfur Species			
Sulfur	%	0.544	22.1
Sulfide	ppm	10.8	87.3
Sulfate	ppm	28.6	
Soluble Salts			
Calcium	ppm	32.5	101
Magnesium	ppm	4.5	28.8
Sodium	ppm	12.4	3
Potassium	ppm	10	0.76
Sulfate-S	ppm	28.6	491
Chloride	ppm	12.9	60.1
Bicarbonate	ppm		<16.4

Metal	Discovery Mine ppm	Faro Mine ppm
Aluminum	22,600	418
Arsenic	40.5	725
Antimony	1.38	71.7
Barium	114	76.4
Beryllium	0.243	0.144
Bismuth	<0.70	10.1
Cadmium	0.252	28.9
Calcium	5,110	1,070
Chromium	83.8	2.82
Cobalt	17.2	139
Copper	53.9	1440
Iron	75,100	386,000
Lead	21.7	13,200
Lithium	37.2	0.617
Magnesium	11,100	1,070
Manganese	338	1,260
Mercury	1.93	
Molybdenum	1.26	2.3
Nickel	63.3	13.9
Phosphorous	595	205
Selenium	1.6	4.23
Silver	0.144	24.3
Silicon	304	140
Strontium	17.1	7.4
Thallium	0.9	9.9
Titanium	2,920	4.95
Tin	<0.3	2.12
Vanadium	60.4	5
Zinc	93.4	23,800

Table 4-2. Composition of Discovery Tailings by Neutron Activation Analysis

Element		Non-Weathered	Error (+/-)	Weathered	Error (+/-)	Change (%)
Aluminum	%	5.82	0.04	4.7	0.03	-19%
Antimony	ppm	0.4	0.04	0.54	0.04	35%
Arsenic	ppm	52	3	127	6	144%
Barium	ppm	552	25	388	69	-30%
Calcium	%	1	0.07	1.25	0.07	25%
Cerium	ppm	51.7	1.3	44.1	1.2	-15%
Cesium	ppm	3.3	0.1	2.34	0.06	-29%
Chromium	ppm	158	9	100	6	-37%
Cobalt	ppm	19.2	0.5	8.51	0.18	-56%
Europium	ppm	1.35	0.03	1.06	0.03	-21%
Gold	ppm	0.29	0.01	2.78	0.06	859%
Hafnium	ppm	3.34	0.26	2.12	0.24	-37%
Iron	%	4.41	0.05	3.28	0.04	-26%
Lanthanum	ppm	24.8	0.4	27	0.6	9%
Manganese	ppm	459	7	349	5	-24%
Nickel	ppm	46	3	ND		
Potassium	%	1.9	0.24	1.59	0.33	-16%
Rubidium	ppm	89	3	68	4	-24%
Samarium	ppm	4.61	0.09	3.57	0.07	-23%
Scandium	ppm	17.3	0.4	10.1	0.2	-42%
Sodium	%	1.4	0.03	0.83	0.02	-41%
Strontium	ppm	120	21	127	19	6%
Tantalum	ppm	0.5	0.03	0.34	0.03	-32%
Terbium	ppm	0.58	0.04	0.48	0.06	-17%
Thorium	ppm	5.31	0.4	3.82	0.29	-28%
Titanium	ppm	3210	150	2330	130	-27%
Tungsten	ppm	12	1	27	2	125%
Uranium	ppm	2.25	0.44	1.16	0.3	-48%
Vanadium	ppm	2.25	0.44	1.16	0.3	-48%
Ytterbium	ppm	1.62	0.25	1.18	2	-27%
Zinc	ppm	165	8	134	7	-19%
Zirconium	ppm	110	16	ND		

Table 4-3. Bacteria Plate Counts

Media	Dilution	Bulk Original	Frozen and Dried	20 °C Cell	1 °C Cell	Insitu Weathered
PCA - Heterotrophs	x10e-5	0	0	11	12	2
	x10e-4	6	0	98	87	0
	x10e-3	38	0	tntc	tntc	7
	x10e-2	tntc	1	tntc	tntc	57
	x10e-1	tntc	8	tntc	tntc	tntc
Total Count (cfu/g)		~50,000	~10	~1,000,000	~1,000,000	~6000
Media 64 Iron oxidizers	x10e-5	0	0	0	0	0
	x10e-4	0	0	0	0	0
	x10e-3	0	0	0	0	2
	x10e-2	0	0	0	0	11
	x10e-1	0	0	0	4	159
Total Count (cfu/g)		0	0	0	40	~1500
Media 238 Acidophilic sulfide oxidizers	x10e-5	0	0	0	0	0
	x10e-4	0	0	0	2	0
	x10e-3	0	0	9	12	5
	x10e-2	32	0	172	198	44
	x10e-1	133	0	tntc	tntc	tntc
Total Count (cfu/g)		~2000	0	~15,000	~20,000	~4500
Media 450 Neutrophilic sulfide oxidizers	x10e-5	2	0	6	20	0
	x10e-4	14	0	104	137	0
	x10e-3	154	0	tntc	tntc	0
	x10e-2	tntc	2	tntc	tntc	0
	x10e-1	tntc	16	tntc	tntc	0
Total Count (cfu/g)		~150,000	~200	~1,000,000	~1,500,000	0

5 DISCUSSION AND ANALYSIS

Using the results from the physical (Section 4.1), thermal (Section 4.2) and microbial characterization (Section 4.3), this chapter presents an analysis of the results and discusses their consequences with respect to the effects of temperature on the generation of acid mine drainage. Since the intent of the investigation was to determine the expected effects at the Discovery Mine, the results from the tests using tailings from Faro mine, as well as other northern sites, will be extrapolated to assess the Discovery site.

5.1 PHYSICAL PROPERTIES ANALYSIS

5.1.1 Grain Size Distribution

As shown in Figure 4-1, the Discovery Mine material has a grain size composition of approximately 35% fine sand, 60% silt and less than 5% clay sized particles. The Faro material is significantly coarser, with approximately 65% fine sand, 35% silt and less than 1% clay sized particles. If grain size alone were to determine the amount of unfrozen water in a sample, the Discovery material would have a significantly higher unfrozen water content, according to capillary pressure / matric suction principles (Williams, 1964). In Figure 4-10 however, this is not the case; therefore, other factors must be contributing to the unfrozen water content.

Another parameter used for modeling unfrozen water content is the material's liquid limit, as shown in Equation 2-14 (Tice, Anderson and Banin, 1976).

$$w'_{u,\theta=-1} = 0.346 \cdot LL - 3.01 \qquad \text{Eq. 2-14}$$

The liquid limit data from Klohn Leonoff (1992) of 40% corresponds to an unfrozen water content of 11% at -1°C. The results from the TDR tests, Figure 4-10, show an

unfrozen water content of 25% at -0.9°C and 4% at –1.5°C for the Discovery tailings. Given the uncertainty involved in both TDR and liquid limit test, this predicted value is within the expected range. However, given the very large change in unfrozen water between these temperatures, the results from the liquid limit prediction are inadequate without further tests. Given the fact that there is less than 5% fines in the tailings, and that liquid limits were not obtainable with the tailings tested in this study, this predicted value is even more questionable. Finally, given the temperature range at the Discovery site, the benefits of knowing the unfrozen water content at -1°C are limited.

5.1.2 Mineralogy

The mineralogical speciation performed on the Discovery tailings showed the presence of quartz, albite, anorthite, muscovite, chlinochlore, gypsum and ferroactinolite. Combining this data with the ICP and NAA metals analyses listing the iron content at under 8% and sulfur at less than 1% suggests that the minerals (such as iron sulfates) which could offer insight into the electrochemical conditions within the tailings are so scarce that no interpretation of the insitu weathering or precipitating conditions is possible.

Furthermore, using acid-base accounting descriptors, the bulk Discovery material has a net neutralizing potential of 9 kg $CaCO_3$ / tonne and a Neutralizing Potential : Acid Potential ratio of 1.5. Given all of these factors, it is not surprising that the Discovery material did not generate acidity in the laboratory. However, as described in Chapter 2 and confirmed in the field, it is the kinetics of the reactions that are the most important, since these tailings were observed to generate significant acidity in the weathered zone.

The Faro material was not tested for mineral species, but it was assessed for metals analysis. These showed a sulfur content of 22% and an iron content of almost 40%. With less than 1% carbonates present, the net neutralizing potential was approximately –690 kg $CaCO_3$ / tonne of material. This is considered extremely acid generating, which was confirmed in the leaching tests. Other tailings in the Canadian Arctic with similar acid generating capacity are from Wellgreen Mine in the YT, and Nanisivik Mine in the

NWT (Klohn Leonoff, 1994). Given these conditions, the Faro material may not be a good surrogate to represent accelerated weathering of the Discovery tailings, but it does provide a 'best case scenario' for determining the qualitative effects of temperature on the acid generating process. This is confirmed further in Section 5.2.

5.2 THERMAL PROPERTIES ANALYSIS

The thermal characterization of the tailings from the Discovery and Faro mines included testing for unfrozen water content and thermal conductivity with temperature. Figure 4-10 shows the results in terms of volumetric unfrozen water content, or unit volume of unfrozen water per total unit soil volume (including ice). This is recalculated in Figure 4-10b as gravimetric unfrozen water content, or mass of unfrozen water per mass of dry soil (% dry weight). For the Faro material, there is a significant difference between the two values, as the specific gravity is especially high with the elevated metals content. Because of this, the volumetric water content is a better measure for comparison purposes; however, to translate from one to the other requires the dry density. In the literature surveyed, some of the data is presented as % dry weight and some as volumetric water content. In many instances, it is uncertain which format has been used.

5.2.1 Discovery Mine – Unfrozen Water

Figure 5-1 compares the volumetric unfrozen water content of the Faro and Discovery tailings with 5 other soils. Except for Hivon (1991), the soils are expected to have very low amount of dissolved solutes. Nevertheless, the figure still demonstrates that the Discovery material has a minimal freezing point depression of approximately 1°C. At temperatures above -1°C, the tailings retain significant unfrozen water. This is likely due to the low solute content within the pore water in addition to the lack of significant fines. The electrical conductivity of the Discovery pore solution was 0.55 dS/m, which corresponds to an ionic strength (Dudas, 1998) of approximately 0.007 moles / L.

$$I = 0.0127 \times EC \qquad \text{Eq. 5-1}$$

where I is ionic strength (moles/L) and EC is electrical conductivity (dS/m).

At temperatures below -1°C, the Discovery tailings exhibit behavior similar to the very fine silty sand with 5 ppt of NaCl, as reported by Hivon (1991). This further supports the idea that the non-weathered material would be relatively non-reactive when frozen. The relevance, therefore, is that if the tailings could be stored in a permafrost state, the amount of water available for chemical reaction would be negligible.

For the case of the tailings already deposited and capped in the delta at Discovery though, the bulk of the material is not likely to experience sub-zero temperatures, due to the adjacent Giauque Lake which acts as a heat source. With a surface temperature of –10°C in March, 1999, 0°C was measured at a depth of 0.75 through 1.25 m from the tailings surface, increasing to +2°C at 2.0 meters (Figure 3-17). Hence, the zone of seasonal freeze-thaw activity in the delta is approximately 1 m. In September of 1998, the tailings profile indicates that the material temperature was above 8°C to a depth of 2.0 meters. Similar conditions were present at the airstrip (Figure 3-17), with a probable frost penetration depth of 1.5m.

Considering oxygen availability, Dave and Blanchett (1999) reported that the oxygen diffusive flux, or amount of oxygen transported across a unit area, across water saturated tailings, is 3.5 g/m^2/year at 25°C. This is reduced to 2.6 at 4°C and 2.3 at 0°C. Unlike the airstrip, the tailings delta samples did not display any weathering profile. Additionally, the water table was sufficiently close to the top of the tailings that matrix suction, generated from the fine-grained material, was sufficient to maintain near-saturated conditions up to the surface of the tailings. Given the anticipated near saturation conditions within the tailings delta and the additional cover added, the infiltration of oxygen is likely to be diffusion dominated and hence the quantity of oxygen would be negligible.

The same report indicates that for a dry waste, with no cover, the oxygen diffusive flux is 10,900 g/m^2/year at 25°C, 5500 g/m^2/year at 3°C and 4200 g/m^2/year at 0°C. Given the

unsaturated conditions beneath the air strip and the deep seasonal freeze-thaw zone. the tailings would be expected to encounter significant weathering conditions if sufficient moisture was available. Unfortunately, no unfrozen water readings were taken for this weathered, unsaturated material, so it is uncertain what the effects of sub-zero conditions would be on their acid generating capacity.

5.2.2 Faro Mine – Unfrozen Water

Figure 5-1 also shows that the unfrozen water content in the Faro tailings was a result of more than capillary pressure or adsorbed water, as the grain size of the Faro tailings were significantly coarser than the Discovery material. Figure 5-2 compares the unfrozen water content of the Faro tailings with a variety of soils having different NaCl concentrations.

The Faro tailings can be classified between a fine sand and a silty sand. Given this fact. the unfrozen water content curve would be expected to lie between those two soils on the graph if its pore fluid had a solute concentration equivalent to 30ppt NaCl. However. it was seen to have even more unfrozen water than the very fine silty sand with 30 ppt NaCl. This confirms Figure 2-9, that the effect of the solutes on unfrozen water is much more significant than the grain size. The electrical conductivity of the pore water was 4.97 dS/m, equivalent to an ionic strength of 0.063 moles/L (Eq 5-1). Considering that solutions with an electrical conductivity greater than 4.0 are considered brines, the Faro tailings pore solution is very concentrated.

5.2.3 Thermal Conductivity

A thermal conductivity probe was used to measure the thermal conductivity of the Discovery and Faro mine tailings (Figure 4-12). As expected, the frozen thermal conductivity of both tailings was higher than the thawed conductivity, with the exception of the temperatures close to 0°C which are ambiguous due to the heat associated with the phase change of water. The frozen thermal conductivity for the Discovery tailings of 3.3

W/m°C is within the range of expected values as shown in Table 5-1, which shows the thermal conductivity for several other mine tailings, in addition to typical soil components. Lupin Mine (NWT) has similar tailings grain size material, in addition to being a gold mine in a similar geological formation. The slight difference might have been due to differences in density (Williams, 1991). The dry densities of the thermal conductivity cells were 2.6 and 1.4 g/cc for the Faro and Discovery tailings respectively: the density of the Lupin tailings was not reported. The thermal conductivity of water is 0.6 W/m°C, as opposed to significantly higher values of 7.7 to 8.8 for quartz. As a saturated soil is compacted, reducing the water content, the thermal conductivity will increase because the volume fraction of mineral grains increases. This is also true of unsaturated soils. Air is an excellent insulator, with a conductivity of 0.025 W/m°C. With a decrease in air voids, the thermal conductivity increases.

Norwest (1998) suggests that the high percentages of metallic minerals (iron sulfate and oxides) do not seem to significantly increase thermal conductivity beyond those expected for natural soil. Without additional tests with control material at known densities, it is not possible to confirm this; however, the work done in this program would suggest otherwise.

For the majority of the published tests, and for the current work, there is a region close to 0°C that has very different behavior, usually resulting in a high peak. Norwest (1998) suggests that this may be due to the onset of solute crystallization at the freezing temperature of the solution. This is a reasonable explanation, as it is the material with the high solute concentrations that displays the peaks. It is unknown however, whether the Norwest (1998) tests were conducted with increasing or decreasing temperature. With a lowering of temperature, with accompanied solute exclusion and precipitation, this hypothesis bears merit. Given that the current tests were run with increasing temperatures, it would require time for the unfrozen material to come to chemical equilibrium and re-precipitate in crystal form.

5.3 BIOTIC EFFECTS ON ACID GENERATION

The microbial test results posed significant uncertainty. As described in Section 4.3, it was initially assumed that the bacteria would be present in all of the bulk samples. After reviewing many of the options available for operating the tests under abiotic conditions, irradiation using a cobalt-60 reactor was employed, as this was believed to result in the least impact upon the soil chemistry and potential acid generation of the tailings.

After the first series of tests using the Discovery material in the humidity and static batch cells did not generate significant acidity, the operation of the batch static cells, including those which had been irradiated, was terminated. It was therefore not possible to determine if there had been any biotic effect in the acid generation, nor possible to confirm the bacteria's presence.

To determine if a lack of bacteria was the cause for the lack of acid generation in the first trial, a bacterial enumeration was conducted. As reported in Chapter 4, a tailings inoculum from several sites revealed that sulfide oxidizing bacteria were present in the humidity cells and in the original bulk material. While this did demonstrate that the bacteria were present in the tailings, it did not explain the lack of acid production. This material was later abandoned because it was believed that the low sulfur content could not generate measurable acid production in the laboratory scale testing within an acceptable time.

One note of interest was the analysis performed on the weathered column of tailings from the airstrip. The surface material provided the only inoculum capable of growing iron oxidizers, and the only inoculum that failed to grow neutrophilic sulfide oxidizers. This suggests that there is an active iron oxidizing zone on the surface of the weathered tailings that has failed to penetrate deep into the unweathered tailings. This may be due to competition between species or to the inability of the iron oxidizers to survive in a neutral environment. Due to the limitations of the scope of the project, the bacteria present were not isolated and identified.

The next stage of tests involved similar humidity cell and batch cell tests. Because uncertainty remained about the biological activity within the tailings, an initial series of enrichment cells were run. The intent was to augment the microbial activity in selected cells by supplying a mature inoculum to the batch cells. As shown in Figure 4-13, these results were again inconclusive as the pH dropped in both the inoculated flasks and the control flasks. These results do show, however, that the activity of the bacteria decreased with temperature. This merely confirms the widely accepted principle that most chemical and microbial activity decreases with temperature. As described in Chapter 2 though, not all bacteria behave in this manner, and that exceptions do exist where the bacteria prefer cooler temperatures.

Because of the uncertainty relating to microbial presence and activity, attempts were made to visual ascertain their presence. At low magnification this was inconclusive, for while bacteria sized particles were present in solution, there was no visible motion typical of active bacteria. The presence of the bacteria was finally confirmed using the transmitting electron microscope, endorsing further bacterial enrichments for inoculating the batch cells.

Given the above, the entire process of assessing the role of bacteria in the generation of acid drainage was extremely difficult. It may be that the opinion of Morin (1998) is valid and sufficient: the chemical and biological components are inseparable and they should be treated together without trying to isolate specific roles or capacities.

In the final round of static batch cells, the microbial inoculum had at least two bacterial populations as shown in Figures 4-14 and 4-15, due to the addition of tailings from the Discovery and Faro sites. It was felt that by combining the bacteria into a single inoculum, the bioactivity rate would be increased and would eliminate the need for further duplicates. A concern was that the bacteria might compete, and reduce the activity of both populations. It is possible that this occurred, but previous work by Battaglia-Brunet et al. (1998) showed that mixing strains of Thiobacillus ferrooxidans.

Thiobacillus thiooxidans and Leptospirillum ferrooxidans produced a more efficient population for pyrite oxidation than any other single or paired population.

5.4 EFECTS OF TEMPERATURE ON HUMIDITY CELLS

Because the humidity cells using Discovery tailings did not generate acidity, the effects of temperature on the weathering of the tailings cannot be discerned; as such, the results will not be analyzed further.

5.4.1 Effects of Temperature on pH for Faro Tailings

The humidity cells comprised the longest ongoing portion of the testing program. As described in Chapter 4, the tailings samples were systematically leached and tested for sulfate and pH. Figure 4-20 shows the results of pH vs time for 20, 3 and 1°C for the Faro mine tailings. All three samples had an initial average pH of approximately 2.7. Beyond this time, there are few similarities.

With the initial low pH, it could be assumed that the tailings environment had already achieved Stage III conditions as described in Figure 2-2. However, because the pH rose quickly in all the cells, it is more likely that the early cycles were merely rinses of the highly soluble and acidic constituents.

The 20°C humidity cells had the greatest initial slope in the plot, which peaked at a pH of approximately 3.8 after 5-6 weeks, then began to slowly decrease. The initial rise in pH is likely due to the early rinsing of the acid in the pore solution. As the rinsing continued, the remaining acid became diluted resulting in a gradual increase in pH. This conforms to published results indicating that there is usually an initial rise (Morin and Hutt, 1997). The slope is steepest at 20°C due to the increased solubility of the acidic material at higher temperatures. Due to the relatively consistent decrease in pH with time after the peak, it is unknown how much more acidic the conditions would have become. If the cells follow the trend displayed by the shake flask test results, then the bacteria species

present in the tailings may be active to pHs below 1. Humidity cell tests previously performed on Faro tailings at standard temperatures (Curragh Resources and SRK, 1991) generated leachate pH of 2.9 after 7 weeks of tests. If this trend was followed, the cells may have already reached their lowest pH.

The best fit line for the 3°C cells had the shallowest slope of increasing pH with time, though the scatter in the early cycles makes this assertion questionable. The peak acidity was achieved at weeks 12-14, after which the pH began to decrease. It is interesting to note that that slope of the downwards curve resembles the slope on the 20° curve. Further testing could confirm this relationship. Also of note is the fact that the pH peaked at 0.5 units higher than at 20°. This may be due to the highly acidic pore water being rinsed as quickly as for the 20° cells, but that the minimal buffering capacity present was less soluble at the lower temperature so that it was not dissipated in the early rinses with the acid. This hypothesis is supported by the curve for the 1°C cells, where the peak pH was even higher.

The error bars on Figures 4-21a-c represent 1 standard deviation from the average of the 3 cells. As explained above, some weeks the samples were dried more or less than others, resulting in a variable concentrated leachate. As this occurred to different cells at different times, the cells experienced slightly different weathering conditions and as such, the variability with time was inevitable. The remainder of the test conditions were uniform across all the samples.

5.4.2 Effects of Temperature on Sulfate Leaching

Using sulfate concentrations as an indicator for acid production did not generate the same shape of curves as pH. Figure 4-20 shows that each temperature experienced an initial drop in sulfate levels, with later increases. The 20°C cells had a concentration peak at approximately 7-8 weeks, then had a significant drop and then another rise.

The initial drop in sulfate is likely due to the initial rinsing of the soluble salts. Following this, the gradual rise represents weathering of the sulfide minerals, indicating active oxidation. The second peak may be due to a subsequent sulfide mineral that was not soluble enough to weather earlier. As described in previous sections, each sulfide mineral has a different solubility; this is especially true of pyrite and pyrrhotite, both of which are present in the Faro tailings (Klohn Leonoff, 1994).

The 3° cells display the same initial decrease in sulfate as the 20° cells, but maintained relatively low sulfate concentrations of approximately 400 mg/L for the first 12 weeks. The sudden increase to approximately 1200 mg/L at week 13 corresponds with the time of the peak in the pH vs Time curve (Fig. 4-20). The onset of increased sulfate production provides further evidence for the onset of the AMD sequence (Fig. 2-2) at this temperature.

The 1° cells also show early sulfate decreases followed by a period of consistent sulfate levels, with an increase in concentration earlier than the 3° cells, after 10 cycles. Additionally, Figure 4-24 shows that after 14 cycles, the 1° cells had released approximately 3200mg of sulfate, 500mg more than the 3° cells. This reversal of expected results is likely only temporary, as the sulfate released in the 1°C cells decreased to approximately 300mg / cycle at cycle 14 from 500mg/cycle at cycle 11, while the 3°C cells have maintained levels above 350 mg/cycle. These figures do not include the sulfate content from first week of leachate, as it is assumed that this sulfate is primarily dissolved sulfate salts and not a function of sulfide oxidation. At the current rates of oxidation, the total sulfate released by the 3° cells would surpass that of the 1°C by cycle 20. Furthermore, Figure 4-20 shows that the pH curves for the two temperatures are very similar. Given that the rates are low (relative to the 20°C cells) over a short period, the differences may be negligible.

5.4.3 Effect of Redox Potential

Early tests for Eh in the Discovery and Faro tailings humidity cells showed that the solution was extremely reactive with the atmosphere, to the extent that the readings would not stabilize. This indicates that the leachate was reacting even after being passed through the filter and may be due to the presence of highly reactive iron (III). In a highly acidic environment with elevated redox potential, iron (III) is the dominant iron species in solution. The presence of Fe^{3+} has been used in numerous studies (Mehling, 1999; Morin, 1998) as an indicator of weathering conditions. These same studies indicate that while Fe^{3+} may be present, for accurate results the solution would have to be tested immediately for iron (III) and therefore also Eh. Given the nature of the humidity cell test wherein the leachate collects in a flask overnight to provide the cell the opportunity to drain, it would be necessary to have an anaerobic sealed collection system to prevent any further reaction and stabilize the Eh readings. This was beyond the financial means of this project given that it provided non-essential, though useful, data for the intended purpose of the investigation.

5.4.4 Humidity Cell Operation

The pH and sulfate analyses were initially conducted at the University of Alberta Soil Science Department. Due to machine malfunctions however, the sulfate testing was transferred to Norwest Labs for the final two months of the testing program.

In the second round of tests (on the Faro tailings), the humidity cells performed very well. By passing the air through the cell, but not forcing it through the sample, the tailings dried without disturbing the sample. As the weeks progressed, there was some deterioration of free flow of leachate. It was found that some cells had to have an initial pressure applied in order to start the flow of water. This may have been due to an air bubble above the membrane, or suction preventing flow, or due to plugging of the membrane. Once the water started draining, it was rare for it to plug again until the following leach cycle.

Early in the testing, the cells were weighed periodically to ensure that they were drying correctly. After prolonged use, this became unnecessary as the consistent moisture content and flow of air was established. On several occasions however, a sample overdried due to a change in cell backpressure. This was verified by monitoring the rate of air bubbling through the outlet port of the cell. If changes in the water level had occurred due to evaporation, the flow increased through that cell. This would result in fluctuations to the pH and/or sulfate levels, as a dried cell would not have any accessible water for oxidization during the dry air phase (Pool and Balderrama, 1994). Additionally, due to decrease in leachate volume, the total sulfate load would be depressed. Despite the presence of a number of questionable outlying data, the humidity cell results as a whole appear to be valid.

5.4.5 Humidity Cells – Comparison to Other Studies

The published literature on similarly conducted tests is very limited. Until recently, acid generation was of little concern in northern regions, so few tests were performed at near-zero temperatures. Some of the other tests performed at low temperatures included leaching columns with tailings from Cullaton Lake Gold Mines, NWT, at 2°C (Dave and Blanchette, 1998), and from Windy Craggy Mine, B.C., at 6-8°C (Dawson and Morin, 1996). The Cullaton Lake material had 2.3% total sulfur, with an AP, NP and NNP of 73, 44, and –29 kg $CaCO_3$/tonne of tailings, significantly less potentially acidic than the Faro material. The data from these tests are shown in Figure 5-3. At 25°C, the pH droped from approximately 7.5 to 3.5 over a period of 2 weeks, then was level for about 30 weeks, when it began to rise steeply. At 2°C, the pH dropped by approximately 1 pH unit over the same period.

At the same time, the leachate was tested for sulfate (Figure 5-4). The 25°C cells showed an early peak of 18,000 ppm sulfate at 4 weeks, then decreased slowly to 4000 ppm at 12 weeks, then to slightly above the 2°C levels at 2000 ppm until the end of the test. The 2°C cells had an initial sulfate leach concentration of 16,000 ppm which decreased rapidly over 3 weeks to 4000 ppm and then to 1500 ppm after 7 weeks and beyond. The

presence of such a ideal peak at 20°C suggests a single sulfide type, making direct comparisons to the current results impossible.

Dave and Blanchette (1999) conclude that based on the total sulfate loading during the active acid production / neutralization periods for the two temperatures, the sulfide oxidation / acid generation rate at 2°C was estimated to be reduced by a factor of between 5-6 of that at 25°C. It is uncertain what means of calculation were employed to determine this value, as the 2°C cells only reached acidic conditions after 1.5 years (Dave and Blanchette, 1998).

Results from humidity cell tests were performed on tailings from Windy Craggy mine (Dawson and Morin, 1996.) show pH and sulfate release for cells at 20° and 6°C (Figures 5-5 and 5-6). The temperature differences between cells is not as large as in the current study or in those from Cullaton Lake; however, with respect to sulfate production rates and leachate pHs, the Windy Craggy samples showed that the pH was lower and the sulfate release rate higher for the higher temperature. Here again, it is seen that quantifying of the effects of temperature is material specific, and little or no general correlation can be made to the results from this study.

The intent of this research was to first determine qualitatively that acid generation would occur at lower temperatures, then to attempt to quantify it. Bearing in mind that each tailings source is different, and that exact field conditions cannot be replicated, the conclusions from this test are that acid drainage does occur at lower temperatures. It is still uncertain if the same amount of acidity would be produced at the lower temperatures, but it appears that the only effect of the temperature was a lag time for depletion of the neutralizing potential. Further tests would reveal if the final slopes of the pH vs time plots for the 20, 3, and 1°C cells are the same (Figure 4-20).

Because of the complex nature of the iron and sulfur species in solution and mineral form, prolonged test data is required to generate accurate rate predictions. As the pH continues to drop, the sulfate levels will continue to increase until the sulfides are

completely reacted. If the trends at the end of the test continued, it would require over 15 years at 20°C and over 30 years for the lower temperatures to achieve complete oxidation, subject to an array of factors, including eventual mineral coating, decrease in weathering area and changes in pH. Unlike the Discovery tailings that contained very low sulfur content, the Faro tailings would be ideal for long term tests, as there would be little concern of sulfide depletion in the sample.

5.5 EFFECTS OF TEMPERATURE ON BATCH TESTS

5.5.1 Predicted Batch Test Results

While not intended to simulate site-specific leaching conditions, the batch cells were intended to provide a means for measuring the change of acidity and of dissolved constituents with time under a set of controlled variables. A similar method, utilizing shake flasks principles (ASTM D3987) but without the agitation, was used by Ahonen and Tuovinen (1990), at 10% solids, to measure the rate of change in pH. In their first trials, elemental sulfur was used as a substrate. Figure 5-7 shows the change in pH with time over 6 months. As expected, the rate of change in pH decreased with temperature. Taking the natural log of the change in pH with time (ln dpH/dt), and plotting against the inverse of temperature as shown in Figure 5-8 reveals an almost linear curve. By extrapolating these results, it is possible that the reactions would continue even to sub-zero temperatures. However, given the complication of the phase change of a portion of the pore fluid below 0°C, the effect on this relationship is uncertain.

In Ahonen and Tuovinen (1991), a similar experiment was conducted using pyrite and pyrrhotite as the substrate. The rate constant in this figure is a measure of the copper (pyrrhotite indicator) and cobalt (pyrite indicator) in solution. As with the elemental sulfur (Figure 5-8), it appears that the oxidation of the sulfides may continue at sub-zero temperatures. Of note in this figure, is that the reaction rate for pyrrhotite at 4°C is similar to the rate for pyrite at 30°C. This demonstrates that sulfide type is an extremely

important factor in determining the potential for AMD. The figure does not indicate, however, if there could be a critical temperature at which all reactions cease.

Figure 5-9 is an idealization of how the sulfur release with time results were expected to appear. Based on shake flask tests, shown in Figure 5-7, the sulfur concentration would increase as the pH decreased. The rate of change of sulfur in solution, or dpH/dt, for 20° would be greater than at 10°, which would be greater than at 3°, down to a critical temperature at which the reactions would cease. Based upon the results from Figure 5-8, it is uncertain at what temperature the reaction would cease. For the reactive material, like pyrrhotite, this critical temperature would likely be significantly lower than for less reactive pyrite. There would likely be a lag time present for the lower temperatures, indicating an acclimatization period for the bacteria, assuming that their role is significant, the duration of which would depend on its strain and history.

Another factor that must be considered is the effect of solute exclusion. As the temperature decreases, the solute concentration increased in the remaining liquid. For systems at temperatures below 0°C, this becomes a factor, as the solutes present are concentrated. As described in Chapter 2, pH also has an effect on the reaction rate, and may be facilitating or restricting for further reactions. The balance between increases in activity due to increased concentration and decreases due to lower temperatures is unknown.

5.5.2 Sources of Error

For the first round of testing, the Discovery tailings batch tests proved unsuccessful at predicting the rate of sulfide oxidation. The cells were tested for pH after 5 months, but revealed no significant change with respect to temperature. This was due to a number of physiological / chemical factors. The first possibility was that the high NP:AP ratio and initial neutral pH of the solution effectively prevented the biochemical component of the AMD process from catalyzing the oxidation and the onset of acid generation. The high

neutralizing potential of the tailings acted as a buffer against the effect that the sulfide oxidizing bacteria may have had.

In addition to the possibilities listed above, there are two possible weaknesses in the system design. A cell could fail when the seal to the flask is broken, allowing water or glycol to leak into the flask. The second possible problem is that the gas transfer membrane failed to allow sufficient oxygen to enter the flasks. Prior to starting, the membranes were tested by adding water into the top of a tube sealed at the base with a membrane. Over the next 24 hours, the water had expelled the air, confirming its transmissivity. Therefore, the apparatus was functional at the outset; however, during the course of the test, blockage may have occurred from condensation on the membrane surface impeding oxygen flow, or merely the inability to pass sufficient oxygen to support the chemical reaction (i.e. the reaction was oxygen limited).

In addition to possible membrane failure, additional variability may exist with the sampling or extracting technique. One possibility is that the water in the cells was not homogeneous, and that extracting different volumes of pore water would result in changes to the extracted water. For this to be true, the pore water in the cells would have to be discontinuous, such as films of unfrozen water, or a change in pore water quality with pore size. In either case, if the extraction method did not draw the pore water uniformly from the entire sample, the leachate quality would vary.

If it was the result of 'pockets' of concentrate, then one would expect there to be a relationship with the leachate volume. The samples were collected in 50 mL vials, and with very few exceptions, these were filled to within 10 mL of the top. Even if the additional 20% experimental error were applied, the results still could not be explained over the ranges of temperatures tested.

Based on the evidence described, it is believed that the membrane failure was the primary cause of the poor results. The next section provides further evidence for this theory.

5.5.3 Consequences of Membrane Failure

Assuming that the membrane did not allow sufficient oxygen supply, several of the results from the 2nd series of batch cell leachate tests can be explained. As seen in Figure 4-29, the 20°, 3° and 0°C data of sulfur concentration vs. time show a curve with a peak at 4 to 5 weeks followed by a decrease in sulfur. If the influx of oxygen was less than the oxygen being utilized in the acid generating reaction, then the system would become increasingly anaerobic. Unlike the humidity cells, the pore water was not being leached, so there could not be a removal of the sulfides from the closed system. Instead, as the oxygen was being depleted, the redox potential was decreasing. As seen on Figure 4-27, the batch cells were operating with conditions denoted by the Area C. This region is very transitional, as it marks the equivalency points between HSO_4^- and SO_4^{2-} as well as of sulfides / sulfates. As such, decreased oxygen concentration would lower the Eh, causing a shift in the system equilibrium. This may explain the wide variability seen in the early tests for sulfate, as the area C traverses the redox zone for the solubility of pyrite. Therefore, if the system was depleting the oxygen supply, the solubility of sulfate would be decreasing, resulting in a precipitation of pyrite or sulfur, and a removal of sulfur/sulfate from the aqueous system.

Given this explanation, it is uncertain why the same trends were not visible in the +1.5°C data. The time independent relationship for the sulfur in solution at –1.5° and -3°C may be explained by an increased lag period for the bacterial activity, or to the slower reaction rates; however, this would not explain the high sulfur concentration at -10°C. The seemingly random data at -10° may be a product of decreased unfrozen water content.

Unlike at -3°, where the samples remained predominantly unfrozen and contained little ice, at -10° the tailings were a solid-bound mass, yet, when the -10°C sample was compressed, the water was released in the same manner as for the higher temperatures.

The samples were not given time to thaw before being compressed, so the water extracted must have been the water that remained unfrozen. Figure 5-1 shows that at -10°, there will still be a 30% unfrozen water content. If this was the case, the solutes may have become concentrated in the unfrozen water. This would explain the elevated sulfur concentrations, as the pure water would have remained in the soil mass.

5.6 CORRELATION BETWEEN HUMIDITY CELLS AND BATCH CELLS

Because the static batch cells did not display any effects of the change in temperatures, no relationship could be drawn between the static and the kinetic weathering procedures. If the batch tests had been effective in evaluating pyrite dissolution with time, the rate of change of the pH on the final slopes of the pH vs time plots (Figure 4-20) for the humidity cells would have been correlated with the rate of change in the batch cells. Insufficient data is available to assume that the first 4 to 5 weeks of data from the 20° and 0°C batch sulfur vs time curves could present a 'bounding' of the oxidation depletion or pyrite dissolution rates for comparison purposes.

5.7 RECOMMENDED CHANGES TO TESTING PROGRAM

In order to obtain weathering curves that facilitate comparisons for changes in pH or metal/sulfate release rates with different temperatures, it is recommended for future testing to use material with a single sulfide source. This would limit the potential for complicating release rates. Otherwise, if a mine has not investigated the sulfide forms present in the parent material, then attempts to predict or compare acid generation from laboratory testing would be of little value. Therefore, the ideal tailings sample for testing to determine the quantitative effects of sub-zero temperatures on acid generation would be a high sulfide material with a single sulfide source (i.e. all pyrrhotite). Though not simulating real field conditions, the relationships determined could be applied in qualitative terms to assist in the characterization of leach tests at actual site conditions.

Few changes would be made to the humidity cell apparatus, as it functioned as expected. If a greater budget were allotted, an air flow meter / regulator on each cell would assist in maintaining equal air flow and consistent drying.

It is uncertain what changes could be made to the batch tests. Theoretically, if a room had 100% relative humidity, the tailings samples could be left open to the atmosphere without concern of dehydration. This would ensure an adequate oxygen supply to the tailings. Operating with the premise that the batch cells successfully used by Ahonen and Tuovinen differed only in moisture content, albeit an extreme difference, the samples could have had a higher moisture content. To resolve the concern of oxygen availability, the samples could be laid in thinner strips, in order to allow oxygen to pass through the saturated frozen material by diffusion rather than advection.

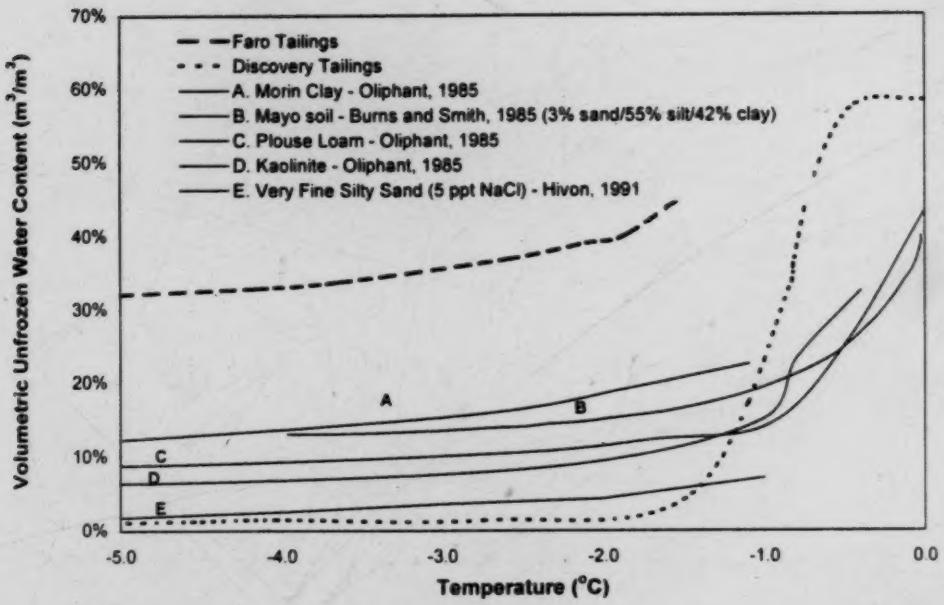

Figure 5-1. Comparison of Volumetric Unfrozen Water Content for 5 Soils with Faro and Discovery Tailings

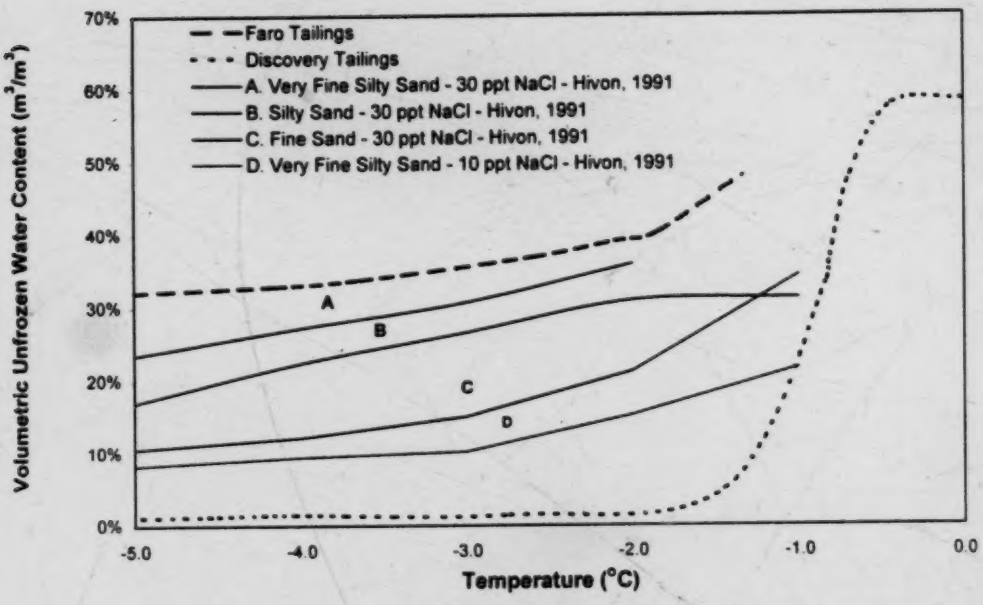

Figure 5-2. Effects of Grain Size and Solute Strength in Volumetric Unfrozen Water Content

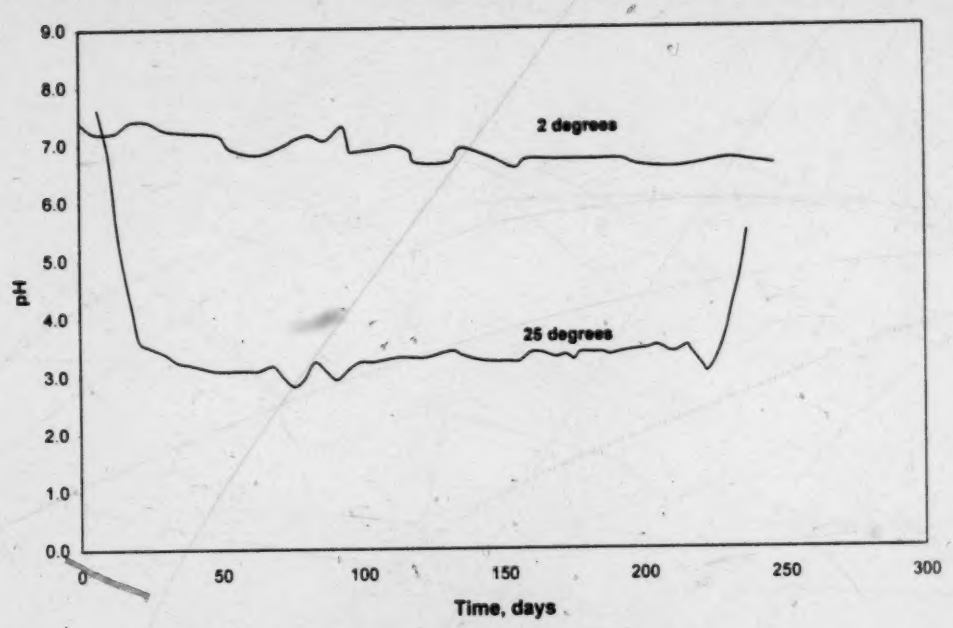

Figure 5-3. Cullaton Lake Humidity Cells - pH vs Time
(Dave and Blanchette, 1998)

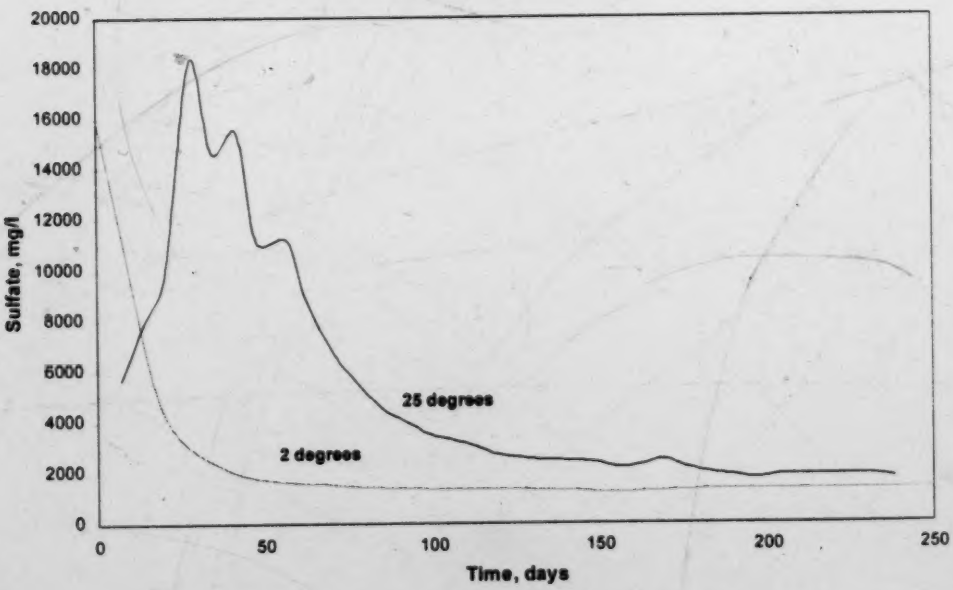

Figure 5-4. Cullaton Lake Humidity Cells - Sulfate vs Time
(Dave and Blanchette, 1998)

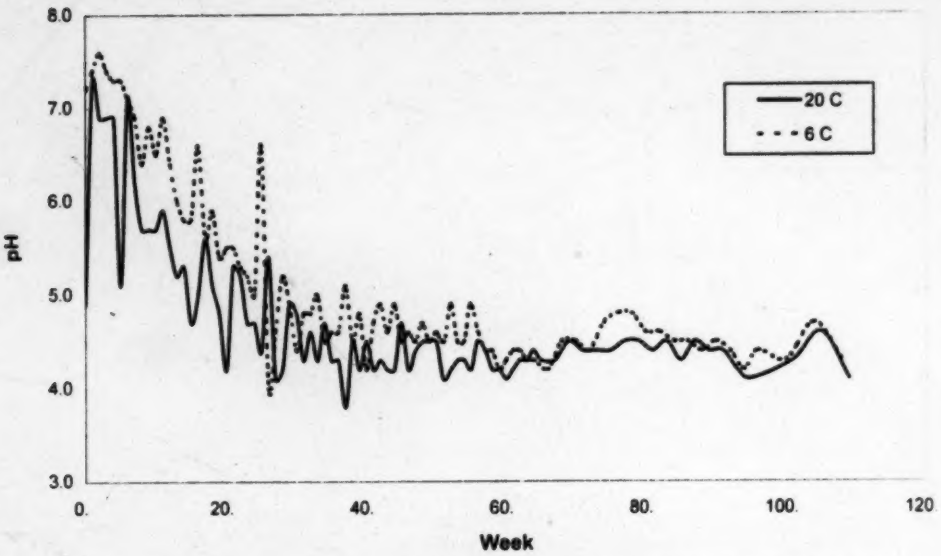

Figure 5-5. Windy Craggy Humidity Cells - pH vs Time at 20∘C and 6∘C (Dawson and Morin, 1996)

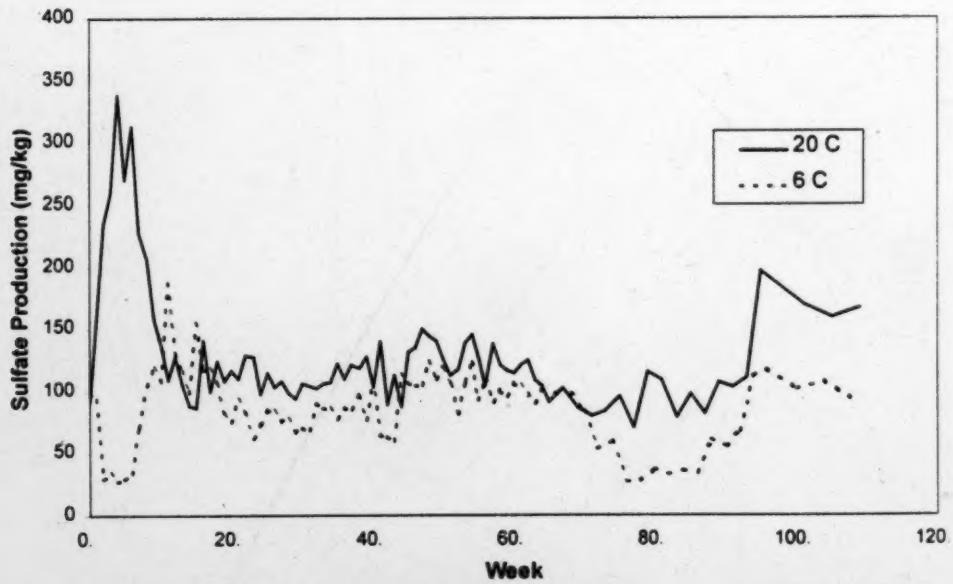

Figure 5-6. Windy Craggy Humidity Cells - Sulfate vs Time at 20∘C and 6∘C (Dawson and Morin, 1996)

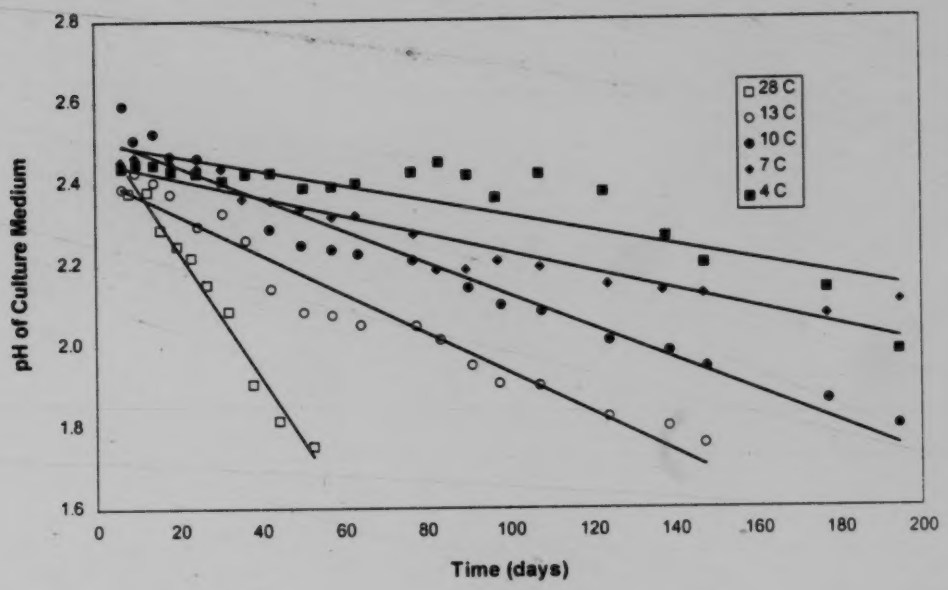

Figure 5-7. pH vs Time for Enrichment Cultures Using Elemental Sulfur at Temperatures Approaching 0°C
(Modified from Ahonen and Tuovinen, 1990)

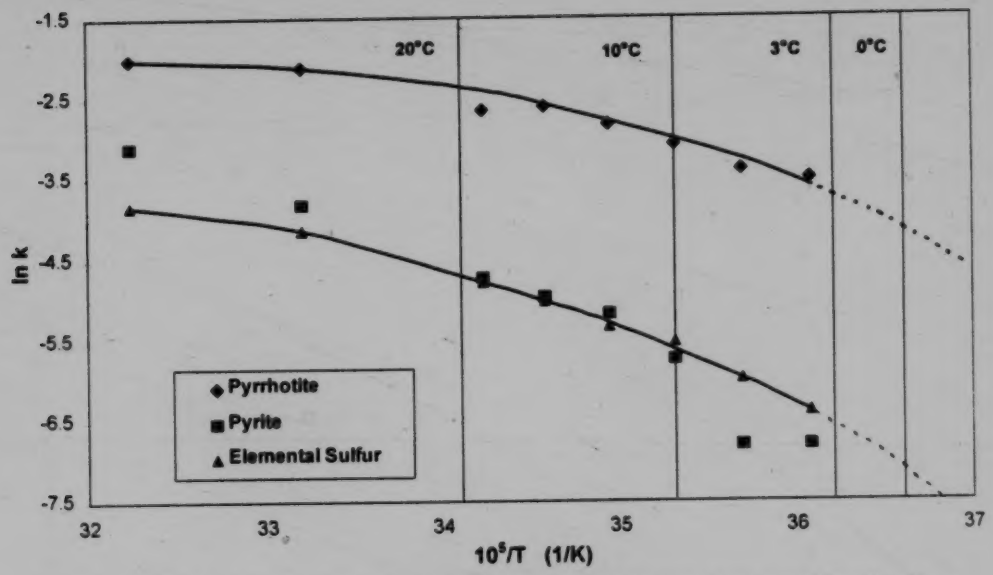

Figure 5-8. Oxidation Reaction Rates with Elemental Sulfur, Pyrite and Pyrrhotite at Temperatures Approaching 0°C
(Modified from Ahonen and Tuovinen, 1990, 1991)

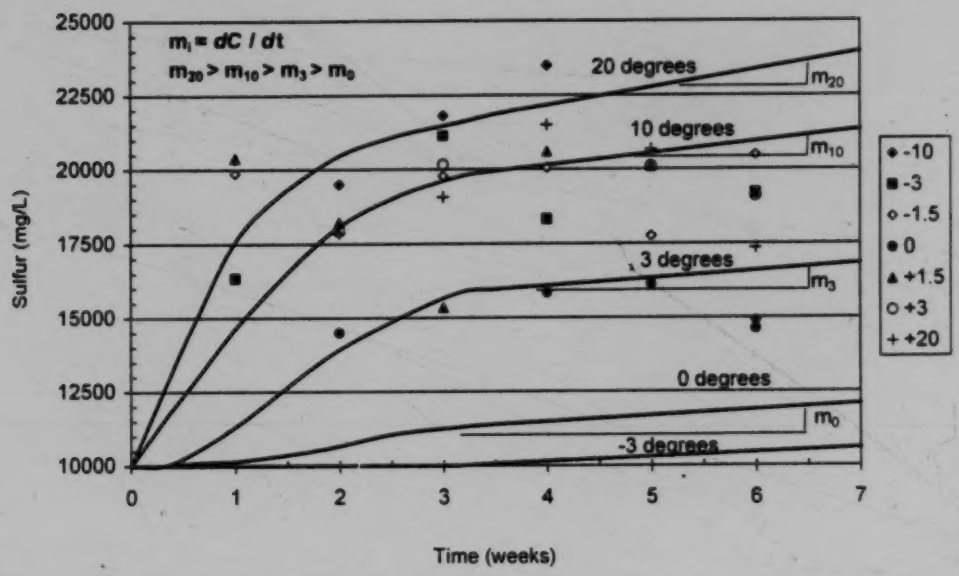

Figure 5-9. Measured and Predicted Behavior of Batch Sulfur Concentration vs Time

Table 5-1. Thermal Conductivities for Various Minerals

	Thermal Conductivty		
	Frozen	**Thawed**	
Faro	5.1	3.1	
Discovery	3.3	1.6	
Silty Sand	4.5	3.0	Norwest, 1998
Lupin	2.7	1.7	Norwest, 1998
(5% clay / 65% silt / 30% sand)			
Quartz		8.8	Williams and Smith, 1989
		7.7	Norwest, 1998
Stone Salt		7.2	Yershov, 1990
Clays (dry)		0.8 - 1.0	Yershov, 1990
Clays (saturated)	1.4 - 1.8	1.2 - 1.4	Yershov, 1990
Organic Matter		0.3	Williams and Smith, 1989
Water (20°C)		0.6	Yershov, 1990
Water (4.1°C)		0.54	Yershov, 1990
Ice (0°C)	2.2		Williams and Smith, 1989
Air		0.025	Williams and Smith, 1989

6 CONCLUSIONS AND RECOMMENDATIONS

The purpose of this research was to determine the effects of temperature on the generation of acid mine drainage at sub-zero temperatures. Despite the fact that the static batch tests did not perform as designed, the reasoning presented in this thesis strongly suggests that the acid generating reactions will continue at temperatures below 0°C, provided that there is unfrozen water present. The rate of oxidation will decrease from that at 20°C, but the oxidation reactions will continue.

Another goal of this research was to determine the effects of temperature on the acid generating mechanisms at the Discovery site, given that despite the extreme temperatures experienced, acidic conditions exist in the airstrip area of the site, as indicated by pH levels below 3.5. An understanding of these mechanisms assists in their management, both in the tailings delta at Discovery mine and similar facilities that experience cold temperatures. Due to the low sulfur content of the Discovery mine tailings (0.54% S), a second experimental program was performed on Faro mine tailings which were significantly richer (22.1% S) to assist in interpreting the effects of temperature.

The unweathered material from Discovery was a sandy silt, with minimal fines, generating weak capillary suction forces. In combination with relatively low ionic concentrations, this resulted in a minimal volume of unfrozen water, 25% volumetric moisture content at -1°C, down to 4% at –1.5°C. Given the extreme conditions at Discovery, any exposed tailings would freeze solid, becoming inert for the winter months. Due to the heat generated from the nearby Giauque Lake, however, the depth of freezing in the delta tailings is only 1m. With the decreased moisture content in the airstrip tailings, this active freeze-thaw zone increases to almost 1.5m.

The thermal conductivity of the saturated frozen Discovery tailings was 3.3 W/m °C; unfrozen, it was 1.6 W/m °C. These values are similar to many soils recorded in the literature, and allow for numerical modeling using standard parameters.

The Discovery material was characterized for AMD catalyzing bacteria. This identified two strains, one that was active in sulfide oxidizing conditions and the other in iron oxidizing conditions. It was discovered that the surface material at the airstrip did not produce any neutrophilic sulfide oxidizers, though it did produce favorable conditions for iron oxidizers and acidophilic sulfide oxidizers. From the unweathered material collected from the tailings delta, the bacteria responded to acidophilic sulfide oxidizing as well as neutrophilic sulfide oxidizing conditions. Due to the very low volumes of unfrozen water in the Discovery tailings though, even if the bacteria on site were active at these low temperatures, the amount of available water, and therefore also access to oxygen, make conditions for acid generation during the winter very unlikely.

The Faro mine tailings revealed a volumetric unfrozen water content of approximately 30%, even at temperatures as low as -20°C. If this site was to experience an increase in precipitation, or if the tailings were water capped and were capable of leaching, these same conclusions may not be transferable, despite experiencing similar thermal conditions. The Faro material also showed higher thermal conductivity levels, 5.1 W/m °C frozen and 3.1 W/m°C unfrozen.

An area of potential research interest is the determination of conditions favorable for establishing an insulated zone of weathering tailings (i.e. the establishment of microclimates within a tailings mass). Parameters to consider include thermal conductivity and the thermal gradient given internal and external temperatures.

The humidity cells using tailings from Discovery Mine did not generate any acidity. Because of this, the cells were discontinued and the batch tests using this material were not tested. The humidity cells using tailings from Faro mine were successful in showing a change in leaching characteristics with time. At 20°C, the leachate reached a peak pH of 3.8 after 5-6 weeks. This peak increased to 4.3 after approximately 13 weeks at 3°C. At the end of the test period, it was indeterminate whether a peak had been reached. The sulfate tracking of the Faro material displayed a 'dual peak', indicating a complex sulfide

system with material containing sulfide minerals with different solubilities. As expected. the 20°C cells generated more sulfate than the cooler temperatures. Due to the complexity of the system, no quantitative relationship was established between temperature and sulfate generation.

The batch cells operated successfully for the first several weeks until the system likely consumed more oxygen than was available. For the first 3-4 weeks, the batches showed an increase in dissolved sulfur with time at temperatures of 20°, 3° and 0°C; however. as the oxygen was depleted, the sulfate in solution precipitated as FeS_2, S, or another intermediate solid. This resulted in fluctuations in the sulfur content for the remainder of the test period, reducing the usefulness of the data. Due to potentially rate limiting steps. no relationship could be made between the humidity cells and the batch tests.

Despite the fact that the test program did not demonstrate acid generation at sub-zero temperatures, the data collected from other test programs, specifically using static shake flask tests at temperatures approaching 0°C, indicate that acid generation below 0°C is likely in the presence of unfrozen water. Given recent discoveries of psychrotrophic strains of Thiobacillus Ferrooxidans and the presence of significant unfrozen water in mine tailings, the potential for generating acidic conditions in permafrost environments or during normal winter months is probable and must be accounted for in spring runoff collection and treatment.

REFERENCES

Ahonen, L. and Tuovinen, O.H., 1990. Kinetics of Sulfur Oxidation at Suboptimal Termperatures. Applied and Environmental Microbiology. Vol. 56, No. 2. pp. 560-562.

Ahonen, L. and Tuovinen, O.H., 1991. Temperature Effects on Bacterial Leaching of Sulfide Minerals in Shake Flask Experiments. Applied and Environmental Microbiology. Vol. 57, No. 1. pp. 138-145.

Anderson, D.M. and Morgenstern, N.R., 1973. Physics, Chemistry and Mechanics of Frozen Ground: A Review. Proceedings of the 2nd International Conference on Permafrost. North American Contribution. National Academy of Sciences, Washington. p.257-289.

Anderson, D.M. and Tice, A.R., 1989. Unfrozen Water Contents of Six Antarctic Soil Materials. Cold Regions Engineering. Proceedings of the 5th International Conference. ASCE; New York, p. 355-366.

Andersland, O.B. and Ladanyi, B., 1994. An Introduction to Frozen Ground Engineering. Chapman Hall, New York, 352p.

ASTM Standard C177-97, 1999. Standard Test Method for Steady-State Heat Flux Measurements and Thermal Transmission Properties by Means of the Guarded-Hot-Plate Apparatus. *In* 1999 Annual Book of ASTM Standards. Vol. 04.06. pp. 21-42.

ASTM Standard D 3152-72, 1999. Standard Test Method for Capillary-Moisture Relationships for Fine-Textured Soils by Pressure-Membrane Apparatus. *In* Annual Book of ASTM Standards. Vol. 04.08. pp. 314-319.

ASTM Standard D 3987-85, 1999. Standard Test Method for Shake Extraction of Solid Waste with Water. *In* Annual Book of ASTM Standards. Vol. 11.04. pp. 14-17.

ASTM Standard D 5334-92, 1992. Standard Test Method for Determination of Thermal Conductivity of Soil and Soft Rock by Thermal Needle Probe Procedure. *In* Annual Book of ASTM Standards. Vol. 04.09. pp. 233-237.

ASTM Standard D 5744, 1996. Standard Test Method for Accelerated Weathering of Solid Materials Using a Modified Humidity Cell. *In* Annual Book of ASTM Standards. Vol. 11.04. pp. 266-278.

Atlas. R.M., 1995. Handbook of Media for Environmental Microbiology. CRC Press. p. 228.

Battaglia-Brunet, F., d'Hugues, P., Cabral, T., Cezac, P., Garcia J.L., and Morin. D., 1998. The Mutual Effect of Mixed Thiobacilli and Leptospirillum Populations on Pyrite Bioleaching. In Mining Engineering, 11(2):195-205.

Beard. P.J. and Cleary, J.P., 1932. The Importance of Temperature for the Survival Time of Bacteria in Foods. J. Prev. Med., 6:141-144.

Black, P.B. 1990. Three Functions that Model Empirically Measured Unfrozen Water Content Data and Predict Relative Hydraulic Conductivity. CRREL Report 90-5. 7p.

Black, P.B. and Tice, A.R., 1989. Comparison of Soil-Freezing Curve and Soil Water Curve Data for Windsor Sandy Loam. Water Resources Research, (25)10: 2205-2210.

Blowes, D.W. and Ptacek, C.J., 1994. Acid-neutralizing Mechanisms in Inactive Mine Tailings. In MAC Short Course Handbook on Environmental Geochemistry of Sulfide Mine-wastes, ed. Jambor, J.L. and Blowes, D.W. pp. 271-292.

Brock, T.D. and Gustafson, J., 1976. Ferric Iron Reduction by Sulfur- and Iron-oxidizing bacteria. Appl. Environ. Microbiology. 32:567-571.

Brickett, L.A., Hammock, R.W. and Edenborn, H.M., 1995. Comparison of Methods Used to Inhibit Bacterial Activity in Sulfide Ore Bioleaching Studies. Hydrometallurgy. 39:293:305.

Burns, C.R. and Smith, M.W., 1985. On the Origin of Aggrational Ice in Permafrost. In Freezing and Thawing of Soil-water Systems. Anderson, D.M. and P.J. Williams (eds). Technical Council on Cold Regions Engineering Monograph. pp. 77-84.

Chen, C.S. and Nagy, S., 1986. Prediction and Correlation of Freezing Point Depression of Aqueous Solutions. Presentation at 1986 Winter Meeting – American Society of Agricultural Engineers, Chicago, Illinois, December 16-19. 17p.

Clark, M.W., Lancaster, G., and McConchie, D., 1996. Total sulphide acidity for the definition and quantitative assessment of the acid sulphate hazard: simple solution or a new suite of problems. The Science of the Total Environment, 183: 249-254.

Coastech Research Inc., 1991. Acid Rock Drainage Prediction Manual. MEND Project 1.16.1b. 130p.

Cornelius, R.J. and Woodcock, J.T., 1958. Pressure Leaching of Manganese Ore, Part 1: Kinetic Aspects. Proc. Australian Inst. Mining Metall., 65p.

Cravotta III, C.A., 1994. Secondary Iron-sulfate Minerals as Sources of Sulfate and Acidity. In Environmental Geochemistry of Sulfide Oxidation, ed. Alpers, C.N. and D.W. Blowes. pp. 345-364.

Cron, B., 1996. Collection of the Faro Tailings Pilot Plant Sample. Prepared by Cron Metallurgical Engineering Ltd.

Cullimore, R., 1998. Personal communication.

Curragh Resources Inc. and Steffen Robertson and Kirsten (BC) Inc., 1991. Down Valley Tailings Impoundment Decommissioning Plan. Report 60635. Prepared for Yukon Territory Water Board.

Dave, N. and Blanchette, M., 1999. Role of Cold Climatic Conditions in Management of Reactive Mining Waste in Northern Canada. In Mining in the Arctic, Udd and Keen (eds). Balkema, Rotterdam. pp. 115-124.

Davé, N., Blanchette, M. and Giziewicz, E., 1996. Roles of Ice, in the Water Cover Option, and Permafrost in Controlling Acid Generation from Sulphide Tailings. Report for Department of Indian and Northern Affairs Canada. MEND Report 1.61.1. 61p.

Dawson, R.F. and Morin, K.F., 1996. Acid Mine Drainage in Permafrost Regions: Issues, Control Strategies and Research Requirements. Report for Department of Indian and Northern Affairs Canada. 59p.

Dudas, M., 1998. SOILS 450 Lecture Notes, University of Alberta

Duke, J., 1999. Personal Communication.

Faure, G., 1991. Principles and Applications of Inorganic Geochemistry. MacMillan Publishing Company, New York. 626p.

Ferguson, K.D. and Morin, K.A., 1991. The Prediction of Acid Rock Drainage – Lessons from the Database. In Second International Conference on the Abatement of Acidic Drainage. Sept. 16-18, Montreal. Vol. 3. pp. 83-106.

Finkelman, R.B. and Giffin, D.E., 1986. "Hydrogen peroxide oxidation: an improved method for rapidly assessing acid-generating potential of sediments and sedimentary rocks". Recreation and Revegetation Research, 5: 521-534.

GEOCON, 1993. Preventing AMD by Disposal of Reactive Tailings in Permafrost. Report for Department of Indian and Northern Affairs Canada. MEND Report 6.1. 98p.

Goresline, H.E., 1961. Historical Development of the Modern Frozen Food Industry. *In* Proceedings - Low Temperature Microbiology Symposium, Campbell Soup Company. Camden. pp. 5-25.

Gould, W.D., Bechard, G. and Lortie, L., 1994. The Nature and Role of Microorganisms in the Tailings Environment. In MAC Short Course Handbook on Environmental Geochemistry of Sulfide Mine-wastes, ed. Jambor, J.L. and D.W. Blowes. pp. 185-199.

Grozic, E., 1997. M.Eng. Thesis. Laboratory Measurements of Unfrozen Water Content Using Time Domain Reflectometry. University of Alberta. 21p.

Grozic, J., 1999. Personal Communication.

Halvorson, H.O, Wolf, J. and Srinivasan, V.R., 1961. Initiation of Growth at Low Temperatures *In* Proceedings - Low Temperature Microbiology Symposium. Campbell Soup Company, Camden. pp. 27-40.

Hayashi, Y., 1991. Micro-macro Freezing of Biological Substances. Third International Symposium on Cold Regions Heat Transfer, June 11-14, University of Alaska Fairbanks. p. 47-56.

Heroux, J. and Rowney, A.C., 1987. Biodegredation Kinetics in Arctic Waters *In* Cold Regions Environmental Engineering – Proceedings of the Second International Confernce, Edmonton, Mar 23-24. pp. 198-209.

Hivon, E.G., 1991. Behaviour of Saline Frozen Soils. Ph. D. Thesis, Department of Civil Engineering, University of Alberta.

Hutchison, I.P. and Ellison, R.D. (ed), 1992. Mining Waste Management. Lewis Publishers, Inc., Chelsea. pp. 127-199.

Ingledew, W.J., 1990. Acidophiles. *In* Microbiology of Extreme Environments. Edwards, C.A. (ed), Open University Press. pp. 33-54.

Jambor, J.L., 1994. Mineralogy of Sulfide-rich Tailings and Their Oxidation Products. In MAC Short Course Handbook on Environmental Geochemistry of Sulfide Mine-wastes. ed. Jambor, J.L. and D.W. Blowes. pp. 59-102.

Klohn Leonoff, 1992. Discovery Mine – Options for Tailings Reclamation. Report for Indian and Northern Affairs Canada. 57p.

Klohn Leonoff, 1994. Acid Rock Drainage Potential in the Northwest Territories – An Evaluatoin of Active and Abondoned Mines. NMEND Study No.2. 47p.

Klohn Leonoff, 1994. Acid Rock Drainage Potential in the Yukon Territory – An Evaluation of Active and Abandoned Mines. NMEND Study No. 3. 39p.

Knapp, R.A., 1987. The Biogeochemistry of Acid Generation in Sulphide Tailings and Waste Rock. In Proceedings – Acid Mine Drainage Seminar/Workshop. Halifax, March 23-26. pp. 47-67.

Koch, A.L., 1994. Growth Measurement. *In* Methods for General and Molecular Bacteriology. American Society for Microbiology. pp. 249-257.

Konrad, J. M, 1989. Unfrozen Water as a Function of Void Ratio in a Clayey Silt. Cold Regions Science and Technology, **18**:49-55.

Konsten, C.M., Brinkman, R. and Andriesse, W., 1988. A field laboratory method to determine total potential and actual acidity in acid sulphate soils. *In* Selected Papers of the Dakar Symposium on Acid Sulphate Soils, ILRI Publ. 44. pp. 106-134.

Krieg, N.R. and Gerhardt, P., 1994. Solid, Liquid/Solid and Semisolid Culture. *In* Methods for General and Molecular Bacteriology. American Society for Microbiology. pp. 216-217.

Lapakko, L., 1987. Prediction of ARD From Duluth Complex Mine Waste in North Eastern Minnesota. Acid Mine Drainage Workshop. DSS Cat. No. En. 40-11-7 11987E. pp. 187-221.

Lawrence, R.W., 1990. Laboratory Procedures for the Prediction of Long Term Weathering Characteristics of Mining Wastes. *In* Acid Mine Drainage: Designing for Closure. GAC-MAC Annual Meeting, May 1990. pp. 131-140.

Leduc, L.G., Trevors, J.T. and Ferroni, G.D., 1993. Thermal characterization of different isolates of Thiobacillus ferrooxidans. FEMS Microbiology Letters, 108, pp. 189-194.

Lefebvre, M., 1997. Feasibility of TDR as an Insitu Tool. M.Sc. Thesis. University of Alberta. 129p.

Lotrario, J.B., Stuart, B.J., Lam, T., Arands, R.R., O'Connor, O.A. and Kosson, D.S., 1995. Effects of Sterilization Methods on the Physical Characteristics of Soil:

Implications for Sorption Isotherm Analyses. Bull. Environ. Contam. Toxicol. 54:668-675.

Lowson, R.T., 1982. Aqueous Oxidation of Pyrite by Molecular Oxygen. Chemical Reviews, 82 (5), pp. 461-497.

Marion, G.M., 2000. Personal Communication.

Marion, G.M. and Grant, S.A., 1997. Physical Chemistry of Geochemical Solutions at Subzero Temperatures. CRREL Special Report 97-10. pp. 349-356.

Marion, G.M., 1995. Freeze-Thaw Processes and Soil Chemistry. CRREL Special Report 95-12. 23p.

McLaren, A.D., 1969. Radiation as a Technique in Soil Biology and Biochemistry. Soil Biology and Biochemistry. 1:63-73.

McMeekin, T.A., Olley, J. and Ratkowsky, D.A., 1988. Temperature Effects on Bacterial Growth Rates *In* Physiological Models in Microbiology, M.J. Bazin and J.I. Prosser (eds.), CRC Press, Boca Raton, Vol. 1, pp. 76-89.

Mehling, P., 1993. Low Temperature Oxidation of Pyrite by Thiobacillus Ferrooxidans. Research Proposal.

Mehling, P., 1999. Personal Communication

Meldrum, J.L., 1998. Determination of the Sulphide Oxidation Potential of Mine Tailings from Rankin Inlet, Nunavut, at Sub-zero Temperatures. MSc. Thesis, Queen's University, Kingston, Ontario. 115p.

Mironenko, M.V., Grant, S.A. and Marion, G.M., 1997. FREZCHEM2 – A Chemical Thermodynaic Model for Electrolyte Solutions at Subzero Temperatures. CRREL Report 97-5. 9p.

Morin, K.A., 1990. Problems and Proposed Solutions in Predictin Acid Mine Drainage with Acid-Base Accounting. In Acid Mine Drainage: Designing for Closure. GAC-MAC Annual Meeting – May 1990.

Morin, K.A. and Hutt, N.M., 1997. Environmental Geochemistry of Minesite Drainage – Practical Theory and Case Studies. MDAG Publishing, Vancouver. 333p.

Morin K.A. and Hutt, N.M., 1998. Internet Case Study for November 1998: Contributions of Bacteria to Sulfide-Mineral Reaction Rates in Natural Environments. www.mdag.com

Morin, K., 1998. Personal communication.

Morin, K.A., Gerencher, E., Jones, C.E. and Konasewich, D.E., 1991. Critical Literature Review of Acid Drainage from Waste Rock. Report for Department of Indian and Northern Affairs Canada. MEND Report 1.11.1. 175p.

Myerson, A.S., 1981. Oxygen Mass Transfer Requirements During Growth of Thiobacillus Ferrooxidans on Iron Pyrite. Biotech & Bioeng., 23, pp. 1413-1416.

Nicholson, R.V., 1994. Iron-sulfide Oxidation Mechanisms: Laboratory Studies. In *MAC The Environmental Geochemistry of Sulfide Mine-wastes*. Short Course Handbook, Vol. 22. Eds. D.W. Blowes and J.L. Jambor. pp. 163-183.

Nicholson, R.V. and Scharer, J.M., 1994. Laboratory Studies of Pyrrhotite Oxidation Kinetics. In Environmental Geochemistry of Sulfide Oxidation, Alpers, C.N. and Blowes, D.W. (eds.)

Norris, P.R. and Johnson, D.B., 1998. Acidophilic Microorganisms. In Extremophiles: Microbial Life in Extreme Environments. Wiley-Liss, Inc., New York. pp. 133-153.

Nordstrom D.K. and Southam, G., 1997. Geomicrobiology of Sulfide Mineral Oxidation. In Geomicrobiology: Interactions Between Microbes and Minerals, Banfield, J.F. and K.H. Nealson (eds). pp. 361-390.

Norwest Mine Services Ltd., 1998. Acid Mine Drainage Behaviour in Low Temperature Regimes – Thermal Properties of Tailings. Report for Environment Canada. Environmental Protection Branch. 26p.

Otwinowski, M., 1994. Quantitative Analysis of Chemical and Biological Kinetics for the Acid Mine Drainage Problem. Report for Department of Indian and Northern Affairs Canada. MEND Report 1.51.1. 76p.

Otwinowski, M., 1995. Scaling Analysis of Acid Rock Drainage. MEND Report 1.19.2. 67p.

Pool, D.L. and Balderrama, R.M., 1994. Evaluation of Humidity Cell Parameters – Their Effect on Precision and Repeatability. Presented at International Lands Reclamation and Mine Drainage Conference. Pittsburg, April 24-29, 1994. pp.326-333.

Ratkowski, D.A., Olley, R.K., McMeekin, T.A. and Ball, A., 1982. Relationship Between Temperature and Growth Rate of Bacterial Cultures, J. Bacteriol, 149,1.

Roberts, D.J., 1999. Personal communication.

Ruijie, C., Horiguchi, K., Guodong, C. and Yuanlin, Z., 1992. The Relationship Between Ice Intrusion Temperature and Confined Pressure. Permafrost. Sixth International

Conference. Proceedings, July 5-9, 1993, Beijing China; South China University of Technology Press; Guangzhou; pp. 1067-1069.

Russell, N.J. and Hamamoto, T., 1998. Psychrophiles. *In* Extremophiles: Microbial Life in Extreme Environments. K. Horikoshi and W.D. Grant (eds.), Wiley-Liss, New York. pp. 25-45.

Sawyer, C.N., McCarty, P.L. and Parkin, G.F., 1994. Chemistry for Environmental Engineering. McGraw-Hill, Inc., New York. p. 516.

Scott, W.J., 1961. Available Water and Microbial Growth. *In* Proceedings - Low Temperature Microbiology Symposium, Campbell Soup Company, Camden. pp. 89-105.

Sheeran, D.E. and Yong, R.W., 1975. Water and Silt Redistribution in Freezing Soils. In Proceedings – Conference on Soil-Water Problems in Cold Regions, Calgary, May 6-7. 1975. pp. 58-69

Singer, P.C., and Stumm, W., 1970. Acidic Mine Drainage: the Rate Determining Step. Science, 167, pp. 1121-1123.

Smith, M.W. and Tice, A.R., 1988. Measurements of Unfrozen Water Contents of Soils: Comparison of the NMR and TDR Methods. CRREL Report 88-11. 11p.

Sobek, A.A., Schuller, W.A., Freeman, J.R. and Smith, R.M., 1978. US EPA Report: EPA 600/2-78-054, 1978

SRK, 1992. Guidelines for ARD Prediction in the North. NMEND Project No. 1. 90 p.

SRK, 1998. Discovery Mine Reclamation Recommended Environmental Monitoring Program. Report No. 1CP001.01-2. Prepared for Public Works and Government Servies. 56p.

Stumm, W., and Lee, G.F., 1961. Oxygenation of Ferrous Iron. Ind. Eng. Chem., 53. pp. 143-146.

Sutherland, D. and Hall, S., 1989. Assessment of Contaminant Leaching and Transport from Abandoned Mines in the Northwest Territories. Data Report for Environment Canada. 30p.

Taylor, M.J., 1987. Physico-chemical Principles in Low Temperature. *In* The Effects of Low Temperature on Biological Systems. Grout, B.W. and G.J. Morris (eds). Edward Arnold Publishers Ltd. London. p. 1-72.

Thurmond V.L. and Brass, G.W., 1987. Geochemistry of Freezing Brines – Low Temperature Properties of Sodium Chloride. CRREL Report 87-13. 11p.

Tice, A.R., Anderson, D.M. and Banin, A., 1976. The Prediction of Unfrozen Water Contents in Frozen Soils from Liquid Limit Determinations. U.S. Army Cold Regions Research Laboratory. CRREL Report 76-8. 9p.

Trevors, J.T., 1996. Sterilization and Inhibition of Microbial Activity in Soil. Journal of Microbiological Methods. 26:53-59.

Trevors, J.T., 1999. Personal Communication.

Tuominen, L., Kairesalo, T., and Hartikainen, H., 1994. Comparison of Methods for Inhibiting Bacterial Activity in Sediment. Applied and Environmental Microbiology. 60(9):3454-3457.

Tuszynski, J.A., Nip, M.L.A. and Sept, D., 1993. Nonlinear Modeling of Chemical Kinetics for the Acid Mine Drainage Problem and Related Physical Topics. MEND Project 1.51.2.

Vincent, W., 1988. Microbial Ecosystems of Antarctica. Cambridge University Press. Cambridge. 291p.

Williams, P.J. and Smith, M.W., 1989. The Frozen Earth: Fundamentals of Geocryology. Cambridge University Press, New York. 306 p.

Williams, P.J., 1964. Unfrozen Water Content of Frozen Soils and Soil Moisture Suction. Geotechnique **14(3)**: 213-246.

Williams, P.J., 1991. Thermal Properties and the Nature of Freezing Soils. Third International Symposium on Cold Regions Heat Transfer, June 11-14, University of Alaska Fairbanks. p. 57-67.

Wolf, D.C., Dao, T.H., Scott, H.D. and Lavy, T.L., 1989. Influence of Sterilization Methods on Selected Soil Microbiological, Physical and Chemical Properties. J. Environ. Qual. 18:39-44.

Xiaozu, X., Lixin, Z., Yousheng, D., Jiacheng, W., Lebedenko I., and Chuvilin, E.M., 1997. Unfrozen Water Content in Multi-crystal Ice. Chinese Science Bulletin, 42. p. 1295-1297.

Yanful, E.K., St. Arnaud, L., and Prairie, R., 1990. Generation and Evolution of Acidic Pore Waters at the Waite Amulet Tailings. MEND Project1.17.1d.

Yershov, E.D., 1990. General Geocryology, Studies in Polar Research. Cambridge University Press, Cambridge. 580p.

Yong, R.N., Cheung, C.H., and Sheeran, D.E., 1978. Prediction of Salt Influence on Unfrozen Water Content in Frozen Soils. Engineering Geology, 13: 137-155.

APPENDIX A

X-Ray Diffraction Patterns

<221697.RAW> ROD-2 UPPER 1 CM. WEATHERED — JADE - Peak List Report

Scan Parameters: Range = 2.0-90.0/0.05, Dwell = 1(sec), Max-I = 19867, Anode = CO — Date: 12-21-99@11:04

Search Parameters: Filter = 11(pts), Threshold = 3.0(sed), Peak-Cutoff = 0.5%, 2-Theta Zero Offset = 0.0(deg)

Note: Intensity data from raw counts, Summit peak location, Wavelength for computing d-spacing = 1.789008<CO, K-alpha1>

#	2-Theta	d(A)	h	k	l	BG	Peak	I%	Area	I%	FWHM	Size(A)	#
1	7.298	14.1548				190	198	1.1	43	1.2	0.264	>1000	1
2	10.239	10.0241				189	1442	8.3	813	14.9	0.284	484	2
3	13.488	7.8199				88	236	1.5	48	1.4	0.181	>1000	3
4	14.804	7.0658				90	666	4.2	137	4.0	0.167	>1000	4
5	20.248	5.0982				99	99	0.6	19	0.5	0.148	>1000	5
6	20.848	4.9810				84	612	3.9	114	3.3	0.148	>1000	6
7	21.849	4.7208				79	237	1.5	41	1.2	0.138	>1000	7
8	23.191	4.4802				77	118	0.8	21	0.6	0.136	>1000	8
9	24.290	4.2594				67	2729	17.6	849	15.7	0.158	>1000	9
10	25.894	4.0383				67	191	1.2	36	1.0	0.148	>1000	10
11	28.677	3.8772				73	131	0.8	23	0.8	0.136	>1000	11
12	27.700	3.7388				75	83	0.5	37	1.1	0.364	304	12
13	28.296	3.6595				104	83	0.5	28	0.7	0.247	518	13
14	29.299	3.5369				89	428	2.8	106	3.1	0.197	871	14
15	29.730	3.4867				121	136	0.9	32	0.9	0.182	>1000	15
16	31.013	3.3459				107	18590	100.0	3440	100.0	0.177	>1000	16
17	32.403	3.2099				114	647	4.2	173	5.0	0.214	662	17
18	32.638	3.1834				113	919	5.9	201	5.8	0.178	>1000	18
19	33.887	3.0893				113	197	1.2	38	1.1	0.190	>1000	19
20	34.850	2.9870				81	137	0.9	32	0.9	0.183	947	20
21	35.533	2.8314				90	83	0.5	20	0.6	0.194	918	21
22	36.456	2.8098				79	119	0.8	27	0.8	0.177	>1000	22
23	36.849	2.8301				65	84	0.5	24	0.7	0.228	993	23
24	39.801	2.8278				86	90	0.6	19	0.5	0.157	>1000	24
25	40.900	2.9801				114	106	0.7	30	0.9	0.218	884	25
26	42.702	2.4686				84	843	5.4	181	5.3	0.172	978	26
27	43.998	2.3879				86	83	0.3	20	0.6	0.301	370	27
28	46.184	2.2620				88	619	4.0	139	4.0	0.179	936	28
29	47.149	2.2365				88	401	2.8	86	2.4	0.188	888	29
30	48.713	2.1280				87	741	4.8	176	5.1	0.189	736	30
31	52.703	2.0152				44	181	1.2	86	2.4	0.372	294	31
32	53.281	1.9956				95	388	2.5	159	4.6	0.328	340	32
33	53.710	1.9901				44	423	2.7	130	3.8	0.244	481	33
34	58.952	1.8178				45	1097	7.1	290	8.4	0.211	808	34
35	64.899	1.8717				80	498	3.1	148	4.2	0.239	822	35
36	66.245	1.6082				88	110	0.7	31	0.9	0.224	873	36
37	70.914	1.5420				89	1026	6.6	320	9.3	0.249	810	37
38	75.987	1.4529				47	144	0.9	44	1.3	0.241	880	38
39	80.852	1.3822				90	529	3.4	128	3.7	0.193	779	39
40	81.180	1.3791				92	901	5.8	193	5.6	0.171	982	40
41	87.958	1.2981				44	156	1.0	43	1.2	0.217	704	41
@	End-of-List												

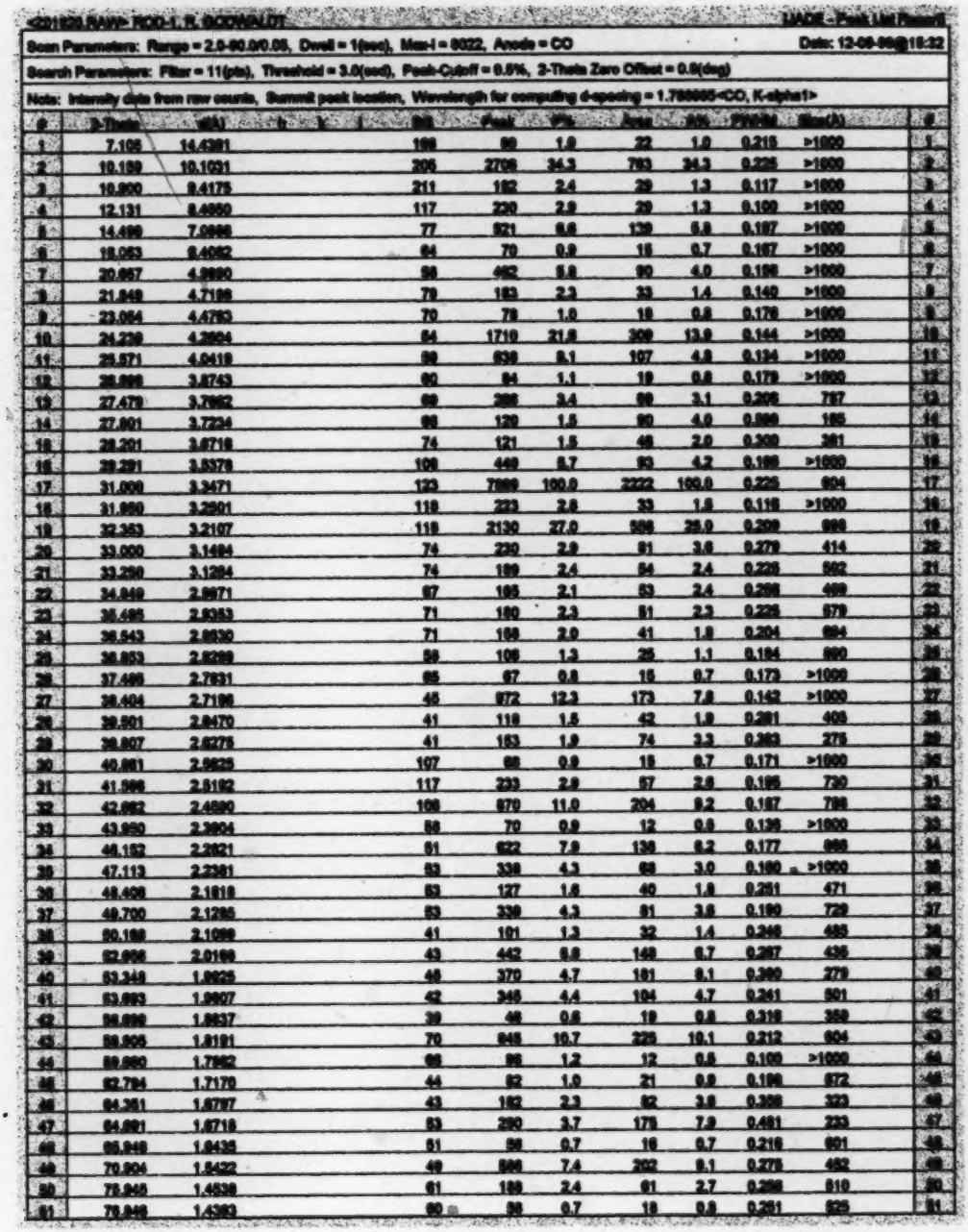

<201820.RAW> ROD-1, R, BOOKHULDT — JADE - Peak List Report

Scan Parameters: Range = 2.0-90.0/0.05, Dwell = 1(sec), Max-I = 8022, Anode = CO — Date: 12-08-98@18:32

Search Parameters: Filter = 11(pts), Threshold = 3.0(sod), Peak-Cutoff = 0.5%, 2-Theta Zero Offset = 0.0(deg)

Note: Intensity data from raw counts, Summit peak location, Wavelength for computing d-spacing = 1.788965<CO, K-alpha1>

#	2-Theta	d(A)	b	I	Bkg	Peak	I%	Area	I%	FWHM	Size(A)	#
1	7.105	14.4391			199	89	1.0	22	1.0	0.215	>1000	1
2	10.159	10.1031			206	2708	34.3	783	34.3	0.225	>1000	2
3	10.900	9.4175			211	182	2.4	29	1.3	0.117	>1000	3
4	12.131	8.4650			117	230	2.9	29	1.3	0.109	>1000	4
5	14.499	7.0998			77	521	6.6	139	6.8	0.197	>1000	5
6	18.083	8.4082			84	70	0.9	15	0.7	0.167	>1000	6
7	20.057	4.9890			96	462	5.8	90	4.0	0.196	>1000	7
8	21.848	4.7199			79	183	2.3	33	1.4	0.140	>1000	8
9	23.054	4.4783			70	78	1.0	18	0.8	0.178	>1000	9
10	24.238	4.2904			84	1710	21.8	309	13.9	0.144	>1000	10
11	25.571	4.0419			98	636	8.1	107	4.8	0.134	>1000	11
12	26.998	3.8743			80	84	1.1	19	0.8	0.179	>1000	12
13	27.479	3.7662			89	266	3.4	69	3.1	0.206	797	13
14	27.901	3.7234			98	120	1.5	90	4.0	0.699	185	14
15	28.201	3.6718			74	121	1.5	46	2.0	0.300	381	15
16	28.291	3.5378			106	449	5.7	93	4.2	0.198	>1000	16
17	31.009	3.3471			123	7899	100.0	2222	100.0	0.225	804	17
18	31.990	3.2901			119	223	2.8	33	1.5	0.118	>1000	18
19	32.353	3.2107			119	2130	27.0	586	26.0	0.209	998	19
20	33.000	3.1484			74	230	2.9	81	3.6	0.279	414	20
21	33.250	3.1284			74	189	2.4	54	2.4	0.228	582	21
22	34.849	2.9971			87	166	2.1	53	2.4	0.298	499	22
23	35.496	2.9353			71	180	2.3	51	2.3	0.226	579	23
24	36.543	2.8830			71	168	2.0	41	1.8	0.204	694	24
25	36.853	2.8289			89	106	1.3	25	1.1	0.184	880	25
26	37.496	2.7931			85	87	0.8	15	0.7	0.173	>1000	26
27	38.404	2.7196			46	972	12.3	173	7.8	0.142	>1000	27
28	39.501	2.8470			41	118	1.5	42	1.9	0.281	406	28
29	39.807	2.6278			41	153	1.9	74	3.3	0.383	275	29
30	40.861	2.5625			107	88	0.9	19	0.7	0.171	>1000	30
31	41.566	2.5192			117	233	2.9	57	2.6	0.195	730	31
32	42.062	2.4590			106	870	11.0	204	9.2	0.187	788	32
33	43.950	2.3904			88	70	0.9	12	0.6	0.136	>1000	33
34	46.152	2.2821			91	622	7.9	136	6.2	0.177	999	34
35	47.113	2.2381			83	338	4.3	68	3.0	0.180	>1000	35
36	48.408	2.1818			83	127	1.6	40	1.8	0.281	471	36
37	48.700	2.1286			83	339	4.3	81	3.6	0.190	729	37
38	50.198	2.1099			41	101	1.3	32	1.4	0.248	485	38
39	52.956	2.0169			43	442	5.6	148	6.7	0.287	436	39
40	53.349	1.9925			46	370	4.7	181	8.1	0.399	279	40
41	53.893	1.9907			42	346	4.4	104	4.7	0.241	601	41
42	56.899	1.8837			39	48	0.6	19	0.8	0.318	358	42
43	58.905	1.8191			70	845	10.7	225	10.1	0.212	804	43
44	59.980	1.7982			66	96	1.2	12	0.6	0.100	>1000	44
45	62.784	1.7170			44	82	1.0	21	0.9	0.196	672	45
46	64.361	1.6797			43	182	2.3	82	3.6	0.358	323	46
47	64.691	1.6719			53	290	3.7	175	7.9	0.481	233	47
48	65.948	1.6436			51	56	0.7	16	0.7	0.216	601	48
49	70.904	1.5422			49	586	7.4	202	9.1	0.275	482	49
50	75.945	1.4539			61	189	2.4	61	2.7	0.298	810	50
51	79.848	1.4263			90	58	0.7	19	0.8	0.251	825	51

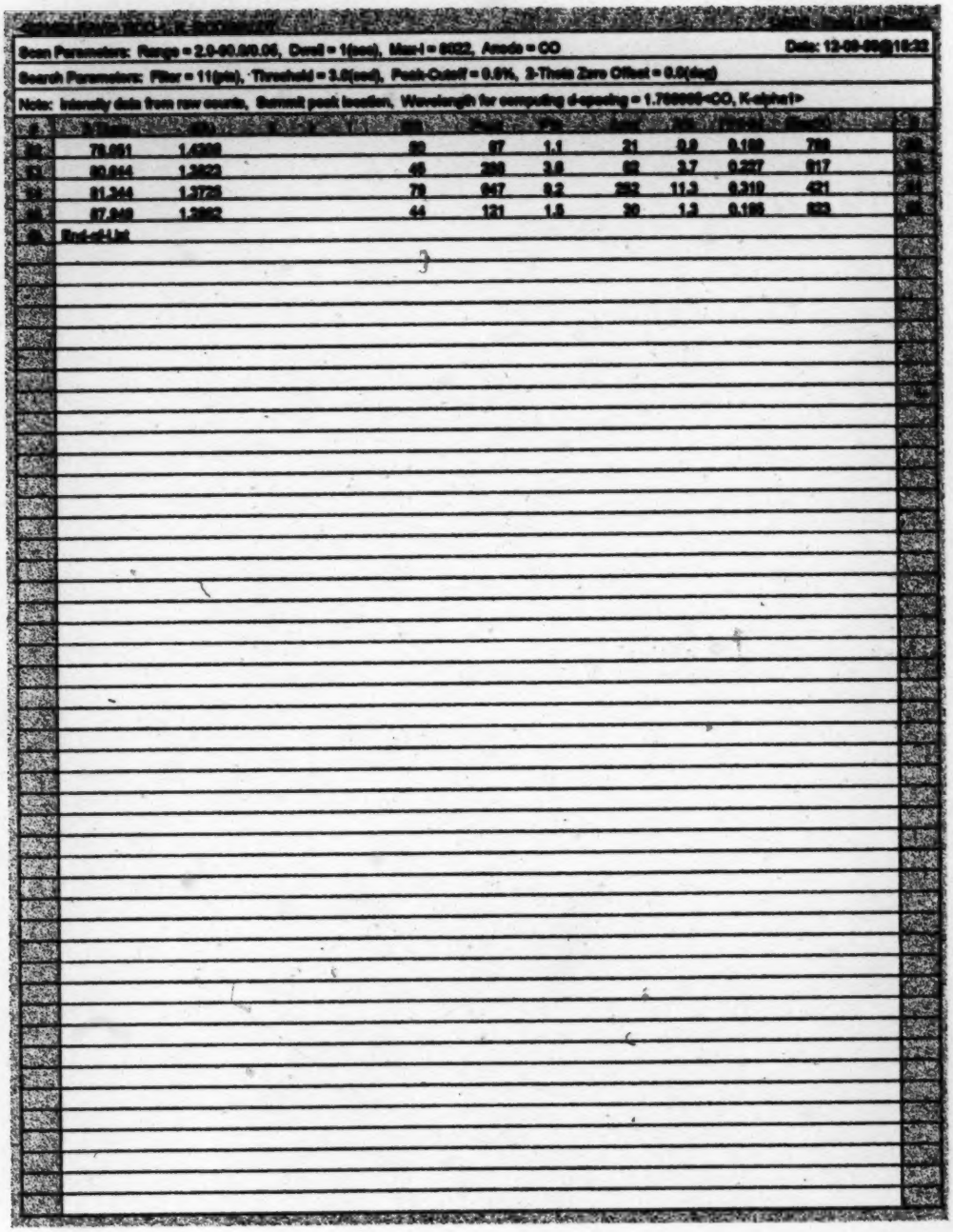

Scan Parameters: Range = 2.0-90.0/0.05, Dwell = 1(sec), Max-I = 8022, Anode = CO Date: 12-09-99@16:22

Search Parameters: Filter = 11(pts), Threshold = 3.0(sec), Peak-Cutoff = 0.5%, 2-Theta Zero Offset = 0.0(deg)

Note: Intensity data from raw counts, Summit peak location, Wavelength for computing d-spacing = 1.789000<CO, K-alpha1>

#	2-Theta	d(A)	I	I%	Area	Area%	FWHM	Left Width	#
30	78.691	1.4368	50	67	1.1	21	0.9	0.189	799
31	80.814	1.3922	46	288	3.8	82	3.7	0.227	917
32	81.344	1.3726	78	947	9.2	262	11.3	0.310	421
33	87.949	1.2862	44	121	1.5	30	1.3	0.195	823
34	End-of-List								

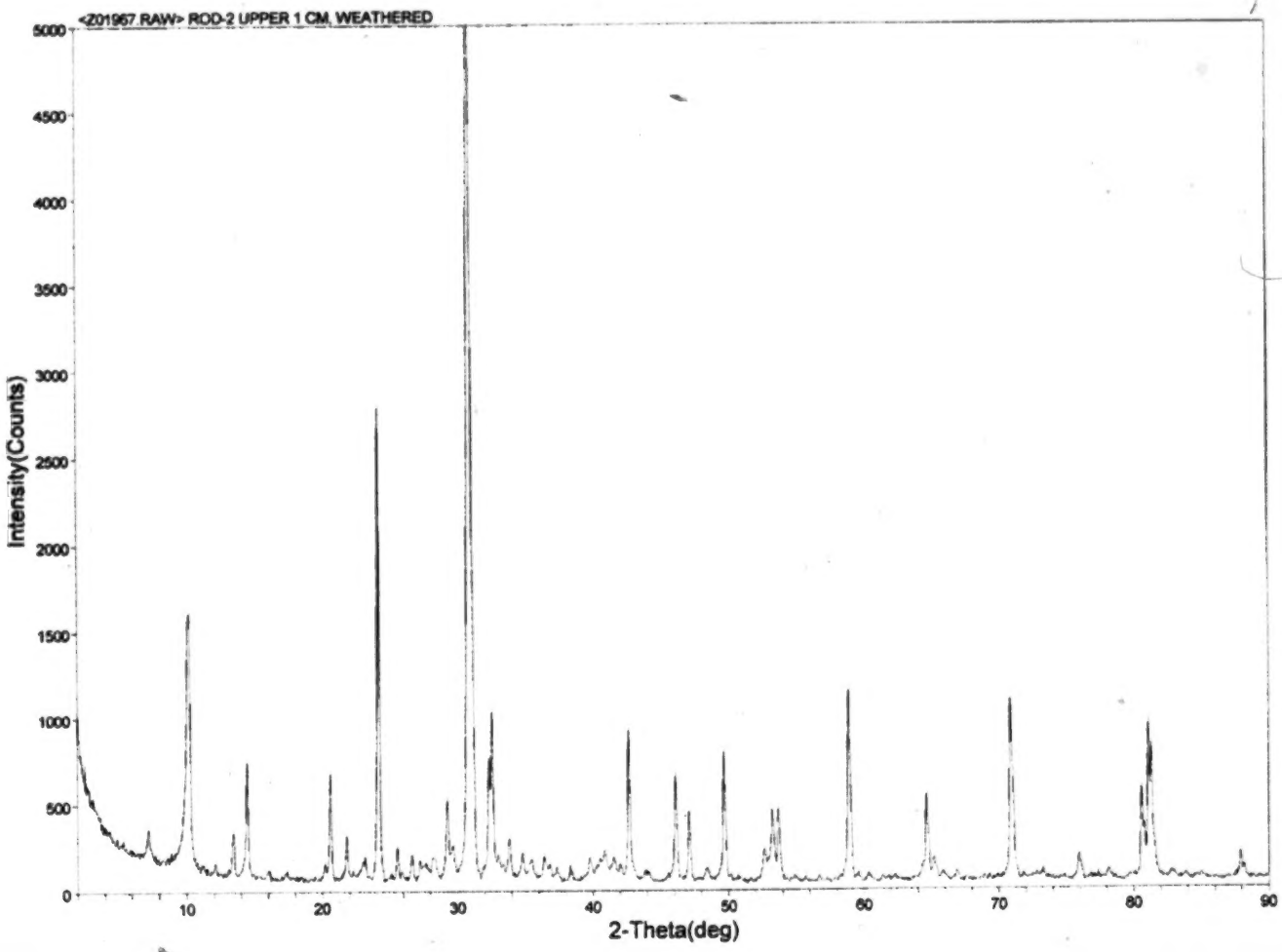
<Z01967.RAW> ROD-2 UPPER 1 CM. WEATHERED
Intensity(Counts)
5000
4500
4000
3500
3000
2500
2000
1500
1000
500
0
10
20
30
40
50
60
70
80
90
2-Theta(deg)

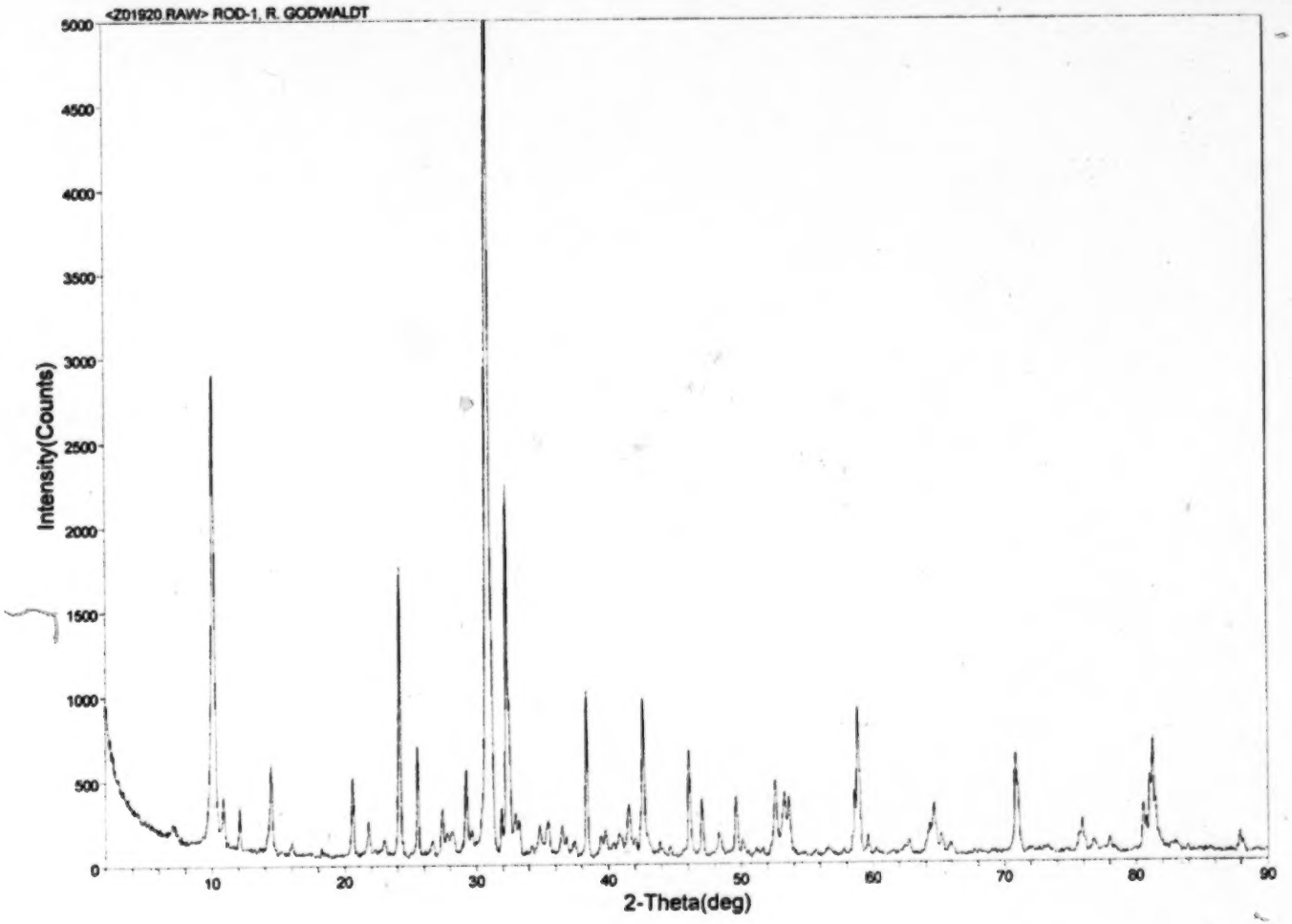
<Z01920.RAW> ROD-1, R. GODWALDT
Intensity(Counts)
5000
4500
4000
3500
3000
2500
2000
1500
1000
500
0
10
20
30
40
50
60
70
80
90
2-Theta(deg)

APPENDIX B

Klohn Leonoff Total Metals Analysis

Norwest Labs

"We Solve Problems"

203 - 20771 Langley Bypass
Langley, B.C. V3A 5E8
(604) 530-4344
FAX 534-9996

Norwest Labs

W.O. 4017
P.O. PB 57430101
October 31, 1991

Klohn Leonoff Ltd.
10200 Shellbridge Way
Richmond, B.C. V6X 2W7

Attention: S. Domvile

S O I L A N A L Y S I S

Total Metals

EPA 3050 - ICP

LAB #	SAMPLE ID	Al	Ba	Be	Cd	Ca	Cr	Cu	Fe	Pb	Mg
		mg/kg									
91-6424	TH4 - 0-24"	27300	114	1.0	< 0.3	7110	92.3	42.5	33300	58	16600
91-6433	Surface Tailings End of pipe of mill	25300	123	1.0	< 0.3	6930	84.3	33.5	33000	60	15600

LAB #	SAMPLE ID	Mn	Mo	Ni	P	K	Na	V	Zn	Co
		mg/kg								
91-6424	TH4 - 0-24"	302	8	45	401	11300	1120	55.5	103	14
91-6433	Surface Tailings End of pipe of mill	250	6	25	532	9960	669	53.8	68.4	8

Norwest Labs

"We Solve Problems"

203 - 20771 Langley Bypass
Langley, B.C. V3A 5E8
(604) 530-4344
FAX 534-9996

Norwest Labs

Klohn Leonoff Ltd.
10200 Shellbridge Way
Richmond, B.C. V6X 2W7

Attention: Serena Domville

W.O. 4017
P.O. PB 57430101
October 29, 1991

SOIL ANALYSIS

LAB #	SAMPLE ID	pH	E.C.	TOTAL ORG. CARBON	TOTAL N	AVAILABLE					AVAILABLE				C.E.C.	TOTAL
						NH4-N	NO3-N	PO4-P	SO4-S	Cl	K	Ca	Mg	Na		
			ms/cm	%	%	ppm					me/100g					ppm
1-6424	TH4 - 0-24"	3.98	4.00	0.012	0.012	76	5.6	3.0	2508	92	0.67	16.8	5.3	2.33	2.7	6105
1-6425	TH4 - 28-36"	7.36	1.12	0.034	0.011	24	4.3	1.9	392	125	0.31	8.1	1.2	0.39	1.6	10730
1-6426	TH6 - 0-18"	3.62	3.30	0.020	0.017	95	5.3	1.5	2964	120	0.15	15.8	2.0	0.65	3.1	18500
1-6427	TH6 - 18-24"	2.55	9.00	0.033	0.028	55	3.6	2.7	4180	85	0.15	10.3	6.8	1.52	2.9	32745
1-6428	TH6 - 24-42"	7.36	1.60	0.024	0.003	26	4.0	1.1	403	82	0.26	5.8	1.7	0.26	0.9	22200
1-6429	TH8 - 0-100cm	4.76	0.30	0.290	0.045	35	3.6	1.9	57	132	0.24	1.3	0.36	0.04	-	278
-6430	TH5 - 0-26"			0.012												
-6431	Soil #1	6.28	1.50	1.71	0.100	26	5.9	57.0	15	-	0.36	7.8	3.5	0.1	16.5	
-6432	Sand & Gravel #2	5.55	1.60	0.80	0.050	94	8.6	4.9	12	-	1.13	2.4	0.5	0.2	6.2	
-6434	Underwater Tailings North Side			0.036												
-6435	Underwater Tailings South Side			0.516												

APPENDIX C

Modified Sobek Test

Modified Acid Base Accounting
(from Coastech Research Inc., 1991)

EQUIPMENT

Aluminum Foil
250 mL flasks
Reciprocating shaking apparatus or other suitable agitation device
Buret, 50 or 100 mL (0.1mL graduation), one for each acid and one for each base
pH meter, equipped with a combination pH electrode

REAGENTS

Distilled (or deionized) water, preferably CO_2-free) strore in container equipped with ascarite tube
Certified grade, 0.1 N hydrochloric acid, for standardization of bases
Approximately 0.1 N sodium hydroxide, standardized
Approximately 0.5 N sodium hydroxide, standardized
Approximately 0.1 N hydrochloric acid, standardized
Approximately 0.5 N hydrochloric acid, standardized
Approximately 25% strength hydrochloric acid, for fizz test

PROCEDURE

1. Crush and pulverize the sample to a target size of 80% minus 200 mesh (Tyler).
2. Submit a sample of the test material for total sulfur and sulfate sulfur analyses.
3. Use certified 0.1N hydrochloric acid to standardize the 0.1N and 0.5N sodium hydroxide solutions, and then use the sodium hydroxide solutions to standardize the 0.1N and 0.5N hydrochloric acid solutions.
4. Place approximately 0.5g of pulverized sample on a piece of aluminum foil or in a small shallow dish. Add one or two drops of 25% HCl to the sample. The presence of carbonate will be indicated by a bubbling or an audible "fizz". Rate the fizz as indicated in Table 1.

Table 1. Volume and Normality of HCl for Use in NP Determination on Basis of Fizz Rating (2g Sample)

Fizz Rating HCl (mL)	HCl (mL)	HCl (Normality
None	20	0.1
Slight	40	0.1
Moderate	40	0.5
Strong	80	0.5

5. Weigh 2.00g of the pulverized sample into a 250mL Erlenmeyer flask and, as a first approximation, add the volume and normality of HCl as indicated by the "fizz" rating in Table 1.
6. Agitate the contents of the flask for 24 hours by placing on a shaking apparatus. At least once in the treatment period, and preferably after approximately 6 hours of reaction, check the pH of the pulp. If the pH is above 2.0, add an appropriate volume of hydrochloric acid of the same strength as originally added.
7. At the end of the shaking period, check the pulp pH. If the total volume and strength of acid was appropriate, the end pH will be in the range 1.5 – 2.0. If the pH is above this range, the amount of acid added is judged to be insufficient for reaction. If the pH is below the range, the amount of acid added is judged to be too high, causing over-reaction. In either case, repeat the test using the next higher of lower volume or strength of HCl as required.
8. Titrate the contents of the flask using 0.1N or 0.5N NaOH (corresponding to the normality of HCl used in Step 5) to pH 8.3. Titrate with NaOH until a constant reading of 8.3 remains for at least 30 seconds.

CALCULATIONS

$$NP = \frac{50\ A \cdot \left[x - \left(\frac{B}{A} \right) \cdot y \right]}{C} \qquad \text{Eq. 1}$$

NP = neutralization potential in kg $CaCO_3$ equivalent per tonne of material
A = normality of HCl
B = normality of NaOH
C = sample weight (g)
x = volume of HCl added
y = volume of NaOH added to pH 7.0 in mL

$$AP = \%\ \ sulfide\ \ sulfur \times 31.25 \qquad \text{Eq. 2}$$

AP = acid potential in kg $CaCO_3$ equivalent per tonne of material

$$NNP = NP - AP \qquad \text{Eq. 3}$$

NNP = Net neutralization potential in kg $CaCO_3$ equivalent per tonne of material

APPENDIX D

Thermal Conductivity Tests

THERMAL CONDUCTIVITY TEST

Date: Apr 22/99

Sample No. 1

Test No: 20 degrees

Temperature (°C): 20.6
Potential Drop, Vr (V): 0.0416
Voltage to Heater Probe, Vp (V): 6.000
Resistance (Ohms): 2.000
Current, I (Amps): 0.0208
Voltage Across Heater, (Vp - Vr): 5.958
Power at Probe Heater (Watts): 0.124
Power per Unite Heated Length of Probe, Q (W/m): 2.637
Probe Length, L (m): 0.047
Thermal Conductivity, λ (W/m°C): 1.538
Slope of Steady State Curve: 0.136

Time Elapsed (seconds)	Ln time (sec)	Outside RTD Reading (Ohms)	Inside RTD Reading (Ohms)	Temperatur (°C)
0.00		108.48	108.31	20.62
5.00	1.61		108.32	20.65
10.00	2.30		108.33	20.68
20.00	3.00		108.36	20.75
30.00	3.40		108.37	20.78
40.00	3.69	108.49	108.39	20.83
50.00	3.91		108.40	20.86
60.00	4.09		108.41	20.88
70.00	4.25	108.5	108.41	20.88
80.00	4.38		108.42	20.91
90.00	4.50		108.43	20.94
100.00	4.61	108.51	108.43	20.94
110.00	4.70		108.44	20.96
120.00	4.79		108.44	20.96
130.00	4.87		108.45	20.99
140.00	4.94		108.45	20.99
150.00	5.01		108.45	20.99
160.00	5.08		108.46	21.01
170.00	5.14	108.52	108.46	21.01
180.00	5.19		108.47	21.04
195.00	5.27	108.53	108.47	21.04
210.00	5.35		108.48	21.06
225.00	5.42		108.48	21.06
240.00	5.48		108.48	21.06
270.00	5.60		108.49	21.09
300.00	5.70		108.49	21.09
330.00	5.80	108.54	108.5	21.12
360.00	5.89		108.5	21.12
390.00	5.97	108.55	108.5	21.12
420.00	6.04		108.51	21.14
450.00	6.11		108.51	21.14
480.00	6.17		108.51	21.14

THERMAL CONDUCTIVITY TEST

Date: Apr 22/99

Sample No. 2 Discovery

Test No: 20 degrees

Temperature (°C): 20.7

Potential Drop, Vr (V): 0.0421

Voltage to Heater Probe, Vp (V): 6.000

Resistance (Ohms): 2.000

Current, I (Amps): 0.0211

Voltage Across Heater, (Vp - Vr): 5.958

Power at Probe Heater (Watts): 0.125

Power per Unite Heated Length of Probe, Q (W/m): 2.668

Probe Length, L (m): 0.047

Thermal Conductivity, **l** (W/m°C): 1.519

Slope of Steady State Curve: 0.140

Time Elapsed (seconds)	Ln time (sec)	Outside RTD Reading (Ohms)	Inside RTD Reading (Ohms)	Temperature (°C)
0.00		108.34	108.19	20.70
5.00	1.61	108.34	108.20	20.73
10.00	2.30		108.22	20.78
20.00	3.00		108.25	20.86
30.00	3.40		108.27	20.91
40.00	3.69		108.28	20.94
50.00	3.91	108.34	108.29	20.96
60.00	4.09	108.35	108.30	20.99
70.00	4.25	108.35	108.31	21.01
80.00	4.38		108.31	21.01
90.00	4.50		108.32	21.04
100.00	4.61		108.33	21.06
110.00	4.70		108.33	21.06
120.00	4.79	108.36	108.34	21.09
130.00	4.87		108.34	21.09
140.00	4.94		108.35	21.12
150.00	5.01		108.35	21.12
160.00	5.08		108.35	21.12
170.00	5.14	108.37	108.36	21.14
180.00	5.19		108.36	21.14
195.00	5.27		108.36	21.14
210.00	5.35		108.37	21.17
225.00	5.42	108.38	108.37	21.17
240.00	5.48		108.38	21.19
270.00	5.60		108.38	21.19
300.00	5.70	108.39	108.39	21.22
330.00	5.80		108.39	21.22
360.00	5.89	108.40	108.4	21.25
390.00	5.97		108.4	21.25
420.00	6.04		108.41	21.27
450.00	6.11	108.41	108.41	21.27
480.00	6.17		108.42	21.30

THERMAL CONDUCTIVITY TEST

Date: Apr 23/99

Sample No. 1 Discovery

Test No: -10.6 degrees

Temperature (°C): -9.1
Potential Drop, Vr (V): 0.0415
Voltage to Heater Probe, Vp (V): 6.000
Resistance (Ohms): 2.000
Current, I (Amps): 0.0208
Voltage Across Heater, (Vp - Vr): 5.959
Power at Probe Heater (Watts): 0.124
Power per Unite Heated Length of Probe, Q (W/m): 2.631
Probe Length, L (m): 0.047
Thermal Conductivity, λ (W/m°C): 3.136
Slope of Steady State Curve: 0.067

Time Elapsed (seconds)	Ln time (sec)	Outside RTD Reading (Ohms)	Inside RTD Reading (Ohms)	Temperature (°C)
0.00		96.95	96.88	-9.06
5.00	1.61		96.90	-9.01
10.00	2.30		96.92	-8.96
20.00	3.00		96.94	-8.91
30.00	3.40		96.95	-8.88
40.00	3.69	96.96	96.96	-8.86
50.00	3.91		96.97	-8.83
60.00	4.09	96.97	96.97	-8.83
70.00	4.25		96.98	-8.81
80.00	4.38		96.98	-8.81
90.00	4.50		96.98	-8.81
100.00	4.61		96.99	-8.78
110.00	4.70	96.98	96.99	-8.78
120.00	4.79		96.99	-8.78
130.00	4.87		96.99	-8.78
140.00	4.94		97.00	-8.75
150.00	5.01		97.00	-8.75
160.00	5.08		97.00	-8.75
170.00	5.14	96.99	97.00	-8.75
180.00	5.19		97.00	-8.75
195.00	5.27		97.00	-8.75
210.00	5.35		97.01	-8.73
225.00	5.42		97.01	-8.73
240.00	5.48		97.01	-8.73
270.00	5.60		97.01	-8.73
300.00	5.70		97.01	-8.73
330.00	5.80	97.00	97.01	-8.73
360.00	5.89		97.02	-8.70
390.00	5.97		97.02	-8.70
420.00	6.04		97.02	-8.70
450.00	6.11		97.02	-8.70
480.00	6.17		97.02	-8.70

THERMAL CONDUCTIVITY TEST

Date: Apr 23/99

Sample No. 2 Discovery

Test No: -10.6 degrees

Temperature (°C): -8.9
Potential Drop, Vr (V): 0.0421
Voltage to Heater Probe, Vp (V): 6.000
Resistance (Ohms): 2.000
Current, I (Amps): 0.0211
Voltage Across Heater, (Vp - Vr): 5.958
Power at Probe Heater (Watts): 0.125
Power per Unite Heated Length of Probe, Q (W/m): 2.668
Probe Length, L (m): 0.047
Thermal Conductivity, **l** (W/m°C): 3.423
Slope of Steady State Curve: 0.062

Time Elapsed (seconds)	Ln time (sec)	Outside RTD Reading (Ohms)	Inside RTD Reading (Ohms)	Temperature (°C)
0.00		96.84	96.82	-8.83
5.00	1.61		96.83	-8.81
10.00	2.30		96.85	-8.75
20.00	3.00		96.88	-8.68
30.00	3.40		96.89	-8.65
40.00	3.69	96.84	96.90	-8.62
50.00	3.91		96.91	-8.60
60.00	4.09		96.91	-8.60
70.00	4.25		96.92	-8.57
80.00	4.38	96.86	96.92	-8.57
90.00	4.50		96.92	-8.57
100.00	4.61		96.93	-8.55
110.00	4.70		96.93	-8.55
120.00	4.79		96.93	-8.55
130.00	4.87		96.93	-8.55
140.00	4.94		96.94	-8.52
150.00	5.01	96.87	96.94	-8.52
160.00	5.08		96.94	-8.52
170.00	5.14		96.94	-8.52
180.00	5.19		96.94	-8.52
195.00	5.27		96.94	-8.52
210.00	5.35		96.94	-8.52
225.00	5.42		96.95	-8.49
240.00	5.48		96.95	-8.49
270.00	5.60		96.95	-8.49
300.00	5.70	96.88	96.95	-8.49
330.00	5.80		96.95	-8.49
360.00	5.89		96.95	-8.49
390.00	5.97		96.95	-8.49
420.00	6.04		96.96	-8.47
450.00	6.11		96.96	-8.47
480.00	6.17		96.96	-8.47

THERMAL CONDUCTIVITY TEST

Date: Apr 24/99

Sample No. 1 Discovery

Test No: -7.7 degrees

Temperature (°C): -6.4

Potential Drop, Vr (V): 0.0415

Voltage to Heater Probe, Vp (V): 5.990

Resistance (Ohms): 2.000

Current, I (Amps): 0.0208

Voltage Across Heater, (Vp - Vr): 5.949

Power at Probe Heater (Watts): 0.123

Power per Unite Heated Length of Probe, Q (W/m): 2.626

Probe Length, L (m): 0.047

Thermal Conductivity, λ (W/m°C): 2.786

Slope of Steady State Curve: 0.075

Time Elapsed (seconds)	Ln time (sec)	Outside RTD Reading (Ohms)	Inside RTD Reading (Ohms)	Temperature (°C)
0.00		97.96	97.90	-6.42
5.00	1.61		97.92	-6.36
10.00	2.30		97.94	-6.31
20.00	3.00		97.95	-6.29
30.00	3.40		97.97	-6.23
40.00	3.69		97.98	-6.21
50.00	3.91		97.99	-6.18
60.00	4.09		97.99	-6.18
70.00	4.25		98.00	-6.16
80.00	4.38		98.00	-6.16
90.00	4.50		98.01	-6.13
100.00	4.61		98.01	-6.13
110.00	4.70		98.01	-6.13
120.00	4.79		98.01	-6.13
130.00	4.87		98.02	-6.10
140.00	4.94		98.02	-6.10
150.00	5.01		98.02	-6.10
160.00	5.08	98	98.02	-6.10
170.00	5.14		98.02	-6.10
180.00	5.19		98.02	-6.10
195.00	5.27	98.01	98.03	-6.08
210.00	5.35		98.03	-6.08
225.00	5.42		98.03	-6.08
240.00	5.48		98.03	-6.08
270.00	5.60	98.02	98.04	-6.05
300.00	5.70		98.04	-6.05
330.00	5.80		98.04	-6.05
360.00	5.89		98.04	-6.05
390.00	5.97	98.03	98.05	-6.03
420.00	6.04		98.05	-6.03
450.00	6.11		98.05	-6.03
480.00	6.17		98.05	-6.03

THERMAL CONDUCTIVITY TEST

Date: Apr 23/99

Sample No. 2

Test No: -7.7 degrees

Temperature (°C): -6.0
Potential Drop, Vr (V): 0.0421
Voltage to Heater Probe, Vp (V): 6.000
Resistance (Ohms): 2.000
Current, I (Amps): 0.0211
Voltage Across Heater, (Vp - Vr): 5.958
Power at Probe Heater (Watts): 0.125
Power per Unite Heated Length of Probe, Q (W/m): 2.668
Probe Length, L (m): 0.047
Thermal Conductivity, λ (W/m°C): 3.283
Slope of Steady State Curve: 0.065

Time Elapsed (seconds)	Ln time (sec)	Outside RTD Reading (Ohms)	Inside RTD Reading (Ohms)	Temperature (°C)
0.00		97.92	97.89	-6.05
5.00	1.61		97.93	-5.95
10.00	2.30		97.94	-5.92
20.00	3.00		97.95	-5.90
30.00	3.40		97.96	-5.87
40.00	3.69		97.97	-5.84
50.00	3.91		97.98	-5.82
60.00	4.09		97.98	-5.82
70.00	4.25		97.99	-5.79
80.00	4.38	97.94	97.99	-5.79
90.00	4.50		97.99	-5.79
100.00	4.61		98.00	-5.77
110.00	4.70		98.00	-5.77
120.00	4.79		98.00	-5.77
130.00	4.87	97.95	98.01	-5.74
140.00	4.94		98.01	-5.74
150.00	5.01		98.01	-5.74
160.00	5.08		98.01	-5.74
170.00	5.14		98.01	-5.74
180.00	5.19		98.01	-5.74
195.00	5.27		98.01	-5.74
210.00	5.35		98.02	-5.71
225.00	5.42		98.02	-5.71
240.00	5.48	97.96	98.02	-5.71
270.00	5.60		98.02	-5.71
300.00	5.70		98.02	-5.71
330.00	5.80		98.02	-5.71
360.00	5.89		98.02	-5.71
390.00	5.97		98.03	-5.69
420.00	6.04		98.03	-5.69
450.00	6.11		98.03	-5.69
480.00	6.17		98.03	-5.69

THERMAL CONDUCTIVITY TEST

Date: Apr 24/99

Sample No. 1 Discovery

Test No: -5.4 degrees

Temperature (°C): -4.0
Potential Drop, Vr (V): 0.0416
Voltage to Heater Probe, Vp (V): 6.000
Resistance (Ohms): 2.000
Current, I (Amps): 0.0208
Voltage Across Heater, (Vp - Vr): 5.958
Power at Probe Heater (Watts): 0.124
Power per Unite Heated Length of Probe, Q (W/m): 2.637
Probe Length, L (m): 0.047
Thermal Conductivity, λ (W/m°C): 3.320
Slope of Steady State Curve: 0.063

Time Elapsed (seconds)	Ln time (sec)	Outside RTD Reading (Ohms)	Inside RTD Reading (Ohms)	Temperature (°C)
0.00		98.89	98.83	-4.00
5.00	1.61		98.84	-3.97
10.00	2.30		98.86	-3.92
20.00	3.00	98.9	98.88	-3.87
30.00	3.40		98.90	-3.82
40.00	3.69		98.91	-3.79
50.00	3.91	98.91	98.91	-3.79
60.00	4.09		98.92	-3.77
70.00	4.25		98.92	-3.77
80.00	4.38	98.92	98.93	-3.74
90.00	4.50		98.93	-3.74
100.00	4.61		98.93	-3.74
110.00	4.70		98.94	-3.71
120.00	4.79		98.94	-3.71
130.00	4.87	98.93	98.94	-3.71
140.00	4.94		98.94	-3.71
150.00	5.01		98.94	-3.71
160.00	5.08		98.95	-3.69
170.00	5.14		98.95	-3.69
180.00	5.19		98.95	-3.69
195.00	5.27		98.95	-3.69
210.00	5.35		98.95	-3.69
225.00	5.42		98.95	-3.69
240.00	5.48		98.96	-3.66
270.00	5.60	98.94	98.96	-3.66
300.00	5.70		98.96	-3.66
330.00	5.80		98.96	-3.66
360.00	5.89		98.96	-3.66
390.00	5.97		98.96	-3.66
420.00	6.04		98.96	-3.66
450.00	6.11		98.96	-3.66
480.00	6.17		98.97	-3.64

THERMAL CONDUCTIVITY TEST

Date: Apr 24/99

Sample No. 2 Discovery

Test No: -5.4 degrees

Temperature (°C): -3.9
Potential Drop, Vr (V): 0.0421
Voltage to Heater Probe, Vp (V): 6.000
Resistance (Ohms): 2.000
Current, I (Amps): 0.0211
Voltage Across Heater, (Vp - Vr): 5.958
Power at Probe Heater (Watts): 0.125
Power per Unite Heated Length of Probe, Q (W/m): 2.668
Probe Length, L (m): 0.047
Thermal Conductivity, λ (W/m°C): 3.209
Slope of Steady State Curve: 0.066

Time Elapsed (seconds)	Ln time (sec)	Outside RTD Reading (Ohms)	Inside RTD Reading (Ohms)	Temperature (°C)
0.00		98.78	98.73	-3.87
5.00	1.61		98.74	-3.84
10.00	2.30		98.76	-3.79
20.00	3.00		98.78	-3.74
30.00	3.40	98.79	98.79	-3.71
40.00	3.69		98.80	-3.69
50.00	3.91		98.81	-3.66
60.00	4.09		98.82	-3.64
70.00	4.25		98.82	-3.64
80.00	4.38	98.8	98.82	-3.64
90.00	4.50		98.83	-3.61
100.00	4.61		98.83	-3.61
110.00	4.70		98.83	-3.61
120.00	4.79		98.83	-3.61
130.00	4.87		98.84	-3.58
140.00	4.94		98.84	-3.58
150.00	5.01		98.84	-3.58
160.00	5.08	98.81	98.84	-3.58
170.00	5.14		98.84	-3.58
180.00	5.19		98.84	-3.58
195.00	5.27		98.85	-3.56
210.00	5.35		98.85	-3.56
225.00	5.42		98.85	-3.56
240.00	5.48		98.85	-3.56
270.00	5.60		98.85	-3.56
300.00	5.70		98.85	-3.56
330.00	5.80	98.82	98.86	-3.53
360.00	5.89		98.86	-3.53
390.00	5.97		98.86	-3.53
420.00	6.04		98.86	-3.53
450.00	6.11		98.86	-3.53
480.00	6.17		98.86	-3.53

THERMAL CONDUCTIVITY TEST

Date: Apr 25/99

Sample No. 1 Discovery
Test No: -2.0 degrees

Temperature (°C): -1.0
Potential Drop, Vr (V): 0.0415
Voltage to Heater Probe, Vp (V): 5.990
Resistance (Ohms): 2.000
Current, I (Amps): 0.0208
Voltage Across Heater, (Vp - Vr): 5.949
Power at Probe Heater (Watts): 0.123
Power per Unite Heated Length of Probe, Q (W/m): 2.626
Probe Length, L (m): 0.047
Thermal Conductivity, λ (W/m°C): 3.492
Slope of Steady State Curve: 0.060

Time Elapsed (seconds)	Ln time (sec)	Outside RTD Reading (Ohms)	Inside RTD Reading (Ohms)	Temperature (°C)
0.00		100.05	99.97	-1.04
5.00	1.61		99.98	-1.01
10.00	2.30		100.00	-0.96
20.00	3.00		100.01	-0.94
30.00	3.40		100.02	-0.91
40.00	3.69		100.02	-0.91
50.00	3.91		100.03	-0.88
60.00	4.09		100.04	-0.86
70.00	4.25		100.04	-0.86
80.00	4.38		100.04	-0.86
90.00	4.50		100.05	-0.83
100.00	4.61	100.06	100.05	-0.83
110.00	4.70		100.05	-0.83
120.00	4.79		100.05	-0.83
130.00	4.87		100.06	-0.81
140.00	4.94		100.06	-0.81
150.00	5.01		100.06	-0.81
160.00	5.08		100.06	-0.81
170.00	5.14		100.06	-0.81
180.00	5.19		100.06	-0.81
195.00	5.27		100.06	-0.81
210.00	5.35		100.06	-0.81
225.00	5.42		100.07	-0.78
240.00	5.48	100.07	100.07	-0.78
270.00	5.60		100.07	-0.78
300.00	5.70		100.07	-0.78
330.00	5.80		100.07	-0.78
360.00	5.89		100.08	-0.75
390.00	5.97		100.08	-0.75
420.00	6.04		100.08	-0.75
450.00	6.11		100.08	-0.75
480.00	6.17		100.08	-0.75

CONDUCTIVITY TEST

Date: Apr 25/99

2

-2.0 degrees

Temperature (°C): -0.9
Potential Drop, Vr (V): 0.0421
Voltage to Heater Probe, Vp (V): 5.980
Resistance (Ohms):
Current, I (Amps): 0.0211
Voltage Across Heater, (Vp - Vr): 5.938
Power at Probe Heater (Watts): 0.125
Power per Unite Heated Length of Probe, Q (W/m): 2.659
Probe Length, L (m): 0.047
Thermal Conductivity, **l** (W/m°C): 3.635
Slope of Steady State Curve: 0.058

Time Elapsed (seconds)	Ln time (sec)	Outside RTD Reading (Ohms)	Inside RTD Reading (Ohms)	Temperature (°C)
0.00		99.95	99.87	-0.91
5.00	1.61		99.88	-0.88
10.00	2.30		99.90	-0.83
20.00	3.00		99.91	-0.81
30.00	3.40		99.92	-0.78
40.00	3.69		99.93	-0.75
50.00	3.91		99.94	-0.73
60.00	4.09		99.94	-0.73
70.00	4.25		99.94	-0.73
80.00	4.38		99.94	-0.73
90.00	4.50	99.96	99.95	-0.70
100.00	4.61		99.95	-0.70
110.00	4.70		99.95	-0.70
120.00	4.79		99.95	-0.70
130.00	4.87		99.96	-0.68
140.00	4.94		99.96	-0.68
150.00	5.01		99.96	-0.68
160.00	5.08		99.96	-0.68
170.00	5.14		99.96	-0.68
180.00	5.19		99.96	-0.68
195.00	5.27		99.97	-0.65
210.00	5.35		99.97	-0.65
225.00	5.42		99.97	-0.65
240.00	5.48		99.97	-0.65
270.00	5.60		99.97	-0.65
300.00	5.70		99.97	-0.65
330.00	5.80		99.98	-0.62
360.00	5.89	99.97	99.98	-0.62
390.00	5.97		99.98	-0.62
420.00	6.04		99.98	-0.62
450.00	6.11		99.98	-0.62
480.00	6.17		99.98	-0.62

THERMAL CONDUCTIVITY TEST

Date: May 14/99

Sample No. 1

Test No: 2.0 degrees

Temperature (°C): 2.0
Potential Drop, Vr (V): 0.041
Voltage to Heater Probe, Vp (V): 5.990
Resistance (Ohms):
Current, I (Amps): 0.0205
Voltage Across Heater, (Vp - Vr): 5.949
Power at Probe Heater (Watts): 0.122
Power per Unite Heated Length of Probe, Q (W/m): 2.595
Probe Length, L (m): 0.047
Thermal Conductivity, λ (W/m°C): 1.721
Slope of Steady State Curve: 0.120

Time Elapsed (seconds)	Ln time (sec)	Outside RTD Reading (Ohms)	Inside RTD Reading (Ohms)	Temperature (°C)
0.00		101.27	101.23	2.23
5.00	1.61		101.24	2.26
10.00	2.30		101.26	2.31
20.00	3.00		101.29	2.39
30.00	3.40		101.31	2.44
40.00	3.69		101.32	2.47
50.00	3.91		101.34	2.52
60.00	4.09	101.28	101.35	2.55
70.00	4.25		101.35	2.55
80.00	4.38		101.36	2.57
90.00	4.50	101.29	101.36	2.57
100.00	4.61		101.37	2.60
110.00	4.70		101.37	2.60
120.00	4.79		101.38	2.62
130.00	4.87	101.3	101.38	2.62
140.00	4.94		101.39	2.65
150.00	5.01		101.39	2.65
160.00	5.08		101.39	2.65
170.00	5.14		101.4	2.68
180.00	5.19	101.31	101.4	2.68
195.00	5.27		101.4	2.68
210.00	5.35		101.4	2.68
225.00	5.42		101.41	2.70
240.00	5.48		101.41	2.70
270.00	5.60	101.32	101.41	2.70
300.00	5.70		101.42	2.73
330.00	5.80		101.42	2.73
360.00	5.89	101.33	101.43	2.75
390.00	5.97		101.43	2.75
420.00	6.04		101.43	2.75
450.00	6.11		101.43	2.75
480.00	6.17	101.34	101.44	2.78

THERMAL CONDUCTIVITY TEST

Date: May 14/99

Sample No. 2

Test No: 2.0 degrees

Temperature (°C): 2.0
Potential Drop, Vr (V): 0.042
Voltage to Heater Probe, Vp (V): 5.990
Resistance (Ohms):
Current, I (Amps): 0.0210
Voltage Across Heater, (Vp - Vr): 5.948
Power at Probe Heater (Watts): 0.125
Power per Unite Heated Length of Probe, Q (W/m): 2.658
Probe Length, L (m): 0.047
Thermal Conductivity, k (W/m°C): 1.550
Slope of Steady State Curve: 0.136

Time Elapsed (seconds)	Ln time (sec)	Outside RTD Reading (Ohms)	Inside RTD Reading (Ohms)	Temperature (°C)
0.00		101.09	101.06	2.18
5.00	1.61		101.07	2.21
10.00	2.30		101.09	2.26
20.00	3.00		101.12	2.34
30.00	3.40		101.14	2.39
40.00	3.69		101.15	2.42
50.00	3.91	101.1	101.16	2.44
60.00	4.09		101.17	2.47
70.00	4.25		101.18	2.49
80.00	4.38		101.19	2.52
90.00	4.50		101.19	2.52
100.00	4.61	101.11	101.2	2.55
110.00	4.70		101.2	2.55
120.00	4.79		101.21	2.57
130.00	4.87		101.21	2.57
140.00	4.94	101.12	101.22	2.60
150.00	5.01		101.22	2.60
160.00	5.08		101.22	2.60
170.00	5.14		101.23	2.62
180.00	5.19		101.23	2.62
195.00	5.27		101.23	2.62
210.00	5.35		101.24	2.65
225.00	5.42	101.13	101.24	2.65
240.00	5.48		101.25	2.68
270.00	5.60	101.14	101.25	2.68
300.00	5.70		101.26	2.70
330.00	5.80		101.26	2.70
360.00	5.89	101.15	101.27	2.73
390.00	5.97		101.27	2.73
420.00	6.04		101.27	2.73
450.00	6.11		101.28	2.75
480.00	6.17		101.28	2.75

THERMAL CONDUCTIVITY TEST

Date: April 29, 2000

Sample No. Faro Mine

Test No: 8

Temperature (°C):	-8.7
Potential Drop, Vr (V):	0.218
Voltage to Heater Probe, Vp (V):	5.970
Resistance (Ohms):	2.000
Current, I (Amps):	0.1090
Voltage Across Heater, (Vp - Vr):	5.752
Power at Probe Heater (Watts):	0.627
Power per Unite Heated Length of Probe, Q (W/m):	13.340
Probe Length, L (m):	0.047
Thermal Conductivity, λ (W/m°C):	5.057
Slope of Steady State Curve:	0.210

Time Elapsed (seconds)	Ln time (sec)	Outside RTD Reading (Ohms)	Inside RTD Reading (Ohms)	Temperature (°C)
0.00		97.64	97.37	-9.12
5.00	1.61	97.64	97.42	-8.99
10.00	2.30	97.64	97.45	-8.91
20.00	3.00	97.64	97.49	-8.81
30.00	3.40	97.64	97.53	-8.70
40.00	3.69	97.64	97.55	-8.65
50.00	3.91	97.64	97.57	-8.60
60.00	4.09	97.64	97.59	-8.55
70.00	4.25	97.65	97.6	-8.52
80.00	4.38	97.65	97.61	-8.49
90.00	4.50	97.65	97.62	-8.47
100.00	4.61	97.65	97.63	-8.44
110.00	4.70	97.65	97.64	-8.42
120.00	4.79	97.66	97.65	-8.39
130.00	4.87	97.66	97.65	-8.39
140.00	4.94	97.66	97.66	-8.36
150.00	5.01	97.66	97.67	-8.34
160.00	5.08	97.66	97.68	-8.31
170.00	5.14	97.67	97.68	-8.31
180.00	5.19	97.67	97.68	-8.31
195.00	5.27	97.67	97.69	-8.29
210.00	5.35	97.67	97.7	-8.26
225.00	5.42	97.67	97.7	-8.26
240.00	5.48	97.68	97.71	-8.23
270.00	5.60	97.68	97.72	-8.21
300.00	5.70	97.69	97.73	-8.18
330.00	5.80	97.69	97.73	-8.18
360.00	5.89	97.69	97.74	-8.16
390.00	5.97	97.69	97.75	-8.13
420.00	6.04	97.7	97.75	-8.13
450.00	6.11	97.7	97.76	-8.10
480.00	6.17	97.7	97.76	-8.10

THERMAL CONDUCTIVITY TEST

Date: April 30, 2000

Sample No. Faro Mine

Test No: 9

Temperature (°C): -8.1
Potential Drop, Vr (V): 0.22
Voltage to Heater Probe, Vp (V): 5.970
Resistance (Ohms): 2.000
Current, I (Amps): 0.1100
Voltage Across Heater, (Vp - Vr): 5.750
Power at Probe Heater (Watts): 0.633
Power per Unite Heated Length of Probe, Q (W/m): 13.457
Probe Length, L (m): 0.047
Thermal Conductivity, I (W/m°C): 5.156
Slope of Steady State Curve: 0.208

Time Elapsed (seconds)	Ln time (sec)	Outside RTD Reading (Ohms)	Inside RTD Reading (Ohms)	Temperature (°C)
0.00		97.91	97.65	-8.39
5.00	1.61	97.91	97.69	-8.29
10.00	2.30	97.91	97.72	-8.21
20.00	3.00	97.91	97.77	-8.08
30.00	3.40	97.91	97.8	-8.00
40.00	3.69	97.92	97.82	-7.95
50.00	3.91	97.92	97.85	-7.87
60.00	4.09	97.92	97.86	-7.84
70.00	4.25	97.92	97.87	-7.82
80.00	4.38	97.92	97.89	-7.77
90.00	4.50	97.92	97.9	-7.74
100.00	4.61	97.93	97.91	-7.71
110.00	4.70	97.93	97.91	-7.71
120.00	4.79	97.93	97.92	-7.69
130.00	4.87	97.93	97.93	-7.66
140.00	4.94	97.93	97.93	-7.66
150.00	5.01	97.94	97.94	-7.64
160.00	5.08	97.94	97.94	-7.64
170.00	5.14	97.94	97.95	-7.61
180.00	5.19	97.94	97.96	-7.58
195.00	5.27	97.94	97.96	-7.58
210.00	5.35	97.94	97.97	-7.56
225.00	5.42	97.95	97.97	-7.56
240.00	5.48	97.95	97.98	-7.53
270.00	5.60	97.95	97.99	-7.51
300.00	5.70	97.96	98	-7.48
330.00	5.80	97.96	98	-7.48
360.00	5.89	97.96	98.01	-7.45
390.00	5.97	97.97	98.02	-7.43
420.00	6.04	97.97	98.02	-7.43
450.00	6.11	97.97	98.03	-7.40
480.00	6.17	97.98	98.03	-7.40

THERMAL CONDUCTIVITY TEST

Date: May 1, 2000

Sample No. Faro Mine

Test No: 10

Temperature (°C): -6.5
Potential Drop, Vr (V): 0.217
Voltage to Heater Probe, Vp (V): 5.940
Resistance (Ohms): 2.000
Current, I (Amps): 0.1085
Voltage Across Heater, (Vp - Vr): 5.723
Power at Probe Heater (Watts): 0.621
Power per Unite Heated Length of Probe, Q (W/m): 13.212
Probe Length, L (m): 0.047
Thermal Conductivity, λ (W/m°C): 5.036
Slope of Steady State Curve: 0.209

Time Elapsed (seconds)	Ln time (sec)	Outside RTD Reading (Ohms)	Inside RTD Reading (Ohms)	Temperature (°C)
0.00		98.37	98.10	-7.22
5.00	1.61	98.37	98.13	-7.14
10.00	2.30	98.37	98.18	-7.01
20.00	3.00	98.37	98.22	-6.91
30.00	3.40	98.37	98.26	-6.81
40.00	3.69	98.38	98.28	-6.75
50.00	3.91	98.38	98.3	-6.70
60.00	4.09	98.38	98.31	-6.68
70.00	4.25	98.38	98.33	-6.62
80.00	4.38	98.38	98.34	-6.60
90.00	4.50	98.38	98.35	-6.57
100.00	4.61	98.39	98.36	-6.55
110.00	4.70	98.39	98.37	-6.52
120.00	4.79	98.39	98.37	-6.52
130.00	4.87	98.39	98.38	-6.49
140.00	4.94	98.4	98.39	-6.47
150.00	5.01	98.4	98.39	-6.47
160.00	5.08	98.4	98.4	-6.44
170.00	5.14	98.4	98.4	-6.44
180.00	5.19	98.41	98.4	-6.44
195.00	5.27	98.41	98.41	-6.42
210.00	5.35	98.41	98.42	-6.39
225.00	5.42	98.41	98.43	-6.36
240.00	5.48	98.41	98.43	-6.36
270.00	5.60	98.42	98.44	-6.34
300.00	5.70	98.42	98.45	-6.31
330.00	5.80	98.43	98.46	-6.29
360.00	5.89	98.43	98.46	-6.29
390.00	5.97	98.43	98.47	-6.26
420.00	6.04	98.43	98.48	-6.23
450.00	6.11	98.43	98.48	-6.23
480.00	6.17	98.44	98.48	-6.23

THERMAL CONDUCTIVITY TEST

Date: May 3, 2000

Sample No. Faro Mine

Test No: 11

Temperature (°C): -5.6
Potential Drop, Vr (V): 0.215
Voltage to Heater Probe, Vp (V): 5.890
Resistance (Ohms): 2.000
Current, I (Amps): 0.1075
Voltage Across Heater, (Vp - Vr): 5.675
Power at Probe Heater (Watts): 0.610
Power per Unite Heated Length of Probe, Q (W/m): 12.980
Probe Length, L (m): 0.047
Thermal Conductivity, λ (W/m°C): 5.118
Slope of Steady State Curve: 0.202

Time Elapsed (seconds)	Ln time (sec)	Outside RTD Reading (Ohms)	Inside RTD Reading (Ohms)	Temperature (°C)
0.00		98.79	98.51	-6.16
5.00	1.61	98.79	98.54	-6.08
10.00	2.30	98.79	98.58	-5.97
20.00	3.00	98.79	98.62	-5.87
30.00	3.40	98.79	98.66	-5.77
40.00	3.69	98.79	98.68	-5.71
50.00	3.91	98.79	98.7	-5.66
60.00	4.09	98.79	98.72	-5.61
70.00	4.25	98.79	98.73	-5.58
80.00	4.38	98.79	98.74	-5.56
90.00	4.50	98.8	98.75	-5.53
100.00	4.61	98.79	98.76	-5.51
110.00	4.70	98.8	98.77	-5.48
120.00	4.79	98.8	98.78	-5.45
130.00	4.87	98.8	98.78	-5.45
140.00	4.94	98.8	98.79	-5.43
150.00	5.01	98.8	98.79	-5.43
160.00	5.08	98.8	98.8	-5.40
170.00	5.14	98.81	98.8	-5.40
180.00	5.19	98.81	98.81	-5.38
195.00	5.27	98.81	98.81	-5.38
210.00	5.35	98.81	98.82	-5.35
225.00	5.42	98.82	98.82	-5.35
240.00	5.48	98.82	98.83	-5.32
270.00	5.60	98.82	98.84	-5.30
300.00	5.70	98.83	98.85	-5.27
330.00	5.80	98.83	98.85	-5.27
360.00	5.89	98.83	98.85	-5.27
390.00	5.97	98.83	98.86	-5.25
420.00	6.04	98.84	98.87	-5.22
450.00	6.11	98.84	98.87	-5.22
480.00	6.17	98.84	98.88	-5.19

THERMAL CONDUCTIVITY TEST

Date: May 4, 2000

Sample No. Faro Mine

Test No: 12

Temperature (°C): -4.5

Potential Drop, Vr (V): 0.22

Voltage to Heater Probe, Vp (V): 6.000

Resistance (Ohms): 2.000

Current, I (Amps): 0.1100

Voltage Across Heater, (Vp - Vr): 5.780

Power at Probe Heater (Watts): 0.636

Power per Unite Heated Length of Probe, Q (W/m): 13.528

Probe Length, L (m): 0.047

Thermal Conductivity, I (W/m°C): 5.022

Slope of Steady State Curve: 0.214

Time Elapsed (seconds)	Ln time (sec)	Outside RTD Reading (Ohms)	Inside RTD Reading (Ohms)	Temperature (°C)
0.00		99.17	98.89	-5.17
5.00	1.61	99.17	98.92	-5.09
10.00	2.30	99.17	98.97	-4.96
20.00	3.00	99.17	99	-4.88
30.00	3.40	99.17	99.04	-4.78
40.00	3.69	99.17	99.06	-4.73
50.00	3.91	99.17	99.08	-4.68
60.00	4.09	99.17	99.1	-4.62
70.00	4.25	99.17	99.11	-4.60
80.00	4.38	99.17	99.12	-4.57
90.00	4.50	99.18	99.13	-4.55
100.00	4.61	99.18	99.14	-4.52
110.00	4.70	99.18	99.15	-4.49
120.00	4.79	99.18	99.16	-4.47
130.00	4.87	99.18	99.16	-4.47
140.00	4.94	99.19	99.17	-4.44
150.00	5.01	99.19	99.18	-4.42
160.00	5.08	99.19	99.19	-4.39
170.00	5.14	99.19	99.19	-4.39
180.00	5.19	99.19	99.2	-4.36
195.00	5.27	99.2	99.2	-4.36
210.00	5.35	99.2	99.21	-4.34
225.00	5.42	99.2	99.22	-4.31
240.00	5.48	99.21	99.22	-4.31
270.00	5.60	99.21	99.23	-4.29
300.00	5.70	99.21	99.24	-4.26
330.00	5.80	99.22	99.25	-4.23
360.00	5.89	99.22	99.26	-4.21
390.00	5.97	99.22	99.26	-4.21
420.00	6.04	99.23	99.27	-4.18
450.00	6.11	99.23	99.28	-4.16
480.00	6.17	99.23	99.28	-4.16

THERMAL CONDUCTIVITY TEST

Date: May 5, 2000

Sample No. Faro Mine

Test No: 13

Temperature (°C):	-4.5
Potential Drop, Vr (V):	0.219
Voltage to Heater Probe, Vp (V):	6.000
Resistance (Ohms):	2.000
Current, I (Amps):	0.1095
Voltage Across Heater, (Vp - Vr):	5.781
Power at Probe Heater (Watts):	0.633
Power per Unite Heated Length of Probe, Q (W/m):	13.469
Probe Length, L (m):	0.047
Thermal Conductivity, I (W/m°C):	5.147
Slope of Steady State Curve:	0.208

Time Elapsed (seconds)	Ln time (sec)	Outside RTD Reading (Ohms)	Inside RTD Reading (Ohms)	Temperature (°C)
0.00		99.34	99.06	-4.73
5.00	1.61	99.34	99.1	-4.62
10.00	2.30	99.34	99.13	-4.55
20.00	3.00	99.34	99.18	-4.42
30.00	3.40	99.34	99.22	-4.31
40.00	3.69	99.34	99.23	-4.29
50.00	3.91	99.34	99.25	-4.23
60.00	4.09	99.35	99.27	-4.18
70.00	4.25	99.35	99.28	-4.16
80.00	4.38	99.35	99.29	-4.13
90.00	4.50	99.35	99.3	-4.10
100.00	4.61	99.35	99.31	-4.08
110.00	4.70	99.35	99.32	-4.05
120.00	4.79	99.36	99.33	-4.03
130.00	4.87	99.36	99.34	-4.00
140.00	4.94	99.36	99.34	-4.00
150.00	5.01	99.36	99.35	-3.97
160.00	5.08	99.36	99.35	-3.97
170.00	5.14	99.36	99.36	-3.95
180.00	5.19	99.36	99.37	-3.92
195.00	5.27	99.37	99.37	-3.92
210.00	5.35	99.37	99.38	-3.90
225.00	5.42	99.37	99.39	-3.87
240.00	5.48	99.38	99.39	-3.87
270.00	5.60	99.38	99.4	-3.84
300.00	5.70	99.38	99.41	-3.82
330.00	5.80	99.39	99.42	-3.79
360.00	5.89	99.39	99.42	-3.79
390.00	5.97	99.39	99.42	-3.79
420.00	6.04	99.4	99.43	-3.77
450.00	6.11	99.4	99.44	-3.74
480.00	6.17	99.4	99.44	-3.74

THERMAL CONDUCTIVITY TEST

Date: May 6, 2000

Sample No. Faro Mine

Test No: 14

Temperature (°C): -3.1
Potential Drop, Vr (V): 0.22
Voltage to Heater Probe, Vp (V): 6.000
Resistance (Ohms): 2.000
Current, I (Amps): 0.1100
Voltage Across Heater, (Vp - Vr): 5.780
Power at Probe Heater (Watts): 0.636
Power per Unite Heated Length of Probe, Q (W/m): 13.528
Probe Length, L (m): 0.047
Thermal Conductivity, λ (W/m°C): 5.262
Slope of Steady State Curve: 0.205

Time Elapsed (seconds)	Ln time (sec)	Outside RTD Reading (Ohms)	Inside RTD Reading (Ohms)	Temperature (°C)
0.00		99.89	99.61	-3.30
5.00	1.61	99.89	99.65	-3.19
10.00	2.30	99.89	99.68	-3.12
20.00	3.00	99.89	99.73	-2.99
30.00	3.40	99.89	99.76	-2.91
40.00	3.69	99.89	99.78	-2.86
50.00	3.91	99.9	99.8	-2.81
60.00	4.09	99.9	99.81	-2.78
70.00	4.25	99.9	99.83	-2.73
80.00	4.38	99.9	99.84	-2.70
90.00	4.50	99.9	99.85	-2.68
100.00	4.61	99.9	99.86	-2.65
110.00	4.70	99.91	99.87	-2.62
120.00	4.79	99.91	99.88	-2.60
130.00	4.87	99.91	99.88	-2.60
140.00	4.94	99.91	99.89	-2.57
150.00	5.01	99.91	99.89	-2.57
160.00	5.08	99.92	99.9	-2.55
170.00	5.14	99.92	99.9	-2.55
180.00	5.19	99.92	99.91	-2.52
195.00	5.27	99.92	99.91	-2.52
210.00	5.35	99.92	99.92	-2.49
225.00	5.42	99.93	99.93	-2.47
240.00	5.48	99.93	99.94	-2.44
270.00	5.60	99.93	99.94	-2.44
300.00	5.70	99.94	99.95	-2.42
330.00	5.80	99.94	99.96	-2.39
360.00	5.89	99.94	99.97	-2.36
390.00	5.97	99.94	99.97	-2.36
420.00	6.04	99.95	99.98	-2.34
450.00	6.11	99.95	99.98	-2.34
480.00	6.17	99.95	99.99	-2.31

THERMAL CONDUCTIVITY TEST

Date: May 9, 2000

Sample No. Faro Mine

Test No: 15

Temperature (°C): -2.6
Potential Drop, Vr (V): 0.22
Voltage to Heater Probe, Vp (V): 6.000
Resistance (Ohms): 2.000
Current, I (Amps): 0.1100
Voltage Across Heater, (Vp - Vr): 5.780
Power at Probe Heater (Watts): 0.636
Power per Unite Heated Length of Probe, Q (W/m): 13.528
Probe Length, L (m): 0.047
Thermal Conductivity, **l** (W/m°C): 5.154
Slope of Steady State Curve: 0.209

Time Elapsed (seconds)	Ln time (sec)	Outside RTD Reading (Ohms)	Inside RTD Reading (Ohms)	Temperature (°C)
0.00		99.95	99.66	-3.17
5.00	1.61	99.95	99.69	-3.09
10.00	2.30	99.95	99.73	-2.99
20.00	3.00	99.95	99.78	-2.86
30.00	3.40	99.95	99.81	-2.78
40.00	3.69	99.95	99.83	-2.73
50.00	3.91	99.95	99.85	-2.68
60.00	4.09	99.95	99.87	-2.62
70.00	4.25	99.95	99.88	-2.60
80.00	4.38	99.95	99.89	-2.57
90.00	4.50	99.96	99.9	-2.55
100.00	4.61	99.96	99.91	-2.52
110.00	4.70	99.96	99.92	-2.49
120.00	4.79	99.96	99.93	-2.47
130.00	4.87	99.96	99.93	-2.47
140.00	4.94	99.96	99.94	-2.44
150.00	5.01	99.97	99.95	-2.42
160.00	5.08	99.97	99.95	-2.42
170.00	5.14	99.97	99.96	-2.39
180.00	5.19	99.97	99.96	-2.39
195.00	5.27	99.97	99.97	-2.36
210.00	5.35	99.98	99.98	-2.34
225.00	5.42	99.98	99.98	-2.34
240.00	5.48	99.98	99.99	-2.31
270.00	5.60	99.99	100	-2.29
300.00	5.70	99.99	100	-2.29
330.00	5.80	99.99	100.01	-2.26
360.00	5.89	100	100.02	-2.23
390.00	5.97	100	100.02	-2.23
420.00	6.04	100	100.03	-2.21
450.00	6.11	100.01	100.04	-2.18
480.00	6.17	100.01	100.04	-2.18

THERMAL CONDUCTIVITY TEST

Date: May 9, 2000

Sample No. Faro Mine

Test No: 16

Temperature (°C): -2.5
Potential Drop, Vr (V): 0.22
Voltage to Heater Probe, Vp (V): 6.000
Resistance (Ohms): 2.000
Current, I (Amps): 0.1100
Voltage Across Heater, (Vp - Vr): 5.780
Power at Probe Heater (Watts): 0.636
Power per Unite Heated Length of Probe, Q (W/m): 13.528
Probe Length, L (m): 0.047
Thermal Conductivity, I (W/m°C): 5.410
Slope of Steady State Curve: 0.199

Time Elapsed (seconds)	Ln time (sec)	Outside RTD Reading (Ohms)	Inside RTD Reading (Ohms)	Temperature (°C)
0.00		100.03	99.75	-2.94
5.00	1.61	100.03	99.79	-2.83
10.00	2.30	100.03	99.82	-2.75
20.00	3.00	100.03	99.87	-2.62
30.00	3.40	100.03	99.9	-2.55
40.00	3.69	100.03	99.92	-2.49
50.00	3.91	100.03	99.94	-2.44
60.00	4.09	100.03	99.95	-2.42
70.00	4.25	100.03	99.97	-2.36
80.00	4.38	100.03	99.98	-2.34
90.00	4.50	100.04	99.99	-2.31
100.00	4.61	100.04	100	-2.29
110.00	4.70	100.04	100.01	-2.26
120.00	4.79	100.04	100.01	-2.26
130.00	4.87	100.04	100.02	-2.23
140.00	4.94	100.04	100.02	-2.23
150.00	5.01	100.04	100.03	-2.21
160.00	5.08	100.04	100.04	-2.18
170.00	5.14	100.05	100.04	-2.18
180.00	5.19	100.05	100.04	-2.18
195.00	5.27	100.05	100.05	-2.16
210.00	5.35	100.05	100.06	-2.13
225.00	5.42	100.05	100.06	-2.13
240.00	5.48	100.05	100.07	-2.10
270.00	5.60	100.06	100.08	-2.08
300.00	5.70	100.06	100.08	-2.08
330.00	5.80	100.06	100.09	-2.05
360.00	5.89	100.07	100.1	-2.03
390.00	5.97	100.07	100.11	-2.00
420.00	6.04	100.07	100.11	-2.00
450.00	6.11	100.08	100.12	-1.97
480.00	6.17	100.08	100.12	-1.97

THERMAL CONDUCTIVITY TEST

Date: May 10, 2000

Sample No. Faro Mine

Test No: 17

Temperature (°C): -1.5

Potential Drop, Vr (V): 0.22

Voltage to Heater Probe, Vp (V): 6.000

Resistance (Ohms): 2.000

Current, I (Amps): 0.1100

Voltage Across Heater, (Vp - Vr): 5.780

Power at Probe Heater (Watts): 0.636

Power per Unite Heated Length of Probe, Q (W/m): 13.528

Probe Length, L (m): 0.047

Thermal Conductivity, λ (W/m°C): 5.583

Slope of Steady State Curve: 0.193

Time Elapsed (seconds)	Ln time (sec)	Outside RTD Reading (Ohms)	Inside RTD Reading (Ohms)	Temperature (°C)
0.00		100.27	99.99	-2.31
5.00	1.61	100.27	100.02	-2.23
10.00	2.30	100.27	100.05	-2.16
20.00	3.00	100.27	100.10	-2.03
30.00	3.40	100.27	100.13	-1.95
40.00	3.69	100.27	100.14	-1.92
50.00	3.91	100.27	100.16	-1.87
60.00	4.09	100.27	100.18	-1.82
70.00	4.25	100.27	100.19	-1.79
80.00	4.38	100.27	100.20	-1.77
90.00	4.50	100.28	100.21	-1.74
100.00	4.61	100.28	100.22	-1.71
110.00	4.70	100.28	100.23	-1.69
120.00	4.79	100.28	100.23	-1.69
130.00	4.87	100.28	100.24	-1.66
140.00	4.94	100.28	100.25	-1.64
150.00	5.01	100.28	100.25	-1.64
160.00	5.08	100.29	100.26	-1.61
170.00	5.14	100.29	100.26	-1.61
180.00	5.19	100.29	100.26	-1.61
195.00	5.27	100.29	100.27	-1.58
210.00	5.35	100.29	100.28	-1.56
225.00	5.42	100.29	100.28	-1.56
240.00	5.48	100.3	100.29	-1.53
270.00	5.60	100.3	100.3	-1.51
300.00	5.70	100.3	100.31	-1.48
330.00	5.80	100.3	100.31	-1.48
360.00	5.89	100.31	100.32	-1.45
390.00	5.97	100.31	100.33	-1.43
420.00	6.04	100.31	100.33	-1.43
450.00	6.11	100.31	100.34	-1.40
480.00	6.17	100.32	100.34	-1.40

THERMAL CONDUCTIVITY TEST

Date: May 11, 2000

Sample No. Faro Mine

Test No: 18

Temperature (°C):	-0.6
Potential Drop, Vr (V):	0.22
Voltage to Heater Probe, Vp (V):	6.000
Resistance (Ohms):	2.000
Current, I (Amps):	0.1100
Voltage Across Heater, (Vp - Vr):	5.780
Power at Probe Heater (Watts):	0.636
Power per Unite Heated Length of Probe, Q (W/m):	13.528
Probe Length, L (m):	0.047
Thermal Conductivity, λ (W/m°C):	10.555
Slope of Steady State Curve:	0.102

Time Elapsed (seconds)	Ln time (sec)	Outside RTD Reading (Ohms)	Inside RTD Reading (Ohms)	Temperature (°C)
0.00		100.71	100.42	-1.19
5.00	1.61	100.71	100.45	-1.12
10.00	2.30	100.71	100.46	-1.09
20.00	3.00	100.71	100.49	-1.01
30.00	3.40	100.71	100.5	-0.99
40.00	3.69	100.71	100.51	-0.96
50.00	3.91	100.71	100.52	-0.94
60.00	4.09	100.71	100.52	-0.94
70.00	4.25	100.71	100.53	-0.91
80.00	4.38	100.71	100.53	-0.91
90.00	4.50	100.71	100.54	-0.88
100.00	4.61	100.71	100.54	-0.88
110.00	4.70	100.71	100.55	-0.86
120.00	4.79	100.71	100.55	-0.86
130.00	4.87	100.71	100.56	-0.83
140.00	4.94	100.71	100.56	-0.83
150.00	5.01	100.71	100.56	-0.83
160.00	5.08	100.71	100.57	-0.81
170.00	5.14	100.71	100.57	-0.81
180.00	5.19	100.71	100.57	-0.81
195.00	5.27	100.71	100.57	-0.81
210.00	5.35	100.71	100.58	-0.78
225.00	5.42	100.71	100.58	-0.78
240.00	5.48	100.71	100.58	-0.78
270.00	5.60	100.71	100.59	-0.75
300.00	5.70	100.72	100.6	-0.73
330.00	5.80	100.72	100.6	-0.73
360.00	5.89	100.72	100.61	-0.70
390.00	5.97	100.72	100.61	-0.70
420.00	6.04	100.72	100.62	-0.68
450.00	6.11	100.72	100.62	-0.68
480.00	6.17	100.72	100.62	-0.68

THERMAL CONDUCTIVITY TEST

Date: May 12, 2000

Sample No. Faro Mine

Test No: 19

Temperature (°C): 0.0
Potential Drop, Vr (V): 0.22
Voltage to Heater Probe, Vp (V): 6.000
Resistance (Ohms): 2.000
Current, I (Amps): 0.1100
Voltage Across Heater, (Vp - Vr): 5.780
Power at Probe Heater (Watts): 0.636
Power per Unite Heated Length of Probe, Q (W/m): 13.528
Probe Length, L (m): 0.047
Thermal Conductivity, λ (W/m°C): 1.959
Slope of Steady State Curve: 0.549

Time Elapsed (seconds)	Ln time (sec)	Outside RTD Reading (Ohms)	Inside RTD Reading (Ohms)	Temperature (°C)
0.00		100.86	100.57	-0.81
5.00	1.61	100.86	100.61	-0.70
10.00	2.30	100.86	100.65	-0.60
20.00	3.00	100.86	100.77	-0.29
30.00	3.40	100.86	100.85	-0.08
40.00	3.69	100.86	100.91	0.08
50.00	3.91	100.86	100.95	0.18
60.00	4.09	100.86	100.99	0.29
70.00	4.25	100.86	101.03	0.39
80.00	4.38	100.86	101.06	0.47
90.00	4.50	100.86	101.08	0.52
100.00	4.61	100.86	101.1	0.57
110.00	4.70	100.86	101.13	0.65
120.00	4.79	100.86	101.15	0.70
130.00	4.87	100.86	101.16	0.73
140.00	4.94	100.86	101.18	0.78
150.00	5.01	100.86	101.2	0.83
160.00	5.08	100.86	101.22	0.88
170.00	5.14	100.86	101.23	0.91
180.00	5.19	100.86	101.24	0.94
195.00	5.27	100.86	101.26	0.99
210.00	5.35	100.86	101.28	1.04
225.00	5.42	100.86	101.3	1.09
240.00	5.48	100.86	101.32	1.14
270.00	5.60	100.86	101.35	1.22
300.00	5.70	100.86	101.38	1.30
330.00	5.80	100.86	101.41	1.38
360.00	5.89	100.86	101.44	1.45
390.00	5.97	100.86	101.47	1.53
420.00	6.04	100.86	101.49	1.58
450.00	6.11	100.86	101.51	1.64
480.00	6.17	100.86	101.54	1.71

THERMAL CONDUCTIVITY TEST

Date: May 13, 2000

Sample No. Faro Mine

Test No: 20

Temperature (°C): 0.7
Potential Drop, Vr (V): 0.22
Voltage to Heater Probe, Vp (V): 6.000
Resistance (Ohms): 2.000
Current, I (Amps): 0.1100
Voltage Across Heater, (Vp - Vr): 5.780
Power at Probe Heater (Watts): 0.636
Power per Unite Heated Length of Probe, Q (W/m): 13.528
Probe Length, L (m): 0.047
Thermal Conductivity, I (W/m°C): 3.046
Slope of Steady State Curve: 0.353

Time Elapsed (seconds)	Ln time (sec)	Outside RTD Reading (Ohms)	Inside RTD Reading (Ohms)	Temperature (°C)
0.00		101.23	100.93	0.13
5.00	1.61	101.23	100.96	0.21
10.00	2.30	101.22	101.00	0.31
20.00	3.00	101.23	101.05	0.44
30.00	3.40	101.22	101.10	0.57
40.00	3.69	101.22	101.14	0.68
50.00	3.91	101.22	101.17	0.75
60.00	4.09	101.23	101.19	0.81
70.00	4.25	101.23	101.22	0.88
80.00	4.38	101.23	101.24	0.94
90.00	4.50	101.23	101.25	0.96
100.00	4.61	101.23	101.27	1.01
110.00	4.70	101.23	101.29	1.06
120.00	4.79	101.23	101.3	1.09
130.00	4.87	101.23	101.32	1.14
140.00	4.94	101.23	101.33	1.17
150.00	5.01	101.23	101.34	1.19
160.00	5.08	101.23	101.35	1.22
170.00	5.14	101.24	101.36	1.25
180.00	5.19	101.24	101.37	1.27
195.00	5.27	101.24	101.38	1.30
210.00	5.35	101.24	101.4	1.35
225.00	5.42	101.24	101.41	1.38
240.00	5.48	101.25	101.42	1.40
270.00	5.60	101.25	101.44	1.45
300.00	5.70	101.26	101.45	1.48
330.00	5.80	101.26	101.47	1.53
360.00	5.89	101.26	101.48	1.56
390.00	5.97	101.27	101.5	1.61
420.00	6.04	101.27	101.51	1.64
450.00	6.11	101.27	101.52	1.66
480.00	6.17	101.28	101.53	1.69

THERMAL CONDUCTIVITY TEST

Date: May 14, 2000

Sample No. Faro Mine

Test No: 21

Temperature (°C):	1.7
Potential Drop, Vr (V):	0.22
Voltage to Heater Probe, Vp (V):	6.000
Resistance (Ohms):	2.000
Current, I (Amps):	0.1100
Voltage Across Heater, (Vp - Vr):	5.780
Power at Probe Heater (Watts):	0.636
Power per Unite Heated Length of Probe, Q (W/m):	13.528
Probe Length, L (m):	0.047
Thermal Conductivity, I (W/m°C):	3.145
Slope of Steady State Curve:	0.342

Time Elapsed (seconds)	Ln time (sec)	Outside RTD Reading (Ohms)	Inside RTD Reading (Ohms)	Temperature (°C)
0.00		101.42	101.12	0.62
5.00	1.61	101.43	101.17	0.75
10.00	2.30	101.42	101.21	0.86
20.00	3.00	101.42	101.26	0.99
30.00	3.40	101.42	101.3	1.09
40.00	3.69	101.42	101.34	1.19
50.00	3.91	101.42	101.37	1.27
60.00	4.09	101.43	101.39	1.32
70.00	4.25	101.42	101.42	1.40
80.00	4.38	101.43	101.44	1.45
90.00	4.50	101.42	101.45	1.48
100.00	4.61	101.43	101.46	1.51
110.00	4.70	101.43	101.49	1.58
120.00	4.79	101.43	101.5	1.61
130.00	4.87	101.43	101.51	1.64
140.00	4.94	101.43	101.53	1.69
150.00	5.01	101.43	101.54	1.71
160.00	5.08	101.43	101.55	1.74
170.00	5.14	101.43	101.56	1.77
180.00	5.19	101.43	101.57	1.79
195.00	5.27	101.44	101.58	1.82
210.00	5.35	101.44	101.59	1.84
225.00	5.42	101.44	101.6	1.87
240.00	5.48	101.45	101.61	1.90
270.00	5.60	101.45	101.63	1.95
300.00	5.70	101.45	101.65	2.00
330.00	5.80	101.46	101.66	2.03
360.00	5.89	101.46	101.68	2.08
390.00	5.97	101.47	101.69	2.10
420.00	6.04	101.47	101.7	2.13
450.00	6.11	101.47	101.71	2.16
480.00	6.17	101.48	101.72	2.18

THERMAL CONDUCTIVITY TEST

Date: May 15, 2000

Sample No. Faro Mine

Test No: 22

Temperature (°C): 3.7
Potential Drop, Vr (V): 0.219
Voltage to Heater Probe, Vp (V): 6.000
Resistance (Ohms): 2.000
Current, I (Amps): 0.1095
Voltage Across Heater, (Vp - Vr): 5.781
Power at Probe Heater (Watts): 0.633
Power per Unite Heated Length of Probe, Q (W/m): 13.469
Probe Length, L (m): 0.047
Thermal Conductivity, I (W/m°C): 3.064
Slope of Steady State Curve: 0.350

Time Elapsed (seconds)	Ln time (sec)	Outside RTD Reading (Ohms)	Inside RTD Reading (Ohms)	Temperature (°C)
0.00		102.1	101.80	2.39
5.00	1.61	102.11	101.83	2.47
10.00	2.30	102.11	101.87	2.57
20.00	3.00	102.11	101.92	2.70
30.00	3.40	102.11	101.97	2.83
40.00	3.69	102.11	102.01	2.94
50.00	3.91	102.11	102.04	3.01
60.00	4.09	102.11	102.06	3.06
70.00	4.25	102.11	102.08	3.12
80.00	4.38	102.11	102.11	3.19
90.00	4.50	102.11	102.13	3.25
100.00	4.61	102.11	102.14	3.27
110.00	4.70	102.11	102.16	3.32
120.00	4.79	102.11	102.17	3.35
130.00	4.87	102.11	102.19	3.40
140.00	4.94	102.12	102.2	3.43
150.00	5.01	102.12	102.21	3.45
160.00	5.08	102.12	102.22	3.48
170.00	5.14	102.12	102.23	3.51
180.00	5.19	102.12	102.24	3.53
195.00	5.27	102.12	102.25	3.56
210.00	5.35	102.12	102.26	3.58
225.00	5.42	102.12	102.27	3.61
240.00	5.48	102.12	102.29	3.66
270.00	5.60	102.13	102.3	3.69
300.00	5.70	102.14	102.32	3.74
330.00	5.80	102.14	102.34	3.79
360.00	5.89	102.14	102.35	3.82
390.00	5.97	102.15	102.36	3.84
420.00	6.04	102.15	102.37	3.87
450.00	6.11	102.16	102.38	3.90
480.00	6.17	102.16	102.39	3.92

THERMAL CONDUCTIVITY TEST

Date: May 20, 2000

Sample No.

Test No: Faro Mine

Temperature (°C):	11.2
Potential Drop, Vr (V):	0.22
Voltage to Heater Probe, Vp (V):	6.000
Resistance (Ohms):	2.000
Current, I (Amps):	0.1100
Voltage Across Heater, (Vp - Vr):	5.780
Power at Probe Heater (Watts):	0.636
Power per Unite Heated Length of Probe, Q (W/m):	13.528
Probe Length, L (m):	0.047
Thermal Conductivity, I (W/m°C):	3.217
Slope of Steady State Curve:	0.335

Time Elapsed (seconds)	Ln time (sec)	Outside RTD Reading (Ohms)	Inside RTD Reading (Ohms)	Temperature (°C)
0.00		104.39	104.06	8.26
5.00	1.61	104.39	104.1	8.36
10.00	2.30	104.39	104.13	8.44
20.00	3.00	104.39	104.19	8.60
30.00	3.40	104.39	104.23	8.70
40.00	3.69	104.39	104.27	8.81
50.00	3.91	104.39	104.3	8.88
60.00	4.09	104.39	104.32	8.94
70.00	4.25	104.39	104.34	8.99
80.00	4.38	104.39	104.36	9.04
90.00	4.50	104.39	104.38	9.09
100.00	4.61	104.39	104.4	9.14
110.00	4.70	104.39	104.42	9.19
120.00	4.79	104.4	104.43	9.22
130.00	4.87	104.4	104.44	9.25
140.00	4.94	104.4	104.45	9.27
150.00	5.01	104.4	104.46	9.30
160.00	5.08	104.4	104.47	9.32
170.00	5.14	104.4	104.48	9.35
180.00	5.19	104.4	104.49	9.38
195.00	5.27	104.41	104.5	9.40
210.00	5.35	104.41	104.51	9.43
225.00	5.42	104.41	104.52	9.45
240.00	5.48	104.41	104.53	9.48
270.00	5.60	104.42	104.55	9.53
300.00	5.70	104.42	104.57	9.58
330.00	5.80	104.42	104.58	9.61
360.00	5.89	104.43	104.59	9.64
390.00	5.97	104.43	104.61	9.69
420.00	6.04	104.44	104.62	9.71
450.00	6.11	104.44	104.63	9.74
480.00	6.17	104.44	104.64	9.77

APPENDIX E

Bacteria Culture Recipes

Culture Media Recipes

ATCC Culture Medium 238 - *Thiobacillus* Medium B

NH_4Cl	0.1 g
KH_2PO_4	3.0 g
$MgCl_2$	0.1 g
$CaCl_2$	0.1 g
$Na_2S_2O_3$-$5H_2O$	5.0 g
Difco agar	15.0 g
Distilled water	1.0 L

Adjust pH to 4.2
Autoclave for 15 minutes at 121 °C.

ATCC Culture Medium 450 - T2 Medium for *Thiobacillus*

Solution A:

$Na_2S_2O_3$-$5H_2O$	5.0 g
NH_4Cl	1.0 g
KNO_3	2.0 g
Difco agar	7.5 g
Distilled water	250 mL

Solution B:

KH_2PO_4	2.0 g
Difco agar	7.5 g
Distilled water	250 mL

Solution C:

$NaHCO_3$	2.0 g
Distilled water	250 mL

Trace Metal Solution

EDTA	50.0 g
$ZnSO_4$	22.0 g
$CaCl_2$	5.54 g
$MnCl_2$	5.06 g
$FeSO_4$	4.99 g
Ammonium molybdate	1.10 g
$CaSO_4$	1.57 g
$CoCl_2$	1.61 g
Distilled water	1.0 L

Adjust pH to 6.0 with KOH

Solution D:

$MgSO_4$-$7H_2O$	0.8 g
$FeSO_4$-$7H_20$ (2%, w/v, in N HCl)	1.0 mL
Trace metal solution	1.0 mL
Distilled water	250 mL

Sterilize the four solutions (A,B,C,D) separately and combine aseptically for the completed medium. The pH of the final medium is 7.0.

ATCC Culture Medium 64 for *Thiobacillus*

Solution A:

$(NH_4)_2SO_4$	0.4 g
KH_2PO_4	0.2 g
$MgSO_4 . 7H_2O$	0.08 g
Distilled water	400 mL

Solution B:

$FeSO_4 . 7H_2O$	10.0 g
1N H_2SO_4	1.0 mL
Distilled water	100 mL

Autoclave solutions A and B separately and combine aseptically.
Adjust pH to 2.8

American Type Culture Collection
www.atcc.org

Iron-oxidizing Medium (Atlas, 1995)

Composition per liter:

$(NH_4)_2SO_4$	3.0g
K_2HPO_4	0.5g
$MgSO_4 \cdot 7H_2O$	0.5g
KCl	0.1g
$Ca(NO_3)_2$	0.01g
$FeSO_4 \cdot 7H_20$ solution	300 mL
H_2SO_4 (10*N*)	1.0 mL

$FeSO_4 \cdot 7H_20$ Solution:
Composition per 300 mL

$FeSO_4 \cdot 7H_20$	44.22 g

Preparation of iron solution: Add $FeSO_4 \cdot 7H_20$ to distilled water and bring volume to 300 mL. Mix thoroughly. Autoclave for 15 min at 15 psi pressure-121°C. Cool to 25°C.

Preparation of medium: Add components, except $FeSO_4 \cdot 7H_20$ solution, to distilled water and bring volume to 700 mL. Mix thoroughly. Gently heat and bring to boil on heating stir plate. Autoclave for 15 min at 15 psi pressure-121°C. Cool to 25°C. Aseptically add 300 mL sterile $FeSO_4 \cdot 7H_20$ solution. Mix thoroughly. Aseptically distribute into sterile flasks.

Pyrite Medium

In the pyrite medium, the $FeSO_4 \cdot 7H_20$ was replaced with 40 g of sterilized bulk Faro tailings estimated at 75% FeS_2.

Sulfur-oxidizing Medium (Roberts, 1999)

Composition per liter:

KH_2PO_4	1.5 g
$CaCl_2$	0.1 g
$MgCl_2 \cdot 6H_20$	0.1 g
NH_4Cl	0.1 g
Elemental sulfur	4.0 g

Preparation of medium: Prepare sterilized sulfur powder by wrapping sulfur powder with aluminum film and autoclaving for 15 min at 112°C. Note the melting point of monoclinic sulfur is 115°C. Sterilize sulfur alone then add into the autoclaved mixture of other components. Aseptically distribute into sterile flasks.

APPENDIX F

pH and Sulfate Tracking for Discovery and Faro Mine Humidity Cells

Faro Mine Tailings Humidity Cell Tracking (20°C)

Cell	Date	#	pH	Cell	Date	#	pH	Cell	Date	#	pH	#	Average	St Dev
M	6-Jan	1	2.9	F	6-Jan	1	2.8	I	6-Jan	1	2.8	1	2.8	0.1
M	7-Jan	2	3.3	F	7-Jan	2	3.0	I	7-Jan	2	2.8	2	3.1	0.2
M	14-Jan	3	3.5	F	14-Jan	3	4.2	I	14-Jan	3	3.0	3	3.6	0.6
M	24-Jan	4	3.5	F	24-Jan	4	4.3	I	24-Jan	4	2.3	4	3.4	1.0
M	27-Jan	5	3.9	F	27-Jan	5	4.0	I	27-Jan	5	3.5	5	3.8	0.3
M	6-Feb	6	4.1	F	6-Feb	6	4.0	I	6-Feb	LOST		6	4.0	0.1
M	13-Feb	7	3.8	F	13-Feb	7	3.6	I	13-Feb	7	3.8	7	3.7	0.1
M	22-Feb	8	3.9	F	22-Feb	8	3.2	I	22-Feb	8	3.7	8	3.6	0.4
M	29-Feb	9	3.7	F	29-Feb	9	3.6	I	29-Feb	9	3.9	9	3.7	0.1
M	7-Mar	10	3.7	F	7-Mar	10	3.6	I	7-Mar	10	3.4	10	3.6	0.1
M	15-Mar	11	4.0	F	15-Mar	11	3.9	I	15-Mar	11	3.4	11	3.8	0.3
M	**21-Mar**	**12**	**6.6**	F	21-Mar	12	3.6	I	21-Mar	12	3.1	12	4.4	1.9
M	**27-Mar**	**13**	**6.6**	F	27-Mar	13	3.5	I	27-Mar	13	3.3	13	4.5	1.9
M	3-Apr	14	3.6	F	3-Apr	14	3.6	I	3-Apr	14	3.0	14	3.4	0.3
M	9-Apr	15	3.3	F	9-Apr	15	3.4	I	9-Apr	15	3.0	15	3.2	0.2
M	15-Apr	16	3.4	F	15-Apr	16	3.3	I	15-Apr	16	2.9	16	3.2	0.2
M	24-Apr	17	3.2	F	24-Apr	17	3.6	I	24-Apr	17	3.2	17	3.3	0.2
M	1-May	18	3.1	F	1-May	18	3.5	I	1-May	18	3.0	18	3.2	0.3
M	8-May	19	3.0	F	8-May	19	3.4	I	8-May	19	3.0	19	3.1	0.2
M	15-May	20	3.0	F	15-May	20	3.3	I	15-May	20	3.0	20	3.1	0.2

Bold - Questionable data

Faro Mine Tailings Humidity Cell Tracking (3°C)

Cell	Date	#	pH	Cell	Date	#	pH	Cell	Date	#	pH	#	Average	St Dev
B	7-Jan	1	3.0	H	7-Jan	1	2.9	D	7-Jan	1	2.4	1	2.8	0.31
B	14-Jan	2	3.5	H	14-Jan	2	3.7	D	14-Jan	2	2.6	2	3.3	0.56
B	24-Jan	3	3.0	H	24-Jan	3	3.1	D	24-Jan	3	2.7	3	2.9	0.18
B	27-Jan	4	3.6	H	27-Jan	4	3.4	D	27-Jan	4	3.0	4	3.3	0.32
B	7-Feb	5	4.2	H	7-Feb	5	4.5	D	7-Feb	5	3.0	5	3.9	0.78
B	14-Feb	6	3.2	H	14-Feb	6	4.0	D	14-Feb	6	3.4	6	3.5	0.38
B	23-Feb	7	3.8	H	23-Feb	7	4.2	D	23-Feb	7	3.7	7	3.9	0.28
B	3-Mar	8	3.9	H	3-Mar	8	4.4	D	3-Mar	8	3.4	8	3.9	0.49
B	12-Mar	9	4.6	H	12-Mar	9	4.9	D	12-Mar	9	3.8	9	4.4	0.58
B	21-Mar	10	3.6	H	21-Mar	10	4.4	D	21-Mar	10	3.9	10	4.0	0.39
B	28-Mar	11	4.6	H	28-Mar	11	4.6	D	28-Mar	11	4.1	11	4.4	0.33
B	4-Apr	12	4.9	H	4-Apr	12	4.6	D	4-Apr	12	3.8	12	4.4	0.55
B	9-Apr	13	4.6	H	9-Apr	13	4.5	D	9-Apr	13	4.5	13	4.5	0.08
B	**25-Apr**	**14**	**4.5**	H	25-Apr	14	4.0	D	25-Apr	14	4.5	14	4.3	0.30
B	**25-Apr**	**15**	**4.0**	H	18-Apr	15	4.4	D	18-Apr	15	4.4	15	4.2	0.22
B	2-May	16	4.2	H	2-May	16	4.4	D	2-May	16	4.3	16	4.3	0.07
B	9-May	17	4.3	H	9-May	17	4.3	D	9-May	17	4.3	17	4.3	0.03

Bold - Questionable data

Faro Mine Tailings Humidity Cell Tracking (1°C)

Cell	Date	#	pH	Cell	Date	#	pH	Cell	Date	#	pH	#	Average	St Dev
C	14-Jan	1	2.7	K	14-Jan	1	2.8	L	14-Jan	1	2.7	1	2.7	0.1
C	24-Jan	2	3.1	K	24-Jan	2	3.1	L	24-Jan	2	2.8	2	3.0	0.2
C	27-Jan	3	3.4	K	27-Jan	3	3.5	L	27-Jan	3	3.1	3	3.3	0.2
C	9-Feb	4	2.9	K	9-Feb	4	3.3	L		4		4	3.1	0.3
C	22-Feb	5	3.8	K	22-Feb	4	3.9	L	22-Feb	5	3.6	5	3.8	0.2
C	29-Feb	6	5.0	K	29-Feb	5	5.0	L	29-Feb	6	3.6	6	4.5	0.8
C	12-Mar	7	4.7	K	12-Mar	7	4.8	L	12-Mar	7	3.7	7	4.4	0.6
C	21-Mar	8	4.3	K	21-Mar	8	4.4	L	21-Mar	8		8	4.3	0.1
C	29-Mar	9	4.6	K	29-Mar	9	4.5	L	29-Mar	9		9	4.6	0.1
C		10		K		10		L	7-Apr	10	4.5	10	4.5	
C	15-Apr	11	4.5	K	15-Apr	11	4.6	L	15-Apr	11	4.7	11	4.6	0.1
C	25-Apr	12	4.4	K	25-Apr	12	4.7	L	25-Apr	12	4.7	12	4.6	0.2
C	4-May	13	4.5	K	4-May	13	4.5	L	4-May	13	4.7	13	4.5	0.1
C	12-May	14	4.4	K	12-May	14	4.2	L	12-May	14	4.7	14	4.4	0.2

Bold - Questionable data
Blank - Sample lost / contaminated

Faro Mine Tailings Humidity Cell Tracking (20°C)

#	CELL	Sample	Vol. (mL)	SO4 mg/L	SO4 mg	SO4 cum.	#	CELL	Sample	Vol. (mL)	SO4 mg/L	SO4 mg	SO4 cum.	#	CELL	Sample	SO4 mg/L	SO4 cum.
1	F	Jan 06	368	944	347	347	1	M	Jan 06	358	1217	436	436	1	average	Jan 06	1080	391
2	F	Jan 07	350	610	213	213	2	M	Jan 07	348	446	155	155	2	average	Jan 07	528	576
3	F	Jan 14	399	983	392	606	3	M	Jan 14	442	553	244	400	3	average	Jan 14	768	894
4	F	Jan 24	387	1013	392	998	4	M	Jan 24	246	1653	407	806	4	average	Jan 24	1333	1293
5	F	Jan 27	403	169	68	1066	5	M	Jan 27	349	1437	501	1306	5	average	Jan 27	803	1578
6	F	Feb 06	330	1943	641	1707	6	M	Feb 06	321	1718	551	1859	6	average	Feb 06	1830	2174
7	F	Feb 13	410	1512	620	2327	7	M	Feb 13	418	1901	795	2654	7	average	Feb 13	1707	2882
8	F	Feb 22	379	1793	680	3006	8	M	Feb 22	426	1601	682	3336	8	average	Feb 22	1697	3563
9	F	Feb 29	313	1609	504	3510	9	M	Feb 29	381	1713	653	3989	9	average	Feb 29	1661	4141
10	F	Mar 07	309	1633	505	4014	10	M	Mar 03	294	1759	517	4506	10	average	Mar 03	1696	4652
11	F	Mar 15	336	1045	351	4366	11	M	Mar 15	311	1489	463	4969	11	average	Mar 15	1267	5059
12	F	Mar 21	403	1247	503	4868	12	M	Mar 21	380	292	111	5080	12	average	Mar 21	770	5365
13	F	Mar 27	324	1221	396	5264	13	M	Mar 27	341	322	110	5189	13	average	Mar 27	772	5618
14	F	Apr 03	420	1046	440	5703	14	M	Apr 03	460	1289	593	5783	14	average	Apr 03	1168	6134
15	F	Apr 10	388	1970	764	6468	15	M	Apr 10	398	2180	868	6650	15	average	Apr 10	2075	6950
16	F	Apr 17	313	1870	585	7053	16	M	Apr 17	348	2320	807	7458	16	average	Apr 17	2095	7647
17	F	Apr 24	459	1670	767	7820	17	M	Apr 24	456	1920	876	8333	17	average	Apr 24	1795	8468
18	F	May 01	442	1400	619	8438	18	M	May 01	454	1400	636	8969	18	average	May 01	1400	9095
19	F	May 09	478	1720	822	9261	19	M	May 09	430	1940	834	9803	19	average	May 09	1830	9923
20	F	May 16	421	1660	699	9959	20	M	May 16	409	1850	757	10560	20	average	May 16	1755	10651

Bold - Questionnable data

Faro Mine Tailings Humidity Cell Tracking (3°C)

#	CELL	Sample	Vol. (mL)	SO4 mg/L	SO4 mg	SO4 cum.
1	B	Jan 07	326	739	241	241
2	B	Jan 14	468	343	160	160
3	B	Jan 24	487	254	124	284
4	B	Jan 27	479	1305	625	909
5	B	Feb 07	384	192	74	983
6	B	Feb 14	453	228	103	1086
7	B	Feb 23	311	286	89	1175
8	B	Mar 03	387	551	213	1388
9	B	Mar 12	397	502	199	1588
10	B	Mar 21	401	421	169	1757
11	B	Mar 28	415	337	140	1897
12	B	Apr 04	392	405	159	2055
13	B	Apr 11	386	1420	548	2603
14	B	Apr 18	415	1270	527	3131
15	B	Apr 25	376	1340	504	3634
16	B	May 02	377	753	284	3918
17	B	May 10	333	951	317	4235

#	CELL	Sample	Vol. (mL)	SO4 mg/L	SO4 mg	SO4 cum.
1	H	Jan 07	347	735	255	255
2	H	Jan 14	482	254	122	122
3	H	Jan 24	451	282	127	249
4	H	Jan 27	368	203	75	324
5	H	Feb 07	232	309	72	396
6	H	Feb 14	338	287	97	493
7	H	Feb 23	368	316	116	609
8	H	Mar 03	279	689	192	801
9	H	Mar 12	364	342	124	926
10	H	Mar 21	433	461	200	1125
11	H	Mar 28	456	328	149	1275
12	H	Apr 04	394	342	135	1409
13	H	Apr 11	461	986	455	1864
14	H	Apr 18	429	1060	455	2319
15	H	Apr 25	358	1220	437	2755
16	H	May 02	428	817	350	3105
17	H	May 10	424	833	353	3458

#	CELL	Sample	SO4 mg/L	SO4 cum.
1	average	Jan 07	248	248
2	average	Jan 14	298	141
3	average	Jan 24	268	267
4	average	Jan 27	754	617
5	average	Feb 07	250	689
6	average	Feb 14	258	789
7	average	Feb 23	301	892
8	average	Mar 03	620	1095
9	average	Mar 12	422	1257
10	average	Mar 21	441	1441
11	average	Mar 28	332	1586
12	average	Apr 04	374	1732
13	average	Apr 11	1203	2234
14	average	Apr 18	1165	2725
15	average	Apr 25	1280	3195
16	average	May 02	785	3512
17	average	May 10	892	3847

Bold - Questionnable data

Faro Mine Tailings Humidity Cell Tracking (1°C)

#	CELL	Sample	Vol. (mL)	SO4 mg/L	SO4 mg	SO4 cum.
1	C	Jan 14	275	616	169	169
2	C	Jan 24	437	410	179	179
3	L	Jan 27	425	267	113	293
4	C	Feb 07	315	438	138	431
5	C	Feb 22	382	406	155	586
6	C	Feb 29	350	420	147	733
7	C	Mar 12	261	487	127	860
8	C	Mar 21	328	444	146	1005
9	C	Mar 29	330	489	161	1167
10	C	Apr 07	333	1280	426	1593
11	C	Apr 16	341	1330	454	2047
12	C	Apr 25	247	954	236	2282
13	C	May 04	345	1350	466	2748
14	C	May 10	347	1010	350	3098

#	CELL	Sample	Vol. (mL)	SO4 mg/L	SO4 mg	SO4 cum.
1	K	Jan 14	270	863	233	233
2	K	Jan 24	420	449	189	189
3	K	Jan 27	404	291	118	306
4	K	Feb 07	309	825	255	561
5	K	Feb 22	357	414	148	709
6	K	Feb 29	323	415	134	843
7	K	Mar 12	277	633	175	1019
8	K	Mar 21	306	845	259	1277
9	K	Mar 29	342	445	152	1429
10	K	Apr 07	344	1270	437	1866
11	K	Apr 16	412	1300	536	2402
12	K	Apr 25	284	1620	460	2862
13	K	May 04	475	745	354	3216
14	K	May 12	337	669	225	3441

#	CELL	Sample	SO4 mg/L	SO4 cum.
1	average	Jan 14	740	201
2	average	Jan 24	429	184
3	average	Jan 27	279	299
4	average	Feb 07	632	496
5	average	Feb 22	410	647
6	average	Feb 29	418	788
7	average	Mar 12	560	939
8	average	Mar 21	645	1141
9	average	Mar 29	467	1298
10	average	Apr 07	1275	1730
11	average	Apr 16	1315	2224
12	average	Apr 25	1287	2572
13	average	May 04	1048	2982
14	average	May 12	840	3270

Bold - Questionnable data

Discovery Mine Humidity Cell Tracking

Sample	Leach Date	Test Date	Cycle #	pH	Sulphate (mg/L) Diluted	Actual
A	19-Jan-99	20-Jan-99	1	7.2		
A	26-Jan-99	3-Feb-99	2	6.8	3.7	18
A	2-Feb-99	3-Feb-99	3	7.8	21.4	107
A	9-Feb-99	10-Feb-99	4	7.7	35.8	179
A	16-Feb-99	17-Feb-99	5	7.6	51.6	258
A	23-Feb-99	24-Feb-99	6	7.6	45.4	227
A	2-Mar-99	3-Mar-99	7	7.4	48.0	240
A	9-Mar-99	10-Mar-99	8	7.4	40.9	204
A	16-Mar-99	17-Mar-99	9	7.5	31.6	158
A	24-Mar-99	31-Mar-99	10	7.1	16.8	84
A	31-Mar-99	31-Mar-99	11	7.5	15.9	79
A	9-Apr-99	10-Apr-99	12		17.4	87
A	16-Apr-99	17-Apr-99	13		32.0	160
B	2-Feb-99	3-Feb-99	1	7.9		
B	9-Feb-99	10-Feb-99	2	7.8	4.9	24
B	16-Feb-99	17-Feb-99	3	7.9	5.0	25
B	23-Feb-99	24-Feb-99	4	7.9	5.4	27
B	2-Mar-99	3-Mar-99	5	7.4		
B	9-Mar-99	10-Mar-99	6	7.7	8.0	40
B	16-Mar-99	17-Mar-99	7	7.8	7.1	35
B	26-Mar-99	31-Mar-99	8	7.5	7.9	39
B	2-Apr-99	3-Apr-99	9		7.1	36
C	19-Jan-99	20-Jan-99		6.9	3.5	18
D	2-Apr-99	3-Apr-99			10.9	55
E	12-Jan-99	20-Jan-99		7.3		
E	19-Jan-99	20-Jan-99		7.2	3.2	16
F	26-Jan-99	3-Feb-99	1	6.3		
F	2-Feb-99	3-Feb-99	2	8.0		
F	9-Feb-99	10-Feb-99	3	7.2		
F	16-Feb-99	17-Feb-99	4	7.5	6.9	34
F	23-Feb-99	24-Feb-99	5	7.4	4.9	25
F	2-Mar-99	3-Mar-99	6	7.2		
F	9-Mar-99	10-Mar-99	7	7.4	4.9	25
F	16-Mar-99	17-Mar-99	8	7.4	4.7	24
F	24-Mar-99	31-Mar-99	9	7.3	9.4	47
F	31-Mar-99	31-Mar-99	10	7.6	15.9	79
F	11-Apr-99	12-Apr-99	11		11.2	56
H	19-Jan-99	20-Jan-99	1	6.2		
H	26-Jan-99	3-Feb-99	2	6.6	3.8	19
H	2-Feb-99	3-Feb-99	3	7.7		

H	9-Feb-99	10-Feb-99	4	7.4	11.9	60
H	16-Feb-99	17-Feb-99	5	7.8	12.6	63
H	23-Feb-99	24-Feb-99	6	7.9	10.0	50
H	2-Mar-99	3-Mar-99	7	7.7		
H	9-Mar-99	10-Mar-99	8	7.8	7.3	37
H	16-Mar-99	17-Mar-99	9	7.7	8.0	40
H	24-Mar-99	31-Mar-99	10	7.5	6.3	32
H	31-Mar-99	31-Mar-99	11	8.0	6.1	30
H	11-Apr-99	12-Apr-99	12		6.8	34
I	2-Feb-99	3-Feb-99	1	7.7		
I	9-Feb-99	10-Feb-99	2	7.8		
I	16-Feb-99	17-Feb-99	3	7.8	6.3	31
I	23-Feb-99	24-Feb-99	4	7.8	4.7	23
I	2-Mar-99	3-Mar-99	5	7.3		
I	9-Mar-99	10-Mar-99	6	7.8	8.0	40
I	16-Mar-99	17-Mar-99	7	7.8	6.4	32
I	26-Mar-99	31-Mar-99	8	7.6	8.9	44
I	2-Apr-99	3-Apr-99	9		6.0	30
J	19-Jan-99	20-Jan-99	11	7.2		
K	12-Jan-99	20-Jan-99	1	7.0	3.7	18
K	26-Jan-99	3-Feb-99	2	6.7		
K	2-Feb-99	3-Feb-99	3	7.4		
K	9-Feb-99	10-Feb-99	4	7.8		
K	16-Feb-99	17-Feb-99	5	7.7	11.3	57
K	23-Feb-99	24-Feb-99	6	7.7	9.3	46
K	2-Mar-99	3-Mar-99	7	7.5	9.7	48
K	9-Mar-99	10-Mar-99	8	7.4	7.5	38
K	16-Mar-99	17-Mar-99	9	7.7	8.7	44
K	24-Mar-99	31-Mar-99	10	7.3	7.8	39
K	31-Mar-99	31-Mar-99	11	7.7	7.0	35
K	9-Apr-99	10-Apr-99	12		9.9	50
K	16-Apr-99	17-Apr-99	13		8.7	44
N	12-Jan-99	20-Jan-99		7.0		
P	2-Feb-99	3-Feb-99	1	7.7		
P	9-Feb-99	10-Feb-99	2	7.7		
P	16-Feb-99	17-Feb-99	3	7.8	7.8	39
P	23-Feb-99	24-Feb-99	4	7.4	3.2	16
P	2-Mar-99	3-Mar-99	5	7.1		
P	9-Mar-99	10-Mar-99	6	7.2	4.9	25
P	16-Mar-99	17-Mar-99	7	7.3	4.6	23
P	26-Mar-99	31-Mar-99	8	7.2	5.8	29
Q	26-Jan-99	3-Feb-99	1	6.8		
Q	2-Feb-99	3-Feb-99	2	7.7		
Q	9-Feb-99	10-Feb-99	3	7.8		

Q	16-Feb-99	17-Feb-99	4	7.5	59.6	298
Q	23-Feb-99	24-Feb-99	5	7.7	49.2	246
Q	2-Mar-99	3-Mar-99	6	7.7	51.1	255
Q	9-Mar-99	10-Mar-99	7	7.5	53.6	268
Q	16-Mar-99	17-Mar-99	8	7.7	38.6	193
Q	24-Mar-99	31-Mar-99	9	7.5	36.4	182
Q	31-Mar-99	31-Mar-99	10	7.7	29.8	149
Q	9-Apr-99	10-Apr-99	11		26.9	134
Q	16-Apr-99	17-Apr-99	12		45.2	226
R	19-Jan-99	20-Jan-99	1	6.8		
R	26-Jan-99	3-Feb-99	2	7.0		
R	2-Feb-99	3-Feb-99	3	7.9		
R	9-Feb-99	10-Feb-99	4	7.6		
R	16-Feb-99	17-Feb-99	5	7.9	13.9	69
R	23-Feb-99	24-Feb-99	6	7.9	9.8	49
R	2-Mar-99	3-Mar-99	7	7.8		
R	9-Mar-99	10-Mar-99	8	7.8	5.4	27
R	16-Mar-99	17-Mar-99	9	7.5	5.3	26
R	24-Mar-99	31-Mar-99	10	7.2	9.3	47
R	31-Mar-99	31-Mar-99	11	7.9	13.2	66
R	11-Apr-99	12-Apr-99	12		8.7	44